SAPIENZA
UNIVERSITÀ DI ROMA

SAPIENZA UNIVERSITY OF ROME
AND
UNIVERSITY OF ROME TOR VERGATA

PH.D. IN ASTRONOMY, ASTROPHYSICS AND SPACE SCIENCE

CYCLE XXX

CMB Anisotropies and Spectral Distortions: Constraining Inflation at Small Scales

Giovanni Cabass
A.Y. 2016/2017

Supervisor: Prof. Alessandro Melchiorri

Co-supervisor: Prof. Enrico Pajer

Coordinator: Prof. Roberto Capuzzo Dolcetta

Deputy Coordinator: Prof. Pasquale Mazzotta

CMB ANISOTROPIES AND SPECTRAL DISTORTIONS: CONSTRAINING INFLATION AT SMALL SCALES

A thesis submitted in partial fulfillment of the requirements for the degree of

Ph.D. in Astronomy, Astrophysics and Space Science

University of Rome "La Sapienza"

Academic Year 2016 – 2017

CANDIDATE:	Giovanni Cabass[a]
SUPERVISOR:	Prof. Alessandro Melchiorri[b]
CO-SUPERVISOR:	Prof. Enrico Pajer[c]

Rome, October 31, 2017

a University of Rome "La Sapienza", giovanni.cabass@gmail.com
b University of Rome "La Sapienza", alessandro.melchiorri@gmail.com
c Utrecht University, enrico.pajer@gmail.com

THESIS PROJECT AND POSSIBLE DEVELOPMENTS

This summary contains the thesis project and its possible developments, together with a list of references, to show what are the topics that I have investigated during the Ph.D.

THESIS WORK

This thesis aims at constraining cosmological inflation, studying the anisotropies in the temperature of the Cosmic Microwave Background (CMB) and the deviations of its spectrum from a black-body form.

Inflation is a period of accelerated, de Sitter-like expansion in the early Universe [1–4]. It has set up the initial conditions for the density perturbations which have later evolved into the structure we observe today. Most of our knowledge about these initial conditions comes from observation of the anisotropies in the temperature of CMB photons [5, 6]. Angular correlation functions of these anisotropies are sensitive to inflationary perturbations on length scales from 10^1 Mpc to 10^4 Mpc. Other probes are needed to constrain inflation on smaller scales: among these there are CMB μ-type spectral distortions [7–13]. These spectral distortions are generated between 2 months and 300 years after the Big Bang, a period of time when photons were not in thermodynamical equilibrium with electrons and baryons. They probe scales far smaller than CMB anisotropies (from 10^{-4} Mpc to 10^{-2} Mpc).

The chief inflationary observable constrained by experiments like WMAP and Planck is the two-point correlation function (power spectrum) of primordial scalar (ζ) and tensor (γ) perturbations [14]. Motivated by the fact that de Sitter isometries are only weakly broken during inflation, the usual parameterization for their dimensionless power spectrum in Fourier space is that of a power-law with spectral index close to zero: $k^3 \langle \zeta\zeta \rangle \propto k^{n_s - 1}$, $k^3 \langle \gamma\gamma \rangle \propto k^{n_t}$. The tilt n_s of scalar perturbations has been detected at $\sim 5\sigma$: however, deviations from a simple power-law spectrum, parameterized by the so-called runnings ($\alpha_s \equiv \frac{dn_s}{d\log k}$, $\beta_s \equiv \frac{d\alpha_s}{d\log k}$, etc.) are still not very well constrained by data [6, 14]. Future CMB spectrometry experiments like PIXIE could prove invaluable for improving the present bounds from CMB anisotropies, Ly-α forest observations [15, 16], and other probes at lower redshift.

When looking for signatures of inflationary dynamics, another important quantity is the three-point correlation function. It measures correlations of a given observable (temperature anisotropies, the number density of galaxies, etc.) at three different points in space. Its importance comes from the fact that we expect it to be very small

(i. e. we expect perturbations to have nearly Gaussian statistics) if there are no interactions between the degrees of freedom that drive inflation [17–19].

Both spectral distortions and temperature anisotropies are sensitive to this non-Gaussianity: for example, if a correlation between spectral distortions and temperature anisotropies is found, single-field inflation (where only one degree of freedom drives the expansion) will be ruled out [20, 21].

During the Ph.D. I have studied these topics mainly in three works:

1. G. Cabass, A. Melchiorri and E. Pajer. "μ-distortions or running: A guaranteed discovery from CMB spectrometry." Phys. Rev. D **93**, no. 8, 083515 (2016). arXiv:1602.05578 [astro-ph.CO];

2. G. Cabass, E. Di Valentino, A. Melchiorri, E. Pajer and J. Silk. "Constraints on the running of the running of the scalar tilt from CMB anisotropies and spectral distortions." Phys. Rev. D **94**, no. 2, 023523 (2016). arXiv:1605.00209 [astro-ph.CO];

3. G. Cabass, E. Pajer and F. Schmidt. "How Gaussian can our Universe be?" JCAP **1701**, no. 01, 003 (2017). arXiv:1612.00033 [hep-th].

The main goal of the first two papers was to study how future CMB spectral distortions experiments could help in constraining the power spectrum of primordial inflationary perturbations, when combined with current data from CMB anisotropy observations (more precisely, measurements from the Planck satellite). We focused mainly on the PIXIE satellite [22], a proposed NASA mission. its goals are the study of the frequency spectrum of both the CMB and other astrophysical sources (such as cosmic dust), which act as a foreground for CMB anisotropy observations:

1. in Phys. Rev. D **93**, no. 8, 083515 (2016) we have shown that, if green-lit, PIXIE will provide a guaranteed discovery. Spectral distortions are sensitive to the amount of power on scales from 10^{-4} Mpc to 10^{-2} Mpc: the smaller the inflationary two-point correlation function is on these scales, the smaller the distortion of the CMB spectrum will be. PIXIE will have the sensitivity necessary to probe the spectral distortions predicted by the standard ΛCDM model: therefore, either it will observe them or we will discover that the scale dependence of the spectrum of primordial perturbations is stronger than what is expected in standard inflationary models (i. e. that the scalar power spectrum is more red-tilted: more precisely, the running α_s is negative);

2. in Phys. Rev. D **94**, no. 2, 023523 (2016), instead, it was shown that PIXIE could give a 85 % improvement on current bounds on the running of the running β_s. This parameter is assumed to

be very small in standard slow-roll inflation scenarios, so that narrowing down the contours is necessary to further confirm the paradigm;

3. in the work JCAP **1701**, no. 01, 003 (2017) we have computed the general form of the observed cosmological three-point correlators in the limit where one point is much farther away than the other two (squeezed limit). This configuration is extremely interesting from the theoretical point of view: in fact, models of inflation where only one degree of freedom drives the expansion predict that the squeezed three-point correlator is extremely small [18, 23, 24]. Therefore any observation of a sizable contribution in this limit would rule them out.

POSSIBLE DEVELOPMENTS

The first possible continuation of the thesis work involves a further study of non-Gaussianity. The same initial conditions which give rise to CMB temperature anisotropies generate spectral distortions: therefore, as mentioned above, we expect a correlation between these two observables. Besides, while temperature anisotropies are linear in the amplitude of inflationary perturbations, spectral distortions are quadratic. Then, the correlation between the two will be sensitive to the primordial three-point function [20, 21, 25–30]. The current goal of [31] is to characterize all the secondary contributions that will add to this correlation, which are expected because of the non-linearity of gravitational evolution. Their calculation is necessary for (very futuristic) PIXIE-like experiments, since they could bias the constraints on primordial non-Gaussianity if not accounted for.

In [32], instead, we are currently studying what is the theoretical prediction for the non-Gaussian halo bias in string theory-inspired inflationary models such as "axion monodromy inflation" [33–35]. Having non-zero primordial non-Gaussianity will give rise to a coupling between long- and short-wavelength perturbations: on small scales, in a patch of size comparable to the long-wavelength mode, dark matter halos will evolve in a "separate universe" with higher (or smaller, depending on the details of the primordial coupling) power spectrum amplitude [36–40]. This will give rise to a modulation of their density by the long-wavelength perturbations that will directly trace the primordial long-short mode coupling (which, in the axion monodromy model, shows an oscillating scale dependence due to the bursts of particle creation occurring during inflation [41]).

Finally, new forecasts for PIXIE should be carried out. Indeed, it has been recently shown in [42] that taking correctly into account foreground contamination will give a $\sim 5\times$ worse sensitivity to spectral

distortions with respect to the original mission target that was put forward in [22].

OTHER WORKS

For coherence of content, only the three papers listed above have been discussed in this thesis. The remaining publications produced during the Ph.D. are the following:

- G. Cabass, M. Gerbino, E. Giusarma, A. Melchiorri, L. Pagano and L. Salvati. "Updated Constraints and Forecasts on Primordial Tensor Modes." Phys. Rev. D **92**, no. 6, 063534 (2015). arXiv:1507.07586 [astro-ph.CO];
- G. Cabass, L. Pagano, L. Salvati, M. Gerbino, E. Giusarma and A. Melchiorri. "Constraints on the early and late integrated Sachs-Wolfe effects from the Planck 2015 cosmic microwave background anisotropies in the angular power spectra." Phys. Rev. D **93**, no. 6, 063508 (2016). arXiv:1511.05146 [astro-ph.CO];
- C. Burigana et al. "Recent results and perspectives on cosmology and fundamental physics from microwave surveys." Int. J. Mod. Phys. D **25**, no. 06, 1630016 (2016). arXiv:1604.03819 [astro-ph.CO];
- E. Di Valentino et al. [CORE Collaboration] "Exploring Cosmic Origins with CORE: Cosmological Parameters." Accepted for publication in JCAP. arXiv:1612.00021 [astro-ph.CO];
- L. Bordin, G. Cabass, P. Creminelli and F. Vernizzi. "Simplifying the EFT of Inflation: Generalized Disformal Transformations and Redundant Couplings." Accepted for publication in JCAP. arXiv:1706.03758 [astro-ph.CO].

REFERENCES

[1] S. W. Hawking, I. G. Moss, and J. M. Stewart. "Bubble collisions in the very early universe." *Phys. Rev.* D26, 2681 (1982).

[2] A. H. Guth and E. J. Weinberg. "Could the Universe Have Recovered from a Slow First Order Phase Transition?" *Nucl. Phys.* B212, 321 (1983).

[3] A. Albrecht and P. J. Steinhardt. "Cosmology for grand unified theories with radiatively induced symmetry breaking." *Phys. Rev. Lett.* 48, 1220 (1982).

[4] A. D. Linde. "A new inflationary universe scenario: A possible solution of the horizon, flatness, homogeneity, isotropy and primordial monopole problems." *Phys. Lett.* B108, 389 (1982).

[5] G. Hinshaw et al. "Nine-Year Wilkinson Microwave Anisotropy Probe (WMAP) Observations: Cosmological Parameter Results." *Astrophys. J. Suppl.* 208 (2013), p. 19. arXiv: 1212.5226 [astro-ph.CO].

[6] P. A. R. Ade et al. "Planck 2015 results. XIII. Cosmological parameters." *Astron. Astrophys.* 594 (2016), A13. arXiv: 1502.01589 [astro-ph.CO].

[7] R. A. Sunyaev and Ya. B. Zeldovich. "The Interaction of matter and radiation in the hot model of the universe." *Astrophys. Space Sci.* 7 (1970), pp. 20–30.

[8] A. F. Illarionov and R. A. Sunyaev. *Soviet Astronomy* 18 (1975), pp. 691–699.

[9] L. Danese and G. De Zotti. *A&A* f107 (39 1982).

[10] C. Burigana, L. Danese, and G. De Zotti. *A&A* 246 (49 1991).

[11] D. J. Fixsen, E. S. Cheng, J. M. Gales, J. C. Mather, R. A. Shafer, and E. L. Wright. "The Cosmic Microwave Background spectrum from the full COBE FIRAS data set." *Astrophys. J.* 473 (1996), p. 576. arXiv: astro-ph/9605054 [astro-ph].

[12] J. Chluba and R. A. Sunyaev. "The evolution of CMB spectral distortions in the early Universe." *Mon. Not. Roy. Astron. Soc.* 419 (2012), pp. 1294–1314. arXiv: 1109.6552 [astro-ph.CO].

[13] R. Khatri and R. A. Sunyaev. "Creation of the CMB spectrum: precise analytic solutions for the blackbody photosphere." *JCAP* 1206 (2012), p. 038. arXiv: 1203.2601 [astro-ph.CO].

[14] P. A. R. Ade et al. "Planck 2015 results. XX. Constraints on inflation." *Astron. Astrophys.* 594 (2016), A20. arXiv: 1502.02114 [astro-ph.CO].

[15] S. Hannestad, S. H. Hansen, F. L. Villante, and A. J. S. Hamilton. "Constraints on inflation from CMB and Lyman alpha forest." *Astropart. Phys.* 17 (2002), pp. 375–382. arXiv: astro-ph/0103047 [astro-ph].

[16] U. Seljak, A. Slosar, and P. McDonald. "Cosmological parameters from combining the Lyman-alpha forest with CMB, galaxy clustering and SN constraints." *JCAP* 0610 (2006), p. 014. arXiv: astro-ph/0604335 [astro-ph].

[17] V. Acquaviva, N. Bartolo, S. Matarrese, and A. Riotto. "Second-Order Cosmological Perturbations from Inflation." *Nucl. Phys.* B667 (2003), pp. 119–148. arXiv: astro-ph/0209156v3.

[18] J. Maldacena. "Non-Gaussian features of primordial fluctuations in single field inflationary models." *JHEP* 013 (May 2003). arXiv: astro-ph/0210603v5.

[19] N. Bartolo, E. Komatsu, S. Matarrese, and A. Riotto. "Non-Gaussianity from Inflation: Theory and Observations." *Phys. Rept.* 402 (2004), pp. 103–266. arXiv: astro-ph/0406398v2.

[20] E. Pajer and M. Zaldarriaga. "A New Window on Primordial non-Gaussianity." *Phys. Rev. Lett.* 109 (2012), p. 021302. arXiv: 1201.5375 [astro-ph.CO].

[21] J. Chluba, E. Dimastrogiovanni, M. A. Amin, and M. Kamionkowski. "Evolution of CMB spectral distortion anisotropies and tests of primordial non-Gaussianity." *Mon. Not. Roy. Astron. Soc.* 466.2 (2017), pp. 2390–2401. arXiv: 1610.08711 [astro-ph.CO].

[22] A. Kogut et al. "The Primordial Inflation Explorer (PIXIE): A Nulling Polarimeter for Cosmic Microwave Background Observations." *JCAP* 1107 (2011), p. 025. arXiv: 1105.2044 [astro-ph.CO].

[23] P. Creminelli and M. Zaldarriaga. "Single field consistency relation for the 3-point function." *JCAP* 0410 (2004), p. 006. arXiv: astro-ph/0407059 [astro-ph].

[24] E. Pajer, F. Schmidt, and M. Zaldarriaga. "The Observed Squeezed Limit of Cosmological Three-Point Functions." *Phys. Rev.* D88.8 (2013), p. 083502. arXiv: 1305.0824 [astro-ph.CO].

[31] G. Cabass, E. Pajer, and D. van der Woude. *In preparation*.

[32] G. Cabass, E. Pajer, and F. Schmidt. *In preparation*.

[33] E. Silverstein and A. Westphal. "Monodromy in the CMB: Gravity Waves and String Inflation." *Phys. Rev.* D78 (2008), p. 106003. arXiv: 0803.3085 [hep-th].

[34] L. McAllister, E. Silverstein, and A. Westphal. "Gravity Waves and Linear Inflation from Axion Monodromy." *Phys. Rev.* D82 (2010), p. 046003. arXiv: 0808.0706 [hep-th].

[35] R. Flauger, L. McAllister, E. Pajer, A. Westphal, and G. Xu. "Oscillations in the CMB from Axion Monodromy Inflation." *JCAP* 1006 (2010), p. 009. arXiv: 0907.2916 [hep-th].

[41] R. Flauger and E. Pajer. "Resonant Non-Gaussianity." *JCAP* 1101 (2011), p. 017. arXiv: 1002.0833 [hep-th].

[42] M. H. Abitbol, J. Chluba, J. C. Hill, and B. R. Johnson. "Prospects for Measuring Cosmic Microwave Background Spectral Distortions in the Presence of Foregrounds." *Mon. Not. Roy. Astron. Soc.* 471 (2017), pp. 1126–1140. arXiv: 1705.01534 [astro-ph.CO].

ABSTRACT

Anisotropies in the angular power spectra of the Cosmic Microwave Background (CMB) temperature and polarization are sourced by inflationary perturbations on scales from 10^1 Mpc to 10^4 Mpc. Deviations of the CMB frequency spectrum from a black-body, instead, can probe inflationary perturbations on scales from 10^{-4} Mpc to 10^{-2} Mpc. These length scales are inaccessible to CMB and large-scale structure measurements. CMB spectral distortions, averaged over the whole sky, constrain the two-point function of primordial perturbations. Correlation of temperature and spectral distortion anisotropies, instead, can constrain their three-point function (making them a probe of primordial non-Gaussianity).

In the first part of this thesis I study what is the level of sensitivity needed, by an experiment measuring the CMB frequency spectrum, to detect the running of the spectral index of inflationary perturbations. I then investigate what is the minimal contribution to the correlation function between temperature and spectral distortion anisotropies that is expected in standard inflationary scenarios. Finally, I discuss what are the secondary contributions (arising from late-time gravitational evolution) to such angular correlation, and how they could bias constraints on primordial non-Gaussianity.

CONTENTS

LIST OF FIGURES

Figures 1.1 and 1.4 were taken from [43, §3.2, §6.1]. Figure 2.1 was taken from [44, §3.2.2]. Figure 2.2 was taken from [45, §3.3.3].

LIST OF TABLES

We review here the conventions about units and notation that are used in this work:

- the metric signature is $(-,+,+,+)$;
- we choose units where $c = \hbar = 1$, in addition to $k_B = 1$;
- we define the Planck mass M_P to be $(8\pi G_N)^{-\frac{1}{2}}$;
- we use the conventions of [46, §3.6] for the Riemann tensor;
- the present time will be denoted by t_0;
- the dimension of the curvature parameter K of a Friedmann-Lemaître-Robertson-Walker metric is L^{-2}: therefore the scale factor a is dimensionless and K is the Gaussian curvature of the space at t_0 (since we choose the scale factor $a(t_0)$ to be 1);
- only in Chapter 1 we will denote with $(\Omega_i)_0$ the present-day ratios between the energy density for a given species i and the energy density of a flat universe, i. e.

  $$(\Omega_i)_0 \equiv \frac{(\rho_i)_0}{3H_0^2 M_P^2} \, .$$

  In the remaining Chapters, the subscript 0 will be omitted;
- greek indices will take the values from 0 to 3. Latin indices from i to k stand for $1, 2, 3$;
- an overdot denotes a derivative with respect to cosmic time t, while a $'$ sign denotes a derivative with respect to conformal time η;
- the convention for the Fourier transform $f(\mathbf{k})$ of $f(\mathbf{x})$ is

  $$f(\mathbf{k}) = \int d^3x \, f(\mathbf{x}) \, e^{-i\mathbf{k}\cdot\mathbf{x}} \, ,$$

  so that the inverse Fourier transform is (for simplicity of notation we will often drop the argument $\mathbf{k}$ of the Fourier modes)

  $$f(\mathbf{x}) = \int \frac{d^3k}{(2\pi)^3} f(\mathbf{k}) \, e^{i\mathbf{k}\cdot\mathbf{x}} \, .$$

  From the above definitions we see that the Dirac delta $\delta^{(3)}(\mathbf{x}-\mathbf{x}')$ in real space is given by

  $$\delta^{(3)}(\mathbf{x}-\mathbf{x}') = \int \frac{d^3k}{(2\pi)^3} e^{i\mathbf{k}\cdot(\mathbf{x}-\mathbf{x}')} \, ,$$

while the Dirac delta $\delta^{(3)}(\mathbf{k}-\mathbf{k}')$ in Fourier space is equal to

$$\delta^{(3)}(\mathbf{k}-\mathbf{k}') = \int \frac{d^3x}{(2\pi)^3} e^{-i(\mathbf{k}-\mathbf{k}')\cdot\mathbf{x}} \; ;$$

- we will often write a Fourier integral as

$$\int \frac{d^3k}{(2\pi)^3} = \int_{\mathbf{k}} \; ;$$

- the translationally and rotationally invariant two-point correlation function of a real variable $f(\mathbf{x})$ in Fourier space (i. e. the power spectrum) is defined by

$$\langle f(\mathbf{k})\, f(\mathbf{k}')\rangle \equiv (2\pi)^3 \delta^{(3)}(\mathbf{k}+\mathbf{k}')\, P_f(k) \; ,$$

or (equivalently) by

$$\langle f(\mathbf{k})\, f^*(\mathbf{k}')\rangle \equiv (2\pi)^3 \delta^{(3)}(\mathbf{k}-\mathbf{k}')\, P_f(k) \; ;$$

- when we encounter derivatives of the potential V for a scalar field ϕ, we use the shorthand

$$\left.\frac{d^n V(\phi)}{d\phi^n}\right|_{\phi=\chi} = V^{(n)}(\chi) \; .$$

For $n \leqslant 3$ we use $','','''$ instead of $(1), (2), (3)$;

- the symmetrizing and antisymmetrizing brackets for $\binom{0}{a}$ tensors are defined as

$$\mathcal{T}_{(m_1 \ldots m_a)} \equiv \frac{1}{a!} \sum_{\Pi} \mathcal{T}_{m_{\Pi(a)} \ldots m_{\Pi(a)}} \; ,$$
$$\mathcal{T}_{[m_1 \ldots m_a]} \equiv \frac{1}{a!} \sum_{\Pi} \delta_{\Pi} \mathcal{T}_{m_{\Pi(a)} \ldots m_{\Pi(a)}} \; ,$$

where the sum is taken over all permutations Π of $1, \ldots a$ and δ_{Π} stands for the parity of the permutation. The generalization to a generic number of upper and lower indices is straightforward;

- when symmetrizing or antisymmetrizing a tensor only on a subset of its indices, we use the vertical brackets $|\cdot|$. E. g.:

$$A_{(\mu} B^{\nu}{}_{|\lambda|} C_{\rho)} = \frac{1}{2}(A_\mu B^\nu{}_\lambda C_\rho + A_\rho B^\nu{}_\lambda C_\mu) \; .$$

The WMAP and Planck satellites have provided a great confirmation of the ΛCDM model [5, 6]:

- they have detected a 5σ deviation from a Harrison-Zeldovich spectrum of primordial perturbations, pointing to slow-roll inflation as the mechanism that generated them. Besides, combined with data from BICEP2/Keck Array [47], they have improved the bounds on the tensor-to-scalar ratio r, greatly disfavoring large-field inflationary models;
- they have provided further evidence for the presence of dark matter (DM) and dark energy (DE), which make up the $\sim 95\,\%$ of the Universe.

Even so, there are still many open questions. For example:

- there is still no detection of primordial B-modes: in fact, one of the main goals of future CMB experiments like CMB Stage IV is to improve the sensitivity to r down to 10^{-3} [48];
- slow-roll inflation predicts a scale dependence for the tilt n_s of the scalar spectrum of order $(1 - n_s)^2$. Since current CMB experiments allow to probe only up to scales $k \sim 10^{-1}\,\mathrm{Mpc}^{-1}$, it is necessary to combine them with other observables to test this prediction;
- are there any relativistic species beyond those predicted by the Standard Model? Besides, the properties of DM and DE are still unknown. For example, we do not know which are the interactions of DM with the Standard Model (what is its annihilation cross-section? Can it decay in Standard Model particles?), or if the current accelerated expansion is driven by vacuum energy or some modification of General Relativity;
- how Gaussian are the statistics of primordial perturbations? Detecting departures from Gaussianity would teach us a great deal about interactions during inflation [19], but often the primordial signal is buried under the contributions of late-time nonlinear gravitational evolution.

This thesis deals mainly with the second and fourth of the above questions, and is structured in the following way:

THE FIRST PART is a review of the basis of the FLRW cosmology. The evolution of the various matter components is presented, along with the so-called "puzzles" of the Hot Big Bang cosmology. I also study how the black-body spectrum of the CMB is generated, along with the mechanisms that can give rise to spectral distortions.

THE SECOND PART contains a review of perturbation theory, and of how the anisotropies in the CMB temperature are computed. The contribution to CMB spectral distortions from Silk damping of acoustic waves in the photon-electron-baryon fluid is also investigated. Finally, I describe how inflation sets up the initial conditions for the evolution of perturbations at late times.

THE THIRD PART contains the scientific research that I carried out during the Ph.D.:

- I start by presenting the constraints from current data on the scale dependence of the primordial scalar power spectrum, together with the forecasts for future CMB spectrometers, which were carried out in [49, 50];
- then I briefly introduce the topic of primordial non-Gaussianity and higher-order correlation functions;
- I conclude with the study, carried out in [51], of the observed squeezed limit of primordial three-point functions, i. e. what is the minimal amount of primordial non-Gaussianity that we can expect to see in late-time observables.

THE APPENDIX contains a brief review of how the likelihood for a CMB experiment is constructed, some intermediate mathematical results for the derivation of the Einstein and fluid equations in a perturbed FLRW cosmology, the mathematical details of the so-called "two-fluid approximation" for the computation of CMB temperature anisotropies, and the Appendices from [49, 51].

Part I

FLRW COSMOLOGY

1 HOT BIG BANG COSMOLOGY AND INFLATION

CONTENTS

In this Chapter we describe the main aspects of the standard cosmological model. We start with an introduction of the Friedmann-Lemaître-Robertson-Walker (FLRW) metric and its properties. We proceed with the derivation and solution of Einstein equations in a FLRW background. Then we discuss what are the "problems of the initial conditions" present in the conventional Big Bang theory. The Chapter ends with the description of the inflationary paradigm and how it offers a solution to such issues. This Chapter is mainly based on [44, §1, §2].

1.1 FLRW SPACETIMES

The Cosmological Principle, supported by many observations (e. g., observations of the Cosmic Microwave Background [52], of Large-Scale Structure [53], and of supernovae [54]), states that the Universe is homogeneous and isotropic on sufficiently large scales.

Mathematically this assumption implies that, on scales larger than $\sim$ 100 Mpc, the Universe is described by a FLRW metric [46, §2.6, §3.5][55, §5.1]. FLRW spacetimes admit a foliation with a "cosmic time" coordinate t and spacelike hypersurfaces Σ_t of constant cosmic time. The hypersurfaces Σ_t are both *homogeneous* (*translationally*-invariant) and

isotropic (*rotationally*-invariant). These conditions imply that the metric is [55, §5.1]

$$\boxed{ds^2 = -dt^2 + \frac{a^2(t)\delta_{ij}dx^i dx^j}{\left(1+\frac{K|x|^2}{4}\right)^2}} \,, \tag{1.1}$$

where we used Cartesian coordinates x^i and the stereographic parameterization of a curved, homogeneous space. In terms of spherical coordinates (r, θ, ϕ), the metric spacetime interval takes the form

$$\boxed{ds^2 = -dt^2 + a^2(t)\left(\frac{dr^2}{1-Kr^2} + r^2 d\Omega^2\right)} \,. \tag{1.2}$$

Before moving on there are a few things to say about eqs. (1.1) and (1.2) for the metric:

- the factor $a(t)$ is the so-called "scale factor": the ratio between a_1^3 and a_2^3 is the ratio between the volumes of Σ_1 and Σ_2;
- the parameter K characterizes the curvature of Σ_t: positively curved hypersurfaces will have $K > 0$, while $K = 0$ and $K < 0$ are for flat and negatively curved hypersurfaces respectively;
- the interval ds^2 above is written in comoving coordinates: observers keep fixed spatial coordinates in the absence of external forces but the physical distance between them is time-dependent, because the universe expands or contracts as $a(t)$ varies.

We see that the evolution of the metric is entirely dictated by that of the scale factor, whose evolution will be related to the energy-momentum tensor via the Einstein field equations: before focusing on the dynamics of $a(t)$, however, we introduce the kinematic concepts of particle horizon, redshifts, and distances in a FLRW background.

1.1.1 *Light cones and horizons*

In General Relativity the causal structure is determined by geodesics with $ds^2 = 0$. These trajectories are studied more easily if one works with conformal time η, defined as

$$\eta(t) \equiv \int_{\hat{t}}^{t} dt' \, \frac{1}{a(t')} \,, \tag{1.3}$$

where $\hat{t}$ is some fixed time. If we consider the conventional Big Bang model, that has a singularity $a(t_{min}) = 0$ at its initial time $t_{min} = 0$ (as we shall see in a moment), we may take $\hat{t}$ to be "the origin of the universe" $\hat{t} = 0$. Using eq. (1.3) along with the coordinate transformation

$$d\chi = \frac{dr}{\sqrt{1-Kr^2}} \,, \tag{1.4}$$

the spacetime interval ds^2 of eq. (1.2) becomes

$$\boxed{ds^2 = a^2(\eta)\{-d\eta^2 + d\chi^2 + F_K(\chi)d\Omega^2\}\ ,} \tag{1.5}$$

where

$$F_K(\chi) \equiv \begin{cases} \dfrac{\sinh^2(\sqrt{|K|}\chi)}{|K|} & \text{if } K < 0\ , \\ \chi^2 & \text{if } K = 0\ , \\ \dfrac{\sin^2(\sqrt{K}\chi)}{K} & \text{if } K > 0\ . \end{cases} \tag{1.6}$$

Eq. (1.5) allows us to fully exploit the property of isotropy, which ensures that it is sufficient to consider radially propagating photons to study the causal properties of the spacetime. Since radial trajectories satisfy $d\Omega = 0$, their worldlines will be entirely specified by the 2-dimensional line element

$$ds^2 = a^2(\eta)(-d\eta^2 + d\chi^2)\ , \tag{1.7}$$

whatever the value of K. This equation says that the metric is like that of Special Relativity, apart from a conformal factor $a^2(\eta)$: therefore the null worldlines of photons have the form

$$\chi = \pm\eta + \chi_0\ , \tag{1.8}$$

and consist of straight lines at $\pm 45°$ in the χ - η plane, as it is depicted in figure 1.1 below.

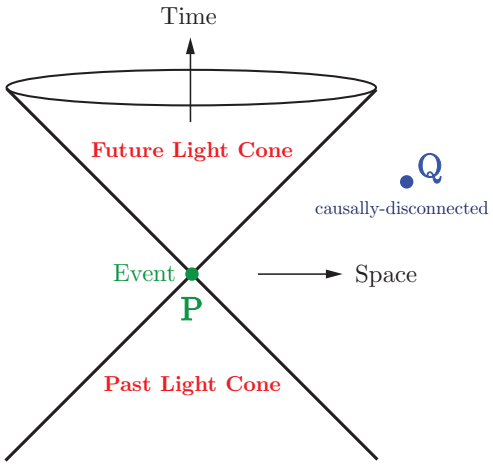

FIGURE 1.1: This figure shows the causal structure of Minkowski spacetime: eqs. (1.5) and (1.7) tell us that a FLRW spacetime possesses the same light cones, whatever its spatial curvature.

With eqs. (1.7) and (1.8) at hand, we are ready to study the so-called "particle horizons". According to eq. (1.8), the maximum distance light is able to travel between a time t_i and a later time t is given by

$$d_p(t, t_i) \equiv a(t)\{\eta(t) - \eta(t_i)\}\ . \tag{1.9}$$

Hence eq. (1.3) gives us the particle horizon, that is

$$d_p(t, t_i) = a(t) \int_{t_i}^{t} dt' \, \frac{1}{a(t')} \, . \tag{1.10}$$

This is the maximum distance from which an observer at time t could have received information: observers separated by a distance larger than $d_p(t, t_i)$ could never have communicated with each other.

As in eq. (1.3), if we consider the conventional Big Bang model with its singularity $a(t_{min}) = 0$ at $t_{min} = 0$, we can take $t_i = 0$. In this case the size of the particle horizon is

$$\boxed{d_p(t, 0) = a(t) \int_{0}^{t} dt' \, \frac{1}{a(t')} \, .} \tag{1.11}$$

1.1.2 *Geodesics*

Let us study in more detail the geodesics of a FLRW universe: this will also help us to set up some notation that will be used in the following Sections. We can distinguish two cases:

- if we have a massive particle of mass m, we can parameterize its worldline with the proper time s. Therefore, the four-velocity $U^\mu = \frac{dx^\mu}{ds}$ will be normalized to -1 [46, §3.3], and the four-momentum P^μ takes the simple form $P^\mu = mU^\mu$. The geodesic equation is then given by

  $$P^\nu \nabla_\nu P^\mu = P^\nu \partial_\nu P^\mu + P^\nu \Gamma^\mu_{\nu\rho} P^\rho = 0 \, , \tag{1.12}$$

  where the Christoffel symbols $\Gamma^\rho_{\mu\nu}$ are computed from the metric using the relation

  $$\Gamma^\rho_{\mu\nu} = \frac{g^{\rho\sigma}}{2} (-\partial_\sigma g_{\mu\nu} + \partial_\mu g_{\nu\sigma} + \partial_\nu g_{\sigma\mu}) \, ; \tag{1.13}$$

- in the case of a massless particle, the proper time is zero and $U_\mu U^\mu = 0$. The momentum of the particle is then given simply by $\frac{dx^\mu}{d\lambda}$, where λ is an affine parameter such that the geodesic equation takes exactly the same form as eq. (1.12) [55, §3.3].

We are now in the position of studying the solutions to the geodesic equation eq. (1.12). We start by introducing the *Hubble rate* H. It is defined as

$$\boxed{H \equiv \frac{\dot{a}}{a} \, ,} \tag{1.14}$$

and sets the time and distance scales of the FLRW spacetime: the characteristic time and length scales of a homogeneous and isotropic universe are H^{-1}. Then, we note that due to the homogeneity of

the background, $\partial_i P^\mu = 0$. Finally, the Christoffel symbols $\Gamma^\rho_{\mu\nu}$ are collected in tab. 1.1. With these results one can show that the geodesic equation takes the form

$$P^0 \frac{dP^\mu}{dt} = -(2\Gamma^\mu_{0j} + \Gamma^\mu_{ij} P^i) P^j \ . \tag{1.15}$$

TABLE 1.1: In this table we collect the Christoffel symbols for the FLRW metric of eqs. (1.1) and (1.2).

Γ^0_{00}	0
Γ^0_{0j}	0
Γ^0_{ij}	$H g_{ij}$
Γ^k_{00}	0
Γ^k_{0j}	$H\delta^k_j$
Γ^k_{ij}	$\frac{g^{kl}}{2}(-\partial_l g_{ij} + \partial_i g_{jl} + \partial_j g_{li})$

Eq. (1.15) can be studied and solved separately in the case of a massive or massless particle:

- for a massive particle we can further distinguish two cases:
  - if the particle is initially at rest in the comoving frame ($P^i = 0$), we see that it will remain at rest because the right-hand side of eq. (1.15) vanishes. From this, we see also that the four-vector $U^\mu = \delta^\mu_0$, which is both timelike and normalized,[1] is the four-velocity of such particles;
  - if the particle is initially moving with some comoving (i. e., relative to the comoving frame) peculiar velocity v^i, related to P^i by

$$P^i = \frac{m v^i}{\sqrt{1 - g_{ij} v^i v^j}} \ , \tag{1.16}$$

we see that the $\mu = 0$ component of eq. (1.15) implies

$$E \frac{dE}{dt} = -\Gamma^0_{ij} = -H p^2 \ , \tag{1.17}$$

where we defined $P^0 \equiv E$ (see [55, §4.3] for details) and $p^2 \equiv g_{ij} P^i P^j$. The constraint $P^\mu P_\mu = -m^2$ implies that $E dE = p dp$, so that

$$\frac{\dot{p}}{p} = -H = -\frac{\dot{a}}{a} \Rightarrow p \propto \frac{1}{a}. \tag{1.18}$$

1 In fact, using the metric of eq. (1.2), we see that $U^\mu U_\mu = g_{\mu\nu} U^\mu U^\nu = -1$.

Therefore, the physical three-momentum of massive particles (and then their peculiar velocity) decays with the expansion of the universe: freely-falling particles will converge on the Hubble flow;

- for a massless particle, the constraint $P^\mu P_\mu = 0$ still implies that $E dE = p dp$. It also says that E is equal to p, so that eq. (1.18) now reads $E \propto a^{-1}$. That is, the energy of a massless particle decays with the expansion of the universe.

1.1.3 *Redshifts*

As we have seen in the previous Section, the fact that our Universe is expanding implies that photons lose energy with time. This is the so-called *redshift*: classically, it corresponds to the fact that the wavelength of propagating electromagnetic waves is stretched by the expansion. Since everything we know about the Universe is inferred by the light we receive from distant objects, it is clear that the redshift is a very important quantity in cosmology. Its expression can be derived either by treating photons classically or quantum mechanically. We will follow the second way, and refer to [55, §4.3][56, §22.5] for two (very detailed) explanations using geometric optics.

For photons, the momentum is inversely proportional to the wavelength of light ($\lambda = 2\pi/p$): since, as we have seen in eq. (1.18), p scales as a^{-1}, the wavelength scales as a. Light emitted at time t_1 with wavelength λ_1 will be observed at $t_0 > t_1$ with wavelength

$$\lambda_0 = \frac{a(t_0)}{a(t_1)}\lambda_1 \ . \tag{1.19}$$

Since $a(t_0) > a(t_1)$, the wavelength of the light increases, $\lambda_0 > \lambda_1$. It is conventional to define the redshift parameter z as

$$z \equiv \frac{\lambda_0 - \lambda_1}{\lambda_1} \Rightarrow 1 + z = \frac{a(t_0)}{a(t_1)} \ . \tag{1.20}$$

It is very important to stress that such redshift of signals is a non-local effect: it is a consequence of how light emitted from *distant objects* travels to us (mathematically, it is a relation between observables on the wordlines of two different observers). In this sense, it is very different from effects like Doppler shifts, which are local. This is usually a source of misconceptions, especially regarding the Hubble redshift-distance relationship and the Hubble flow of galaxies.

1.1.4 *Distances*

There are mainly two concepts of distance of observational relevance in cosmology: the *luminosity distance* and the *angular diameter distance*. In order to define them, we need three other notions:

PHYSICAL DISTANCE It is the time-dependent distance between two points on a spatial section at a cosmic time t (or at a conformal time η) as calculated with the FLRW metric. Using the metric of eq. (1.5), we see that for a flat FLRW universe it is just $a\chi$. We call d this distance.

COMOVING DISTANCE It is obtained from the physical distance by removing the scale factor that multiplies it. From eq. (1.8) we see that the comoving distance between us and some object emitting light at redshift z (i. e. at a time $t_1 < t_0$) is given by

$$d^{co} = \int_{t_1}^{t_0} dt\, \frac{1}{a(t)} = \int_0^z dz'\, \frac{1}{H(z')} \,. \tag{1.21}$$

Besides, for flat spatial hypersurfaces we can further distinguish a comoving wavelength (λ) from a physical one ($a\lambda$), and comoving Fourier modes of modulus k from physical modes of modulus $\frac{k}{a}$.

METRIC DISTANCE Called d_m, it is the distance between two points on a hypersurface at fixed η and χ. For infinitesimal displacements, $ds^2 = F_K(\chi)d\Omega^2 \equiv d_m^2 d\Omega^2$. If the curvature K of spatial sections is zero, d_m and the comoving distance coincide.

While the comoving distance and the metric distance are not observable, they play an important role in the definition of the luminosity distance d_L and the angular diameter distance d_A:

LUMINOSITY DISTANCE Suppose we know objects that behave like *standard candles*: these are objects that have a known absolute luminosity L.[2] Then, it is possible to use the observed flux F ($\equiv$ energy per second per receiving area) from such objects to measure their distance. In a static Euclidean space, the flux-luminosity relation for an object at a fixed comoving distance χ is given by

$$F = \frac{L}{4\pi\chi^2} \,. \tag{1.22}$$

In a FLRW universe, this relation is changed for three reasons:

- at the time t_0, when the light reaches the Earth, the proper area of a sphere that is drawn around the object and crosses the Earth is $4\pi d_m^2$;
- the energy of photons at the reception point differs from the energy at emission by a factor of $(1+z)^{-1}$;
- the same factor enters in the expression for the number of photons crossing a unit receiving area *in a unit time*, since

2 For example, Supernovae of Type IA are believed to be standard candles [54].

the time intervals for the source and observer differ by factor $(1+z)^{-1}$.[3]

Therefore, eq. (1.22) becomes

$$F = \frac{L}{4\pi d_m^2 (1+z)^2} = \frac{L}{4\pi d_L^2}, \text{ with } d_L \equiv d_m(1+z) \ . \tag{1.23}$$

ANGULAR DIAMETER DISTANCE In addition to standard candles, we can have access to *standard rulers*, i. e. objects of known physical size D. This is the case, for example, of fluctuations in the CMB. If we assume, as we did before, that the light from an object at a comoving distance χ from the Earth is emitted at a time t_1, and that the object subtends an angle $\delta\theta$ in the sky, the formula for the distance of the object from us (in a static Euclidean space) would be

$$d_A = \frac{D}{\delta\theta} \ . \tag{1.24}$$

In a FLRW universe, the relation between the physical transverse size D and its angular size in the sky is also modified:

- the comoving length of a small arc of angular size $\delta\theta$ is not just $\chi\delta\theta$, but $a(t_1)F_K(\chi)\delta\theta$, as we see from eq. (1.5);
- then, expressing it in terms of redshift z and d_m, eq. (1.24) becomes

$$d_A = \frac{d_m}{1+z} \ . \tag{1.25}$$

We will see in the Section 1.2.1 how the angular diameter distance plays an important role in elucidating what are the so-called "puzzles" of Hot Big Bang picture (see fig. 1.2).

1.1.5 *Dynamics of FLRW spacetimes*

The dynamics of the universe are dictated by those of the scale factor, which in turn is governed by the Einstein equations

$$G_{\mu\nu} = \frac{T_{\mu\nu}}{M_P^2} \ , \tag{1.26}$$

where $G_{\mu\nu}$ is the Einstein tensor $R_{\mu\nu} - \frac{R}{2}g_{\mu\nu}$ and $T_{\mu\nu}$ is the energy-momentum tensor.

What about $T_{\mu\nu}$? Its decomposition in the case of a generic fluid of four-velocity U^μ normalized to $U_\mu U^\mu = -1$ is [56, §22.3][57][58, §4]

$$T_{\mu\nu} = \rho U_\mu U_\nu + pP_{\mu\nu} + 2Q_{(\mu}U_{\nu)} + \Sigma_{\mu\nu} \ , \tag{1.27}$$

where:

3 That is, the relation between the physical time intervals at emission and reception is $dt_0 = (1+z)dt_1$.

- $P^{\mu}{}_{\nu} = \delta^{\mu}{}_{\nu} + U^{\mu}U_{\nu}$ is the projection tensor on 3-dimensional spatial sections orthogonal to U^{μ};
- the energy density (ρ) and isotropic pressure (p) of the fluid are related to $T_{\mu\nu}$ by

$$\boxed{\begin{aligned} \rho &= T_{\mu\nu}U^{\mu}U^{\nu} \ , && \text{(1.28a)} \\ p &= \frac{1}{3}T_{\mu\nu}P^{\mu\nu} \ ; && \text{(1.28b)} \end{aligned}}$$

- Q_{μ} is the energy-momentum transfer four-vector, and it is obtained from the energy-momentum tensor by

$$Q_{\mu} = -P^{\nu}{}_{\mu}T_{\nu\rho}U^{\rho} \ ; \tag{1.29}$$

- the symmetric and traceless tensor $\Sigma_{\mu\nu}$ is the anisotropic stress tensor. Its expression in terms of $T_{\mu\nu}$ is

$$\Sigma_{\mu\nu} = P^{\rho}{}_{(\mu}P^{\lambda}{}_{\nu)}T_{\rho\lambda} - \frac{1}{3}h^{\rho\lambda}T_{\rho\lambda}P_{\mu\nu} \ . \tag{1.30}$$

In the case of a fluid whose energy and momentum are conserved (and ours is the case), Q_{μ} is equal to 0. Besides, in a FLRW cosmology:

- the energy-momentum tensor is that of a *geodesic* (U^{μ} is a geodesic vector field) *perfect* fluid (the anisotropic stress tensor is also 0);
- in order to maintain spatial homogeneity and isotropy ρ and p will be functions of t only;
- as we have seen in Section 1.1.2, the worldlines of the geodesic perfect fluid with zero peculiar velocity are those with four-velocity $U^{\mu} = \delta^{\mu}_{0}$.

Once everything is inserted in eq. (1.26) we end up with the system of the two "Friedmann equations", that is

$$\boxed{\begin{aligned} H^2 &= \frac{\rho}{3M_P^2} - \frac{K}{a^2} \ , && \text{(1.31a)} \\ \dot{H} + H^2 &= -\frac{1}{6M_P^2}(\rho + 3p) \ , && \text{(1.31b)} \end{aligned}}$$

while the conservation of the energy-momentum tensor $\nabla_{\mu}T^{\mu\nu} = 0$ (or the combination of eqs. (1.31), if you wish) instead gives

$$\boxed{\dot{\rho} = -3H(\rho + p) \ .} \tag{1.32}$$

Eq. (1.31b) tells us that in an expanding universe filled with ordinary matter (that is one satisfying $\rho + 3p \geqslant 0$, the so-called "strong energy condition") one must have $\ddot{a} < 0$. This leads to a singularity in the finite past at a time t_{min} (that may be set to 0): it is the Big Bang singularity, which would signal the breakdown of the classic theory of General Relativity. We will see later how inflation pushes this singularity in the infinite past, effectively getting around this issue.

1.1.6 *Solutions of Friedmann equations*

In this Section we study eqs. (1.31) and their solutions. We start by writing down the equation of state that links the energy density with the isotropic pressure, that is

$$p = w\rho \ . \tag{1.33}$$

The less restrictive energy conditions on the energy-momentum tensor (see [46, §4.6] for details) say that $|w|$ must be $\leqslant 1$. In this range of $|w|$ we distinguish the following values for w, each corresponding to the dominance of a particular form of matter:

MATTER DOMINANCE This case corresponds to the dominance of non-relativistic matter and has $w = 0$.

RADIATION DOMINANCE This case corresponds to the dominance of relativistic matter and has $w = \frac{1}{3}$.

Λ DOMINANCE This case corresponds to the dominance of a cosmological constant term in the Einstein-Hilbert action. It has $w = -1$.

If we now combine the equation of state with the conservation of energy, eq. (1.32), we get

$$\frac{d\log\rho}{d\log a} = -3(1+w) \ . \tag{1.34}$$

This differential equation can be easily integrated and, if w does not depend on t, the solution is

$$\rho(a) \propto a^{-3(1+w)} \ . \tag{1.35}$$

Plugging this ρ into eq. (1.31a) and integrating it, one finds that the time evolution of the scale factor is given by

$$\boxed{a(t) \propto \begin{cases} t^{\frac{2}{3}(1+w)} & \text{if } w \neq -1 \ , \\ e^{Ht} \text{ with } H = \text{const.} & \text{if } w = -1 \ . \end{cases}} \tag{1.36}$$

A summary of these results is given in tab. 1.2.

If more than one (relativistic or not) matter species contributes significantly to ρ and p, the total energy density and total isotropic pressure will be

$$\rho = \sum_i \rho_i \ , \tag{1.37a}$$

$$p = \sum_i p_i \ , \tag{1.37b}$$

TABLE 1.2: Solutions of Friedmann equations for a flat FLRW metric dominated by matter (MD), radiation (RD), and cosmological constant (ΛD). The entries for $\rho(a)$, $a(t)$ and $a(\eta)$ indicate what these quantities are proportional to.

Dominance	w	$\rho(a)$	$a(t)$	$a(\eta)$	$\eta_{\min}$
MD	0	a^{-3}	$t^{\frac{2}{3}}$	η^2	0
RD	$\frac{1}{3}$	a^{-4}	$t^{\frac{1}{2}}$	η	0
ΛD	-1	a^0	e^{Ht}	$-\eta^{-1}$	$-\infty$

where i runs over all the species (baryons, photons, etc.). From these ρ_i and p_i and their equations of state one defines the ratios

$$\Omega_i \equiv \frac{\rho_i}{\rho_{cr}} \Rightarrow \Omega = \sum_i \Omega_i \ , \tag{1.38}$$

with the "critical energy density" ρ_{cr} (the energy density of a flat FLRW universe) being[4]

$$\rho_{cr} \equiv 3H^2 M_P^2 \ . \tag{1.39}$$

Now, thanks to eq. (1.35), we can write eq. (1.31a) as

$$\left(\frac{H}{H_0}\right)^2 = \sum_i (\Omega_i)_0 a^{-3(1+w_i)} + (\Omega_K)_0 a^{-2} \ , \tag{1.40}$$

where Ω_K (i. e. the curvature contribution) is

$$\Omega_K \equiv -\frac{K}{(aH)^2} \ , \tag{1.41}$$

and we took $a_0 = 1$ for simplicity. If we evaluate the above equation at the present time we obtain the "consistency relation"

$$\sum_i (\Omega_i)_0 + (\Omega_K)_0 = 1 \ . \tag{1.42}$$

Current observations, mainly those of the Cosmic Microwave Background (CMB) and of Large-Scale Structure (LSS), tell us that the ratios $(\Omega_i)_0$ are those of tab. 1.3.
The first thing we notice from looking at tab. 1.3, together with eqs. (1.41) and (1.42), is that K is constrained to be very close to zero:[5] therefore we can (and will, for the rest of this thesis) focus on a *flat* FLRW metric. These results also tell us that our present Universe is composed approximately of:

4 In fact eq. (1.31a) with $\rho = \rho_{cr}$ implies that K must be equal to zero.
5 At least when fitting cosmological data with the standard ΛCDM parameterization [6]. We refer to [6, 60] for an analysis of the constraints on $(\Omega_K)_0$ in extended (i. e. non-ΛCDM) models.

TABLE 1.3: 68 % confidence limits for $(\Omega_i)_0$ of baryon (b), cold dark matter (cdm) and dark energy (Λ), as from [59]. We recall that h and H_0 are related by $H_0 h^{-1} = 100\,\mathrm{km\,s^{-1}\,Mpc^{-1}}$.

$(\Omega_b)_0 h^2$	$(\Omega_{cdm})_0 h^2$	$(\Omega_\Lambda)_0 h^2$
0.02214 ± 0.00024	0.1187 ± 0.0017	0.692 ± 0.010

- a 5 % of ordinary matter;
- a 27 % of (cold) dark matter;
- a 68 % of dark energy that satisfies an equation of state with $w \approx -1$, hence the subscript Λ.

1.2 PUZZLES OF THE HOT BIG BANG THEORY

After this introduction, we are now going to explain how the conventional Big Bang theory requires a particular fine-tuned set of initial conditions if one wants the Universe to evolve into its current state.

1.2.1 *Horizon problem*

In Section 1.1.1 we saw that the maximum distance light can travel from $t = 0$ to a given time t is

$$d_p(t,0) = a(t) \int_0^t dt' \, \frac{1}{a(t')} = a(t)\{\eta(t) - \eta_{min}\} \, . \tag{1.43}$$

In the conventional Big Bang expansion one has $w \geqslant 0$: this means (see tab. 1.2) that η_{min} is equal to 0, leading to a *finite* $d_p(t,0)$. The consequence is that at early times there is a large number of *causally disconnected* regions (see fig. 1.2 for details), and this goes against the experimentally verified homogeneity of the CMB. How could these regions have thermalized if they were not in causal contact? More precisely, the characteristic size of the anisotropies in the CMB angular power spectrum is given by the angle at which the horizon at recombination is seen today (as we will see in the next Chapters). Neglecting factors of order 1, this angle is $\theta \approx \frac{\eta_{rec}}{\eta_0}$: from fig. 1.2, we see that $\frac{\eta_{rec}}{\eta_0} \approx 1°$. The argument can then be turned around: i. e., we do indeed see that the CMB temperature is the same (up to one part in 10^{-5}) in regions separated by $\approx 1°$ in the sky. This tells us that the the Universe is made up by $(\eta_{rec}/\eta_0)^{-3} \approx 10^4$ regions ("separate universes") that were not in causal contact at recombination.

One way to solve this puzzle would be just saying that the initial density perturbations were *exactly* such that the right degree of uniformity is observed in the Cosmic Microwave Background, and that they

also possessed the right level of fluctuations to explain the formation of the structure we observe today. This approach, however, is not very satisfactory since it amounts to very fine-tuned initial conditions for our Universe.

1.2.2 *Flatness problem*

In addition to the initial distribution of density inhomogeneities, the velocities of the fluid are also needed to completely characterize the "Cauchy problem of the universe". If the universe has to remain homogeneous at late times, the initial fluid velocities must take very precise values: if they are too small there would be a quick recollapse, if they are too big the expansion would be so rapid that structure formation could not occur.

This fine-tuning of the initial velocities is called "flatness problem". The name derives from the Newtonian treatment of gravity: in this formalism one shows that the starting value for the kinetic energy of fluid particles is related to the curvature parameter K, and one sees how too little initial kinetic energy leads to a closed universe ($K > 0$), while too large initial kinetic energy leads to an open universe ($K < 0$).

With this said, one can be more quantitative: choosing for simplicity the case of a single species of matter and combining eq. (1.31a) with eq. (1.34), one finds that

$$\frac{d|\Omega - 1|}{d \log a} > 0 \Leftrightarrow 1 + 3w > 0 \, . \tag{1.44}$$

Consequently, when dealing with ordinary matter (for which w is always larger than zero), $\Omega = 1$ is an unstable fixed point of the Friedmann equations: in the standard Big Bang cosmology the near-flatness observed today ($(\Omega_K)_0 \approx 0$) requires an unnatural adjustment at $\Omega \approx 1$ of the total density parameter in the early Universe.

1.3 CLASSICAL DYNAMICS OF INFLATION

Everything is ready to present the theory of inflation, and to show how it fixes the problems of the classical Big Bang cosmology that we have presented in the preceding Section.

1.3.1 *Solution of the horizon problem*

We reformulate the horizon problem in way that will make its solution more evident: in eq. (1.11) we obtained the physical particle horizon $d_p(t, 0)$: the *comoving* (particle) horizon, then, is

$$\boxed{d_p^{co}(a) = \int_0^a d \log a' \, \frac{1}{a' H(a')} \, ,} \tag{1.45}$$

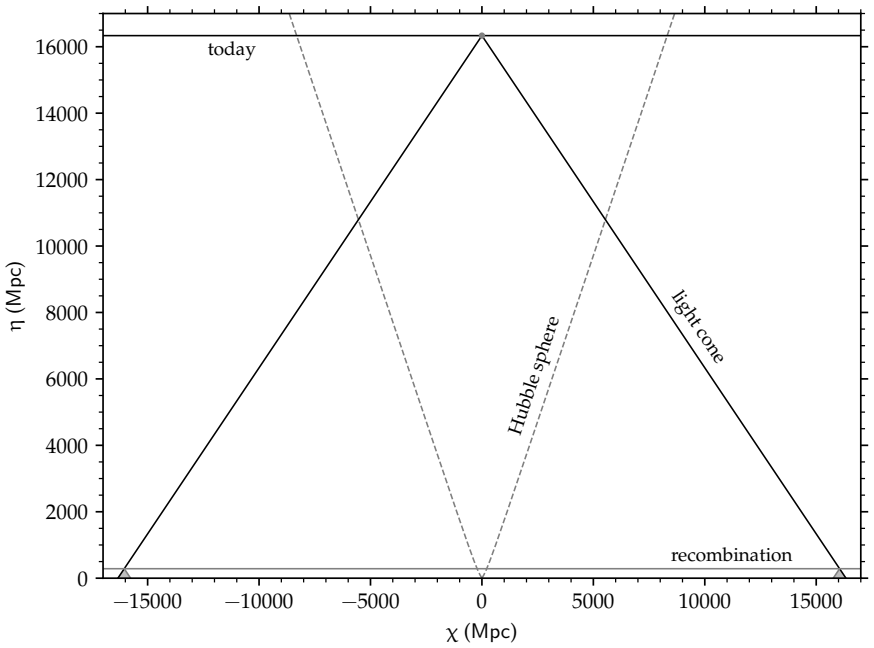

FIGURE 1.2: Spacetime diagram of standard Big Bang cosmology (neglecting the period of Λ dominance that starts around $a/a_0 \approx 0.5$), with its horizon problem: two points on a fixed surface of constant η are in causal contact if their past light cones intersect at $\eta = \eta_{\text{min}}$ (the Big Bang). Because η_{min} is zero, the LSS (last-scattering surface: it is the set of points situated at a distance such that photons emitted from there at the time of recombination are reaching us now. These are the photons we detect today as CMB radiation) consists of many causally disconnected patches that will not be in thermal equilibrium with each other.

where $(aH)^{-1}$ is the "comoving Hubble radius" (recall that $a(t)$ is equal to 0 for $t = 0$). The properties of d_p^{co} and $(aH)^{-1}$ are:

COMOVING PARTICLE HORIZON If at a time t two particles are at a comoving distance larger than $d_p^{co}(t)$, they could *never* have communicated with each other.

COMOVING HUBBLE RADIUS If at a given time t two particles are separated by a comoving distance larger than the comoving Hubble radius at that time, they are unable to influence each other *now*.

The distinction between the two is crucial: it is possible that the comoving particle horizon is much larger than $(aH)^{-1}$ at the present time, so that particles *cannot communicate today* but *were in causal contact early on*. This is the solution to the horizon problem.

From eq. (1.45) one sees that an early phase of decreasing Hubble radius gets the job done: in this way the comoving Hubble radius in

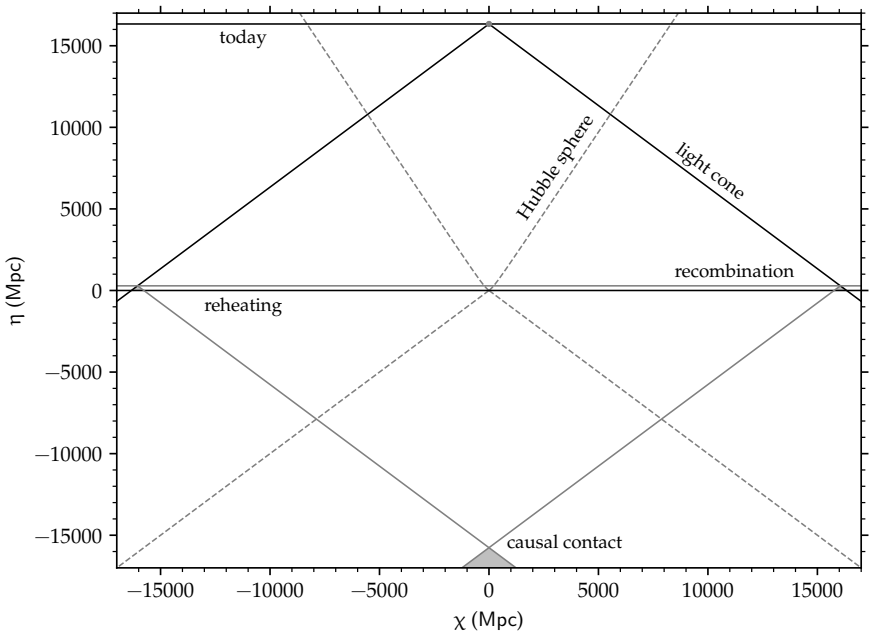

FIGURE 1.3: Spacetime diagram of inflationary cosmology for $H \approx$ const.: the singularity $a = 0$ is pushed at $\eta = \eta_{min} \to -\infty$, and eq. (1.50) says that the scale factor blows up at $\eta = 0$. This is due to the assumption of an almost de Sitter space, which means that inflation will continue forever (with $\eta = 0$ corresponding to $t \to +\infty$). In reality when inflation ends at some finite time the approximation of eq. (1.50) breaks down: this is why $\eta = 0$ stands for the end of inflation, and there will be a smooth transition (the so-called *reheating phase*) from inflation to the standard radiation-dominated era.

the past would have been much larger than what it is now, and the contributions to d_p^{co} would come mostly from those times.

1.3.2 *Solution of the flatness problem*

We have seen how the second fine-tuning issue of the Hot Big Bang theory derives from eq. (1.44). With a little manipulation we can rewrite it as

$$|\Omega - 1| = \frac{|K|}{(aH)^2} \ . \tag{1.46}$$

If in the past the comoving Hubble radius decreases, the solution $\Omega = 1$ becomes an attractor. This solves the flatness problem.

1.3.3 *Spacetime diagram of inflation*

The defining trait of inflation is that of a shrinking comoving Hubble radius. By means of eq. (1.31b) we can recast it as

$$\boxed{\frac{d}{dt}\left(\frac{1}{aH}\right) < 0 \Leftrightarrow \ddot{a} > 0 \Leftrightarrow \rho + 3p < 0 \,,} \tag{1.47}$$

from which we deduce that:

- inflation is a period of accelerated expansion. If we introduce the quantities ε_H and N, defined by

$$\varepsilon_H \equiv -\frac{\dot{H}}{H^2} \,, \tag{1.48a}$$

$$\frac{dN}{dt} \equiv -H \Rightarrow N_1 - N_2 = -\log\frac{a_1}{a_2} \,, \tag{1.48b}$$

  eq. (1.47) is transformed into

$$\varepsilon_H = \frac{d\log H}{dN} < 1 \,; \tag{1.49}$$

- during the inflationary epoch the strong energy condition is violated.

In the next Section we are going to see how during inflation the Hubble rate is approximately constant: since we want a period of expansion, this constant must be larger than zero. In this case, thanks to eq. (1.3), one has

$$\eta \approx -\frac{1}{aH} \text{ with } H \approx \text{const.} \,. \tag{1.50}$$

Thus eq. (1.9) implies that the comoving particle horizon is not finite, and the horizon problem does not appear. What about the flatness problem? The comoving Hubble radius is decreasing, so the results of Section 1.3.2 apply. The resulting spacetime diagram is that of fig. 1.3 in the previous page.

1.3.4 *Single-field slow-roll inflation*

The simplest way in which one is able to violate the strong energy condition is to take ρ and p to be those of a single scalar field ϕ: the "inflaton". We do not specify the physical nature of the inflaton: indeed, there is no need to do it because in the Effective Field Theory of Inflation ϕ is nothing more than a "clock" that parametrizes the evolution of the inflationary energy density [61, 62]. The dynamics of ϕ (minimally) coupled to gravity are governed by the action

$$\begin{aligned} S &= S_G + S_M \\ &= \frac{M_P^2}{2}\int d^4x\,\sqrt{-g}\,R - \frac{1}{2}\int d^4x\,\sqrt{-g}\,\left\{(\nabla\phi)^2 + 2V(\phi)\right\} \,, \end{aligned} \tag{1.51}$$

which we will examine more thoroughly in Chapter 4. The field ϕ can depend only on time if the symmetries of a FLRW background must be satisfied, and the resulting field equations for the scale factor are nothing else but eqs. (1.31) with

$$\rho = \frac{\dot{\phi}^2}{2} + V(\phi) \,, \tag{1.52a}$$

$$p = \frac{\dot{\phi}^2}{2} - V(\phi) \,, \tag{1.52b}$$

while for ϕ one has

$$\ddot{\phi} + 3H\dot{\phi} + V'(\phi) = 0 \,. \tag{1.53}$$

With the energy density and isotropic pressure given above, the parameter w in the case of a single scalar field is

$$\boxed{w = \frac{\frac{\dot{\phi}^2}{2} - V(\phi)}{\frac{\dot{\phi}^2}{2} + V(\phi)}} \,, \tag{1.54}$$

and we can have accelerated expansion if the potential energy is sufficiently larger than the kinetic energy. What are the means to achieve this? The original formulation of inflation in [63] was to have ϕ evolve from a false vacuum (where the kinetic energy is close to zero, but the potential energy is larger than zero) to the true minimum of the potential via quantum tunnelling. However it was realized that the expansion would have prevented the bubbles of the new phase from coalescing, so the Universe would never have moved to the state it is in today [1, 2].

Therefore the idea of a potential with a local minimum was abandoned in [3, 4], moving to one with a very shallow slope leading to the ground state: the field would have *slowly rolled* towards the bottom of the potential as depicted in fig. 1.4 in the next page, maintaining its kinetic energy small and allowing for $\ddot{a} > 0$. In fact with some manipulations we find that ε_H is

$$\varepsilon_H = \frac{\dot{\phi}^2}{2H^2 M_P^2} = \frac{3}{1 + \frac{2V(\phi)}{\dot{\phi}^2}} \,, \tag{1.55}$$

so if $\dot{\phi}^2$ is smaller than $V(\phi)$ then $\varepsilon_H < 1$, and eq. (1.47) holds. Having $\dot{\phi}^2 \ll V(\phi)$ leads to $\varepsilon_H \ll 1$ and $p \approx -\rho$, hence to the de Sitter limit. What about the duration of inflation? It will be sustained for long enough to solve the horizon and flatness problems only if $\varepsilon_H < 1$ for a sufficiently large number of Hubble times: this requires that a second parameter, called η_H and defined as

$$\eta_H = -\frac{d \log \varepsilon_H}{dN} = 2\varepsilon_H + \frac{2\ddot{\phi}}{H\dot{\phi}} \,, \tag{1.56}$$

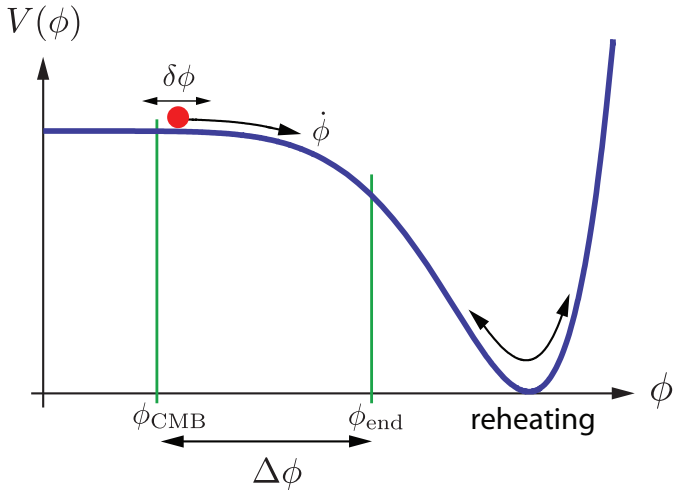

FIGURE 1.4: This figure shows the mechanism of single-field slow-roll inflation, where the field ϕ rolls down a potential $V(\phi)$: when the potential energy dominates over the kinetic energy $\ddot{a}$ is larger than zero, and the acceleration stops when $\dot{\phi}^2 \approx V(\phi)$. Fluctuations observed in the CMB are created at $\phi_{\rm CMB}$ (often called $\phi_\star$ in the literature). After inflation ends the inflaton ϕ oscillates around the minimum of the potential, and its energy density is converted into radiation in the process called "reheating".

satisfies $|\eta_H| < 1$ ($|\eta_H| \ll 1$ in the de Sitter limit).

In the slow-roll regime the conditions $\varepsilon_H \ll 1$ and $|\eta_H| \ll 1$ can be reformulated as constraints on the shape of the inflationary potential

$$\varepsilon_V(\phi) \ll 1, \text{ with } \varepsilon_V(\phi) \equiv \frac{M_P^2}{2}\left(\frac{V'(\phi)}{V(\phi)}\right)^2 , \tag{1.57a}$$

$$|\eta_V(\phi)| \ll 1, \text{ with } \eta_V(\phi) \equiv M_P^2 \frac{V''(\phi)}{V(\phi)} , \tag{1.57b}$$

where the Planck mass is introduced to make these "potential slow-roll parameters" (ε_H and η_H are the "Hubble slow-roll parameters", instead) manifestly dimensionless. The Hubble and potential slow-roll parameters are related by the "slow-roll approximation": in the upcoming Chapters we will often stop at the first order of this approximation, that says (one may refer to [64, 65] for a complete treatment of the slow-roll expansion)

$$\varepsilon_H \approx \varepsilon_V , \tag{1.58a}$$

$$\eta_H \approx -2\eta_V + 4\varepsilon_V . \tag{1.58b}$$

Inflation ends when $\ddot{a} = 0$: this corresponds to $\varepsilon_H = 1$ (thus to $\varepsilon_V \approx 1$) and to the violation of the slow-roll assumption. The number of e-folds of inflation occurred at a time t is given by

$$N(t) = \log\frac{a_{\rm end}}{a(t)} = \int_t^{t_{\rm end}} dt'\, H(t') = \int_{\phi(t)}^{\phi_{\rm end}} d\phi\, \frac{H}{\dot{\phi}} . \tag{1.59}$$

If we stop at first order in slow-roll, and assume $\dot{\phi} > 0$ (as in fig. 1.4), eq. (1.59) becomes

$$\boxed{N(t) \approx \frac{1}{M_P^2} \int_{\phi(t)}^{\phi_{end}} d\phi \, \frac{V(\phi)}{V'(\phi)} = \int_{\phi(t)}^{\phi_{end}} \frac{d\phi}{M_P} \frac{1}{\sqrt{2\varepsilon_V(\phi)}} \, .} \tag{1.60}$$

The above results can also be used to estimate how much inflation is actually needed to solve the horizon and flatness problems of the standard Hot Big Bang cosmology. At least, we need to require that scales k of order of the comoving Hubble radius today had been inside the comoving Hubble radius during inflation, i. e. that

$$(a_0 H_0)^{-1} < (a_I H_I)^{-1} \, . \tag{1.61}$$

For simplicity, we can neglect not only the period of Λ dominance but also the matter-dominated epoch, and assume that reheating happens instantaneously after the end of inflation. Then $H \propto a^{-2}$ after the end of inflation. Assuming the reheating temperature to be $T_{reh} \sim T_{end} \approx 10^{15}$ GeV, we have (we will see in the next Chapter that temperature scales as $1/a$)

$$\frac{a_0 H_0}{a_{end} H_{end}} = \frac{a_0}{a_{end}} \left(\frac{a_{end}}{a_0} \right)^2 = \frac{a_{end}}{a_0} = \frac{T_0}{T_{end}} \approx 10^{-28} \, , \tag{1.62}$$

where we have used $T_0 \approx 10^{-3}$ eV (i. e. $T_0 \approx 2.7$ K). Eq. (1.61), then, tells us that

$$(a_I H_I)^{-1} \gtrsim 10^{28} (a_{end} H_{end})^{-1} \, . \tag{1.63}$$

Since H is almost constant during inflation, this relation turns into $\log \frac{a_{end}}{a_I} = N_I \gtrsim 64$: that is, around 60 e-folds of inflation are needed.

Before moving on to the next Chapter, it is important to point out that the fundamental microscopic origin of inflation is still unknown: there are many models whose predictions are within the experimental uncertainties. For a nice review of the most common potentials (and on inflationary theory in general) we refer to [43, §6.5], while for a compendium of *all* the inflationary models in the literature see [66].

2

THE CMB FREQUENCY SPECTRUM

CONTENTS

As we have seen in the previous Chapter, the Universe emerged in a very dense state after the end of inflation and reheating. The interactions between particles were so fast (much faster than the Hubble rate) that thermodynamic equilibrium was established, and the state of the Universe was that of a plasma at a single temperature T. As the Universe expanded, the plasma cooled down, and the first light elements (hydrogen, helium and lithium) formed. At some point, the temperature had dropped enough for the first stable atoms to exist, and then for photons to start free-streaming. In this Chapter, we are going to review briefly the thermal history of the Hot Big Bang, with a glance at neutrino decoupling, recombination, etc. In the second part, we study in more detail how the CMB black-body spectrum (and possible deviations from it) are formed. This Chapter is mainly based on [44, §2, §3][45].

2.1 THERMAL HISTORY

Suppose we have some particles that interact with each other with a rate of interaction Γ. If $\Gamma \gg H$, then interactions are so fast that thermal equilibrium is established, and particles can be described by a single distribution function in phase space, characterized by a temperature T. Conversely, if $\Gamma \ll H$, the particle species under consideration does not interact efficiently anymore with the other particles in the thermal bath, and decouples from it.

What can we say about Γ in the Standard Model? The rate of interactions for a reaction $1+2 \rightleftarrows 3+4$, with particle densities $n_1 \sim n_2 \sim n$, is given by $n \langle \sigma v \rangle$, where σ and v are, respectively, the cross-section and the relative velocity in the center-of-mass frame and $\langle \ldots \rangle$ indicates an average over the velocity distribution. In the Standard Model, where interactions between 1, 2, 3 and 4 are mediated by gauge bosons, from dimensional analysis we can write $\langle \sigma v \rangle \sim \alpha^2/T^2$ for $v \sim 1$, where $\alpha = g^2/4\pi$. Then, using $n \sim T^3$ and the Friedmann equation $\rho = 3H^2 M_P^2 \sim T^4$, we see that for $\alpha \sim 10^{-2}$ thermal equilibrium is achieved for $10^2\,\mathrm{GeV} \lesssim T \lesssim 10^{16}\,\mathrm{GeV}$.

Conversely, consider for example weak interactions: below the electroweak symmetry breaking scale, $T \lesssim 10^2\,\mathrm{GeV}$, the $W^\pm$ and Z^0 bosons are massive, and the cross-section for weak interactions becomes that of Fermi theory, i. e. $\langle \sigma v \rangle \sim G_F^2 T^2$, with $G_F \approx 1.17 \times 10^{-5}\,\mathrm{GeV}^{-2}$. The strength of the weak interactions decreases as the temperature of the Universe drops, and becomes $\mathcal{O}(H)$ around $T_w^{dec} \approx 1\,\mathrm{MeV}$. Around this temperature, particles that interact with the plasma only through weak interactions decouple.

In the next Sections we will investigate these concepts more thoroughly. We conclude this introduction with a summary of the key events in the history of the Universe. A detailed treatment of all these events can be found on [67] and references therein:

BARYOGENESIS This is the epoch when the asymmetry between matter and antimatter that we observe today in the Universe was generated. Baryogenesis models try to derive the observed baryon-to-photon ratio $\frac{n_b}{n_\gamma} \approx 10^{-9}$.

ELECTROWEAK PHASE TRANSITION At a temperature $T \approx 10^2\,\mathrm{GeV}$, the Higgs mechanism gives mass to the $W^\pm$ and Z^0 bosons. The cross-section of weak interactions goes from a $\langle \sigma v \rangle \sim E^{-2}$ behavior to a $\langle \sigma v \rangle \sim E^2$ one.

QCD PHASE TRANSITION Around $T \sim \Lambda_{QCD} \approx 150\,\mathrm{MeV}$ the strong interaction between quarks and gluons becomes important, and baryons ($|qqq\rangle$) and mesons ($|q\bar{q}\rangle$) states are formed.

DARK MATTER FREEZE-OUT If dark matter is a weakly-interacting massive particle (WIMP), it will decouple (its abundance will freeze-out) around $T \sim T_w^{dec} \approx 1\,\mathrm{MeV}$.

NEUTRINO DECOUPLING Neutrinos interact with the plasma only through weak interactions: therefore they will also decouple around $T \sim T_w^{dec}$.

ELECTRON-POSITRON ANNIHILATION Around $T \approx m_e$, the reaction $e^+ + e^- \rightleftarrows \gamma + \gamma$ can proceed only from left to right (because photons are not energetic enough to create e^+-e^- pairs).

Electrons and positrons then annihilate, and their energy is transferred to the thermal bath, heating it. Neutrinos have decoupled before e^+-e^- annihilation, so they are not heated.

BIG BANG NUCLEOSYNTHESIS At $T \approx 10^{-1}$ MeV light elements were formed.

RECOMBINATION When the photon temperature drops low enough that the reaction $H + \gamma \to e^- + p$ is disfavored, neutral hydrogen forms.

PHOTON DECOUPLING Around the time neutral hydrogen forms, photons decouple from the plasma. Indeed, photons and electrons interact mainly through Compton scattering $e^- + \gamma \rightleftarrows e^- + \gamma$: after recombination, the density of free electrons drops sharply and the photon mean free path becomes longer than the horizon. Photons then stream freely through the Universe and are today observed as the CMB.

2.1.1 *Equilibrium thermodynamics*

When we talk about thermal equilibrium in the Hot Big Bang phase, we are using the language of statistical mechanics. The system is then described by a *distribution function* f in phase space [56, §22.6], which is defined in terms of the measurements made by a local Lorentz observer at a given point x^μ in spacetime as the number $\delta\mathcal{N}$ of particles that occupy a spatial volume $\delta\mathcal{V}_{\mathbf{x}}$ and have (physical) momentum (defined as in Section 1.1.2) in a small region of size δP^i around some P^i, i. e. occupy some volume $\delta\mathcal{V}_{\mathbf{P}}$ in momentum space. The distribution function f is then defined as the ratio

$$f \equiv \frac{\delta\mathcal{N}}{\delta\mathcal{V}_{\mathbf{x}}\delta\mathcal{V}_{\mathbf{P}}} \,. \tag{2.1}$$

Notice that we have defined it in terms of $\mathbf{x}$ only (since we are focusing on a specific local Lorentz observer, who has a proper definition of time), and $\mathbf{P}$ only (since $P^0 > 0$ is fixed uniquely by $P^\mu P_\mu = -m^2$). For a generic observer O^μ, then, we can define [56, §22.6]

$$d\mathcal{N} \equiv f(t, \mathbf{x}, E(\mathbf{P}), \mathbf{P}) \, \frac{\sqrt{h}\, d^3x\, d^3P}{(2\pi)^3 E(\mathbf{P})} \,, \tag{2.2}$$

where [58, §4]:

- the coordinates $(t, \mathbf{x})$ are locally adapted to the observer (i. e. we have $O_\mu \propto \delta^0_\mu$ in these coordinates);
- $h_{\mu\nu}$ is the induced metric on the surfaces of constant t;
- P^i are the covariant spatial components of the physical three-momentum;

- $\frac{d^3P}{E(\mathbf{P})}$ is the Lorentz-invariant volume element on the mass hyperboloid, and the positive-energy solution of $P^\mu P_\mu = -m^2$ is selected in the relation $E = E(\mathbf{P})$.

Given a distribution function f, we can define the number density current N^μ and the energy-momentum tensor $T^{\mu\nu}$ with a procedure called "taking moments of f".[1] More precisely, we have (dropping the arguments of f for simplicity of notation)

$$N^\mu = \int \frac{d^3P}{(2\pi)^3 E} f P^\mu \,, \tag{2.3a}$$

$$T^{\mu\nu} = \int \frac{d^3P}{(2\pi)^3 E} f P^\mu P^\nu \,. \tag{2.3b}$$

Matching with the definitions of eqs. (1.27), (1.28), (1.29), (1.30), we can extract the energy density ρ, the isotropic pressure p, etc. Regarding the number density, recall that a perfect fluid has four-velocity of energy transport U^μ equal to the four-velocity of particle number transport, i.e. one can write $N^\mu = nU^\mu$, where n is the particle number density.[2] This definition allows to extract also n from eqs. (2.3).

Things become more simple for perfect fluids in a FLRW background: indeed, due to homogeneity and isotropy, f for a given particle species i can depend only on cosmic time t and the energy E of the particle. Then, it is straightforward to show that (recalling that $p^2 \equiv g_{ij}P^iP^j$, see Section 1.1.2)

$$\boxed{n = \int \frac{d^3P}{(2\pi)^3} f(E) \,,} \tag{2.4a}$$

$$\boxed{\rho = \int \frac{d^3P}{(2\pi)^3} E\, f(E) \,,} \tag{2.4b}$$

$$\boxed{p = \frac{1}{3}\int \frac{d^3P}{(2\pi)^3} \frac{p^2}{E} f(E) \,.} \tag{2.4c}$$

Having seen how n, ρ and p are defined, we proceed by introducing three important concepts in the study of the thermal history of our Universe:

KINETIC EQUILIBRIUM A system of particles is said to be in kinetic equilibrium if the particles exchange energy and momentum efficiently. This leads to a state of maximum entropy in which the distribution functions are given by the Fermi-Dirac and Bose-Einstein distributions, i.e.

$$\boxed{f(E) = \frac{g}{e^{\frac{E-\mu}{T}} \pm 1} \,,} \tag{2.5}$$

1 We will see how this procedure works in more detail in Section 3.3. For the moment, we refer to [56, §22.6][58, §4][67, §5] for more details.

2 This need not be the case for an imperfect fluid, as we will see in Section 3.3.1.

where g is the number of internal degrees of freedom (e. g. spin), the $+$ ($-$) sign is for fermions (bosons), and μ is the chemical potential.

CHEMICAL EQUILIBRIUM A system of particles is said to be in chemical equilibrium with respect to some reaction if the rate of forward and reverse reactions is the same. For a reaction $A + B + \cdots \rightleftarrows C + D + \ldots$, this implies

$$\sum_i^{A,B,\ldots} \mu_i = \sum_i^{C,D,\ldots} \mu_i \ . \tag{2.6}$$

For example, we will see that at redshifts $z \gtrsim 2 \times 10^6$ photons and electrons are in chemical equilibrium with respect to double Compton scattering, i. e. $e^- + \gamma \leftrightarrows e^- + \gamma + \gamma$. This implies that the photon chemical potential is zero at $z \gtrsim 2 \times 10^6$.

THERMAL EQUILIBRIUM Finally, a system of particles is in thermal equilibrium if they are both in kinetic and chemical equilibrium. Such particles share the same temperature T.

2.1.2 *Densities, pressure and entropy*

Using eqs. (2.4), (2.5), we can compute the number and energy densities of massive and massless particles, assuming chemical equilibrium (so that all chemical potentials vanish). Recalling that $E(\mathbf{P}) = \sqrt{p^2 + m^2}$, it is straightforward to show that:

- in the ultra-relativistic limit $T \gg m$, the integrals can be done in terms of the Riemann ζ function. They are given by

$$n = \frac{g\zeta(3)}{\pi^2} T^3 \times \begin{cases} 1 & \text{for bosons} \ , \\ \frac{3}{4} & \text{for fermions} \ , \end{cases} \tag{2.7a}$$

$$\rho = \frac{g\pi^2}{30} T^4 \times \begin{cases} 1 & \text{for bosons} \ , \\ \frac{7}{8} & \text{for fermions} \ , \end{cases} \tag{2.7b}$$

$$p = \frac{\rho}{3} \ ; \tag{2.7c}$$

- in the limit $T \ll m$, instead, the integrals become

$$n = g\left(\frac{mT}{2\pi}\right)^{\frac{3}{2}} e^{-\frac{m}{T}} \ , \tag{2.8a}$$

$$\rho = mn \ , \tag{2.8b}$$

$$p = nT \ll \rho \ . \tag{2.8c}$$

Comparing eqs. (2.7) with eqs. (2.8), one can see that there is an exponential "Boltzmann suppression" of n, ρ and p as T drops below

m. This is the annihilation of particles and antiparticles: when the temperature drops below the mass, the energies of the particles in the thermal bath are not high enough for pair production and then cannot balance the annihilation. We will see in a moment how this is relevant for the temperature of the Cosmic Neutrino Background (CνB).

Through eqs. (2.7) it is possible to define the so-called *effective number of relativistic species*, $g_*(T)$. Calling T the photon temperature and ρ_r the energy density of radiation (i. e. the sum of energy densities over all relativistic species), it is just defined as

$$g_*(T) \equiv \frac{30\rho_r}{\pi^2 T^4} \,. \tag{2.9}$$

One can distinguish two contributions to g_*: these are the contribution of relativistic particles (with $T \gtrsim m$) in thermal equilibrium with photons, i. e.

$$g_*^{\text{th}}(T) \equiv \sum_{i=b} g_i + \frac{7}{8}\sum_{i=f} g_i \,, \tag{2.10}$$

and the contribution of relativistic particles decoupled from photons (which can have a different temperature, $T_i \neq T$, from photons), i. e.

$$g_*^{\text{dec}}(T) \equiv \sum_{i=b} g_i \left(\frac{T_i}{T}\right)^4 + \frac{7}{8}\sum_{i=f} g_i \left(\frac{T_i}{T}\right)^4 \,. \tag{2.11}$$

If all particles are in thermal equilibrium with photons, to compute $g_*(T)$ it is enough to use eq. (2.9) and discard a given species from the sum once they annihilate. Things are different if there is some contribution from $g_*^{\text{dec}}(T)$, since it is necessary to know the ratio $\frac{T_i}{T}$. This can be done by using the conservation of entropy in equilibrium.[3]

In absence of chemical work, i. e. when the number of particles in the system does not change if the volume is held fixed (so that $\mu = 0$), the first law of thermodynamics for the entropy density s reads as

$$\partial_\mu \rho = \frac{\rho + p}{n}\partial_\mu n + nT\partial_\mu s \,. \tag{2.12}$$

Using the continuity equations for n and ρ, i. e. $\nabla_\mu N^\mu = 0$ and $U_\mu \nabla_\nu T^{\mu\nu} = 0$, it is possible to show that $s = \frac{\rho+p}{T}$ is conserved, i. e. that $s \propto a^{-3}$. From eqs. (2.7b), (2.7c), then, we see that for a collection of particles of different species s takes the form

$$s = \sum_i \frac{\rho_i + p_i}{T} \equiv \frac{2\pi^2}{45}\{\underbrace{g_{*,S}^{\text{th}}(T) + g_{*,S}^{\text{dec}}(T)}_{\equiv g_{*,S}(T)}\}T^3 \,, \tag{2.13}$$

where we used that the total energy density ρ is $\approx \rho_r$ in radiation dominance. From this definition, and eqs. (2.9), (2.10), it is clear that

3 There are non-equilibrium processes in which entropy is not conserved. However, these yield a negligible correction to this computation, since the result will be dominated by the entropy of the photons [44, §3.2.5].

$g_*^{\rm th}(T) = g_{*,S}^{\rm th}(T)$. However, since for decoupled species $s_i \propto T_i^3$ from eqs. (2.7b), (2.7c) (their entropy will be conserved separately once they decouple), one has that

$$g_{*,S}^{\rm dec}(T) \equiv \sum_{i=b} g_i \left(\frac{T_i}{T}\right)^3 + \frac{7}{8}\sum_{i=f} g_i \left(\frac{T_i}{T}\right)^3 \neq g_*^{\rm dec}(T) \ . \tag{2.14}$$

The conservation of entropy, then, takes the form

$$\frac{d(g_{*,S}(T)T^3a^3)}{dt} = 0 \Rightarrow T \propto \frac{1}{\sqrt[3]{g_{*,S}(T)}\, a} \ . \tag{2.15}$$

Away from particle mass thresholds $T \sim m_i$, i. e. where the particle species i becomes non-relativistic, $g_{*,S}(T)$ is constant and T scales as a^{-1}. Whenever, instead, a particle species annihilates, its entropy is transferred to the plasma, heating it up and causing T to decrease less slowly than a^{-1}. It is very important to stress that the entropy is transferred only to the particles that the annihilating species was in equilibrium with. As we will see in the next Section, this is the reason why the temperatures of the CMB and the CνB are different.

2.1.3 *Cosmic neutrino background*

Neutrinos are coupled to the plasma via weak interaction. At temperatures below the scale of electroweak symmetry breaking, the cross-section for weak interactions scales as $\langle\sigma v\rangle \propto T^2$. Then, the interaction rate $\Gamma = n\langle\sigma v\rangle$ scales as T^5. Using the first Friedmann equation, eq. (1.31a), and eq. (2.15), during radiation dominance, one can easily see that the Hubble rate scales as

$$H = \sqrt{\frac{\rho_r}{3M_P^2}} \approx \frac{\pi}{3}\sqrt{\frac{g_*(T)}{10}}\frac{T^2}{M_P} \sim \frac{T^2}{M_P} \ . \tag{2.16}$$

Therefore, Γ becomes $\lesssim H$ around 1 MeV (a more precise calculation gives $T_w^{\rm dec} \approx 0.8\,$MeV).

After the decoupling of weak interactions, neutrinos move freely along geodesics preserving their Fermi-Dirac distribution. Their entropy will be conserved: then, using the results of the previous Section, T_ν scales as a^{-1}. If $g_{*,S}(T)$ is constant, also the photon temperature scales in the same way: however, particle annihilations can inject energy in the plasma and make T decrease more slowly than a^{-1}. This indeed happens because of e^+-e^- annihilation, which happens right after $T_w^{\rm dec}$, when the temperature drops below the electron mass.

The increase in the temperature of photons can be computed using eq. (2.15). Neglecting neutrinos and other decoupled species in eqs. (2.13), (2.14), and using the fact that $g_\gamma = g_{e^+} = g_{e^-} = 2$, the photon temperature increases of a factor $\sqrt[3]{11/4}$ after e^+-e^- annihilation, i. e.

$$\frac{(aT)|_{T<m_e}}{(aT)|_{T\gtrsim m_e}} = \sqrt[3]{\frac{11}{4}} \ . \tag{2.17}$$

Since aT_ν is conserved, the ratio $\frac{T_\nu}{T}$ for $T \lesssim m_e$ is

$$\frac{T_\nu}{T} = \sqrt[3]{\frac{4}{11}}\,, \tag{2.18}$$

while the number of relativistic species is

$$g_*(T) = 2 + \frac{7}{8} \times 2N_{\text{eff}} \times \left(\frac{4}{11}\right)^{\frac{4}{3}}\,, \tag{2.19a}$$

$$g_{*,S}(T) = 2 + \frac{7}{8} \times 2N_{\text{eff}} \times \left(\frac{4}{11}\right)\,. \tag{2.19b}$$

In eqs. (2.19), N_{eff} is the so-called "effective number of neutrino species": in the Standard Model it is equal to 3,[4] while it can be higher if there are other relativistic degrees of freedom around $T \approx 1\,\text{MeV}$ (or lower, as it happens in scenarios involving a period of matter domination before the beginning of the Hot Big Bang epoch, due to the presence of a non-relativistic massive particle which then decays. We refer to [70–72] for details). The evolution of $g_*(T)$ and $g_{*,S}(T)$ is shown in fig. 2.1.

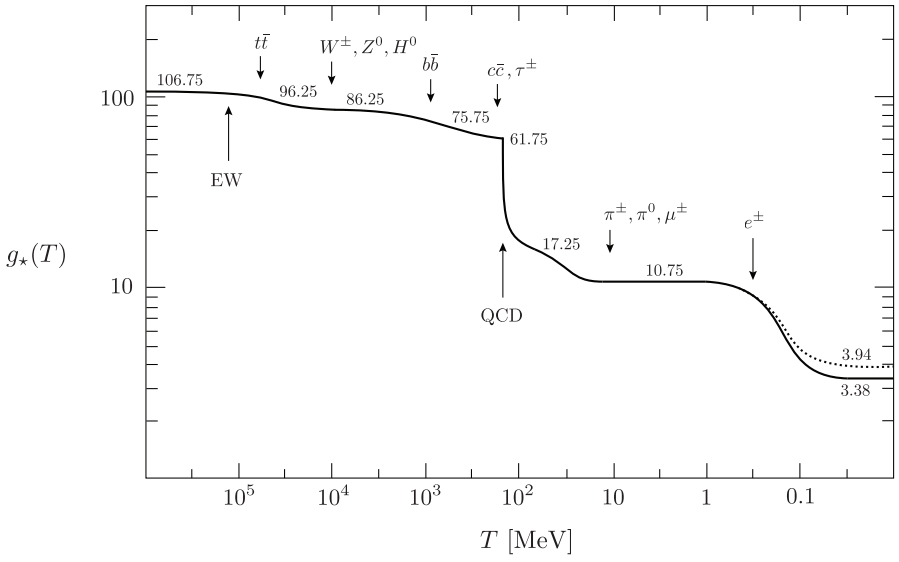

FIGURE 2.1: This plot shows the evolution of $g_*(T)$ (full line) and $g_{*,S}(T)$ (dotted line) as a function of T. We see that they are equal up to $T \approx 0.5\,\text{MeV}$, when neutrinos decouple from the plasma, while $g_*(T) = 3.38$ and $g_{*,S}(T) = 3.94$ after $T \approx m_e$ (for $N_{\text{eff}} = 3$). The plot also shows that the transitions of a particle species from relativistic to non-relativistic behavior is not instantaneous. About 80 % of the particle-antiparticle annihilations takes place in the interval $\frac{m}{6} \lesssim T \lesssim m$ [44, §3.2.2].

4 Taking into account corrections to the neutrino distribution function (i. e. deviations from the Fermi-Dirac form) and the fact that neutrino decoupling is not instantaneous raises this number to 3.046 [68, 69].

2.1.4 *Recombination and CMB decoupling*

In the previous Sections we assumed (kinetic) equilibrium, so that the distribution functions assumed the Bose-Einstein or Fermi-Dirac form. There are, however, many processes in the early Universe where this assumption does not hold. The tool needed to describe the evolution is the Boltzmann equation. In its simplest form,[5] it says that the number of particles of a given species i is conserved in absence of interactions, i. e.

$$\boxed{\frac{dn_i}{dt} + 3Hn_i = C[n_1, \dots] \,,} \tag{2.20}$$

where the *collision term* C encodes the effect of interactions of the particle i with the other species. In this Section we will consider only interactions of the form $1+2 \rightleftarrows 3+4$. In this case, the collision term can be written as

$$C[n_1, \dots n_4] = -\alpha n_1 n_2 + \beta n_3 n_4 \,, \tag{2.21}$$

where α is the thermally averaged cross-section $\langle \sigma v \rangle_{1+2\to 3+4}$ for the process $1+2 \to 3+4$: the first term on the right-hand side of eq. (2.21) says that the higher α is (and/or the higher the densities of the species 1 and 2 are), the faster $n_1 a^3$ is depleted. The parameter β can be related to α by noticing that $n_1 a^3$ must be constant in chemical equilibrium (indeed, in this case the number of particles in a fixed physical volume $V \propto a^3$ does not change, because there is no process that yields a net production or destruction of particles): the collision term must then vanish when the number densities are those derived from eqs. (2.5), (2.6), i. e.

$$\beta = \left(\frac{n_1 n_2}{n_3 n_4} \right) \Bigg|_{eq} \alpha \,. \tag{2.22}$$

Using $N_i \equiv \frac{n_i}{s}$ as variables, eq. (2.20) becomes

$$\boxed{\frac{d \log N_1}{d \log a} = -\frac{\Gamma_1}{H} \left\{ 1 - \left(\frac{N_1 N_2}{N_3 N_4} \right) \Bigg|_{eq} \frac{N_3 N_4}{N_1 N_2} \right\} \,,} \tag{2.23}$$

where $\Gamma_1 \equiv n_2 \langle \sigma v \rangle_{1+2\to 3+4}$. The qualitative behavior of the solution of eq. (2.23) is the following:

- for $\Gamma_1 \gg H$, the system tends towards chemical equilibrium. Suppose indeed that we start with $N_{i>1} \sim N_{i>1}^{eq}$. If $N_1 \gg N_1^{eq}$, the right-hand side of eq. (2.23) is negative and particles of the species 1 are destroyed until $N_1 \to N_1^{eq}$. If, on the other hand, we start with $N_1 \ll N_1^{eq}$, particles are produced until $N_1 \to N_1^{eq}$;

5 We will study it in more detail in Sections 2.2 and 3.3.

- for $\Gamma_1 \ll H$, N_1 tends to a constant, the "relic abundance".

An example of out-of-equilibrium process where the above evolution takes place is recombination. This is the period of time in the early Universe when the first atoms formed. At temperatures above $\approx 1\,\text{eV}$, the plasma was composed of free electrons, photons (tightly coupled to electrons via Compton scattering) and nuclei (interacting with electrons via Coulomb scattering). When the temperature became low enough, the formation of neutral hydrogen became viable (i. e. photons were not energetic enough to allow the reaction $H + \gamma \to p + e^-$). Then, the density of free electrons dropped sharply and photons decoupled from matter. The quantity that one wants to track during recombination is the free electron fraction X_e, defined as

$$X_e \equiv \frac{n_e}{n_b} \,, \tag{2.24}$$

where n_b is the baryon density.

The goal is then to solve eq. (2.23) with $N_1 = N_e$, in order to find the relic abundance of electrons. However, the onset of recombination can be estimated in the following way. If we assume equilibrium, the number densities of electrons, protons and hydrogen atoms take the form of eq. (2.8a), i. e.

$$n_i^{\text{eq}} = g_i \left(\frac{m_i T}{2\pi}\right)^{\frac{3}{2}} e^{\frac{\mu_i - m_i}{T}} \text{ for } i = e, p, H \,, \tag{2.25}$$

where we have included the chemical potentials, which were absent from the calculations of Section 2.1.2. Assuming $\mu_\gamma = 0$, chemical equilibrium of the reaction $H + \gamma \rightleftarrows p + e^-$ implies $\mu_H = \mu_p + \mu_e$. Considering the ratio

$$\left(\frac{n_H}{n_e n_p}\right)\bigg|_{\text{eq}} = \frac{g_H}{g_e g_p}\left(\frac{2\pi}{T}\frac{m_H}{m_e m_p}\right)^{\frac{3}{2}} e^{\frac{m_p + m_e - m_H}{T}} \,, \tag{2.26}$$

then, gets rid of the chemical potentials. Using $g_e = g_p = 2$, $g_H = 4$,[6] and neglecting the binding energy $B_H \equiv m_p + m_e - m_H$ in the prefactor (but not in the exponent), we arrive at

$$\frac{n_H}{n_e^2}\bigg|_{\text{eq}} = \left(\frac{2\pi}{m_e T}\right)^{\frac{3}{2}} e^{\frac{B_H}{T}} \,, \tag{2.27}$$

where we also used the fact that the Universe is not electrically charged so $n_e = n_p$. Using the baryon-to-photon ratio $\eta_b \equiv \frac{n_b}{n_\gamma}$, and neglecting all other nuclei except protons, one arrives at the Saha equation, i. e.

$$\boxed{\left(\frac{1 - X_e}{X_e^2}\right)\bigg|_{\text{eq}} = \frac{2\eta_b \zeta(3)}{\pi^2}\left(\frac{2\pi T}{m_e}\right) e^{\frac{B_H}{T}} \,.} \tag{2.28}$$

6 Recall that $|\frac{1}{2}\rangle \otimes |\frac{1}{2}\rangle = |0\rangle \oplus |1\rangle$.

Eq. (2.28), which assumes that the relic abundance of electrons is the equilibrium one, allows to estimate the recombination temperature. We can define T_{rec} as the temperature at which 90 % of the electrons have combined with protons to form hydrogen (i. e. when $X_e = 10^{-1}$). Using $B_H = 13.6\,\text{eV}$ one finds $T_{rec} \approx 0.3\,\text{eV}$. For $T_0 \approx 2.7\,\text{K}$, the redshift of recombination is $z_{rec} \approx 1300$. Since matter-radiation equality is at $z_{m\text{-}r} \approx 3500$, recombination occurs in matter dominance.

It is also possible to compute when the photons and electrons (coupled through Compton scattering $e^- + \gamma \rightleftarrows e^- + \gamma$) stop interacting. The interaction rate $\Gamma_e \approx n_e \sigma_T$ (where σ_T is the Thomson scattering cross-section and we take $v \approx 1$) is decreasing because of recombination: using eq. (2.28) one sees that it becomes of order of the Hubble rate at $T_{dec} \approx 0.27\,\text{eV}$, corresponding to $z_{dec} \approx 1100$.

We conclude this Section with some brief comments:

- the Saha equation gives the correct prediction for T_{rec}, but solving the full Boltzmann equation eq. (2.23) is necessary to compute correctly the electron fraction after freeze-out;
- the recombination temperature is $\approx 10^2\times$ smaller than the binding energy of the hydrogen atom. The reason is that, also if $T \lesssim B_H$, there are photons energetic enough to ionize a hydrogen atom in the high-frequency tail of the photon distribution. This effect is amplified by the fact that there are very many photons for each hydrogen atom ($\eta_b \approx 10^{-9}$);
- T_{rec} and T_{dec} are fairly close. However, solving the full Boltzmann equation shows that the free electron fraction has a 10 % drop from recombination to decoupling. This means that a large degree of neutrality is necessary for our Universe to become transparent to photon propagation;
- while recombination happens after matter-radiation equality, it is important to stress that z_{rec} is not deep into matter dominance. At recombination the ratio $\frac{\rho_r}{\rho_m}$ is still high enough to leave an observable signature in the CMB angular power spectrum, through the early ISW effect [73, §9.2.2].

In this Section we have used the equilibrium distributions to arrive at the Saha equation. In reality, the distributions deviate from the Bose-Einstein, Fermi-Dirac and Maxwell-Boltzmann forms: while electrons and ordinary matter are well described by Maxwell-Boltzmann distributions up to $z \approx 10$ [45], when electron and protons combine to form an hydrogen atom, the energy emitted can distort the photon spectrum. The study of the *cosmological recombination lines* is a very rich and promising field of research [74, 75] These spectral distortions will be investigated in the next Section.

2.2 CMB BLACK-BODY SPECTRUM

We have seen in Section 2.1.2 that, in kinetic equilibrium with zero chemical potential, the photon frequency spectrum takes the *black-body* form, i. e. (using eq. (2.5) with $\mu_\gamma = 0$ and $g_\gamma = 2$)

$$I_\gamma(E) = \frac{E^3 f_\gamma^{BB}(E)}{2\pi^2} = \frac{E^3}{\pi^2}\frac{1}{e^{\frac{E}{T}} - 1} \,, \tag{2.29}$$

where the intensity I_γ is defined from the relation

$$\rho_\gamma = \int_0^{+\infty} dE\, I_\gamma(E) = \frac{\pi^2 T^4}{15} \,, \tag{2.30}$$

and it is usually plotted in units of $\mathrm{erg\,s^{-1}\,cm^{-2}\,Hz^{-1}\,sr^{-1}}$ in the literature. From now on we will define $f_\gamma^{BB}(E)$ to be just $(e^{\frac{E}{T}} - 1)^{-1}$, i. e. without the factor g_γ.

The black-body frequency spectrum is uniquely identified by the temperature T, with the maximum of the intensity being around $\frac{\nu_{max}}{T} \approx 58.8\,\mathrm{GHz\,K^{-1}}$ ($\lambda_{max} T \approx 5.10\,\mathrm{mm\,K}$). For a black-body spectrum, besides, the ratio $\frac{\rho_\gamma}{n_\gamma}$ is fixed in terms of T as

$$\left.\frac{\rho_\gamma}{n_\gamma}\right|_{BB} = \frac{\pi^4 T}{30\zeta(3)} \,. \tag{2.31}$$

What happens if we do a small change in the temperature, $T \to T' = T + \delta T$? The black-body spectrum will change as (defining $x \equiv E/T$, with $\frac{x'}{x} = \frac{T}{T'}$)

$$\delta f_\gamma^{BB} = \frac{1}{e^{x'} - 1} - \frac{1}{e^x - 1} = \frac{x e^x}{(e^x - 1)^2}\frac{\delta T}{T} + \mathcal{O}\left(\frac{\delta T}{T}\right)^2 \,, \tag{2.32}$$

so that

$$\frac{\Delta I_\gamma}{T^3} = \frac{x^3}{\pi^2}\underbrace{\frac{x e^x}{(e^x - 1)^2}}_{\equiv G(x)}\frac{\delta T}{T} + \mathcal{O}\left(\frac{\delta T}{T}\right)^2 \,, \tag{2.33}$$

where we can call $G(x)$ the *spectrum of a temperature shift*. However, the change in the total energy and total number of photons will satisfy the relation

$$\boxed{\frac{\delta n_\gamma}{n_\gamma} - \frac{3}{4}\frac{\delta \rho_\gamma}{\rho_\gamma} = 0 \,.} \tag{2.34}$$

This tells us that if we inject some energy in the photon field, but we are not able to change accordingly the number of photons, the spectrum will deviate from a black-body. More precisely, *the distortion of eq.* (2.32) *will not be thermalized*.

The goal of this Section is to study in more detail when and how this happens in our Universe, and which kind of spectral distortions of the CMB can arise.

2.2.1 *General assumptions*

In order to thermalize a distortion, we need to create photons: two processes that achieve this are thermal Bremsstrahlung (BR) and double Compton emission (DC). These processes efficiently create photons at low energies: it is Compton scattering that redistributes these soft photons in the high-frequency tail of the spectrum, restoring full equilibrium.

The relevant epoch for spectral distortions of the photon spectrum is at $z \lesssim 2 \times 10^6$: indeed, thermalization was very efficient above this redshift, and any residual distortion from this epoch will be very small [45, §3]. Other two assumptions that we are going to make in this Section are the following:

- we are going to neglect the perturbations in the cosmic fluid. These perturbations are very important for the *creation* of spectral distortions (as we will see in Section 3.4), but are negligible when one wants to study the thermalization process;
- the distribution function of electrons, protons and ordinary matter is assumed to be of the Maxwell-Boltzmann form at one common temperature T_e and with fixed chemical potentials. Up until recombination, as we have seen in Section 2.1.4, T and T_e are very close, i. e. photons and electrons are in thermal equilibrium (actually T_e tends to deviate from the photon temperature T as the Universe expands, in a process called "adiabatic cooling". This is due to the difference in adiabatic indices of photons and electrons). After photon decoupling, the energy/momentum transfer between electrons and other matter is still very fast, and they share a common temperature T_e up to $z \approx 10$ [45, §3][76, 77].

2.2.2 *Photon Boltzmann equation*

The Boltzmann equation eq. (2.20) for particle number densities that was used in Section 2.1.4 is a general consequence of the Boltzmann equation for the distribution function f in phase space. On a FLRW background, $f = f(t, E)$ evolves as (we drop the subscript γ on f, from now on)

$$\boxed{\dot{f} - H\frac{\partial f}{\partial \log E} = C[f]\ .} \tag{2.35}$$

The left-hand side includes the effects of gravity (more precisely, the effects of the cosmological expansion), while the right-hand side describes how f varies when particles interact with each other in between their geodesic motion through spacetime. In absence of collisions, it is easy to see that, given any function $f_0(E)$, the function $f_0(E \times a)$

solves eq. (2.35). This, in turn, can be used to show that temperature redshifts as a^{-1} for f_0 given by eq. (2.5) with $\mu = 0$.

Taking moments of eq. (2.35) directly yields the continuity equations for number and energy densities, defined in eqs. (2.4a), (2.4b), with the appropriate source terms describing the heat transfer due to interactions. In order to describe electrons and baryons this is enough. In order to study the evolution of photons, instead, one needs the full equation eq. (2.35), with the appropriate collision terms. Consider for example Compton scattering, i. e.

$$e^-(p) + \gamma(k) \rightleftarrows e^-(p') + \gamma(k') \,, \tag{2.36}$$

whose kinematics is depicted in fig. 2.2. Neglecting the photon polarization (as we are doing throughout), the collision term $C[f]|_{CS}$ reads (see, e. g., [78])

$$\begin{aligned} C[f]|_{CS} = \frac{1}{2E(p)} \int Dp' \, Dk \, Dk' \, (2\pi)^4 \delta^{(4)}(p + k - p' - k') \\ \times |\mathcal{M}|^2 \mathcal{F}(p, p', k, k') \,, \end{aligned} \tag{2.37}$$

where $Dp = \frac{d^3p}{2(2\pi)^3 E(p)}$, $\mathcal{M}$ is the matrix element of the interaction eq. (2.36), and the statistical factor is

$$\begin{aligned} \mathcal{F}(p, p', k, k') = f_e(\mathbf{p}') f_\gamma(\mathbf{k}')\{1 + f_\gamma(\mathbf{k})\} \\ - f_e(\mathbf{p}) f_\gamma(\mathbf{k})\{1 + f_\gamma(\mathbf{k}')\} \,, \end{aligned} \tag{2.38}$$

with the $(1 + f)$ factors accounting for induced scattering (Pauli-blocking has been dropped).

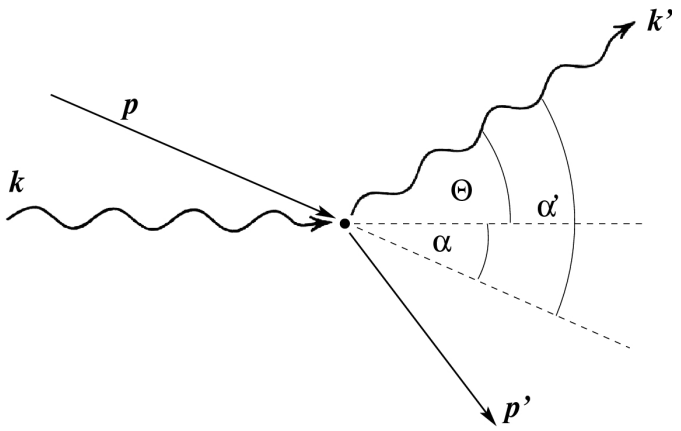

FIGURE 2.2: Scattering angles for $e^-(p) + \gamma(k) \rightleftarrows e^-(p') + \gamma(k')$.

In the early Universe, photons undergo many interactions with free electrons. The most important processes are Compton scattering, Bremsstrahlung and double Compton scattering.[7] Among these, Compton scattering is efficient (and the fastest) for most times, while BR and DC are especially important before $z \approx 5 \times 10^4$.

7 Notice that there can also be non-standard processes (e. g. decaying particles) that add a photon source term.

Compton scattering and Kompaneets equation

We start by studying the kinematics of Compton scattering, using the conventions of fig. 2.2 for the scattering angles. Energy and momentum conservation implies that the photon energy changes by a factor

$$\frac{E'}{E} = \frac{1-\beta\mu}{1-\beta\mu'+\frac{E}{\gamma m}(1-\cos\Theta)} \ , \tag{2.39}$$

where the β and γ factors of the electron have their usual Special Relativity definition, and we have defined $\mu \equiv \cos\alpha$, $\mu' \equiv \cos\alpha'$. There are two interesting regimes:

- if $\beta = 0$, we are in the recoil-dominated regime. For $E \ll m_e$, the photon energy shift becomes

$$\frac{E'}{E} \approx 1 - \frac{E}{m}(1-\cos\Theta) \ . \tag{2.40}$$

  Therefore we see that, averaging over angles, the fractional energy decrease is

$$\left\langle \frac{\Delta E'}{E} \right\rangle_\Theta \approx -\frac{E}{m_e} \ ; \tag{2.41}$$

- if $0 < \beta \ll 1$ and $E \ll m_e$, so that $\beta \gg \frac{E}{\gamma m_e}$, we are in the Doppler-dominated regime. In this limit, one can approximate the energy shift as

$$\frac{E'}{E} \approx \frac{1-\beta\mu}{1-\beta\mu'} \approx 1 - \beta(\mu-\mu') - \beta^2(\mu-\mu')\mu' \ , \tag{2.42}$$

  so that

$$\left\langle \frac{\Delta E'}{E} \right\rangle_\Theta \approx \frac{\beta^2}{3} \ . \tag{2.43}$$

  Averaging over the electron velocity distribution, which is assumed to be of the Maxwell-Boltzmann form, the fractional energy gain is proportional to

$$\left\langle \frac{\Delta E'}{E} \right\rangle_{\Theta,\beta} \approx \frac{T_e}{m_e} \equiv \theta_e \ . \tag{2.44}$$

  A more careful analysis, which takes into account the angular dependence of the scattering cross-section, i. e. (in the Thomson limit)

$$\frac{d\sigma}{d\Omega} \approx \frac{3\sigma_T}{16\pi}(1+\cos^2\Theta) \text{ for } \beta \ll 1, \frac{\Delta E'}{E} \ll 1 \ , \tag{2.45}$$

  gives an average fractional energy gain due to Doppler boosting equal to $4\theta_e$.

These limits prove useful to understand the terms appearing on the right-hand side of the *Kompaneets equation* for the evolution of f [79], i. e.

$$\boxed{\begin{aligned}\left.\frac{\partial f}{\partial \tau}\right|_{CS} &\approx \frac{\theta_e}{x_e^2}\frac{\partial}{\partial x_e}\left\{x_e^4\left[\frac{\partial f}{\partial x_e}+f(1+f)\right]\right\} \\ &= \frac{\theta_e}{x^2}\frac{\partial}{\partial x}\left\{x^4\left[\frac{\partial f}{\partial x}+\frac{T}{T_e}f(1+f)\right]\right\} .\end{aligned}} \tag{2.46}$$

The $\approx$ sign is present in eq. (2.46) because it is obtained from eqs. (2.35), (2.37) by stopping at second order in an expansion in $\langle\frac{\Delta E'}{E}\rangle_{\Theta,\beta}$ (where the average is taken over the scattering cross-section and the electron velocity distribution),[8] and assuming that the photon distribution does not have sharp features [79, 81]. In eq. (2.46) we have defined

$$x_e \equiv \frac{E}{T_e} , \tag{2.47a}$$

$$d\tau \equiv \sigma_T n_e dt , \tag{2.47b}$$

where $\tau(t)$ is the optical depth. If we write $T = T_0(1+z)$, where T_0 is the current temperature of the CMB ($T_0 = 2.7255\,K$ [11]), we see that switching from $(\frac{\partial}{\partial t}, \frac{\partial}{\partial \log E})$ to $(\frac{\partial}{\partial \tau}, \frac{\partial}{\partial x})$ absorbs the redshift term of eq. (2.35). Besides, we see that:

- the second term in the curly brackets is the Doppler boosting term. It describes the diffusion of photons in energy due to the Doppler effect and thus depends on the electron temperature, as it is shown in eq. (2.44);
- the first term, instead, describes the downward scattering of photons due to the recoil effect of eq. (2.41), with the $(1+f)$ factor accounting for Bose-enhancement/stimulated recoil.

Taking moments of the Kompaneets equation, we can derive equations for the evolution of the photon energy density and number density. Since Compton scattering conserves the number of photons, we expect that $\frac{d(na^3)}{dt} = 0$. Indeed, the integral of the right-hand side of eq. (2.46) with respect to $dx\,x^2$ vanishes. The integral over $dx\,x^3$, instead, is not zero, but gives the evolution equation for ρ_γ, i. e.

$$\left.\frac{\partial \rho_\gamma}{\partial \tau}\right|_{CS} \approx 4\theta_e \rho_\gamma \left(1 - \frac{T_e^{eq}}{T_e}\right) , \tag{2.48}$$

with the *Compton equilibrium temperature* defined by

$$T_e^{eq} \equiv \frac{T\int_0^{+\infty} dx\, x^4\, f(1+f)}{4\int_0^{+\infty} dx\, x^3\, f} . \tag{2.49}$$

8 This assumption does not hold if electrons are hot, since the change in the energy of the photon after the scattering will not be small. This happens, e. g., when one studies the Sunyaev-Zeldovich effect in very hot clusters [80]: we refer to Section 2.3.2 for details.

Electrons are heated (cooled) and photons lose (gain) energy if $T_e < T_e^{eq}$ ($T_e > T_e^{eq}$). Since T_e^{eq} and T are not very far from each other (they are actually the same if f has the black-body form), one can see that the ratio $\frac{T}{T_e}$ controls the energy exchange between electrons and photons: if T_e is lower than T, there can be a cooling of the photon gas. We will encounter this effect in the next Sections, under the name of *adiabatic cooling*. Finally, we note that the time-scale of energy transfer from electrons to photons is $t_{e\gamma} = (4\sigma_T n_e \theta_e)^{-1}$, which is smaller than an Hubble time up to $z \approx 5 \times 10^4$. At this point, *Comptonization* becomes inefficient and the shape of the CMB spectral distortion changes: we will see this in more detail in Section 2.3.3.

Bremsstrahlung and double Compton scattering

Bremsstrahlung and double Compton scattering are, respectively, the lowest order radiative corrections to Coulomb and Compton scattering where the photon number changes. For Bremsstrahlung, one needs to worry mainly on electron-ion processes, since the $e^- + e^- \to e^- + e^- + \gamma$ interaction is inefficient at the redshifts of interest [82]. Their collision terms are given by

$$\left.\frac{\partial f}{\partial \tau}\right|_{BR} \approx \frac{K_{BR} e^{-x_e}}{x_e^3}\left\{1 - (e^{x_e} - 1) f\right\} , \tag{2.50a}$$

$$\left.\frac{\partial f}{\partial \tau}\right|_{DC} \approx \frac{K_{BR} e^{-2x}}{x^3}\left\{1 - (e^{x_e} - 1) f\right\} , \tag{2.50b}$$

where K_{BR} and K_{DC} are z- and E-dependent functions, whose expression can be found in [45, §1, §2]. We refer to, respectively, [83] and [12] for a derivation: here we note that they can be approximated by

$$K_{BR} \approx 1.4 \times 10^{-6} \left(\frac{\bar{g}_{eff}}{3.0}\right)\left(\frac{\Omega_b h^2}{0.022}\right)(1+z)^{-\frac{1}{2}} , \tag{2.51a}$$

$$K_{DC} \approx \frac{16\pi^3}{45}\alpha\theta^2 \approx 1.7 \times 10^{-20}(1+z)^2 , \tag{2.51b}$$

where $\theta \equiv \frac{T}{m_e}$, α is the fine-structure constant, $\bar{g}_{eff}$ is the BR thermally averaged "Gaunt factor" [83], which encodes the details of the electron-ion interaction, and eq. (2.51b) is valid in the limit that the scattering photon in the $e^- + \gamma \to e^- + \gamma + \gamma$ interaction does not lead to a large recoil of the electron. Comparing eq. (2.51a) and eq. (2.51b) shows that, while Bremsstrahlung is more efficient in the past, the bulk of the thermalization process is controlled by double Compton scattering, which becomes more important than Bremsstrahlung emission around $z \approx 3.7 \times 10^5$ [9].

2.2.3 *Final set of evolution equations*

Eqs. (2.46), (2.50) give the final evolution equation for the photon distribution function, which we can write as

$$\begin{aligned}\frac{\partial f}{\partial \tau} = \frac{\theta_e}{x^2}\frac{\partial}{\partial x}\left\{x^4\left[\frac{\partial f}{\partial x} + \frac{T}{T_e}f(1+f)\right]\right\} \\ + \left\{1-(e^{x_e}-1)f\right\}\left(\frac{K_{BR}e^{-x_e}}{x_e^3} + \frac{K_{BR}e^{-2x}}{x^3}\right) + S(\tau, x)\ ,\end{aligned} \tag{2.52}$$

where we have added explicitly a photon source term, which can arise in non-standard models (e. g. one could consider some dark matter particle decaying into photons): it adds both energy and photons to the photon field. From eq. (2.52) we also see that, when DC and BR dominate, the equilibrium ($\frac{\partial f}{\partial \tau} = 0$) distribution is driven towards the black-body form at a temperature T_e.

Eq. (2.52) needs to be complemented by an evolution equation for the electron temperature (or, equivalently, the electron energy density). While the photon temperature scales as a^{-1}, the adiabatic index of electrons is $\gamma_e = 5/3$ (as for a monoatomic ideal gas). Therefore, the perfect gas law, for $p_e = n_e T_e$, gives $T_e \propto V^{1-\gamma_e} = a^{-2}$. For this reason, an useful quantity to track is the ratio $r_e \equiv \frac{T_e}{T}$: its evolution equation reads [45, §3.4]

$$\begin{aligned}\frac{dr_e}{d\tau} = \frac{\dot{Q}}{\alpha_h \theta \sigma_T n_e} + \frac{4\rho_\gamma}{\alpha_h m_e}(r_e^{eq} - r_e) \\ - \frac{H}{\sigma_T n_e} r_e - \frac{4\rho_\gamma(\mathcal{H}_{BR}+\mathcal{H}_{DC})}{\alpha_h m_e} r_e\ ,\end{aligned} \tag{2.53}$$

where $\alpha_h \equiv \frac{3}{2}(n_e + n_H + n_{He})$ is the heat capacity of the medium and $\dot{Q}$ is the electron heating term, i. e. the equivalent of the photon source term S. The BR and DC heating terms, $\mathcal{H}_{BR}$ and $\mathcal{H}_{DC}$, can be computed by taking the appropriate moments of eq. (2.52). The second and third terms on the right-hand side of eq. (2.53) show how the expansion tends to drive $T_e \propto a^{-2}$, while Compton scattering tends to bring T_e close to $T_e^{eq} \approx T$.

The above evolution equations can be solved numerically: a great simplification occurs if one expands the photon distribution function in small perturbations around the black-body form. In this way, as usual with linearized equations, a Green's function method can be used to solve eqs. (2.52), (2.53) for arbitrary source terms S and $\dot{Q}$ (the go-to code being `CosmoTherm`). In the next Sections we will see, instead, in which limits some analytical results for f can be obtained.

2.3 y- AND μ-DISTORTIONS

In this Section, we discuss some analytic approximations for the spectral distortions caused by early energy release. We start by introducing the Compton-y and μ-distortions, which are the classic types

of distortions first studied in [7, 80]. In the so-called y-distortion era, $z \lesssim 5 \times 10^4$, DC and BR emission and photon transport from low to high frequencies are already inefficient, so that at high frequencies the distortion shape is purely determined by Compton scattering. In contrast, during the μ-era ($5 \times 10^4 \lesssim z \lesssim 2 \times 10^6$), thermalization works very well and the amplitude of the distortion evolves significantly. The *distortion visibility functions* will describe how efficiently these distortions are thermalized, and which fraction of the energy released in the plasma actually ends up modifying the black-body spectrum.

2.3.1 y-*distortions*

As we have seen in Section 2.2.2, more precisely when we derived eq. (2.48), the energy exchange between photons and electrons due to Compton scattering, along with the redistribution of photons in energy, becomes inefficient around $z \approx 5 \times 10^4$. If we neglect Bremsstrahlung and double Compton scattering in eq. (2.52), since at these redshifts DC is not fast enough with respect to the Thomson rate $t_T \equiv (\sigma_T n_e)^{-1}$ and BR is a subleading correction until recombination [45, §4.4], the evolution of f will be dictated by the Kompaneets equation eq. (2.46) only.

Suppose that we start with at $\tau = 0$ with a black-body spectrum. If we evolve the distribution for a small time $\delta\tau$, the distribution will change as

$$\delta f \approx (\theta_e - \theta) \underbrace{G(x)\left\{x\frac{e^x+1}{e^x-1} - 4\right\}}_{\equiv Y_{SZ}(x)} \delta\tau \,, \tag{2.54}$$

where the parameter y, defined as

$$\boxed{y \equiv \int_0^\tau d\tau'(\theta_e - \theta) \,,} \tag{2.55}$$

determines the time-scale over which the approximation of eq. (2.54) holds. y measures the *energy transfer* between photons and electrons. Indeed, integrating eq. (2.54) against $dx\, x^3$ shows that $\frac{\delta\rho_\gamma}{\rho_\gamma} = 4y$:[9] therefore, the *Compton* y*-distortion* arises in the limit of inefficient energy exchange between electrons and photons. This distortion of the CMB was first studied in [80], and then applied to hot electrons residing inside the potential wells of clusters of galaxies, giving rise to the Sunyaev-Zeldovich (SZ) effect, which we discuss briefly in the next Section. The shape of the y-distortion, defined in eq. (2.54) as $Y_{SZ}(x) \equiv \left(x \coth \frac{x}{2} - 4\right) G(x)$, is shown in fig. 2.3.

9 Notice that the integral of eq. (2.54) against $dx\, x^2$ vanishes, as it is expected since Compton scattering does not change the number of photons.

2.3.2 *Sunyaev-Zeldovich effect*

The CMB spectrum acquires a y-distortion when photons travel through clusters of galaxies. These are the largest virialized objects in our Universe, with typical masses $10^{13} M_\odot \lesssim M \lesssim 10^{14} M_\odot$, containing up to $\approx 10^3$ galaxies. They also host a hot plasma with free electrons at temperature $T_e = \mathcal{O}(\text{keV})$ at typical densities $n_e \approx 10^{-3}\,\text{cm}^{-3}$. The hot electrons, then, can scatter CMB photons and distort their spectrum, in a process called *thermal* Sunyaev-Zeldovich (tSZ) effect. The typical y-parameter of massive clusters is of order $10^{-5} \div 10^{-4}$.

Before proceeding, we note that the assumptions of this Section are inadequate to accurately compute the distortions due to the thermal SZ effect. Indeed, the electrons inside clusters can have thermal velocities up to $\mathcal{O}(10^{-1})$: in this case, relativistic corrections become important and the Kompaneets equation loses its validity. Besides, if the cluster is moving with respect to the CMB, there will be an additional Doppler shift in the CMB temperature towards the cluster. This shift is of purely kinematical origin: for this reason the effect is called *kinematic* Sunyaev-Zeldovich (kSZ) effect.

2.3.3 *μ-distortions*

In the regime where the parameter y of eq. (2.55) is much larger than 1, energy exchange is very efficient and the photon distribution tends towards $\frac{\partial f}{\partial \tau} = 0$. Solving the Kompaneets equation under this assumption gives

$$f = \frac{1}{e^{x_e + \mu_0} - 1} \,, \tag{2.56}$$

i. e. a Bose-Einstein distribution at a temperature T_e, with dimensionless chemical potential μ_0. In the rest of this work we will use the above definition of chemical potential, related to that of eq. (2.5) by

$$\mu_{\text{here}} = \left(-\frac{\mu}{T} \right) \Big|_{\text{there}} \,. \tag{2.57}$$

The solution with $\mu_0 < 0$ is unphysical, because $x_e + \mu_0$ could vanish for some positive frequency $x_{e,0} > 0$: what would happen, instead, is that the photons would form a Bose-Einstein condensate at $x_e = 0$, with $\mu_0 = 0$ elsewhere [84, 85]. In a real plasma, actually, BR and DC emission will prevent even this from happening [8, 86].

How can we fix the constant μ_0? Suppose to start with a black-body spectrum for photons, and electrons at $T_e = T = T_{e,i}$. If we change the number and energy density of the photon field as

$$\rho_{\gamma,f} = \rho_{\gamma,i}(1 + \epsilon_\rho) \,, \tag{2.58a}$$

$$n_{\gamma,f} = n_{\gamma,i}(1 + \epsilon_n) \,, \tag{2.58b}$$

and wait until the distribution function has reached the Bose-Einstein equilibrium form, it is possible to relate the final electron temperature $T_{e,f} = T_{e,i} + \delta T_e$ and the chemical potential μ_0 to ϵ_ρ and ϵ_n. Assuming small deviations $\mu_0 \ll 1$, $\delta T_e \ll T_{e,i}$, the solution is

$$\delta T_e = \frac{540\{\zeta(3)\}^3\epsilon_n - \pi^6\epsilon_\rho}{4\{\pi^6 - 480[\zeta(3)]^3\}} \approx -0.5185\epsilon_n + 0.6389\epsilon_\rho \,, \tag{2.59a}$$

$$\mu_0 = -\frac{3\pi^4\zeta(3)(4\epsilon_n - 3\epsilon_\rho)}{2\{\pi^6 - 480[\zeta(3)]^3\}} \approx -1.866\epsilon_n + 1.401\epsilon_\rho \,. \tag{2.59b}$$

From eq. (2.59b) we see that for $\epsilon_\rho = \frac{4}{3}\epsilon_n$ we have no distortion, as we have already seen in eq. (2.34): in this case, only the temperature of the black-body spectrum is increased after scattering has redistributed all photons.

Suppose now that we are given some frequency spectrum, to which we want to fit some spectral dependence.[10] More precisely, we assume that we want to fit a small distortion from a black-body. How do we define the μ-distortion shape? Expanding eq. (2.56) for small μ_0 gives

$$f = \frac{1}{e^{x_e} - 1} - \mu_0\frac{G(x_e)}{x_e} + \mathcal{O}(\mu_0^2) \,, \tag{2.60}$$

suggesting that we fit a μ-distortion using the shape $M(x) \equiv -\frac{G(x)}{x}$ (see fig. 2.3). However, recalling that Compton scattering conserves the number of photons, a better definition turns out to be

$$M^*(x) \equiv \frac{3}{\kappa^c}\left\{G(x)\left(\frac{\pi^2}{18\zeta(3)} - \frac{1}{x}\right)\right\} \,, \tag{2.61}$$

where, following [45, §4.2.2], we defined

$$\frac{3}{\kappa^c} \equiv \frac{9\pi^4\zeta(3)}{\{2\pi^6 - 810[\zeta(3)]^2\}} \approx 1.401 \,. \tag{2.62}$$

In this way, the integral of $M^*(x)$ over $dx\, x^2$ vanishes (as it does the integral of Y_{SZ} for the y-distortion), and the relative change of the photon energy density is normalized to 1. In the rest of this Section, however, we will use the definition of μ_0 which derives from eq. (2.60) for analytical calculations (using the fact that at linear order in μ_0 we can drop the difference between x_e and x): the matching with eq. (2.61) is straightforward. We refer to fig. 2.3 for a plot of the black-body, temperature shift, y-distortion and μ-distortion shapes of the photon frequency spectrum. The plot shows that the important feature of a μ-distortion is that it is shifted towards lower frequencies with respect to the y-distortion. This makes it distinguishable from $G(x)$ and $Y_{SZ}(x)$, so that observing a μ-distortion is a clear indication for a signal created in the pre-recombination era, deep into the thermal history of our Universe.

10 This is exactly what happens when analyzing CMB data: see Appendix A for details.

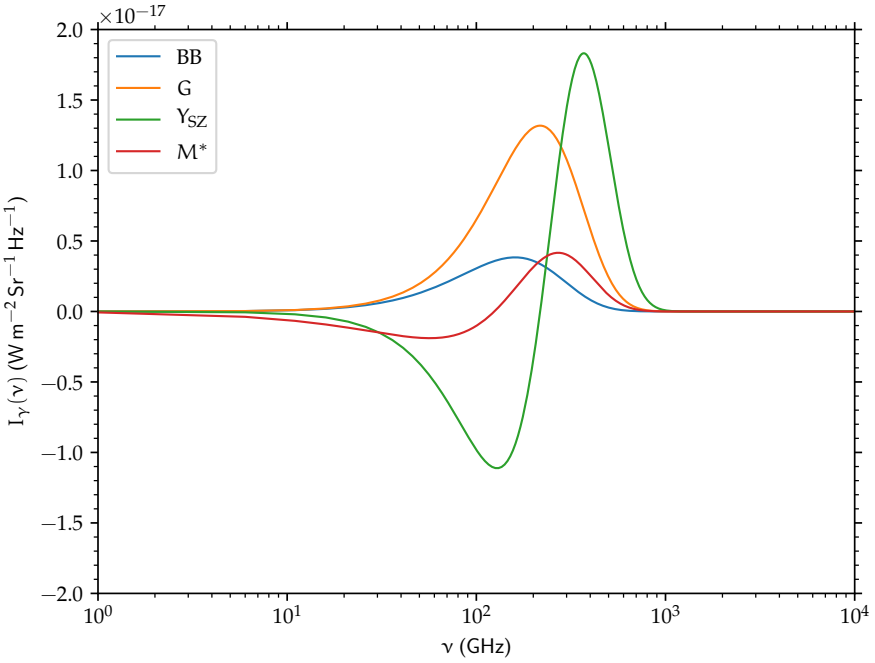

FIGURE 2.3: This plot shows the black-body, G, Y_{SZ} and M^* shapes of the photon frequency spectrum, i.e. $I_\gamma(\nu) = \frac{2h\nu^3}{c^2} f_\gamma(\nu)$, where $f_\gamma(x)$ are the occupation numbers of eqs. (2.29), (2.33), (2.54), (2.61). The dimensionless amplitudes of these spectra must be fitted to data. We plot the intensities as functions of frequency for $T = 2.7255\,K$.

2.3.4 *Distortion visibility functions*

The picture that arises from Sections 2.3.1 and 2.3.3 is the following: given a small energy increase ϵ_ρ and/or small photon production ϵ_n, the CMB spectrum will be distorted according to

$$\delta f(x) = \underbrace{\frac{(\epsilon_\rho)|_y}{4}}_{\equiv y} Y_{SZ}(x) + \underbrace{\left\{ (\epsilon_\rho)|_\mu - \left(\frac{4\epsilon_n}{3}\right)\Big|_\mu \right\}}_{\equiv \mu_0} M(x)\,, \tag{2.63}$$

where the subscripts indicate that the energy release and photon production happen during the "μ-era" ($5\times10^4 \lesssim z \lesssim 2\times10^6$) or the "y-era" ($z \lesssim 5\times10^4$). Two aspects are missing from this analysis:

- we have not included photon production (i.e. Bremsstrahlung and double Compton scattering) into the picture but assumed that only Compton scattering changes the photon field. This will be mostly relevant for the evolution of μ-distortions, since not all energy release or photon production eventually is visible as a distortion. That is, the *distortion visibility function* is smaller than unity because thermalization reduces the effective amount of energy release that survives as a distortion. This is implicitly

hidden in the definition of $(\epsilon_\rho)|_\mu$ and $(\epsilon_n)|_\mu$ of eq. (2.63), and is mainly relevant for the μ-distortion, when BR and DC can still create soft photons and affect the photon number density;

- the second point is that the transition between the μ- and the y-era is not abrupt, but occurs over a range of redshifts. In the intermediate regime the distortion is not only given by the superposition of μ- and y-distortion, but has a much richer spectral dependence.

In this Section we will study in more detail how the μ-distortion visibility function is defined and computed, referring to [12, 87, 88] for details about the computation of the residual distortions from the μ-y transition.

Assuming that the only relevant distortion is of the μ-type, from eqs. (2.59b), (2.62) we can see that

$$\frac{d\mu_0}{d\tau} = \frac{3}{\kappa^c}\frac{d\log(\rho_\gamma a^4)}{d\tau} - \frac{4}{\kappa^c}\frac{d\log(n_\gamma a^3)}{d\tau} \,. \tag{2.64}$$

Therefore, it is necessary to compute the energy release and photon production terms from the Boltzmann equation, eq. (2.52).

Regarding the first term on the right-hand side of eq. (2.64), one can show that BR and DC contributions cancel with the energy exchange from Compton scattering, eq. (2.48) once the equilibrium temperature is computed correctly [89]: therefore, one only needs to consider the electron heating term Q_e^*, i. e.

$$\frac{d\log(\rho_\gamma a^4)}{d\tau} \approx \frac{\dot{Q}_e^*}{\rho_\gamma} \,, \tag{2.65}$$

where $\dot{Q}_e^*$ is different from $\dot{Q}$ in eq. (2.53) because it includes also the contribution from adiabatic cooling of electrons [12, 89].

The photon production term $\frac{d\log(n_\gamma a^3)}{d\tau}$ is more complicated. We know that at low frequencies the CMB spectrum is pushed into equilibrium with the electrons, so that it is best to describe the distortion with respect to a black-body at the electron temperature plus a small μ-type distortion, as in eq. (2.60): since we are working at linear order in the distortions from a black-body, we can neglect the difference between the electron temperature and the photon temperature in $\delta f = -\mu_0 \frac{G(x_e)}{x_e} \approx -\mu_0 \frac{G(x)}{x}$.

If we now integrate eq. (2.52) against $dx\, x^2$ assuming the distribution function to be a black-body plus a small μ-type perturbation, we find a diverging answer unless the chemical potential is a function of frequency, and vanishes faster than $-\frac{\log x}{x^2}$ for $x \to 0$. The reason is that, at small frequencies, Bremsstrahlung and double Compton emission can still create photons, so the assumption of a constant, non-zero chemical potential is incorrect in the Rayleigh-Jeans region [7]. In order to compute its spectral dependence, one needs to look

at the full Boltzmann equation. A simplification arises from the fact that, since we are interested in small frequencies only, we can expand eq. (2.52) for $x \to 0$. Calling $\Lambda(\tau, x) \equiv K_{BR} + K_{DC} e^{-x}$, the stationary solution for the chemical potential must satisfy

$$x^2 \frac{d^2\mu}{dx^2} + 2x\frac{d\mu}{dx} - \frac{\Lambda(\tau, x)}{x^2\theta} = 0 \,. \tag{2.66}$$

The BR and DC emission coefficients are only weakly dependent on frequency for $x \ll 1$. We can thus replace $\Lambda(\tau, x) \approx x_c^2\theta$, where the critical frequency x_c can be determined numerically. Eq. (2.66), then, takes the form

$$\frac{d}{dx}\left(x^2\frac{d\mu}{dx}\right) - \frac{x_c^2}{x^2}\mu = 0 \,, \tag{2.67}$$

which has the simple solution $\mu(\tau, x) = \mu_0(\tau) e^{-\frac{x_c(\tau)}{x}}$.[11]

Using this approximate solution, the photon production term in eq. (2.64) takes the form

$$\frac{d\log(n_\gamma a^3)}{d\tau} \approx \frac{x_c\theta}{2\zeta(3)}\mu_0(\tau) \,, \tag{2.68}$$

so that eq. (2.64) becomes

$$\frac{d\mu_0}{d\tau} = \frac{3}{\kappa^c}\frac{\dot{Q}_e^*}{\rho_\gamma} - \frac{2x_c\theta}{\kappa^c\zeta(3)}\mu_0 \,. \tag{2.69}$$

Assuming that the chemical potential vanishes at early times, only the inhomogeneous solution survives. If we define the *thermalization optical depth* $\tau_\mu(z)$ as

$$\boxed{\tau_\mu(z) \equiv \frac{2}{\kappa^c\zeta(3)}\int_0^z dz' \, \frac{x_c\theta}{(1+z')t_T H} \,,} \tag{2.70}$$

the solution reads

$$\boxed{\begin{aligned}\mu_0(z) &= \frac{3}{\kappa^c}\int_z^{+\infty} dz' \, \frac{\dot{Q}_e^*}{\rho_\gamma}\frac{e^{-\{\tau_\mu(z')-\tau_\mu(z)\}}}{(1+z')H} \\ &\approx \frac{3}{\kappa^c}\int_0^{+\infty} dz' \, \frac{d(Q_e^*/\rho_\gamma)}{dz'}\underbrace{e^{-\{\tau_\mu(z')-\tau_\mu(z)\}}}_{\equiv \mathcal{J}_\mu(z',z)} \,.\end{aligned}} \tag{2.71}$$

The function $\mathcal{J}_\mu(z', z)$ is the *spectral distortion visibility function* between the heating redshift z' and z. It determines the fraction of energy injected at z' that is still visible as a distortion at z. For $\mathcal{J}_\mu(z', z) \approx 1$, most of the energy is still stored in the distortion, while

11 One can see that at $z \approx 2 \times 10^5$, when photon transport from Compton scattering becomes inefficient and μ_0 becomes for all practical purposes time-independent, the critical frequency is $x_c \approx 5 \times 10^{-2}$, corresponding to $\nu_c \approx 3\,\text{GHz}$ (which is outside of the coverage of current (Planck) and proposed (PIXIE) experiments).

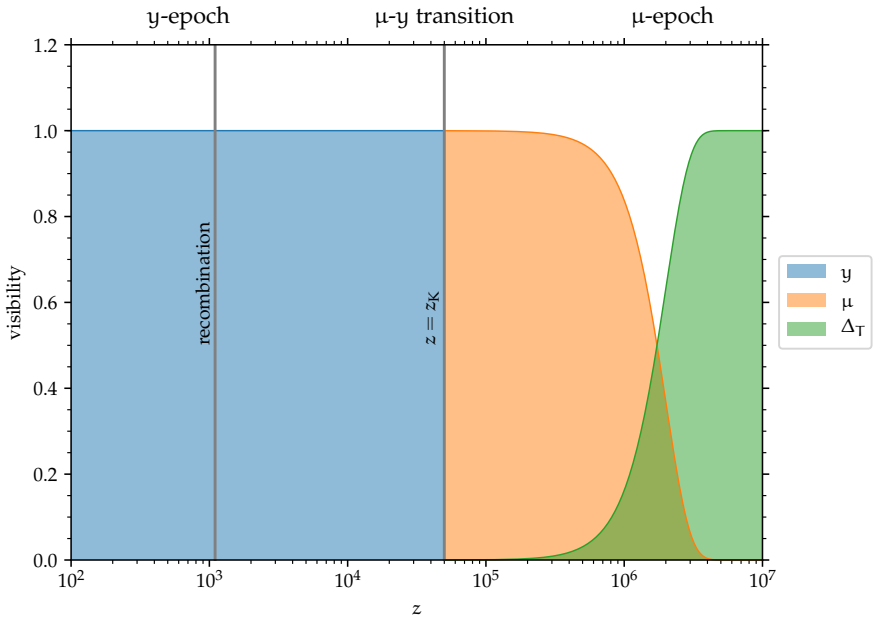

FIGURE 2.4: Formation of primordial distortions. At low redshifts ($z \lesssim z_K = 5 \times 10^4$), a y-distortion is formed with distortion visibility close to unity, while at high redshifts a μ-distortion appears. The energy release has to be weighted with the μ-distortion visibility function which drops exponentially at $z_{DC} \approx 2 \times 10^6$ (leading to a pure temperature shift Δ_T), and is basically equal to 1 at $z \approx 2 \times 10^5$ (i. e. the redshift at which photon transport from low to high frequencies by Compton scattering becomes inefficient).

for $\mathcal{J}_\mu(z', z) \ll 1$, most of the energy was thermalized and converted into a temperature shift. For redshifts above the Comptonization redshift $z_K \equiv 5 \times 10^4$, where the distortion is of the μ-shape, the visibility function $\mathcal{J}_\mu(z', 0)$ can be approximated as [9, 10, 90]

$$\mathcal{J}_\mu(z', 0) = e^{-(z'/z_{DC})^{\frac{5}{2}}} \,, \tag{2.72}$$

where the DC thermalization redshift is given by [90]

$$z_{DC} = 1.98 \times 10^6 \left(\frac{\Omega_b h^2}{0.022}\right)^{-\frac{2}{5}} \left(\frac{T_0}{2.7255\,K}\right)^{\frac{1}{5}} \left(\frac{1 - Y_p/2}{0.88}\right)^{-\frac{2}{5}} \,, \tag{2.73}$$

with Y_p being the ^4He number density fraction. Such result includes only DC emission in the computation of the thermalization optical depth. Indeed, it is double Compton scattering, and not Bremsstrahlung, that controls the bulk of the thermalization process: we refer to [45, §4.5.2] for details.[12] We can extend this formalism below z_K in a straightforward way: after Compton scattering becomes inefficient, the distortions do not thermalize, and the energy release goes completely

12 More precisely, see fig. 4.9.

into a y-distortion. The resulting correction to the CMB black-body occupation number, at redshift $z = 0$, reads

$$\boxed{\delta f(x) = y Y_{SZ}(x) + \mu_0 M(x) + \Delta_T G(x) \,,} \tag{2.74}$$

where (see also fig. 2.4)

$$\boxed{\begin{aligned} y &= \frac{1}{4}\int_0^{+\infty} dz\, \frac{d(Q_e^*/\rho_\gamma)}{dz}\, \Theta(z_K - z) \,, && \text{(2.75a)} \\ \mu_0 &= \frac{3}{\kappa^c}\int_0^{+\infty} dz\, \frac{d(Q_e^*/\rho_\gamma)}{dz}\, \mathcal{J}_\mu(z,0)\Theta(z - z_K) \,, && \text{(2.75b)} \\ \Delta_T &= \frac{1}{4}\int_0^{+\infty} dz\, \frac{d(Q_e^*/\rho_\gamma)}{dz}\, \{1 - \mathcal{J}_\mu(z,0)\Theta(z - z_K)\} \,. && \text{(2.75c)} \end{aligned}}$$

In this Chapter we already discussed some sources of $\frac{d(Q_e^*/\rho_\gamma)}{dz}$ that can lead to a distortion of the CMB spectrum. The adiabatic cooling effect, introduced in Section 2.2.2, takes the form [12, 86]

$$\left.\frac{d(Q_e^*/\rho_\gamma)}{dz}\right|_{ac} = -\frac{45\{2n_H(z) + 3n_{He}(z)\}}{2\pi^2(1+z)T^3} \,,$$

where we see that it leads to a *negative* spectral distortion because energy is *extracted* from the photon field in order to keep electrons at $T_e \approx T$. There are other sources of distortions, like the Sunyaev-Zeldovich effect, the contribution from recombination,[13] and possibly the effect of annihilating or decaying dark matter particles (see, e. g., [12]). In the next Chapters, we are going to be mostly dealing with another effect, i. e. the spectral distortions coming from *Silk damping of acoustic waves* in the photon-electron-baryon fluid. This effect is a probe of inflationary perturbations at very small scales. In order to see this, we have to depart from the assumption of a FLRW background and add some perturbations to the metric and to matter: this will be the topic of the next Chapters.

13 Photons emitted by atoms during the recombination process will distort the CMB spectrum at specific frequencies, corresponding to the recombination lines: we refer to [91], and references therein, for details.

Part II

THE PERTURBED UNIVERSE

3

COSMOLOGICAL PERTURBATION THEORY

CONTENTS

So far, we have treated the spacetime as perfectly homogeneous and isotropic. To understand the formation and evolution of large-scale structures, we have to introduce inhomogeneities. As long as these perturbations remain relatively small, we can treat them in perturbation theory. This allows to expand the Einstein equations order-by-order in perturbations of the metric and the stress-energy tensor.

The Chapter is based mainly on [44, §4, §5][92] (for the treatment of CMB anisotropies) and [20, 93] (for the calculation of μ-distortions anisotropies). The Arnowitt-Deser-Misner (ADM) formalism used to obtain the perturbed Einstein and matter equations is reviewed in Appendix B: for further details we refer to [55, §10, §E][56, §21][94].

3.1 NEWTONIAN PERTURBATION THEORY

In order to gain some intuition, one can start from Newtonian perturbation theory. Indeed, on scales well inside the Hubble radius and for non-relativistic matter (e. g. cold dark matter and baryons after decoupling), Newtonian gravity is a good approximation of General Relativity.

3.1.1 *Static spacetime*

Consider a non-relativistic fluid with mass density ρ, pressure $p \ll \rho$ and velocity $\mathbf{u}$. The equations of motion are obtained simply by

imposing mass and momentum conservation: in absence of external forces (i. e. for zero pressure) these would just be

$$\dot{\rho} + \partial_i(\rho u^i) = 0 \,, \tag{3.1a}$$
$$D_t \mathbf{u} = 0 \,, \tag{3.1b}$$

where the convective derivative $D_t = \partial_t + u^i \partial_i$ measures how the fluid velocity and the fluid mass density change along the trajectory of a given fluid element. Expanding eqs. (3.1), and adding a non-zero pressure gradient as an external force, gives the continuity and Euler equations, i. e.

$$\dot{\rho} + u^i \partial_i \rho = 0 \,, \tag{3.2a}$$
$$\dot{u}^i + u^j \partial_j u^i = -\frac{\partial_i p}{\rho} - \partial_i \Phi \,. \tag{3.2b}$$

The gravitational potential Φ is determined by the Poisson equation, which reads as

$$\partial^2 \Phi = \frac{\rho}{2M_P^2} \,. \tag{3.3}$$

Expanding all the dynamical variables X in small perturbations δX around a background $\bar{X}$, it is easy to see that $\bar{\rho} = \text{const.}$, $\bar{p} = \text{const.}$, $\bar{\mathbf{u}} = 0$ and $\bar{\Phi} = 0$ are a solution for the background, while the perturbations must satisfy the equations

$$\frac{\partial \delta\rho}{\partial t} = -\bar{\rho} \partial_i u^i \,, \tag{3.4a}$$
$$\bar{\rho} \dot{u}^i = -\partial_i \delta p - \bar{\rho} \partial_i \Phi \,, \tag{3.4b}$$
$$\partial^2 \Phi = \frac{\delta\rho}{2M_P^2} \,. \tag{3.4c}$$

Combining the time derivative of eq. (3.4a) with the divergence of eq. (3.4b),[1] one can arrive at a system of two partial differential equations for $\delta\rho$ and the gravitational potential, i. e.

$$\frac{\partial^2 \delta\rho}{\partial t^2} - c_s^2 \partial^2 \delta\rho = \bar{\rho} \partial^2 \Phi \,, \tag{3.5a}$$
$$\partial^2 \Phi = \frac{\delta\rho}{2M_P^2} \,. \tag{3.5b}$$

In order to obtain eq. (3.5a), we assumed an equation of state for the fluid. This means that in the rest frame of the fluid it is possible to write p as a function of ρ: the *speed of sound* c_s^2, then, is just the functional derivative $\frac{\delta p}{\delta \rho}$. Because of the symmetries of the background, c_s^2 is a constant in a static spacetime, while it can only depend on time when $H \neq 0$.

1 As we will see in Section 3.3.1, this procedure allows to obtain a closed equation for $\delta\rho$ and Φ only on sub-Hubble scales.

It is a trivial step to plug eq. (3.5b) in eq. (3.5a), to arrive at a (sourced) wave equation for $\delta\rho$. Being a linear PDE, such equation can be solved by going to Fourier space: the solution for $\delta\rho_{\mathbf{k}}$ is given by a superposition of plane waves, with frequency $\omega(k)$ equal to

$$\omega^2(k) = c_s^2 k^2 - \frac{\bar{\rho}}{2M_P^2} \,. \tag{3.6}$$

Therefore, we see that for wavelengths shorter than the *Jeans length*, defined as

$$\boxed{k_J^2 \equiv \frac{\bar{\rho}}{2c_s^2 M_P^2}} \,, \tag{3.7}$$

matter perturbations oscillate, while on large scales ($k < k_J$) they grow exponentially.

3.1.2 *Expanding spacetime*

In an expanding space, $\mathbf{x}_{\text{phys.}} = a(t)\mathbf{x}$ ($\mathbf{x}_{\text{phys.}}$ being the physical coordinates and $\mathbf{x}$ being the comoving coordinates), eqs. (3.1) will still hold when written in terms of $\mathbf{x}_{\text{phys.}}$. Therefore, when we switch to comoving coordinates, they become (up to linear order in perturbations)

$$\frac{\partial\rho}{\partial t} - Hx^i\partial_i\rho + \frac{\partial_i\{\rho(Hax^i + v^i)\}}{a} = 0 \,, \tag{3.8a}$$

$$\dot{v}^i + Hv^i = -\frac{\partial_i p}{a\rho} - \frac{\partial_i\Phi}{a} \,. \tag{3.8b}$$

The Poisson equation, instead, simply becomes

$$\partial^2\Phi = \frac{a^2\rho}{2M_P^2} \,. \tag{3.9}$$

In the above equations, spatial derivatives are with respect to $\mathbf{x}$, and the peculiar velocity $\mathbf{v}$ (which starts at first order in perturbations) is related to $\mathbf{u}$ by

$$\mathbf{u} = \dot{\mathbf{x}}_{\text{phys.}} = H\mathbf{x}_{\text{phys.}} + \mathbf{v} \,, \tag{3.10}$$

where $H\mathbf{x}_{\text{phys.}}$ is the Hubble flow.

At zeroth order in perturbations, assuming $\bar{p} = 0$ for non-relativistic matter, the mass density simply evolves as $\bar{\rho} \propto a^{-3}$. If we introduce the *density contrast* $\delta \equiv \frac{\delta\rho}{\bar{\rho}}$, it is straightforward to see that the first-order equations become

$$\dot{\delta} = -\frac{\partial_i v^i}{a} \,, \tag{3.11a}$$

$$\dot{v}^i + Hv^i = -\frac{\partial_i \delta p}{a\bar{\rho}} - \frac{\partial_i\Phi}{a} \,, \tag{3.11b}$$

$$\partial^2\Phi = \frac{a^2\bar{\rho}\delta}{2M_P^2} \,. \tag{3.11c}$$

Eq. (3.11b) confirms that, in absence of pressure or gravitational perturbations, peculiar velocities decay as a^{-1} with the expansion of the universe.

Now, as we did in Section 3.1.1, we can combine eq. (3.11c), the time derivative of eq. (3.11a), and the divergence of eq. (3.11b) to arrive at a single equation for the fractional density perturbation δ. Assuming, as before, a speed of sound c_s^2 relating $\delta\rho$ and δp, we see that the equation governing the evolution of δ is

$$\boxed{\ddot{\delta} + 2H\dot{\delta} - \frac{c_s^2 \partial^2 \delta}{a^2} = \frac{\bar{\rho}\delta}{2M_P^2} \, .} \tag{3.12}$$

This implies the same Jeans length as in eq. (3.7), but unlike the case of a static spacetime, it now depends on time because $\bar{\rho}$ and c_s^2 are not forced to be constants. Compared to eqs. (3.5), the equation of motion in the expanding spacetime includes a friction term $\propto H\dot{\delta}$. This has two effects: Below the Jeans length, the fluctuations oscillate with decreasing amplitude. Above the Jeans length, the fluctuations experience power-law growth, rather than the exponential growth we found in Section 3.1.1.

The above equation for δ can be used to follow the evolution of matter perturbations (δ_m) inside the Hubble radius (with the caveat that the right-hand side of eq. (3.12) must be replaced with a sum over all the gravitating matter species, since it originally derives from the Poisson equation for Φ). We will then solve it, focusing separately on the radiation-dominated, matter-dominated and Λ-dominated epochs. Besides, we will neglect small effects due to baryons (that will be considered in Section 3.3.1), so that $\delta_m = \delta_{cdm}$, for which $c_s^2 = 0$. Finally, we assume *adiabatic* perturbations: as we will see in Section 3.2.4, this implies that all matter species i satisfy

$$\frac{\delta_i}{1+w_i} = \frac{\delta_j}{1+w_j} \; \forall \, i, j \, . \tag{3.13}$$

Therefore, for $w_i = \mathcal{O}(1)$, all δ_i are comparable and the total density perturbation, that sources Φ, is dominated by the species that is dominant in the background.

Radiation dominance

As we will see in more detail in 3.3.1, radiation fluctuations on scales smaller than the Hubble radius oscillate as sound waves (supported by large radiation pressure) and their time-averaged density contrast vanishes [95]. Therefore, assuming adiabatic perturbations, the matter density contrast during radiation dominance satisfies the simple equation (recalling that the speed of sound is zero)

$$\ddot{\delta}_m + 2H\dot{\delta}_m = 0 \, . \tag{3.14}$$

Using $H = \frac{1}{2t}$ during the radiation-dominated epoch, we see that the growing mode solution of eq. (3.14) is $\delta_m \propto \log t \sim \log a$. We see that the rapid expansion due to the effectively unclustered radiation makes the growth of δ_m only logarithmic.

Matter dominance

During the matter-dominated epoch, using $H = \frac{2}{3t}$ and $\bar{\rho} = 3M_P^2 H^2 \approx \bar{\rho}_m$, eq. (3.12) becomes

$$\ddot{\delta}_m + \frac{4\dot{\delta}_m}{3t} - \frac{2\delta_m}{3t^2} = 0 \, . \tag{3.15}$$

With a power-law ansatz, $\delta_m \propto t^p$, it is easy to see that the growing mode solution of eq. (3.15) has $p = \frac{2}{3}$. Therefore, we see that during matter domination the dark matter fluctuations grow proportionally to the scale factor.

Λ dominance

If dark energy is a cosmological constant, it will not cluster ($\delta_\Lambda = 0$): therefore, for adiabatic perturbations, during Λ dominance the evolution equation for δ_m on sub-Hubble scales will be the again given by eq. (3.14), but with a different Hubble rate H. Indeed, $H = \text{const.}$ for a cosmological constant, so it is easy to see that the growing mode solution for δ_m will just be $\delta_m = \text{const.}$: density perturbations stop to grow once dark energy starts to dominate.

These three results can be combined under the form of a "transfer function", $T(z, k)$, which describes how the primordial perturbations set up by inflation are post-processed: schematically, $\delta_m(z, \mathbf{k}) = T(z, k)\delta_m(+\infty, \mathbf{k})$. The transfer function $T(z, k)$ depends only on the magnitude k and not on the direction of $\mathbf{k}$, because the perturbations are evolving on a homogeneous and isotropic background. The square of the Fourier mode $\delta_m(z, \mathbf{k})$, that defines the matter power spectrum, will then be proportional to $T^2(z, k)$. We will not investigate this further in this Section, and refer to [44, §5][96, §7] for details.

3.2 RELATIVISTIC PERTURBATION THEORY

The Newtonian treatment of cosmological perturbations is inadequate on scales larger than the Hubble radius, and for relativistic fluids (like photons and neutrinos): the correct description of perturbations requires General Relativity. In this Section we will describe how one can derive the relativistic equations for a perfect fluid coupled to gravity (referring to Appendix B for the mathematical details), discuss briefly the gauge problem of cosmological perturbation theory (see [97] and references therein), and conclude with an explanation of the difference between adiabatic and isocurvature initial conditions.

3.2.1 *Einstein and fluid equations*

We will consider fluids interacting only through gravity. Therefore their energy-momentum tensors will be separately conserved. We can then focus on a single fluid plus gravity: the generalization of the equations to the case of multiple fluids is straightforward. Furthermore, until we arrive at Section 3.3.1, we will consider only perfect fluids. Calling U^μ the velocity of energy and particle transport, satisfying $U_\mu U^\mu = -1$, the stress-energy tensor $T^{\mu\nu}$ and number density current N^μ take the form

$$\boxed{\begin{aligned} N^\mu &= n U^\mu \,, \qquad (3.16a)\\ T^{\mu\nu} &= (\rho + p) U^\mu U^\nu + p g^{\mu\nu} \,. \qquad (3.16b) \end{aligned}}$$

Since the universe admits a foliation in terms of a "cosmic time" coordinate t and corresponding spacelike hypersurfaces Σ_t, an ADM decomposition of the metric is useful. The normal n^μ to the hypersurfaces of constant t will have components

$$\boxed{\begin{aligned} n^0 &= \frac{1}{N} \,, \qquad (3.17a)\\ n^i &= -\frac{N^i}{N} \,, \qquad (3.17b) \end{aligned}}$$

where N and N^i are, respectively, the lapse function and the shift vector (not to be confused with the spatial components of the number density current). The spacetime interval ds^2 is decomposed as

$$\boxed{ds^2 = -N^2 dt^2 + h_{ij}(dx^i + N^i dt)(dx^j + N^j dt) \,,} \qquad (3.18)$$

with $h_{\mu\nu} = g_{\mu\nu} + n_\mu n_\nu$ being the metric on the hypersurfaces Σ_t. Using eqs. (3.17), (3.18) it is straightforward to see that $n_\mu n^\mu = -1$.

The three-metric $h_{\mu\nu}$ and the normal one-form n_μ allow to write down a "$3+1$" decomposition of all tensorial quantities. For our purposes it will be useful to decompose the fluid four-velocity U^μ as

$$U^\mu = \gamma(n^\mu + v^\mu) \,, \qquad (3.19)$$

where $n_\mu v^\mu = 0$. The normalization condition for U^μ implies that

$$\gamma = \frac{1}{\sqrt{1 - v^2}} \,, \qquad (3.20)$$

where $v^2 \equiv h_{\mu\nu} v^\mu v^\nu$. Since we assume that $\bar{v}^\mu = 0$ (peculiar velocities decay anyway), we see that $\gamma = \mathcal{O}(2)$. From eq. (3.19) one can project the conservations of the stress-energy tensor and of the number density current along n^μ and orthogonal to it: these will yield the relativistic form of the fluid equations (energy, momentum and particle number

conservation). We refer to Appendix B for details on how to derive these equations.

The system of fluid equations must be supplemented by the Einstein equations, eq. (1.26). It is possible to write an ADM decomposition of these as well. Since the Einstein tensors has two (symmetric) slots, there are three possibilities, that we call $\parallel\parallel$, $\parallel\perp$ and $\perp\perp$:

- the projection of both indices along the normal vector n^μ ($\parallel\parallel$) gives the lapse constraint;
- the projection of one index along n^μ, and the other orthogonal to it ($\parallel\perp$), gives the shift constraint;
- the projection of both indices on the hypersurfaces of constant time ($\perp\perp$) gives the dynamical Einstein equations. These can be further decomposed in a trace part, a trace-free part and a "curl" part. The first two are obtained just by tracing $G^{\mu\nu}$ with $h_{\mu\nu}$, and by subtracting $\frac{(h^{\rho\sigma}G_{\rho\sigma})h^{\mu\nu}}{3}$ to $h^\mu{}_\rho h^\nu{}_\sigma G^{\rho\sigma}$, while the latter can be defined through the volume element $\varepsilon_{\mu\nu\rho\sigma}n^\sigma$ on Σ_t. We refer to [58, §A.1] for details: in any case, we will see that it is not necessary to consider the curl part of the $\perp\perp$ Einstein equations if we work with scalar perturbations only.

We again refer to Appendix B for details on how to decompose the Einstein equations in the $3+1$ formalism: in the next Section we will instead discuss the gauge freedom that is available in choosing the foliation and the coordinates on the surfaces of constant time.

3.2.2 *Gauge freedom and gauge fixing*

Given a foliation t of spacetime, with coordinates x^i on Σ_t, we have still the freedom of choosing another one simply by redefining $t = t' + \delta t(t', \mathbf{x}')$. As long as δt is small, the new time coordinate will still be future-directed and timelike, and then will define a new foliation of the manifold. On top of this freedom, we can choose whatever coordinate system we want on the hypersurfaces of constant time. This is nothing but the coordinate freedom of General Relativity.

For example, consider a fluid with four-velocity u^μ that satisfies $u_{[\mu}\nabla_\nu u_{\rho]} = 0$: the Frobenius theorem implies that u^μ is (at least locally) hypersurface-orthogonal [55, §B.3], i. e. that there exist a function t such that $u_\mu \propto \partial_\mu t$.[2] It is then possible to choose t as a time coordinate (so that $u_\mu \propto \delta^0_\mu$), write the four-dimensional metric in the

2 We notice that the condition of hypersurface orthogonality implies that the vorticity $\omega_{\mu\nu} = h_{[\mu}{}^\rho \nabla_\rho u_{\nu]}$ is equal to zero (the converse is not true, in general [55, §9.2]: zero vorticity implies that u^μ is hypersurface-orthogonal only if the four-acceleration $u^\nu\nabla_\nu u^\mu$ vanishes). Indeed, it is possible to show that a barotropic fluid without vorticity can always be described by a derivatively coupled scalar field ϕ [98].

form of eq. (3.18), and use the remaining freedom in the choice of the spatial coordinates on Σ_t to write h_{ij} as

$$h_{ij} = a^2 e^{2\zeta} (e^{\gamma})_{ij} \ , \tag{3.21}$$

where the matrix γ_{ij} is transverse and traceless, i. e. $\gamma_{ii} = 0$, $\partial_i \gamma_{ij} = 0$.

A different coordinate system that one can choose is *Newtonian gauge*. At linear order in perturbations, we can use the freedom of redefining the spatial coordinates to put h_{ij} in the form

$$h_{ij} = a^2 (1 - 2\Psi) \delta_{ij} \ , \tag{3.22}$$

where we have dropped the tensor modes γ_{ij}. Then, considering only scalar modes, it is possible to do a time redefinition that puts g_{0i} to 0. After these coordinate changes the metric takes the form

$$ds^2 = -(1 + 2\Phi) dt^2 + a^2 (1 - 2\Psi) \delta_{ij} dx^i dx^j \ . \tag{3.23}$$

Before proceeding, we stress the following points:

- if we consider also vector modes, g_{0i} will not be zero. However, g_{0i} is not a dynamical variable, and will be constrained to zero if the peculiar velocity v^i has only a longitudinal component (i. e. if $v^i = \partial_i v$). This is ensured by the scalar-vector-tensor (SVT) decomposition theorem, that ensures that perturbations of different helicities do not mix at linear order in perturbation theory [99, §B.2];
- in Newtonian gauge, the coordinate time is not the same as the one in the *comoving gauge* of eq. (3.21), since now U_μ will not be proportional to δ^0_μ (equivalently, v^i is not zero in this gauge).

As it is the case for all gauge theories, one must be careful to isolate physical perturbations from fictitious gauge modes: in this respect, gauge-invariant variables play a central role. At linear order in perturbation theory, these are combinations of metric and matter perturbations that do not change under a linearized coordinate redefinition, i. e.

$$x^\mu = \tilde{x}^\mu + \xi^\mu(\tilde{x}) = \tilde{x}^\mu + \xi^\mu(x) + \mathcal{O}(2) \ , \tag{3.24}$$

where ξ^μ starts at $\mathcal{O}(1)$ and ξ^i can be further decomposed in a transverse and longitudinal part. We will discuss these gauge-invariant variables in more detail in Section 4.8, when we derive the initial conditions for metric and matter perturbations that are set up from inflation. In the rest of this Chapter, we will work in a fixed gauge, and make sure that the final result of any computation is indeed an observable (this will happen, e. g., when we compute the CMB anisotropy spectrum in Section 3.3).

3.2.3 *Perturbative expansion of field equations*

We are now in the position to write down the Einstein equations and the conservation of energy-momentum in Newtonian gauge. First of all, we notice that the trace-free part of the $\perp\perp$ projection of Einstein equations implies that, in absence of anisotropic stresses, the two potentials Φ and Ψ are equal. The remaining equations are:

LAPSE CONSTRAINT

$$\frac{\delta\rho}{2M_P^2} = \frac{\partial^2\Phi}{a^2} - 3H(\dot{\Phi} + H\Phi) \ . \tag{3.25}$$

SHIFT CONSTRAINT With $v^i = \partial_i v$, it is given by

$$\dot{\Phi} + H\Phi = -\frac{a^2(\bar{\rho} + \bar{p})v}{2M_P^2} \ . \tag{3.26}$$

TRACE PART OF $\perp\perp$ EINSTEIN EQUATIONS

$$\frac{\delta p}{2M_P^2} = 3H^2\Phi + 4H\dot{\Phi} + 2\dot{H}\Phi + \ddot{\Phi} \ . \tag{3.27}$$

ENERGY CONSERVATION Assuming an equation of state w for the background and a speed of sound c_s^2 for perturbations, and working in conformal time η, it is given by

$$\delta' = -(1+w)(\theta - 3\Phi') - 3\mathcal{H}\delta(c_s^2 - w) \ , \tag{3.28}$$

where we defined $\mathcal{H} \equiv aH$, $\theta \equiv a\partial^2 v$.

DIVERGENCE OF EULER EQUATION Contracting the spatial components of $\nabla_\mu T^{\mu\nu}$ with ∂_i gives

$$0 = \frac{w'\theta}{1+w} + \partial^2\Phi + \theta' + \frac{c_s^2\partial^2\delta}{1+w} + \mathcal{H}(1-3w)\theta \ . \tag{3.29}$$

3.2.4 *Adiabatic and isocurvature perturbations*

We conclude this Section with a discussion of the initial conditions for the Einstein and conservation equations, in the case of multiple matter species. These are given for $\eta \to 0$, i.e. when all the modes of observational interest were outside of the horizon. We will see in Section 4.8 that inflation sets up the initial conditions for the Newtonian potential Φ. Therefore, the super-horizon limit of eq. (3.25) can be used to read off the initial condition for the density contrast δ (after using the Friedmann equation eq. (1.31a) to rewrite $\delta\rho$ in terms of δ and H). However, things are more complicated in the presence of more than one matter species, because Φ is sourced by all components: in this case, the differences between the density perturbations of various species must be also provided as initial condition. One can then distinguish two cases:

ADIABATIC INITIAL CONDITIONS These initial conditions satisfy

$$S_{i,j} \equiv \frac{\delta_i}{1+w_i} - \frac{\delta_j}{1+w_j} = 0 \;\forall\, i,j \;. \tag{3.30}$$

ISOCURVATURE INITIAL CONDITIONS They are simply defined by having a non-zero $S_{i,j}$.

In the rest of this work, we will consider only adiabatic initial conditions: current data are consistent with this assumption, and in single-field inflation only this kind of perturbations are excited. To see this, we can look at the reheating process: the inflaton ϕ must be coupled to the Standard Model if we want it to decay, inflation to end, and the radiation-dominated epoch to begin. Consider the hypersurfaces of constant inflaton, $\phi = \bar{\phi}(t)$. Given a Standard Model particle χ_i, and a rate $\Gamma_i(\phi)$ for the process $\phi \to \chi_i\chi_i$. Once $\Gamma_i(\phi)$ becomes comparable to the Hubble rate (i. e. on the *reheating surface*), the inflaton decays in χ_i. The relic density of the particle i will be fixed by the decay rate, which in turn is only a function of the inflaton v.e.v. Therefore, in this gauge there will be no density perturbations at the end of inflation. In a general gauge, where the inflaton perturbations are restored by a time shift

$$t = \tilde{t} + \delta t = \tilde{t} + \frac{\delta\phi}{\dot{\bar{\phi}}} \;, \tag{3.31}$$

the densities of the various species i will be determined by

$$\bar{\rho}_i(t) = \bar{\rho}_i(\tilde{t} + \delta t) = \bar{\rho}_i(\tilde{t}) + \dot{\bar{\rho}}_i(\tilde{t})\delta t \;\forall\, i \;, \tag{3.32}$$

so that eq. (3.30) is automatically satisfied. In passing, we notice that if there are other fields active during inflation that can decay into the Standard Model, the picture above will not hold and isocurvature perturbations can be generated (we refer to [73, §14] and references therein for details).

3.3 CMB ANISOTROPIES

We are now in the position to discuss how the CMB temperature anisotropies that we observe today in the sky are generated. A full treatment would require writing down the collisional Boltzmann equations for photons, electrons+baryons, and dark matter in a perturbed universe, expand them up to first order in small fluctuations around the FLRW background, and solve the coupled system of PDEs. For a single species, we can write the Boltzmann equation as

$$\boxed{\frac{Df}{d\lambda} = p^\mu \frac{\partial f}{\partial x^\mu} + \frac{DE}{d\lambda}\frac{\partial f}{\partial E} + \frac{Dl^\mu}{d\lambda}\frac{\partial f}{\partial l^\mu} = C[f] \;,} \tag{3.33}$$

where λ is an affine parameter along the particle trajectory such that P^μ is the four-momentum of the particle. As we discussed in Section 3.2.1, we have decomposed the four-momentum as

$$P^\mu = E(n^\mu + l^\mu) \,, \tag{3.34}$$

with $n_\mu l^\mu = 0$, and $h_{\mu\nu} l^\mu l^\nu$ is fixed by the on-shell condition $P^\mu P_\mu = -m^2$. Therefore, the distribution function is naturally a function of E and l^μ. For $C[f] = 0$ (i. e. in absence of collisions) the particles follow geodesics, $P^\nu \nabla_\nu P^\mu = 0$: from the geodesic equation, it is then possible to derive the evolution of the energy ($\frac{DE}{d\lambda}$) and the three-momentum ($\frac{Dl^\mu}{d\lambda}$), and from them obtain the evolution of the distribution function (see [58, §4] and Section 3.3.2 for details). Eq. (3.33) is the Boltzmann equation for a single particle species, with distribution function f: different species will be coupled directly via the collision term $C[f_1, \dots]$, and indirectly by gravity.

However, we will proceed in a different way. As we have seen in Section 2.1.1, we can take moments of the Boltzmann equations:

- for dark matter, we can neglect all moments beyond the zeroth and the first one. Higher moments will be suppressed by powers of $\langle \frac{p}{E} \rangle \sim \frac{T}{m}$, that is very small for cold dark matter. Besides, we assume that dark matter is collision-less, i. e. that it interacts with other species only through gravity. Therefore we can set to zero the right-hand side of eq. (3.33). The result is that the relevant equations for dark matter perturbations are just the relativistic form of the continuity and Euler equation (with zero speed of sound); [3]

- baryons and electrons are effectively combined in a single fluid thanks to Coulomb scattering. In turn, Compton scattering tightly couples electrons to photons. Therefore, we effectively end up with a photon-electron-baryon perfect fluid, where the higher moments of the photon distribution function beyond the monopole (i. e. the energy density of the fluid) and the dipole (i. e. the fluid velocity) are suppressed by the photon mean free path $t_T = (\sigma_T n_e)^{-1}$. Indeed, consider a point in space: photons arriving to it from different directions last-scattered off very nearby electrons if Compton scattering is efficient (i. e. the photon mean free path is very small). These nearby electrons most likely had a temperature very similar to the point of observation. Therefore, photons from all directions have the same temperature: this means that only the monopole of the distribution is

3 This is not exactly true [100]: also in the case of dark matter there will be viscous corrections, and a non-zero speed of sound will be generated by non-linearities. The higher moments in the Boltzmann hierarchy, in this case, will be suppressed not because of the strength of interactions (as it happens for photons+electrons+baryons, where t_T/H^{-1} is very small) but because dark matter particles could have moved only for a finite distance given the finite age of the Universe.

relevant. In the presence of a bulk velocity of the electron-baryon fluid, the same argument will hold once we go to the electron-baryon fluid rest frame. However, it is important to stress that this is just an approximation: the non-zero photon mean free path will lead to corrections to the perfect fluid behavior, encoded in *viscous coefficients* that modify the stress-energy tensor from its perfect fluid form, can make the velocity of energy transport differ from that of particle number transport, etc. (see also [101, §6, §7, §B.10] for some analytical work emphasizing the fluid dynamic approach);

- photons, electrons and baryons are tightly coupled until recombination. Then photons decouple from electrons and baryons, which in turn fall into the dark matter potential wells, and free-stream to us: the photon distribution function will just follow the collision-less Boltzmann equation in a perturbed universe, as the photons travel from the last-scattering surface to us (of course, reionization around $z \approx 6$ and any other process that re-couples photons to free electrons must be also taken into account. We will not go into the details of these effects in this Section: we refer to [73, §9.2.3][96, §8.7.2] for details).

Therefore, we have the following picture: up until recombination, we can solve the coupled Einstein and fluid equations for dark matter and photons+electrons+baryons (Section 3.3.1). At decoupling, we just follow the perturbations of the photon distribution function through the collision-less Boltzmann equation up to the observation point, deriving the expression for the CMB temperature anisotropies that we see in the sky today (Section 3.3.2). The two-fluid approximation of Section 3.3.1 is based on [92][99, §3.3.3], while more general references for both Sections 3.3.1 and 3.3.2 are [96, §7, §8][102, §9, §10].

3.3.1 *Two-fluid approximation*

As we have discussed above, we need to solve the fluid and Einstein equations of Section 3.2.3 for the dark matter perturbations (subscript: cdm) and the photon-electron-baryon fluid (subscript: bγ). If we define the "baryon loading" $R \equiv \frac{3\bar{\rho}_b}{4\bar{\rho}_\gamma}$, it is straightforward to see that for adiabatic perturbations we have

$$w_{b\gamma} = \frac{1}{3+4R}\,, \tag{3.35a}$$

$$c^2_{s,b\gamma} = \frac{1}{3(1+R)}\,, \tag{3.35b}$$

while $w_{cdm} = 0$ and $c^2_{s,cdm} = 0$ are both equal to zero. If we furthermore define $u \equiv \theta/k$ in eqs. (3.28), (3.29) and use the adiabatic relation

between δ_b and δ_γ, we see that the system of equations for δ_γ and $u_{b\gamma} \equiv u_\gamma$ simplify to

$$\delta'_{cdm} = -k u_{cdm} + 3\Phi' \,, \tag{3.36a}$$
$$u'_{cdm} = -\mathcal{H} u_{cdm} + k\Phi \,, \tag{3.36b}$$
$$\delta'_\gamma = -\frac{4}{3} k u_\gamma + 4\Phi' \,, \tag{3.36c}$$
$$(1+R) u'_\gamma = -R\mathcal{H} u_\gamma + \frac{1}{4} k\delta_\gamma + (1+R) k\Phi \,, \tag{3.36d}$$
$$k(\Phi' + \mathcal{H}\Phi) = \frac{a^2}{2M_P^2} \sum_{\substack{i = \\ \{cdm, b\gamma\}}} (\bar{\rho}_i + \bar{p}_i) u_i \,. \tag{3.36e}$$

where we used the shift constraint equation eq. (3.26) to close the system, following [92]. In Appendix C we solve eqs. (3.36) numerically: however, we also need the initial conditions. These are set up deeply into radiation domination, when all modes of interest were outside the horizon: by taking the $\eta \to 0$ limit of eqs. (3.36) we see that the initial conditions for the matter fluctuations are

$$\delta_\gamma = -2\Phi \,, \tag{3.37a}$$
$$\delta_{cdm} = \frac{3}{4} \delta_\gamma \,, \tag{3.37b}$$
$$u_\gamma = -\frac{1}{4} \frac{k}{\mathcal{H}} \delta_\gamma \,. \tag{3.37c}$$
$$u_{cdm} = u_\gamma \,. \tag{3.37d}$$

As we will see in Section 4.8, the initial conditions for the Newtonian potential Φ (which becomes a constant on super-horizon scales) are set up by inflation: for now we can just take the initial Φ to be equal to 1, thereby extracting the primordial perturbations from the transfer functions.

We are interested in following perturbations, more precisely the "effective temperature perturbation" $\Phi + \frac{\delta_\gamma}{4}$, up to decoupling. Indeed, as we will see in more detail in the next Section, $\Phi + \frac{\delta_\gamma}{4}$ is the local temperature perturbation minus the redshift photons suffer when climbing out from the potential well of the dark matter perturbation (Φ is negative for an overdensity, as we can see from the sub-horizon limit of eq. (3.25) after we expand it in Fourier modes). Besides, we will see that the main contribution to the temperature anisotropies we observe at a given angular scale θ comes from $\Phi(\eta_{rec}, k) + \frac{\delta_\gamma(\eta_{rec}, k)}{4}$ at $k \approx \frac{\pi}{\theta d^{co}_{rec}}$, where $d^{co}_{rec} = \eta_0 - \eta_{rec} \approx \eta_0$ is the comoving distance to the last-scattering surface.

While from eqs. (3.37) we see that scales that are outside the horizon at recombination are not post-processed and will mainly contain the information from inflation, for $k \gg k_{rec} \equiv \eta_{rec}^{-1}$ we can try to get some

insight from Newtonian perturbation theory. Plugging eq. (3.36d) into the time derivative of eq. (3.36c), we obtain

$$\delta_\gamma'' = 4\Phi'' + 4R c_{s,b\gamma}^2 k\mathcal{H} u_\gamma - c_{s,b\gamma}^2 k^2 \delta_\gamma - \frac{4}{3}k^2\Phi \ . \tag{3.38}$$

On sub-horizon scales we can drop $k\mathcal{H}u_\gamma$. Besides, since recombination happens during matter dominance, Φ'' will be negligible for adiabatic perturbations: indeed, when a single species with constant equation of state w dominates the energy and pressure budget of the universe, combining eqs. (3.25), (3.27) leads to

$$0 = \Phi'' + 3(1+w)\mathcal{H}\Phi' + wk^2\Phi \ . \tag{3.39}$$

For $w = 0$, the growing-mode solution for the potential is $\Phi = \text{const.}$ If we further consider a constant speed of sound, we see that the equation for δ_γ is that of a forced harmonic oscillator with frequency $\omega^2 = c_{s,b\gamma}^2 k^2$, i. e.

$$\boxed{\delta_\gamma'' + c_{s,b\gamma}^2 k^2 \delta_\gamma = -\frac{4}{3}k^2\Phi \ .} \tag{3.40}$$

Taking the $\eta \to 0$ limit and imposing that $\delta_\gamma \to -2\Phi = \text{const.}$ selects only the cosine solution (this limit is not mathematically consistent with the approximations used to arrive at eq. (3.40), but it gets the right initial conditions for δ_γ). We also see that the effect of baryons (via R) is to shift the equilibrium point of the oscillations of $\Phi + \frac{\delta_\gamma}{4}$ by $-R\Phi$. In an expanding universe, $c_{s,b\gamma}^2$ will be slowly-varying: the WKB approximation can then be used to show that

$$\frac{\delta_\gamma(\eta, k)}{4} + (1+R)\Phi(\eta, k) \propto \cos k r_s \ , \tag{3.41}$$

where the *sound horizon* $r_s(\eta)$ is given by

$$r_s(\eta) = \int_0^\eta d\eta' \, c_{s,b\gamma}(\eta') \ . \tag{3.42}$$

Other corrections will come from the fact that the potential Φ also evolves, especially at the earlier times when radiation dominates the expansion rate (e. g. this will affect the proportionality factor of eq. (3.41), for sub-horizon modes). However, the qualitative result of an *acoustic oscillation* of $\Phi + \frac{\delta_\gamma}{4}$, and the shift of its equilibrium point by baryons, remains:

- the photon-electron-baryon fluid is attracted by the gravitational potential sourced by dark matter, reaching the maximum compression. The photon pressure, then, pushes the fluid out from the potential well, reaching its maximum decompression. These oscillations continue until recombination;

- the shifting of the equilibrium point due to $R \neq 0$ has significant phenomenological consequences. In fact, this shift breaks the oscillations symmetry, with baryons enhancing the compression phase into potential wells;
- we see that the typical angular scale of variation of CMB temperature anisotropies in the sky is $\theta \sim \frac{r_s(\eta_{rec})}{\eta_0} \sim \frac{\eta_{rec}}{\eta_0}$.

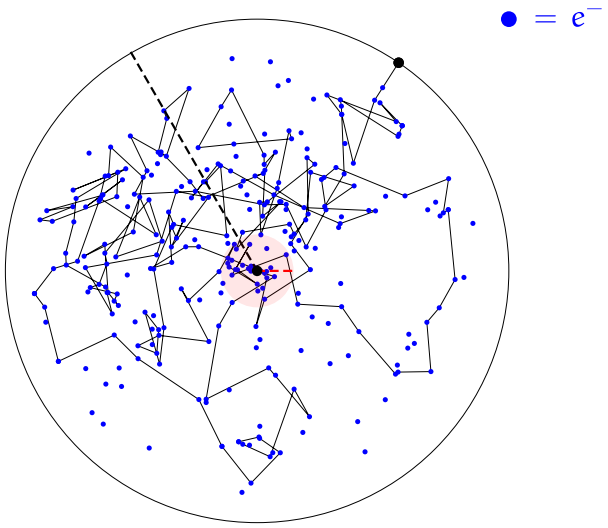

FIGURE 3.1: Free motion of photons in space washes out inhomogeneities in their spatial distribution. The flux of photons from an overdense region is higher than that from an underdense one, so the free motion smoothes out the density contrast. This is a kinematic effect, whose spatial scale (the *Silk damping* scale) is determined by the distance that photons travel in characteristic time (i. e. the Hubble time in a cosmological context). Perturbations of wavelength shorter than this length are suppressed.

By assuming perfect tight coupling, i. e. a mean free path of photons equal to zero, the above solutions are still missing some important physics: the approximation of the photons and electrons and baryons moving together as a single fluid is just an approximation. It is valid only if the scattering rate of photons off electrons is infinite. Of course this condition is not met: photons travel a finite distance in between scatters (see fig. 3.1), given by the mean free path $\lambda_{mpf} = t_T = (\sigma_T n_e)^{-1}$. If the density of electrons is very large, then the mean free path is correspondingly small. In the course of a Hubble time, the number of photon scatterings is $\sigma_T n_e H^{-1}$, and each scatter contributes to the random walk of the photon. The total distance traveled in the course of a random walk is the mean free path times the

square root of the total number of steps. Therefore, in a Hubble time a cosmological photon moves a mean distance

$$\lambda_D \sim \lambda_{mfp}\sqrt{\frac{\sigma_T n_e}{H}} = \frac{1}{\sqrt{\sigma_T n_e H}} \,. \tag{3.43}$$

Any perturbation on scales smaller than λ_D can be expected to be washed out. In Fourier space this will correspond to damping of all modes with $k \gtrsim \lambda_D^{-1}$: more precisely, in eq. (3.41), the effective temperature perturbation (and δ_γ, u_γ themselves) will be damped by a factor

$$\delta_\gamma(\eta, k) \propto e^{-\frac{k^2}{k_D^2}} \cos k r_s \,, \tag{3.44}$$

where we defined k_D as [96, §8.4][103–105][4]

$$k_D^2(\eta) \equiv \int_0^\eta \frac{d\eta'}{a(\eta')} \frac{1}{6(1+R)\sigma_T n_e}\left(\frac{R^2}{1+R} + \frac{8}{9}\right) . \tag{3.45}$$

Putting aside factors of order unity, eq. (3.45) says that $1/k_D \sim \sqrt{\eta t_T/a}$, which agrees with the estimate of eq. (3.43). This result for the damping of short-scale modes (the so-called "Silk damping") follows directly by writing down the full Boltzmann hierarchy, expanded in the limit of small λ_{mpf}. In the fluid approximation this amounts to adding viscous corrections to the number density current and the stress-energy tensor: for example, the stress-energy tensor of a perfect fluid would get a correction $\Delta T_{\mu\nu}$ parameterized as (we refer to [93][101, §6, §7, §B.10][107, §7.4.1] for details)

$$\begin{aligned}\Delta T_{\mu\nu} = &-2\eta\left\{\nabla_{(\mu}u_{\nu)} + u_{(\mu}u^\lambda \nabla_{|\lambda|}u_{\nu)}\right\} \\ &+ \left(\frac{2\eta}{3} - \zeta\right)(\nabla_\lambda u^\lambda)(g_{\mu\nu} + u_\mu u_\nu) + \mathcal{O}(\nabla^2) \,,\end{aligned} \tag{3.46}$$

where η and ζ are the shear viscosity and bulk viscosity, respectively. However we stress that, as in any Effective Field Theory expansion, the expression for the viscous coefficients in terms of t_T can be derived only by matching with the microscopic theory (i. e. the the Boltzmann hierarchy itself, in this case).

We are now in the position of solving eqs. (3.36), (3.37) numerically, following [92]. The details are spelled out in Appendix C: here we stress that we assume $\Lambda = 0$, so that the background evolution is dictated only by matter and radiation, and can be solved analytically [44, §5.2.3]. Fig. 3.2 shows the sources $\Phi + \frac{\delta_\gamma}{4}$ and u_γ evaluated at recombination, for varying wavenumber k: we see that the behavior discussed above is reproduced by the numerical solution.

4 Taking into account photon polarization, the factor $\frac{8}{9}$ is replaced by $\frac{16}{15}$ [106].

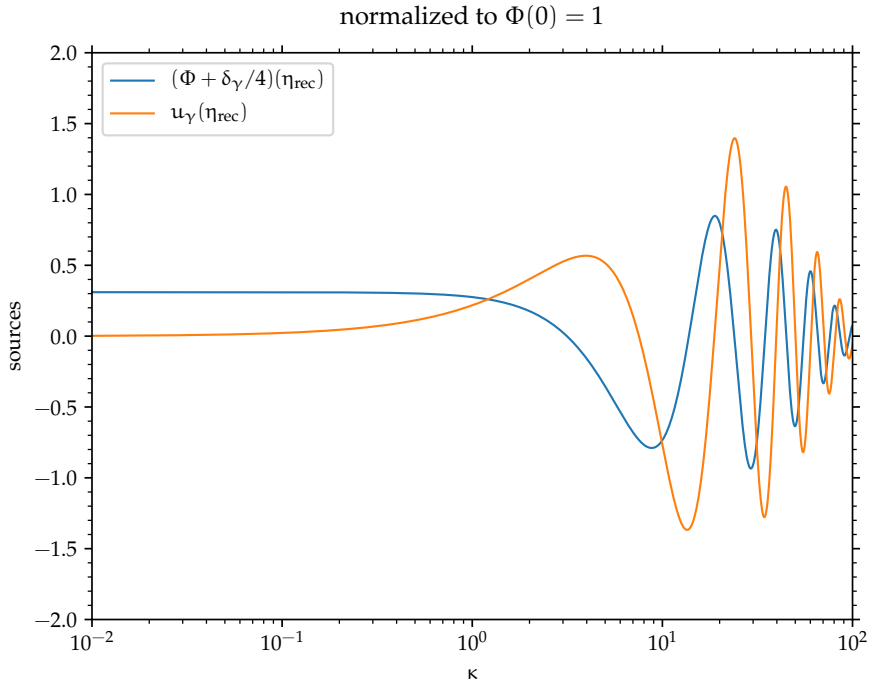

FIGURE 3.2: Photon perturbations at $\eta = \eta_{\rm rec}$, for varying k, assuming $\Lambda = 0$, $\Omega_m h^2 = 0.13$, $\Omega_b h^2 = 0.02$ and $a_{\rm rec} = 1100$. We defined $\kappa \equiv k\eta_r$, where $\eta_r \equiv (4a_{\rm rec}/\Omega_m H_0^2)^{1/2} \approx 501.4\,{\rm Mpc}$ is the would-be conformal time at recombination if there had been only matter dominance after the Big Bang (we refer to Appendix C for details). The Newtonian potential Φ has been set to 1 for $\eta \to 0$ (i. e. deeply into radiation dominance).

3.3.2 *Free-streaming after decoupling*

As we discussed in the previous Section, after decoupling we can follow photon perturbations from the last-scattering surface to us using the collision-less Boltzmann equation. Several comments are in order:

- we can parameterize the photon momentum in eq. (3.33) as $P^\mu = E(n^\mu + l^\mu)$, where n^μ is the normal to the surfaces of constant time in Newtonian gauge (see the discussion at the beginning of Section 3.2.1), $n_\mu l^\mu = 0$, and the on-shell condition implies that

$$h_{\mu\nu} l^\mu l^\nu = 1 \,, \tag{3.47a}$$

$$E^2 = h_{\mu\nu} P^\mu P^\nu \equiv p^2 \,; \tag{3.47b}$$

- the photon phase-space distribution function has the black-body form, i. e. (we will often suppress the arguments for simplicity of notation)

$$f = \frac{2}{e^{\frac{E}{T}} - 1} \,, \tag{3.48}$$

where the temperature $T = \bar{T}(1+\Theta)$ depends on $x^\mu = (t, \mathbf{x})$ and $l^\mu = (0, \mathbf{l})$ *only*, and we used $g_\gamma = 2$;

- the assumption of tight coupling at recombination, i. e. the fact that the photon-baryon-electron is approximated as a perfect fluid (characterized only by energy density, pressure density and velocity), means that the temperature perturbation Θ takes the form

$$\boxed{\Theta = \frac{\delta_\gamma}{4} + l_\mu (v^\mu)_\gamma \ ,} \tag{3.49}$$

where $(v^\mu)_\gamma$ for the photon fluid is defined by eqs. (3.19), (3.20). Indeed, we can take moments of the photon distribution of eq. (3.48) in a local Lorentz frame adapted to the fluid, and see that they reproduce the definitions of Section 3.2.1 (eqs. (3.16), more precisely) for a photon fluid with density contrast δ_γ and velocity $(v^\mu)_\gamma$;

- in Newtonian gauge (restoring the potential Ψ for a moment), we can write l^i as

$$l^i = \frac{\hat{p}^i}{a(1-\Psi)} \ , \tag{3.50}$$

where $\delta_{ij}\hat{p}^i\hat{p}^j = 1$. From eq. (3.50) we have that

$$p^i = p l^i = \frac{p\hat{p}^i}{a(1-\Psi)} \ , \tag{3.51}$$

at leading order in perturbations. Recalling from eq. (3.26) that $(v^i)_\gamma = \partial_i v_\gamma$, and that (dropping for a moment the subscript γ)

$$\left.\begin{aligned} u^i &= a v^i \\ u^i &= -\frac{\partial_i u}{\sqrt{-\partial^2}} \end{aligned}\right\} \Rightarrow \theta = a\partial_i v^i = -\frac{\partial^2 u}{\sqrt{-\partial^2}} = \sqrt{-\partial^2}\, u \ , \tag{3.52}$$

or, equivalently, that

$$\left.\begin{aligned} u^i &= a v^i \\ u^i &= -i\hat{k}^i u \end{aligned}\right\} \Rightarrow \theta = a(ik^i)v^i = ku \ , \tag{3.53}$$

we have

$$l_\mu (v^\mu)_\gamma = \hat{\mathbf{p}} \cdot \mathbf{u}_\gamma + \mathcal{O}(2) \ , \tag{3.54}$$

where we used

$$l_i = a(1-\Psi)\hat{p}^i + \mathcal{O}(2) \ . \tag{3.55}$$

If we go to Fourier space, and call $\chi \equiv \hat{\mathbf{p}} \cdot \hat{\mathbf{k}}$, eq. (3.54) becomes

$$l_\mu (v^\mu)_\gamma = -i\chi u_\gamma \ . \tag{3.56}$$

We have now all the ingredients to solve the collision-less Boltzmann equation from $\eta_{\rm rec}$ to η_0. As we have seen in eq. (3.33), it is given by

$$0 = P^\mu \frac{\partial f}{\partial x^\mu} + \frac{DE}{d\lambda}\frac{\partial f}{\partial E} + \left(h^\mu{}_\nu \frac{Dl^\nu}{d\lambda}\right)\frac{\partial f}{\partial l^\mu} \,, \tag{3.57}$$

where we used the fact that only the projected part of $\frac{Dl^\mu}{d\lambda}$ will survive when contracted with $\frac{\partial f}{\partial l^\mu}$ (we refer to [58, §4][108] for a proof). The evolution equations for E and l^μ are dictated by the photon geodesic equation. The derivation of these equations is deferred to Appendix B: for now we just note that the last term on the right-hand side of eq. (3.57) will be second-order in perturbations (i. e. lensing is a second-order effect, since the photon direction l^μ is unchanged by geodesic motion in a FLRW background and the zeroth-order phase-space distribution depends only on the photon energy. Indeed, as we can see from eq. (3.49), $\frac{\partial f}{\partial l^\mu} = \mathcal{O}(1)$). If we further use the fact that eq. (3.57) is linear in f, it is straightforward to arrive at two equations for $\bar{T}$ and Θ only, i. e.

$$\frac{d\log \bar{T}}{dt} = -H \,, \tag{3.58a}$$

$$0 = \dot{\Theta} + \frac{\hat{p}^i}{a}\partial_i\Theta - \dot{\Psi} + \frac{\hat{p}^i}{a}\partial_i\Phi \,. \tag{3.58b}$$

Eq. (3.58a) is self-explanatory. Going to conformal time, eq. (3.58b) becomes

$$0 = \Theta' + \hat{p}^i\partial_i\Theta - \Psi' - \Phi' + \Phi' + \hat{p}^i\partial_i\Phi \,, \tag{3.59}$$

which, using the method of characteristics, is solved by

$$\begin{aligned}(\Theta+\Phi)(\eta,\mathbf{x},\hat{\mathbf{p}}) = {}& (\Theta+\Phi)(\eta_{\rm rec},\mathbf{x}-\hat{\mathbf{p}}\Delta\eta,\hat{\mathbf{p}}) \\ & + \int_{\eta_{\rm rec}}^{\eta} d\eta'\, S_{\rm ISW}(\eta',\mathbf{x}-\hat{\mathbf{p}}\Delta\eta) \,,\end{aligned} \tag{3.60}$$

where we defined

$$\Delta\eta \equiv \eta - \eta_{\rm rec} \,, \tag{3.61a}$$

$$S_{\rm ISW}(\eta,\mathbf{x}) \equiv (\Psi'+\Phi')(\eta,\mathbf{x}) \,. \tag{3.61b}$$

Indeed, we have

$$\begin{aligned}\frac{\partial(\Theta+\Phi)(\eta,\mathbf{x},\hat{\mathbf{p}})}{\partial\eta} = {}& -\hat{p}^i \frac{\partial(\Theta+\Phi)(\eta_{\rm rec},y^i,\hat{\mathbf{p}})}{\partial y^i}\bigg|_{\mathbf{y}=\mathbf{x}-\hat{\mathbf{p}}\Delta\eta} \\ & + S_{\rm ISW}(\eta,\mathbf{x}-\hat{\mathbf{p}}\Delta\eta) \\ & - \hat{p}^i\int_{\eta_{\rm rec}}^{\eta} d\eta' \frac{S_{\rm ISW}(\eta',\mathbf{y})}{\partial y^i}\bigg|_{\mathbf{y}=\mathbf{x}-\hat{\mathbf{p}}\Delta\eta} \,,\end{aligned} \tag{3.62}$$

and

$$\begin{aligned}\hat{p}^i\frac{\partial(\Theta+\Phi)(\eta,\mathbf{x},\hat{\mathbf{p}})}{\partial x^i} = {}& \hat{p}^i \frac{\partial(\Theta+\Phi)(\eta_{\rm rec},y^i,\hat{\mathbf{p}})}{\partial y^i}\bigg|_{\mathbf{y}=\mathbf{x}-\hat{\mathbf{p}}\Delta\eta} \\ & + \hat{p}^i\int_{\eta_{\rm rec}}^{\eta} d\eta' \frac{S_{\rm ISW}(\eta',\mathbf{y})}{\partial y^i}\bigg|_{\mathbf{y}=\mathbf{x}-\hat{\mathbf{p}}\Delta\eta} \,.\end{aligned} \tag{3.63}$$

Evaluating eq. (3.60) at $\eta = \eta_0$ and restoring $\Phi = \Psi$, we see that the present temperature anisotropy $\Theta(\eta_0, \mathbf{x}, \hat{\mathbf{p}})$ is given by

$$\boxed{\begin{aligned}\Theta(\eta_0, \mathbf{x}, \hat{\mathbf{p}}) = &\left(\frac{\delta_\gamma}{4} + \Phi\right)(\eta_{\rm rec}, \mathbf{x} - \hat{\mathbf{p}}\Delta\eta_0) \\ &+ \hat{\mathbf{p}} \cdot \mathbf{u}_\gamma(\eta_{\rm rec}, \mathbf{x} - \hat{\mathbf{p}}\Delta\eta_0) \\ &+ \int_{\eta_{\rm rec}}^{\eta_0} d\eta' \, S_{\rm ISW}(\eta', \mathbf{x} - \hat{\mathbf{p}}\Delta\eta_0) \, .\end{aligned}} \tag{3.64}$$

In the left-hand side of eq. (3.64) we have put to zero two terms:

- first of all, the Newtonian potential today is unobservable (or, equivalently, only the potential difference between recombination and the observation point is a physical observable).[5] Therefore, we have absorbed $\Phi(\eta_0, \mathbf{x})$ in the average measured temperature by the observer at $(\eta_0, \mathbf{x})$;
- the second term we have put to zero is the Doppler term $\hat{\mathbf{p}} \cdot \mathbf{u}_\gamma(\eta_0, \mathbf{x})$, which is due to the motion of the observer at $(\eta_0, \mathbf{x})$ with respect to the CMB (recall eq. (3.19)). This effect results in a large dipole anisotropy, which must be taken into account when CMB data are analyzed but is not relevant for this discussion.

We see, then, how $\Theta(\eta_0, \mathbf{x}, \hat{\mathbf{p}})$ is made up of three contributions:

SACHS-WOLFE EFFECT It is the relative frequency shift of photons induced by the difference in gravitational potentials at emission (i. e. at recombination) and detection.

DOPPLER EFFECT At the last scattering epoch, the baryon-electron-photon medium moves with respect to the conformal Newtonian frame with a non-zero velocity, and this generates a Doppler shift in the photon temperature.

INTEGRATED SACHS-WOLFE EFFECT It also reflects the change of the photon frequency due to gravitational potentials, now depending on time. If a photon passes through a region with negative potential whose magnitude grows in time, it first "dives" into the potential well and then gets out from the deeper well. As a result, the photon loses energy.

Once we have the observed temperature anisotropy as a function of $\hat{\mathbf{p}}$, we can expand it in spherical harmonics $Y_{\ell m}(\hat{\mathbf{p}})$ on the sky. More precisely, given $\Theta(\eta_0, \mathbf{x}, \hat{\mathbf{p}})$ we can define its $a_{\ell m}$ spherical harmonic coefficients by

$$\Theta(\eta_0, \mathbf{x}, \hat{\mathbf{p}}) = \sum_{\ell=0}^{\infty} \sum_{m=-\ell}^{\ell} a_{\ell m}(\eta_0, \mathbf{x}) \, Y_{\ell m}(\hat{\mathbf{p}}) \, . \tag{3.65}$$

5 As always in General Relativity, only (second) derivatives of the potential can be measured by a local observer (Einstein equivalence principle).

Correspondingly, we extract the coefficients $a_{\ell m}$ by

$$a_{\ell m}(\eta_0, \mathbf{x}) = \int d\hat{\mathbf{p}}\, \Theta(\eta_0, \mathbf{x}, \hat{\mathbf{p}})\, Y^*_{\ell m}(\hat{\mathbf{p}}) \ , \tag{3.66}$$

where the integration is on the unit sphere. The coefficient for $\ell = 0$, which is just the angular average of the temperature anisotropy on the sky, can be re-absorbed in the definition of $\bar{T}(\eta_0)$. The $\ell = 1$ multipole, instead, will pick up the local Doppler term $\hat{\mathbf{p}} \cdot \mathbf{u}_\gamma(\eta_0, \mathbf{x})$ that we have discussed (and discarded) in the previous paragraph. From the $a_{\ell m}$ coefficients, then, we can define the *angular power spectrum*, i. e.

$$\langle a_{\ell m} a^*_{\ell' m'} \rangle \equiv C_\ell \delta_{\ell\ell'} \delta_{mm'} \Rightarrow C_\ell = \frac{1}{2\ell + 1} \sum_{m=-\ell}^{\ell} |a_{\ell m}|^2 \ , \tag{3.67}$$

where we assumed statistical isotropy in eq. (3.67), so that the coefficients $a_{\ell m}$ are uncorrelated at different ℓ and m. If we recall from eq. (3.64) that $\Theta(\eta_0, \mathbf{x}, \hat{\mathbf{p}})$ is a function of $\mathbf{x} - \hat{\mathbf{p}}\Delta\eta_0$, we can write it in Fourier space as

$$\Theta(\eta_0, \mathbf{x}, \hat{\mathbf{p}}) = \int \frac{d^3k}{(2\pi)^3} \Theta(\eta_0, \mathbf{k}, \hat{\mathbf{p}}) e^{i\mathbf{k}\cdot\mathbf{x}} e^{-i\mathbf{k}\cdot\hat{\mathbf{p}}\Delta\eta_0} \ , \tag{3.68}$$

where

$$\begin{aligned} \Theta(\eta_0, \mathbf{k}, \hat{\mathbf{p}}) = &\left(\frac{\delta_\gamma}{4} + \Phi \right)(\eta_{rec}, \mathbf{k}) + \hat{\mathbf{p}} \cdot \mathbf{u}_\gamma(\eta_{rec}, \mathbf{k}) \\ &+ \int_{\eta_{rec}}^{\eta_0} d\eta'\, S_{ISW}(\eta', \mathbf{k}) \ . \end{aligned} \tag{3.69}$$

Using the Rayleigh expansion of a plane wave, i. e.[6]

$$e^{-i\mathbf{k}\cdot\hat{\mathbf{p}}\Delta\eta_0} = 4\pi \sum_{\ell=0}^{+\infty} \sum_{\ell=-m}^{m} i^{-\ell} j_\ell(k\,\Delta\eta_0) Y^*_{\ell m}(\hat{\mathbf{k}}) Y_{\ell m}(\hat{\mathbf{p}}) \ , \tag{3.70}$$

and matching with eq. (3.65), one can find the expression of the $a_{\ell m}(\eta_0, \mathbf{x})$ in terms of $\Theta(\eta_0, \mathbf{k}, \hat{\mathbf{p}})$. Things are simpler for the Sachs-Wolfe (SW) and Integrated Sachs-Wolfe (ISW) effects, since for them $\Theta(\eta_0, \mathbf{k}, \hat{\mathbf{p}})$ does not depend on $\hat{\mathbf{p}}$. For the Doppler shift, some more work is needed to translate the $\hat{\mathbf{p}}$-dependence into a ℓ-dependence (we refer to [96, §8.5.1] for details: the $\hat{\mathbf{p}} \cdot \mathbf{u}_\gamma$ term gives rise to a different combination of Bessel functions $j_\ell(k\,\Delta\eta_0)$). If we focus only on the SW term for simplicity, we find

$$\begin{aligned} a_{\ell m}(\eta_0, \mathbf{x}) = 4\pi \int \frac{d^3k}{(2\pi)^3} e^{i\mathbf{k}\cdot\mathbf{x}} &\underbrace{\left(\frac{\delta_\gamma}{4} + \Phi \right)(\eta_{rec}, \mathbf{k})}_{\equiv S_{SW}(\eta_{rec}, \mathbf{k})} \\ &\times i^{-\ell} j_\ell(k\,\Delta\eta_0) Y^*_{\ell m}(\hat{\mathbf{k}}) \ , \end{aligned} \tag{3.71}$$

6 The complex conjugation between the two spherical harmonics can be interchanged.

which also defines the Fourier transform $a_{\ell m}(\eta_0, \mathbf{k})$. We can now compute the angular power spectrum: taking the ensemble average of $a_{\ell m} a^*_{\ell' m'}$ at $(\eta_0, \mathbf{x})$, we see that

$$\begin{aligned}\langle a_{\ell m} a^*_{\ell' m'} \rangle = (4\pi)^2 \int_{\mathbf{k}} \int_{\mathbf{k}'} & e^{i(\mathbf{k}-\mathbf{k}')\cdot\mathbf{x}} \\ & \times \langle S_{SW}(\eta_{rec}, \mathbf{k})\, S^*_{SW}(\eta_{rec}, \mathbf{k}') \rangle \\ & \times i^{-\ell+\ell'} j_\ell(k\,\Delta\eta_0) j_{\ell'}(k'\,\Delta\eta_0) \\ & \times Y^*_{\ell m}(\hat{\mathbf{k}}) Y_{\ell' m'}(\hat{\mathbf{k}}') \ .\end{aligned} \tag{3.72}$$

As we will see in the next Chapter, the ensemble average in eq. (3.72) is fixed by the initial conditions for the Newtonian potential Φ deep into radiation dominance, which in turn are set up by inflation. More precisely, eq. (3.44) has a proportionality factor equal to $-\frac{8}{3}\Phi_{MD}$, where Φ_{MD} is the value of the potential on super-horizon scales $k\eta \ll 1$ *during matter dominance* (when recombination happens). Indeed, we have that $\delta_\gamma = \frac{4}{3}\delta_{cdm}$ for adiabatic perturbations, and the relativistic Poisson equation eq. (3.25) tells us that $\delta_{cdm} = -2\Phi$ on super-horizon scales when dark matter fluctuations are the main source for the Newtonian potential (as it happens in the matter-dominated epoch). Thus, the normalization factor for $\delta_\gamma(\eta_{rec}, k)$ at $k\eta_{rec} \ll 1$ is fixed by

$$\frac{\delta_\gamma}{4} \to -\frac{2\Phi_{MD}}{3} \Rightarrow \Phi + \frac{\delta_\gamma}{4} \to \frac{\Phi_{MD}}{3} \ . \tag{3.73}$$

As we will see in more detail in Section 4.8, the value of Φ on super-horizon scales drops of a factor $\frac{9}{10}$ as we transition from radiation to matter dominance. Therefore, we have

$$\Phi_{MD} = \frac{9}{10}\Phi_{RD} \ . \tag{3.74}$$

Φ_{RD} was set to 1 in Section 3.3.1. We will see that it is just $-\frac{2}{3}\zeta$, where the *comoving curvature perturbation* ζ is defined during inflation by eq. (3.21) in comoving gauge. It becomes a constant on super-horizon scales: with ζ here we denote such constant value. Therefore the initial conditions for δ_γ, and the ensemble average of the $a_{\ell m}$ coefficients, are fixed by

$$\Phi_{MD} = -\frac{3}{5}\zeta \ . \tag{3.75}$$

These results are confirmed by fig. 3.2 (apart from small corrections coming from the fact that recombination does not truly happen deeply into matter dominance, and from the fact that baryons are also present): then, in order to proceed it suffices to notice that $\langle S_{SW}(\eta_{rec}, \mathbf{k})\, S^*_{SW}(\eta_{rec}, \mathbf{k}') \rangle$ will just be proportional to the *power spectrum* of ζ, i. e.

$$\begin{aligned}\langle S_{SW}(\eta_{rec}, \mathbf{k})\, S^*_{SW}(\eta_{rec}, \mathbf{k}') \rangle &\propto \langle \zeta(\mathbf{k})\, \zeta^*(\mathbf{k}') \rangle \\ &= (2\pi)^3 \delta^{(3)}(\mathbf{k}-\mathbf{k}')\, P_\zeta(k) \ ,\end{aligned} \tag{3.76}$$

where we used homogeneity and isotropy to write the two-point function of ζ in terms of its power spectrum $P_\zeta(k)$. If we call $\Delta^2_{SW}(k)$ the proportionality factor in the above equation (which, again, can depend only on k because of homogeneity and isotropy), we can write eq. (3.72) as

$$\begin{aligned}\langle a_{\ell m} a^*_{\ell' m'}\rangle = (4\pi)^2 \int_{\mathbf{k}} & \Delta^2_{SW}(k)\, P_\zeta(k) \\ & \times i^{-\ell+\ell'} j_\ell(k\Delta\eta_0) j_{\ell'}(k\Delta\eta_0) \\ & \times Y^*_{\ell m}(\hat{\mathbf{k}}) Y_{\ell' m'}(\hat{\mathbf{k}}) \ ,\end{aligned} \tag{3.77}$$

where we see that translational invariance ensures that the observed angular power spectrum does not depend on the observation point $\mathbf{x}$. If we do the angular integral in $d\hat{\mathbf{k}}$, and use the closure relation

$$\int d\hat{\mathbf{k}}\, Y^*_{\ell m}(\hat{\mathbf{k}}) Y_{\ell' m'}(\hat{\mathbf{k}}) = \delta_{\ell\ell'}\delta_{mm'} \ , \tag{3.78}$$

we arrive at

$$\boxed{C_\ell = \frac{2}{\pi}\int_0^{+\infty} dk\, k^2 \Delta^2_{SW}(k)\, P_\zeta(k)\, j^2_\ell(k\Delta\eta_0) \ .} \tag{3.79}$$

The derivation of the previous paragraph for the angular power spectrum, eq. (3.79), can be carried out for the full combination of SW, Doppler and ISW effects of eq. (3.64). When computing the C_ℓ coefficients, there will be cross-terms between the different source functions. E. g., the Sachs-Wolfe and the Doppler terms are out of phase with one another (see fig. 3.2): at the places where the monopole contributes least to the anisotropies, at its troughs, the dipole contributes the most. This means that the dipole is not as important in the power spectrum as one might naively think, since it adds incoherently to the monopole. Among other effects that are not considered by eq. (3.79), we have:

- we have approximated photon decoupling as instantaneous, but (as we have seen in Section 2.1.4) photon decoupling takes quite a long time. This prevents us from seeing very small scales in the CMB anisotropy spectrum. More precisely, instead of considering as initial conditions for the free-streaming evolution the photon monopole and dipole just at $\eta = \eta_{rec}$, the sources $\Phi(\eta_{rec})$, $\delta_\gamma(\eta_{rec})$ and $u_\gamma(\eta_{rec})$ must be replaced with a convolution over the photon visibility function, which gives the probability that a photon last-scatters at a redshift η. As a result, the C_ℓ coefficients get a suppression $\sim \exp(-\ell^2/\Delta\ell^2)$, where $\Delta\ell \approx 2800$. We refer to [73, §9.3] for a more detailed analysis: in Section 3.3.1 and Appendix C we added a fudge factor directly in the sources, following [92];

- at reionization, the light from the first stars, quasars and dwarf galaxies makes our Universe less transparent to CMB photons.

The density of free electrons become sizable again, and the probability for a photon to "live through" the reionization epoch (starting at t_{rei}) is $\exp(-\tau_{rei})$, where the optical depth of reionization is given by

$$\tau_{rei} = \int_{t_{rei}}^{t_0} dt\, \sigma_T n_e \ , \tag{3.80}$$

with the integration being performed along the photon worldline. Photons that rescatter at $z = z_{rei}$ at given place in the Universe have last scattered at recombination anywhere on a sphere of coordinate radius $\eta_{rei} - \eta_{rec} \approx \eta_{rei}$. Since the direction of photon propagation changes randomly, photons coming to an observer from a given direction gather from the whole of that sphere. Hence, the contribution of rescattered photons to anisotropy at angular scales smaller than $\Delta\theta_{rei} = \frac{\eta_{rei}}{\eta_0}$ is washed out, and the remaining anisotropy is due to photons that have not rescattered. On the other hand, the anisotropy at angular scales larger than $\Delta\theta_{rei}$ remains intact, since the regions of the coordinate size η_{rei} at recombination are not resolved at these angular scales. At the level of the angular power spectrum, this implies a suppression of the C_ℓ coefficients by $\exp(-2\tau_{rei})$ for $\ell > \frac{\pi\eta_0}{\eta_{rei}}$;

- we have not included (massive) neutrinos in the computation of the sources in Section 3.3.1. The effective number of neutrino species and the neutrino mass have an important impact on CMB anisotropies, and are one of the most important targets of upcoming experiments (we refer to [109–114] and references therein for details).

Current codes, like CAMB, take all these effects into account, in addition to solving the Boltzmann hierarchy to higher order in moments (i.e. beyond the monopole and the dipole): in fig. 3.3 we show the temperature angular power spectrum as a function of ℓ, computed by CAMB, for the Planck best-fit cosmological parameters [6].

3.3.3 *CMB polarization*

We conclude this Section with a word on polarization. One would expect the polarizations of the CMB photons to be completely random: however, a net linear polarization is induced by Thomson scattering between photons and free electrons, either at decoupling or during a later epoch of reionization, if the incoming radiation field has a quadrupole component [96, §10.5, §10.6]. In the case of isotropic (in the rest frame of the electron) incoming radiation, the outgoing radiation remains unpolarized: this is because orthogonal polarization directions cancel out [115, 116].

How does one characterize these fluctuations in the photon polarization? Polarization is not a scalar field, so the standard expansion

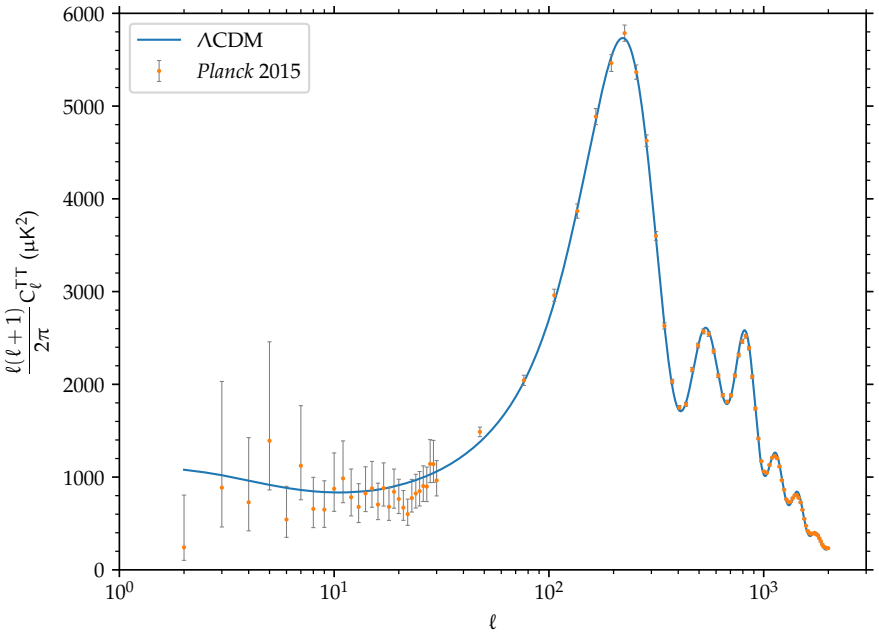

FIGURE 3.3: The blue curve shows the angular power spectrum C_ℓ^{TT} of temperature anisotropies for the Planck best-fit cosmological parameters [6], while the orange points (with gray lines) show Planck data points and errors. Errors become larger at small ℓ because of cosmic variance. Since the ensemble average over different universes that appears in the definition of the C_ℓ coefficients cannot (for obvious reasons) be taken, we construct an estimator $\hat{C}_\ell$ of the C_ℓ, defined as

$$\hat{C}_\ell \equiv \frac{1}{2\ell+1} \sum_{m=-\ell}^{\ell} |a_{\ell m}|^2 \ .$$

The expected squared difference between $\hat{C}_\ell$ and C_ℓ is the cosmic variance, and for Gaussian anisotropies is equal to

$$\langle (\hat{C}_\ell - C_\ell)^2 \rangle = \frac{2C_\ell^2}{2\ell+1} \ .$$

Therefore, at large angular scales we do not have many different regions (that we assume are corresponding to different realizations of the underlying stochastic field: *ergodic hyphotesis*) over which to sample the distribution from which the $a_{\ell m}$ are drawn, and there will be an intrinsic uncertainty in our knowledge of the C_ℓ.

in spherical harmonics does not apply. Instead, one starts from the anisotropy tensor, that is a 2×2 tensor $I_{ij}(\hat{\mathbf{p}})$ defined on the sky (the directions i and j are those orthogonal to $\hat{\mathbf{p}}$) at the observation point $(\eta_0, \mathbf{x})$. From I_{ij} one constructs:

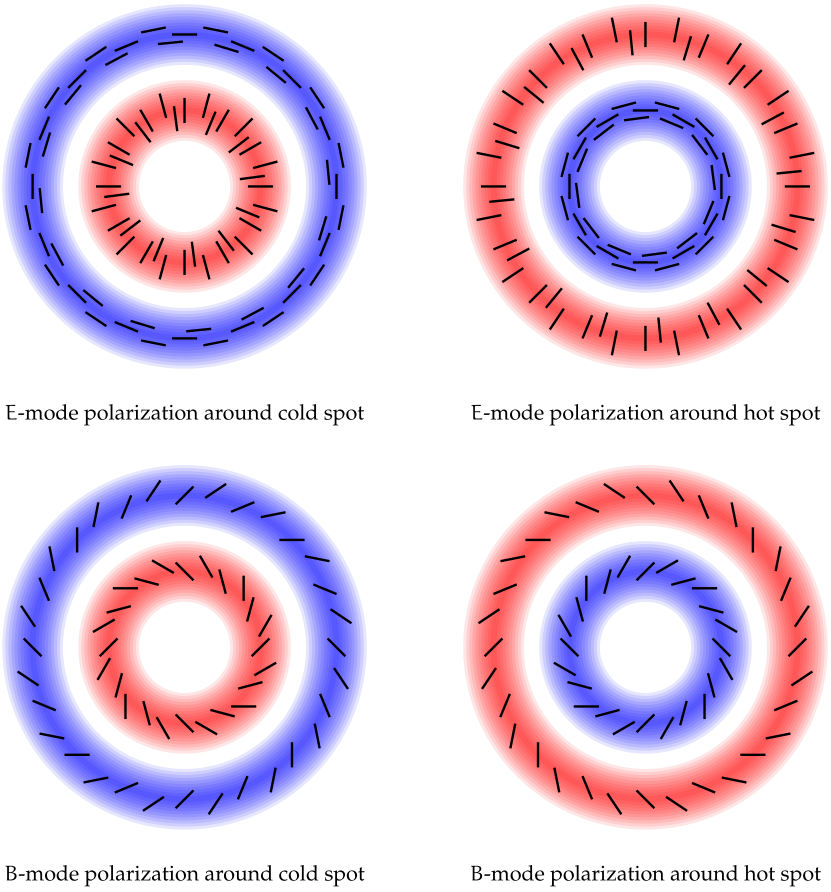

E-mode polarization around cold spot

E-mode polarization around hot spot

B-mode polarization around cold spot

B-mode polarization around hot spot

FIGURE 3.4: This figure shows how both E- and B-mode polarization patterns are rotationally-invariant, but behave differently under reflections through the plane orthogonal to $\hat{\mathbf{p}}$: the E-modes stay unchanged, while the positive and negative B-modes get interchanged. Another way to characterize them is that the E field is divergence- and curl-free (with $E < 0$ around cold spots in the sky and $E > 0$ around hot ones), contrary to the B one which is divergence-less but has vorticity different from zero at every point in the sky.

- the "Stokes parameters" Q and U, which are

$$Q = \frac{1}{4}(I_{11} - I_{22}) \,, \tag{3.81a}$$

$$U = \frac{1}{2} I_{12} \,. \tag{3.81b}$$

  These two parameters are related to the magnitude and angle of polarization through

$$P = \sqrt{Q^2 + U^2} \,, \tag{3.82a}$$

$$\alpha = \frac{1}{2} \arg(Q + iU) \,; \tag{3.82b}$$

- the scalar (spin-0) $\frac{1}{4}(I_{11} + I_{22})$, which is nothing but the temperature anisotropy itself.

Since the spin-2 fields Q and U are not invariant under rotations in the plane perpendicular to $\hat{\mathbf{p}}$, they cannot be expanded as in eq. (3.65): the spin-2 spherical harmonics $Y^{(s)}_{\ell m}$ (with $(s) = \pm$) must be used instead, leading to [117, 118]

$$Q(\hat{\mathbf{p}}) \pm iU(\hat{\mathbf{p}}) = \sum_{\ell=0}^{+\infty} \sum_{m=-\ell}^{\ell} a^{\pm}_{\ell m} Y^{\pm}_{\ell m}(\hat{\mathbf{p}}) \ . \tag{3.83}$$

The last step is the introduction of the linear combinations

$$a^{E}_{\ell m} \equiv -\frac{1}{2}(a^{+}_{\ell m} + a^{-}_{\ell m}) \ , \tag{3.84a}$$

$$a^{B}_{\ell m} \equiv -\frac{1}{2i}(a^{+}_{\ell m} - a^{-}_{\ell m}) \ , \tag{3.84b}$$

and, from there, of the spin-0 fields

$$E(\hat{\mathbf{p}}) \equiv \sum_{\ell=0}^{+\infty} \sum_{m=-\ell}^{\ell} a^{E}_{\ell m} Y_{\ell m}(\hat{\mathbf{p}}) \ , \tag{3.85a}$$

$$B(\hat{\mathbf{p}}) \equiv \sum_{\ell=0}^{+\infty} \sum_{m=-\ell}^{\ell} a^{B}_{\ell m} Y_{\ell m}(\hat{\mathbf{p}}) \ . \tag{3.85b}$$

These fields are much more convenient to use (due to their scalar nature), and completely specify the linear polarization field. The properties of E- and B-modes are illustrated in figure 3.4.

Along with the multipole moments $a_{\ell m}$ of eq. (3.65) (that from now on we will denote with $a^{T}_{\ell m}$), the coefficients $a^{E}_{\ell m}$ and $a^{B}_{\ell m}$ are everything we need to compute power spectra and cross-correlations of temperature and polarization fluctuations. The angular correlation of eq. (3.67) is then generalized to

$$\boxed{C^{XY}_{l} \equiv \frac{1}{2l+1} \sum_{m=-\ell}^{\ell} \langle a^{X}_{\ell m} (a^{Y}_{\ell m})^{*} \rangle \text{ with } X, Y = T, E, B \ .} \tag{3.86}$$

Given that both temperature and polarization anisotropies are created by primordial density fluctuations, we expect a non-zero cross-correlation XY = TE. The TB and EB cross-correlations, instead, are equal to 0 for symmetry reasons).

This decomposition in E- and B-modes is fundamental in modern cosmology, as [117, 118] (but see [96, § 10.9], also) have shown. In fact these two works have demonstrated that:

- scalar perturbations (energy density fluctuations in the plasma) can lead to a quadrupole component for the incoming radiation field. The result, though, is *only* E-*modes and no* B-*modes*;
- vector perturbations (vorticity in the plasma) also produce a quadrupole component. They create *mainly* B-*modes*, but the expansion of the universe damps vorticity so their contribution is expected to be negligible;

- tensor perturbations (gravitational waves) stretch and squeeze space in orthogonal directions. They produce *both* E- *and* B-*modes*.

The point is that *tensors generate* B-*modes where scalars do not*, so a detection of B-modes by experiments can be a sign of primordial gravitational waves generated by inflation. The problem is that polarized radiation is also emitted by electrons gyrating in the galactic magnetic field (synchrotron radiation) or by dust (aligned particles of carbon, graphite and other silicates). Besides gravitational lensing can turn E-modes in B-modes. Therefore a detection of B-mode polarization in the CMB is not automatically a "smoking gun" for inflation: one has to also take into account the contributions of these foregrounds.

We conclude this brief survey of CMB polarization with the equivalents of eq. (3.79) for XY different from TT:

- for XY = EE, TE we are considering, respectively, the angular power spectrum of the E field and the angular cross-correlations between the temperature anisotropies and E-modes. Both of them are dominated by scalar fluctuations, so one can write

$$\boxed{\begin{aligned} C_\ell^{EE} &= \frac{2}{\pi}\int dk\, k^2 \overbrace{P_\zeta(k)}^{\text{inflation}}\overbrace{\Delta_{E,\ell}(k)\Delta_{E,\ell}(k)}^{\text{transfer function}}\,, \qquad (3.87a)\\ C_\ell^{TE} &= \frac{2}{\pi}\int dk\, k^2 \underbrace{P_\zeta(k)}_{\text{inflation}}\underbrace{\Delta_{T,\ell}(k)\Delta_{E,\ell}(k)}_{\text{transfer function}}\,, \qquad (3.87b)\end{aligned}}$$

  where, in eq. (3.79), we would have defined $\Delta_{T,\ell}$ as

$$\Delta_{T,\ell}(k) \equiv \Delta_{SW}(k)\, j_\ell(k\Delta\eta_0)\ ; \qquad (3.88)$$

- for XY = BB we are studying the angular power spectrum of B-modes. The equivalent of eq. (3.79) is

$$\boxed{C_\ell^{BB} = \frac{4}{\pi}\int dk\, k^2 \underbrace{P_\gamma(k)}_{\text{inflation}}\underbrace{\Delta_{B,l}(k)\Delta_{B,l}(k)}_{\text{transfer function}}\,,} \qquad (3.89)$$

  where the power spectrum of tensor perturbations during inflation is the Fourier transform of the two-point function of the spin-2 metric perturbation γ_{ij} of eq. (3.21), computed during inflation (the overall factor of 2 with respect to eqs. (3.87) accounts for the two polarizations, + and ×, of γ_{ij}: we refer to Section 4.3 for details). Since $P_\gamma(k)$ only appears in eq. (3.89), the power spectra of B-modes is a probe of the strength of tensor perturbations.

3.4 CMB μ-DISTORTIONS FROM SILK DAMPING

We conclude this Chapter with an overview of how μ-type spectral distortions from Silk damping are generated. The physical picture

is that dissipation erases all sound waves on small scales and homogeneously redistributes their energy, hence heating the photons and generating a μ-distortion. In Section 2.3.4 we have seen how (recalling that $\frac{3}{\kappa^c} \approx 1.4$)

$$\mu_0 = \frac{3}{\kappa^c}\int_0^{z_{DC}} dz\, \frac{d(Q_e^*/\rho_\gamma)}{dz}\, \Theta(z - z_K)\ , \tag{3.90}$$

where $z_{DC} = 2\times 10^6$, $z_K = 5\times 10^4$ and we have approximated the μ-distortion visibility function of eq. (2.75b) as a simple Theta function, i. e. $\mathcal{J}_\mu(z,0) = \Theta(z_{DC} - z)$. Therefore we only need to compute the rate of heating $Q_e^* \equiv Q$, and we will have an expression for the chemical potential $\mu_0 \equiv \mu$.

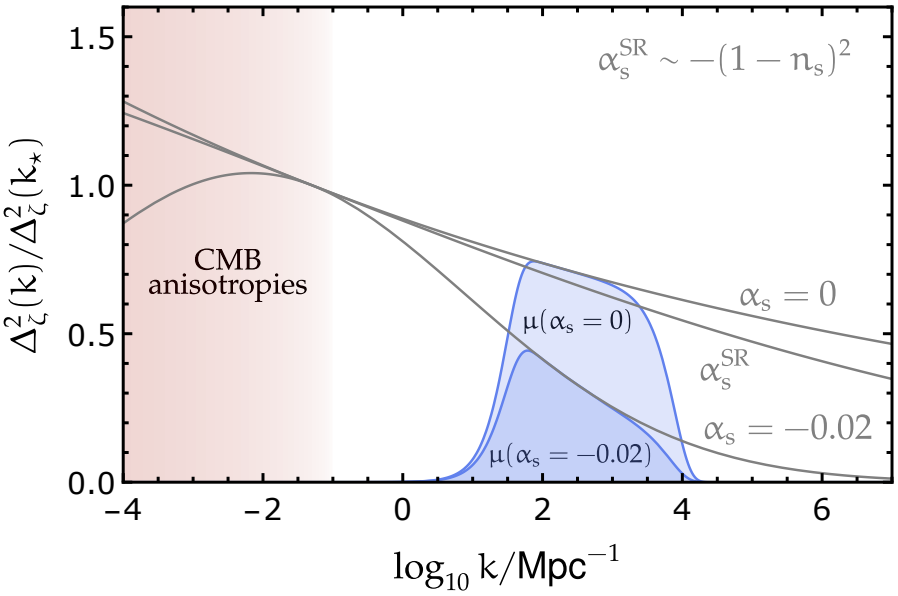

FIGURE 3.5: The average μ-distortion seen in the sky is a direct probe of the power spectrum of scalar perturbations during inflation on scales complementary to those probed by the CMB, as we see from eq. (3.101). The dimensionless power spectrum $\Delta^2_\zeta(k)$ is usually parameterized as a power-law, i. e.

$$\Delta^2_\zeta(k) = A_s\left(\frac{k}{k_\star}\right)^{n_s - 1 + \alpha_s \log\frac{k}{k_\star}}\ ,$$

where $k_\star$ (fixed to $5\times 10^{-2}\,\mathrm{Mpc}^{-1}$ in the plot), n_s is the "tilt" ($n_s \approx 0.96$ from Planck data [6]) and α_s is the "running" (which slow-roll inflation predicts to be $\alpha_s^{SR} \sim -(1-n_s)^2$). From the plot we see that μ is very sensitive to the running α_s.

In flat space, the energy of a wave δ is [93]

$$Q(\eta, \mathbf{x}) = \bar\rho \frac{c_s^2}{1+c_s^2}\,\langle \delta^2(\eta,\mathbf{x})\rangle_p\ , \tag{3.91}$$

where $\langle\ldots\rangle_p$ denotes an average over the period of oscillation. Since large-scale perturbations do not dissipate anyway, we can extend

this flat-space result to a perturbed FLRW universe. Besides, we will neglect the effect of baryons in the following (referring to [93] for a more detailed treatment): therefore, the overall relativistic factor $c_{s,\gamma}^2/(1+c_{s,\gamma}^2)$ of eq. (3.91) is

$$\frac{c_{s,\gamma}^2}{1+c_{s,\gamma}^2} \approx \frac{1}{4} \,, \tag{3.92}$$

for $c_{s,\gamma}^2 \approx w_\gamma = \frac{1}{3}$. Now, we know from Section 3.3.1 that acoustic waves δ_γ in the photon-electron-baryon fluid oscillate according to

$$\delta_\gamma(\eta, k) \sim \cos k r_s \,, \tag{3.93}$$

where $r_s(\eta)$ is defined in eq. (3.42). However, while in Section 3.3.1 we were focusing on acoustic oscillations in the matter-dominated epoch, μ-distortions are created deeply into radiation dominance. For this reason, we must be careful about the normalization of δ_γ. During radiation domination, the Newtonian potential obeys eq. (3.39) with $w_\gamma = 1/3$. Imposing $\Phi \to \Phi_{RD} = -\frac{2}{3}\zeta$ on super-horizon scales, we have

$$\Phi(\eta, k) = -2\zeta(k)\frac{j_1(kr_s)}{kr_s} \,. \tag{3.94}$$

If we use the Poisson equation eq. (3.25) with $\delta \approx \delta_\gamma$ during radiation domination (for adiabatic perturbations), we see that inside the horizon δ_γ oscillates around 0 with maximum amplitude 4ζ. Adding the Silk damping term, we have

$$\delta_\gamma(\eta, k) = -4\zeta(k) e^{-\frac{k^2}{k_D^2}} \cos k r_s \,, \tag{3.95}$$

where the Silk damping scale $k_D^2(\eta)$ is defined in eq. (3.45). Since the damping scale $k_D^2(\eta)$ decreases with time (indeed, we have $k_D(z) \approx 4.1(1+z)^{3/2} \times 10^{-6}\,\mathrm{Mpc}^{-1}$), the amplitude of the acoustic waves (and then their energy) is also decaying with time, so that

$$\frac{d(Q/\bar{\rho}_\gamma)}{dz} > 0 \,, \tag{3.96}$$

and we will have a positive μ-distortion. Combining eq. (3.91) with eq. (3.95), we find [20, 25]

$$\begin{aligned} \mu(z_K, x) &= 4.6 \int_{\mathbf{k}_1} \int_{\mathbf{k}_2} \zeta(k_1)\zeta(k_2) e^{i(\mathbf{k}_1+\mathbf{k}_2)\cdot\mathbf{x}} \\ &\qquad \times \langle \cos(k_1 r_s)\cos(k_2 r_s)\rangle_p \, e^{-(k_1^2+k_2^2)/k_D^2}\Big|_{z_K}^{z_{DC}} \\ &\approx \int_{\mathbf{k}_1} \int_{\mathbf{k}_2} \zeta(k_1)\zeta(k_2) W_\mu(k_1, k_2) e^{i(\mathbf{k}_1+\mathbf{k}_2)\cdot\mathbf{x}} \,, \end{aligned} \tag{3.97}$$

where we have approximated $\langle \cos(k_1 r_s)\cos(k_2 r_s)\rangle_p \approx \frac{1}{2}$ and we defined the window function $W_\mu(k_1, k_2)$ as

$$W_\mu(k_1, k_2) \equiv 2.3\, e^{-(k_1^2+k_2^2)/k_D^2}\Big|_{z_K}^{z_{DC}} \,. \tag{3.98}$$

If we write $\mu(z_K, x)$ in Fourier space, i. e.

$$\mu(z_K, k) = \int d^3x\, e^{-i\mathbf{k}\cdot\mathbf{x}} \int_{\mathbf{k}_1} \int_{\mathbf{k}_2} \zeta(k_1)\zeta(k_2) W_\mu(k_1, k_2) e^{i(\mathbf{k}_1+\mathbf{k}_2)\cdot\mathbf{x}} \,, \quad (3.99)$$

and we evolve it from z_K to $z = 0$ using the Sachs-Wolfe approximation of eq. (3.71), we see that the $a^\mu_{\ell m}$ coefficients at the observation point $(\eta_0, \mathbf{x})$ are given by

$$a^\mu_{\ell m} = 4\pi \int_{\mathbf{k}} e^{i\mathbf{k}\cdot\mathbf{x}} \mu(z_K, k) i^{-\ell} j_\ell(k\Delta\eta_0) Y^*_{\ell m}(\hat{\mathbf{k}}) \,, \quad (3.100)$$

where $\Delta\eta_0$, now, is $\eta_0 - \eta_K$. If we consider the sky average $\ell = 0$ (so that $Y^*_{\ell m}(\hat{\mathbf{k}}) = \frac{1}{4\pi}$, and take the ensemble average $\langle a^\mu_{00}\rangle$, we see that the expected value of the observed chemical potential is equal to (as expected, the dependence on the observation point $\mathbf{x}$ drops out due to translational invariance)

$$\boxed{\begin{aligned} \langle a^\mu_{00}\rangle &= \int_{\mathbf{k}_1} P_\zeta(k_1) W_\mu(k_1, k_1) j_0(0) \\ &= \int_0^{+\infty} \frac{dk}{k} \Delta^2_\zeta(k) W_\mu(k, k) \,, \end{aligned}} \quad (3.101)$$

where we defined the *dimensionless power spectrum* $\Delta^2_\zeta(k)$ as

$$\Delta^2_\zeta(k) \equiv \frac{k^3 P_\zeta(k)}{2\pi^2} \,. \quad (3.102)$$

Therefore, we see that μ is a direct probe of the power spectrum of ζ on scales between $k_D(z_K) \approx 46\,\mathrm{Mpc}^{-1}$ and $k_D(z_{DC}) \approx 1.1 \times 10^4\,\mathrm{Mpc}^{-1}$ (see fig. 3.5).

4

INITIAL CONDITIONS FROM INFLATION

CONTENTS

In this Chapter we will compute, following [18], the power spectra of primordial scalar and tensor fluctuations. Then, we will see how the super-horizon values of these perturbations act as initial conditions for the late-time evolution we studied in Chapter 3. We will conclude with a review of the phenomenological parameterizations of the primordial scalar power spectrum.

4.1 GAUGE CHOICE AND QUADRATIC ACTIONS

We will focus on single-field, slow-roll inflation. The action is that of eq. (1.51), i. e.

$$S = \frac{M_P^2}{2}\int d^4x\,\sqrt{-g}\,R - \frac{1}{2}\int d^4x\,\sqrt{-g}\,\left\{(\nabla\phi)^2 + 2V(\phi)\right\}\,. \tag{4.1}$$

How many degrees of freedom are present? The metric will contain 4 scalar perturbations (g_{00}, g_{ii}, $g_{0j} \sim \partial_j B$, $g_{ij} \sim \partial_i\partial_j E$), 2 vector perturbations (g_{0j}, with $\partial_j g_{0j} = 0$, and $g_{ij} \sim \partial_{(i}\hat{E}_{j)}$, with $\partial_i \hat{E}_i = 0$) and one transverse and traceless tensor perturbation g_{ij}. Furthermore, we will have one scalar perturbation $\delta\phi$ coming from ϕ. One vector perturbation can be set to zero by means of a coordinate change, while the shift constraint equation will enforce the second vector perturbation to zero (since there are no sources for it in the matter sector). If we choose the time coordinate so that $\delta\phi = 0$ (comoving gauge), all degrees of freedom will be contained in the metric. The ADM decomposition of the metric will read as in eq. (3.18), i. e.

$$ds^2 = -N^2dt^2 + h_{ij}(dx^i + N^i dt)(dx^j + N^j dt)\,, \tag{4.2}$$

and we can use the remaining gauge freedom to put the spatial metric in the form

$$h_{ij} = a^2 e^{2\zeta} (e^{\gamma})_{ij} \ , \tag{4.3}$$

where $\gamma_{ii} = \partial_i \gamma_{ij} = 0$. Correspondingly, the action of eq. (4.1) will be decomposed as

$$\begin{aligned} S = \frac{M_P^2}{2} \int d^4x \, N\sqrt{h} \left({}^{(3)}R + \frac{E_{ij}E^{ij} - E^2}{N^2} \right) \\ + \frac{1}{2} \int d^4x \, N\sqrt{h} \left\{ \frac{\dot{\bar{\phi}}^2}{N^2} - 2V(\bar{\phi}) \right\} \ , \end{aligned} \tag{4.4}$$

where we defined $E_{ij} \equiv NK_{ij}$ ($K_{\mu\nu}$ being the extrinsic curvature of the surfaces of constant time), $E \equiv h_{ij}K^{ij}$, and we used the $3+1$ decomposition of the Ricci scalar, which is given by [55, §E.2]

$$R = {}^{(3)}R + K_{\mu\nu}K^{\mu\nu} - K^2 + 2\nabla_\mu (Kn^\mu - A^\mu) \ , \tag{4.5}$$

with $A^\mu \equiv n^\nu \nabla_\nu n^\mu$.

The variables N and N^i are non-dynamical (their equations of motion do not involve time derivatives), so they can be integrated out to find the action for scalar and tensor fluctuations. If we are interested in up to the cubic action for ζ and γ_{ij}, we just need them at first order: in fact, the second- and third-order lapse and shift perturbations will multiply the zeroth-order lapse and shift equations, which vanish since the background solves the zeroth-order equations of motion (we refer to [119] for a proof[1]). Then, N and N^i will not contain tensor modes, since we cannot form a scalar from the transverse and traceless γ_{ij} at first order in perturbations. Using the fact that the extrinsic curvature can be written as

$$E_{ij} = \frac{\dot{h}_{ij} - 2\,{}^{(3)}\nabla_{(i}N_{j)}}{2} \ , \tag{4.6}$$

where ${}^{(3)}\nabla_i$ is the covariant derivative on surfaces of constant time and $N_i = h_{ij}N^j$, the constraint equations become

$$0 = {}^{(3)}R - 2V(\bar{\phi}) - \frac{E_{ij}E^{ij} - E^2}{N^2} - \frac{\dot{\bar{\phi}}^2}{N^2} \ , \tag{4.7a}$$

$$0 = {}^{(3)}\nabla_i \left(\frac{E^i{}_j - E\delta^i{}_j}{N} \right) . \tag{4.7b}$$

If we define

$$N = 1 + \delta N \ , \tag{4.8a}$$

$$N^i = \partial_i \psi \ , \tag{4.8b}$$

1 Actually, it is possible to prove that the solution of the constraints at order n is enough to find the action for ζ and γ_{ij} up to order $2n+1$ [65].

eqs. (4.8) are solved by

$$\delta N = \frac{\dot{\zeta}}{H} , \tag{4.9a}$$

$$\psi = -\frac{\zeta}{a^2 H} + \varepsilon_H \partial^{-2} \dot{\zeta} , \tag{4.9b}$$

where ε_H is the slow-roll parameter defined in eq. (1.55), i. e.

$$\varepsilon_H = -\frac{\dot{H}}{H^2} = \frac{\dot{\bar{\phi}}^2}{2H^2 M_P^2} . \tag{4.10}$$

After plugging eq. (4.9) in eq. (4.4), and expanding up to second order in perturbations, we can find the quadratic actions for ζ and γ. These are equal to [18]

$$\boxed{S_\zeta = M_P^2 \int d^4x \, \varepsilon_H a^3 \left\{ \dot{\zeta}^2 - a^{-2} (\partial_k \zeta)^2 \right\} ,} \tag{4.11a}$$

$$\boxed{S_\gamma = \frac{M_P^2}{8} \int d^4x \, a^3 \left\{ (\dot{\gamma}_{ij})^2 - a^{-2} (\partial_k \gamma_{ij})^2 \right\} .} \tag{4.11b}$$

We will start from the scalar action: once we have solved the equations of motion for ζ we will be able to translate the results also to γ_{ij}.

4.2 DYNAMICS OF THE SCALAR DEGREE OF FREEDOM

We start with the Fourier decomposition of the comoving curvature perturbation, that is

$$\zeta(t, \mathbf{x}) = \int \frac{d^3k}{(2\pi)^3} \zeta(t, \mathbf{k}) e^{i\mathbf{k}\cdot\mathbf{x}} . \tag{4.12}$$

From eq. (4.11a) we see that each $\zeta(t, \mathbf{k})$ is a harmonic oscillator with time dependent mass, whose equation of motion is

$$\frac{d\left(a^3 \varepsilon_H \dot{\zeta}(t, \mathbf{k})\right)}{dt} + a \varepsilon_H k^2 \zeta(t, \mathbf{k}) = 0 . \tag{4.13}$$

It is a simple matter, then, to quantize the system: we promote $\zeta(t, \mathbf{k})$ and $\dot{\zeta}(t, \mathbf{k})$ to q-numbers by writing (see [55, § 14.2] and [120, § 3.2] for a more exhaustive treatment of quantization on curved spacetimes)

$$\zeta(t, \mathbf{k}) = r_k(t) a_{\mathbf{k}} + r_k^*(t) a_{-\mathbf{k}}^\dagger , \tag{4.14}$$

where the mode functions $r_k(\eta)$ are general classical solutions of eq. (4.13). These are solutions to a second-order linear differential equation, so they will depend on two arbitrary constants of integration. In principle, these constants are fixed in the following way:

- if the operators $a_{\mathbf{k}}$ and $a_{\mathbf{k}}^\dagger$ must satisfy the standard creation and annihilation commutation relations, the mode functions will have to satisfy a particular normalization condition. For a scalar field in Minkowski spacetime this condition would be

$$r_k^* \dot{r}_k - r_k \dot{r}_k^* = -i ; \tag{4.15}$$

- the second constant is fixed by choosing a vacuum state $|0\rangle$ for the fluctuations, annihilated by all $a_{\mathbf{k}}$.

How can we proceed during inflation? By inspection of eq. (4.13) we see that for early times, when a mode of physical wavelength $a\lambda$ is well inside the horizon, the ratio of $a\lambda$ to the Hubble scale H^{-1} is very small and the mode feels like it is in a flat spacetime. So we can take as $|0\rangle$ the usual vacuum of Minkowski space for an observer in the far past. When the mode is outside the horizon during inflation, instead, the solutions of eq. (4.13) quickly become constant.

Let us see, now, what happens in de Sitter space. The action for a massless scalar s is given by

$$S = \frac{1}{2}\int_{-\infty}^{0} d\eta \int d^3x \, \frac{1}{H^2\eta^2}\left\{(s')^2 - (\partial_k s)^2\right\} , \tag{4.16}$$

and it is straightforward to show that the classical solutions $s_k^{\mathrm{cl.}}$, in this case, are given by [120, §5.4]

$$\boxed{s_k^{\mathrm{cl.}}(\eta) = \frac{H}{\sqrt{2k^3}}(1 - k\eta)e^{ik\eta} .} \tag{4.17}$$

Very late times correspond to small $|\eta|$, and we see that the mode function $s_k^{\mathrm{cl.}}$ becomes a constant in this limit. The two-point function of the massless scalar is instead given by

$$\begin{aligned}\langle s(\eta,\mathbf{k})\, s(\eta,\mathbf{k}')\rangle &= (2\pi)^3\delta(\mathbf{k}+\mathbf{k}')|s_k^{\mathrm{cl.}}(\eta)|^2 \\ &= (2\pi)^3\delta(\mathbf{k}+\mathbf{k}')\frac{H^2}{2k^3}(1+k^2\eta^2) ,\end{aligned} \tag{4.18}$$

and for modes well outside the horizon (for which $k|\eta| \ll 1$, since in de Sitter space $\eta = -(aH)^{-1}$) it becomes

$$\langle s_{\mathbf{k}}(\eta) s_{\mathbf{k}'}(\eta)\rangle \sim (2\pi)^3\delta(\mathbf{k}+\mathbf{k}')\frac{H^2}{2k^3} . \tag{4.19}$$

Going back to the inflationary computation we see that, if one knew the solution to eq. (4.13), the two-point function of $\zeta(t,\mathbf{k})$ would be simply calculated as

$$\langle \zeta(t,\mathbf{k})\, \zeta(t,\mathbf{k}')\rangle = (2\pi)^3\delta(\mathbf{k}+\mathbf{k}')|r_k(t)|^2 . \tag{4.20}$$

In the slow-roll limit, however, it is possible to estimate the late-time behavior (after the time of horizon crossing, that is) of the mode function by the corresponding result in de Sitter space, taking as value for H the Hubble constant at the moment of horizon crossing $k = a(t)H(t)$. The reason is that at late times $r_k(t)$ is constant while at early times the flat spacetime approximation is valid. We also note that the action of eq. (4.11a) contains an overall factor of ε_H: it enters in the normalization of the classical solution, therefore to compute

the super-horizon ($\eta \to 0$) two-point function for ζ we have to use the result of eq. (4.19) with

$$s(0,\mathbf{k}) = \sqrt{2\varepsilon_H}\,\zeta(0,\mathbf{k}) = \frac{\dot{\phi}}{H}\zeta(0,\mathbf{k}) \ , \tag{4.21}$$

where ε_H is evaluated at horizon crossing $k = a(t)H(t)$. Recalling the definition of power spectrum for ζ, then, we see that

$$\boxed{P_\zeta(0,k) \equiv P_\zeta(k) = \frac{1}{4M_P^2k^3}\frac{H^2}{\varepsilon_H}\bigg|_{k=aH}} \ . \tag{4.22}$$

4.3 DYNAMICS OF THE TENSOR DEGREES OF FREEDOM

We start from expanding the tensor perturbation γ_{ij} in a Fourier integral. This expansion is given by

$$\gamma_{ij}(t,\mathbf{x}) = \int \frac{d^3k}{(2\pi)^3} \sum_{p=+,\times} \epsilon_{ij}^p(\mathbf{k})\gamma^p(t,\mathbf{k})e^{i\mathbf{k}\cdot\mathbf{x}} \ , \tag{4.23}$$

with

$$\delta^{ik}\delta^{jl}\epsilon_{ij}^p(\mathbf{k})\epsilon_{kl}^q(\mathbf{k}) = 2\delta^{pq} \ , \tag{4.24a}$$

$$\delta^{ij}\epsilon_{ij}^p(\mathbf{k}) = 0 \ \forall\,\mathbf{k},p \ , \tag{4.24b}$$

$$k^i\epsilon_{ij}^p(\mathbf{k}) = 0 \ \forall\,\mathbf{k},p \ . \tag{4.24c}$$

Eqs. (4.24b), (4.24c) impose constraints on the symmetric three-tensors ϵ_{ij}^p, and this is why they actually depend only on the magnitude k of $\mathbf{k}$. If we insert this expression for h_{ij} into the tensor quadratic action S_γ we find the sum of two copies of the scalar quadratic action S_ζ, one for the $+$ polarization and one for the $\times$ polarization. However the difference is that S_γ is not multiplied by the slow-roll parameter ε_H: therefore, the power spectrum of tensor modes (which is the same for both polarizations) is given by [18]

$$\boxed{P_\gamma(k) = \frac{2}{M_P^2k^3}H^2|_{k=aH}} \ . \tag{4.25}$$

4.4 POWER SPECTRA IN THE SLOW-ROLL APPROXIMATION

We recall that for an operator O the power spectrum P_O in Fourier space is defined by

$$\langle O(t,\mathbf{k})\,O(t\mathbf{k}')\rangle \equiv (2\pi)^3\delta(\mathbf{k}+\mathbf{k}')P_O(t,k) \ . \tag{4.26}$$

The *dimensionless* power spectrum Δ_O^2 for the same quantity is instead defined as

$$\boxed{\Delta_O^2(t,k) \equiv \frac{k^3}{2\pi^2}P_O(t,k)} \ , \tag{4.27}$$

where the overall factor $\propto k^3$ ensures that the real space variance of the dimensionless power spectrum is given by the momentum-space integral $\int_0^{+\infty} d\log k\, \Delta^2_O(t,k)$. The final results of this analysis are listed in tab. 4.1 below.

TABLE 4.1: Power spectra for scalar and tensor modes for $\eta \to 0$ at leading order in slow-roll [18].

$P_\zeta(k)$	$\dfrac{1}{4M_P^2k^3}\dfrac{H^2}{\varepsilon_H}\Big\vert_{k=aH}$
$\Delta^2_\zeta(k)$	$\dfrac{1}{8\pi^2M_P^2}\dfrac{H^2}{\varepsilon_H}\Big\vert_{k=aH}$
$P_\gamma(k)$	$\dfrac{2}{M_P^2k^3}H^2\vert_{k=aH}$
$\Delta^2_\gamma(k)$	$\dfrac{1}{\pi^2M_P^2}H^2\vert_{k=aH}$

4.5 INFLATIONARY OBSERVABLES

The scalar and tensor dimensionless power spectra $\Delta^2_s(k)$ and $\Delta^2_t(k)$ are related to those of ζ and γ_{ij} by

$$\Delta^2_s(k) = \Delta^2_\zeta(k)\ , \tag{4.28a}$$

$$\Delta^2_t(k) = 2\Delta^2_\gamma(k)\ , \tag{4.28b}$$

where the factor of 2 in equation (4.28b) derives from the sum over the two polarizations $+$ and $\times$. These equations show us two important results:

- since the scalar action is slow-roll suppressed, $\Delta^2_s(k)$ is slow-roll "enhanced" by a factor of ε_H^{-1};
- the same thing does not happen for $\Delta^2_t(k)$, so tensor modes are more difficult to detect.[2]

This property of primordial fluctuations is encoded in the "tensor-to-scalar ratio" r, whose expression in terms of the slow-roll parameters ε_H and η_H (that we defined in Section 1.3.4) is

$$r(k) = \frac{\Delta^2_t(k)}{\Delta^2_s(k)} = 16\varepsilon_H|_{k=aH}\ . \tag{4.29}$$

Another observable one can consider is the "spectral index", that we already introduced in fig. 3.5: the condition $k = aH$ in tab. 4.1 leads to additional momentum dependence of the dimensionless power spectra,

2 Another reason is that tensor modes (like vector modes) decay once they come back into the horizon [121, 122].

even if the explicit factor of k^3 has been removed. One parameterizes this dependence with

$$n_s(k) - 1 = \frac{d\log\Delta_s^2(k)}{d\log k} = -\eta_H|_{k=aH} - 2\varepsilon_H|_{k=aH} \,, \tag{4.30a}$$

$$n_t(k) = \frac{d\log\Delta_t^2(k)}{d\log k} = -2\varepsilon_H|_{k=aH} \,, \tag{4.30b}$$

that hold at first order in slow-roll. With these definitions, $n_s(k) = 1$ and $n_t(k) = 0$ correspond to "scale-invariant" spectra. In the following we will consider only the scalar spectral index, because experiments are not yet sensitive enough to detect n_t.

If we now use the potential slow-roll parameters instead of the Hubble ones, recalling the relations of eqs. (1.58), we find that

$$\boxed{\begin{aligned} &\Delta_s^2(k) = \frac{1}{24\pi^2}\frac{1}{M_P^4}\frac{V}{\varepsilon_V}\bigg|_{k=aH} \,, && (4.31a)\\ &r(k) = 16\varepsilon_V|_{k=aH} \,, && (4.31b)\\ &n_s(k) = 1 + 2\eta_V|_{k=aH} - 6\varepsilon_V|_{k=aH} \,, && (4.31c) \end{aligned}}$$

where ε_V and η_V are functions of the potential and of its first and second derivatives (respectively) evaluated at $\phi = \bar\phi(t)$. Experiments will give us the values of the scalar and tensor spectra at a "pivot" scale $k_\star$, where the scalar and tensor spectra are normalized (recall fig. 3.5). The scale $k_\star$ has crossed the horizon at the time $t_\star$ at which $k_\star = a_\star H_\star$): using eqs. (4.31) we relate these measurements directly to the shape of the inflationary potential driving the period of accelerated expansion. In fact one is able to reconstruct the derivatives of the potential at $\bar\phi_\star = \bar\phi(t_\star)$ and from there its power series.

4.6 THE ENERGY SCALE OF INFLATION AND THE LYTH BOUND

In this short Section we study what one can learn about the inflationary epoch by measuring primordial gravitational waves. We begin from relating the energy scale of inflation to the strength of these primordial gravitational waves. The starting point is eq. (4.29) for the tensor-to-scalar ratio

$$r(k) = \frac{\Delta_t^2(k)}{\Delta_s^2(k)} \,, \tag{4.32}$$

which one can rewrite as

$$r(k) = \frac{2}{\pi^2 M_P^2}\frac{H^2|_{k=aH}}{\Delta_s^2(k)} \approx \frac{2}{3\pi^2 M_P^4}\frac{V|_{k=aH}}{\Delta_s^2(k)} \,, \tag{4.33}$$

since during slow-roll the kinetic energy is negligible. If we now substitute in this formula the measured value of the dimensionless scalar power spectrum, which is of order 10^{-9} [123], we arrive at the

equation (we are dropping the dependence on k here, because we are just interested in the orders of magnitude)

$$\boxed{\sqrt[4]{V} \approx \sqrt[4]{\frac{r}{0.01}} \times 10^{16}\,\text{GeV}\,.} \tag{4.34}$$

Therefore having a tensor-to-scalar ratio of order 10^{-1} corresponds to an energy scale of order $10^{16}\,\text{GeV}$.

Now we arrive at the Lyth bound [124], which relates the intensity of tensor fluctuations to the excursion in field space during inflation. If we combine eq. (4.31b) with the expression for the number of e-folds N at first order in slow-roll, i. e. (we assume $\dot{\bar{\phi}} > 0$, as in fig. 1.4)

$$N(t) = \int_{\bar{\phi}(t)}^{\bar{\phi}_{\text{end}}} \frac{d\bar{\phi}}{M_P} \frac{1}{\sqrt{2\varepsilon_V(\bar{\phi})}}\,, \tag{4.35}$$

we find that

$$\frac{d\bar{\phi}}{dN} = -M_P\sqrt{\frac{r(\bar{\phi})}{8}}\,. \tag{4.36}$$

If we now use the fact that ε_V (and then r) does not evolve much during slow-roll (since also $|\eta_V|$ is much smaller than 1), we find that (again dropping the dependence on k)

$$\boxed{\frac{\bar{\phi}_{\text{end}} - \bar{\phi}_{\text{CMB}}}{5\,M_P} \equiv \frac{(\Delta\bar{\phi})_{\text{slow-roll}}}{M_P} \approx \sqrt{\frac{r}{0.01}}\,,} \tag{4.37}$$

where $\bar{\phi}_{\text{CMB}}$ (recall fig. 1.4) is the value of the inflaton at the time at which the fluctuations measured in the CMB are generated. Hence values of r of order 10^{-1} translate into a trans-Planckian displacement $(\Delta\bar{\phi})_{\text{slow-roll}} \gtrsim M_P$ during inflation: this is why models predicting a large amount of primordial gravitational waves are called "large-field models".[3]

4.7 BEYOND POWER-LAW SPECTRA

The result of eq. (4.30a) for the tilt of the scalar power spectrum can be cast in a different way: from the definition of spectral index we have that, for constant $n_s(k) - 1$, $\Delta^2_\zeta(k)$ can be written as

$$\Delta^2_\zeta(k) = A_s\left(\frac{k}{k_\star}\right)^{n_s-1}\,, \tag{4.38}$$

where

$$A_s = \frac{1}{8\pi^2 M_P^2}\frac{H^2}{\varepsilon_H}\bigg|_{aH=k_\star}\,, \tag{4.39a}$$

$$n_s - 1 = -\eta_H|_{aH=k_\star} - 2\varepsilon_H|_{aH=k_\star}\,. \tag{4.39b}$$

3 For an analysis of large field models from an effective field theory point of view we refer the reader to [43, §28.3, §28.4].

However, it is possible to extend eq. (4.39) to higher order in an expansion in $\log \frac{k}{k_\star}$. More precisely, we can write

$$\Delta^2_\zeta(k) = A_s \left(\frac{k}{k_\star}\right)^{n_s - 1 + \frac{\alpha_s}{2}\log\frac{k}{k_\star} + \frac{\beta_s}{6}\log^2\frac{k}{k_\star} + \dots}, \tag{4.40}$$

where α_s is the "running of the spectral index", β_s the "running of the running of the spectral index", etc. In the slow-roll approximation, we can match the phenomenological parameters of eq. (4.40) to time derivatives of the Hubble parameter at the pivot scale by using the relations

$$N - N_\star = -\log\frac{k}{k_\star}\,, \tag{4.41a}$$

$$1 - n_s = 2\varepsilon_H - \frac{1}{\varepsilon_H}\frac{d\varepsilon_H}{dN}\,, \tag{4.41b}$$

where N is the number of e-folds from the end of inflation, decreasing as time increases (i. e. $Hdt = -dN$). The running of ε_H up to third order in N is given, then, by

$$\varepsilon_H(N) = \varepsilon_H(N_\star) + \sum_{i=1}^{3} \frac{\varepsilon_H^{(i)}}{i!}(N - N_\star)^i\,, \tag{4.42}$$

with

$$\varepsilon_H^{(i)} \equiv \left.\frac{d^i\varepsilon_H}{dN^i}\right|_{N=N_\star}. \tag{4.43}$$

The coefficients $\varepsilon_H^{(i)}$ can be related to $n_s - 1$, α_s and β_s by using eq. (4.41b). Indeed, differentiating it with respect to N and then using eq. (4.41a), one can find the coefficients of the Taylor expansion of $\varepsilon_H(N)$ in terms of the parameters describing the scale dependence of the primordial spectrum $\Delta^2_\zeta(k)$. More precisely, the system of equations to solve is (calling $\varepsilon_H|_\star \equiv \varepsilon_H(N_\star)$)

$$\varepsilon_H^{(1)} = (n_s - 1)\varepsilon_H|_\star + 2(\varepsilon_H|_\star)^2\,, \tag{4.44a}$$

$$\varepsilon_H^{(2)} = -\alpha_s\varepsilon_H|_\star + 4\varepsilon_H|_\star\varepsilon_H^{(1)} + (n_s - 1)\varepsilon_H^{(1)}\,, \tag{4.44b}$$

$$\begin{aligned}\varepsilon_H^{(3)} = {}& \beta_s\varepsilon_H|_\star - 2\alpha_s\varepsilon_H^{(1)} \\ & + (n_s - 1)\left\{-\alpha_s\varepsilon_H|_\star + 4\varepsilon_H|_\star\varepsilon_H^{(1)} + (n_s - 1)\varepsilon_H^{(1)}\right\} \\ & + 4\left\{\varepsilon_H|_\star\left[-\alpha_s\varepsilon_H|_\star + 4\varepsilon_H|_\star\varepsilon_H^{(1)} + (n_s - 1)\varepsilon_H^{(1)}\right]\right. \\ & \left. + (\varepsilon_H^{(1)})^2\right\}.\end{aligned} \tag{4.44c}$$

4.8 CONNECTION TO OBSERVATIONS

As we have seen in Section 4.1, ζ and γ_{ij} are conserved on super-horizon scales, given that there are no mass terms in their Lagrangians

eqs. (4.11). Then, we can use these two variables to connect the inflationary epoch to the Hot Big Bang era. The main problem is finding gauge-invariant variables that reduce to ζ and γ_{ij} in comoving gauge, so that we can then equate their super-horizon value to that of the Newtonian gauge variables of Section 3.3.1.

4.8.1 *Scalar mode*

We start from studying the scalar mode ζ. Given a generic first-order metric $g_{\mu\nu}$ equal to

$$g_{00} = -(1+2\Phi) \,, \tag{4.45a}$$

$$g_{0j} = a(\partial_j B + \hat{B}_j) \,, \tag{4.45b}$$

$$g_{ij} = a^2(1-2\Psi)\delta_{ij} + a^2\partial_i\partial_j E + a^2\partial_{(i}\hat{E}_{j)} + a^2\gamma_{ij} \,, \tag{4.45c}$$

with $\partial_j\hat{B}_j = \partial_i\hat{E}_i = 0$, and the stress-energy tensor of a fluid with four-velocity $U^\mu = \gamma(n^\mu + v^\mu)$ (n^μ being the normal to the surfaces of constant time and v^i equal to $\partial_i v$), it is straightforward to see that the combination $-\Psi + a^2 H v$ is gauge-invariant. Indeed, consider for example the case of a time redefinition $t = \tilde{t} + \delta t(\tilde{t}, \tilde{\mathbf{x}})$: under this transformation we have

$$\tilde{\Psi} = \Psi - H\delta t \,, \tag{4.46a}$$

$$\tilde{v} = v - \frac{\delta t}{a^2} \,, \tag{4.46b}$$

so that $-\Psi + a^2 H v$ does not change.

In comoving gauge during inflation, $-\Psi + a^2 H v$ reduces to our ζ, since for $\delta\phi = 0$ the stress-energy tensor is unperturbed (so $v = 0$). Besides, we see that ζ is indeed conserved for $\eta \to 0$, so that also the gauge-invariant combination $-\Psi + a^2 H v$ will be conserved on super-horizon scales and can be used to match to the Newtonian gauge variables at horizon re-entry during radiation dominance. Using the shift constraint equation for a fluid with equation of state w, we can rewrite $-\Psi + a^2 H v$ as

$$\begin{aligned} -\Psi + a^2 H v &= -\Psi - \frac{2M_P^2}{\bar{\rho}(1+w)}(H\dot{\Psi} + H^2\Psi) \\ &= -\Psi - \frac{2}{3(1+w)}\left(\frac{\dot{\Psi}}{H} + \Psi\right) \,, \end{aligned} \tag{4.47}$$

so that for $\dot{\Psi} \to 0$ on super-horizon scales we obtain

$$\boxed{-\Psi + a^2 H v \to -\Psi - \frac{2\Psi}{3(1+w)} = -\frac{5+3w}{3(1+w)}\Psi \,.} \tag{4.48}$$

For $\Psi = \Phi$, in absence of anisotropic stress, we obtain the initial conditions used in the previous Chapter. Besides, we see that as w goes from $\frac{1}{3}$ to 0 as we go from radiation dominance to matter dominance, the super-horizon value of the Newtonian potential drops of a factor of $\frac{9}{10}$.

4.8.2 *Tensor modes*

The same line of reasoning of the previous Section can be applied to the tensor modes γ_{ij}. Things are far simpler in this case, since at linear order in perturbations γ_{ij} is gauge-invariant. Indeed, if we take the linearized coordinate transformation of eq. (3.24), i. e.

$$x^\mu = \tilde{x}^\mu + \xi^\mu(\tilde{x}) = \tilde{x}^\mu + \xi^\mu(x) + \mathcal{O}(2) \ , \tag{4.49}$$

we see that neither ξ^0 nor $\xi^i = \partial_i \xi_L + \hat{\xi}^i$ (with $\partial_i \hat{\xi}^i = 0$) can contain a spin-2 perturbation at this order.

Therefore, the super-horizon value of γ_{ij} (and of its power spectrum) obtained in Section 4.3 can be directly used as initial condition for the tensor modes in any other gauge at horizon re-entry.

Part III

SCIENTIFIC RESEARCH

5

μ OR α_s: A GUARANTEED DISCOVERY

CONTENTS

In this Chapter we discuss the implications for single-field slow-roll inflation of a PIXIE-like experiment that will measure μ-distortions at the level of 10^{-8}. The Chapter is based on the work Phys. Rev. D **93**, no. 8, 083515 (2016).

5.1 INTRODUCTION

The recent measurements of CMB anisotropies made by the Planck satellite experiment [14] have provided, once again, a spectacular confirmation of the ΛCDM cosmological model and determined its parameters with an impressive accuracy. Also, numerous new ground based or balloon borne CMB telescopes are currently gathering data or under development. Moreover, several proposals for a new satellite experiment like PIXIE [22], PRISM [125, 126], COrE [127], and LiteBIRD [128] are under discussion.

In summary, two main lines of investigation are currently pursued: CMB polarization and spectral distortions. Improving current measurements of CMB polarization is partially motivated by the inflationary paradigm. As we have seen in Chapter 4, the simplest models of inflation predict a nearly scale-invariant (red-tilted) spectrum of primordial scalar perturbations, in perfect agreement with the latest experimental evidence. Inflation also predicts a stochastic background of gravitational waves: a discovery of this background (e. g. through measurements of CMB B-mode polarization [117, 118]) with a tensor-to-scalar ratio $r \sim 10^{-2}$ would correspond to inflation occurring at the GUT scale (see Section 4.6). Planned and/or proposed CMB experiments could detect this background, and measure the tensor-to-scalar ratio $r \sim 0.01 \times (E_{\rm inflation}/10^{16}\,{\rm GeV})^4$ with a relative error of order 10^{-2}, if inflation occurs at these energies [129, 130]. This would be a spectacular confirmation of the inflationary theory. However, the energy scale of inflation could be orders of magnitude lower than the GUT scale.

In this case, the stochastic background would be out of the reach of upcoming or planned experiments.

On the other hand, CMB μ-type spectral distortions are an unavoidable prediction of the ΛCDM model, since they are generated by the damping of primordial fluctuations [7, 90] with an amplitude of order $\mu = \mathcal{O}(10^{-8})$ (for this reason, it will be useful to define the parameter $\mu_8 \equiv \mu \times 10^8$, that will be used in the rest of this and the following Chapters).

While a measurement of CMB spectral distortions could shed light on several aspects of physics beyond ΛCDM such as, e. g., gravitino decay [131], cosmic strings [132], magnetic fields [133], hidden photons [134], and dark matter interactions [135], just to name a few, it is important to stress that spectral distortions could provide significant information on inflation through the contribution coming from primordial perturbations [136–140].

Indeed, as we have shown in Section 4.7, in a typical inflationary model the spectral index n_s of scalar perturbations is expected to have a small (and often negative) running, of order $|\alpha_s| \sim (1 - n_s)^2$ [141–143]. State-of-the art CMB observations by the Planck experiment [6, 14] are fully compatible with an exact power law spectrum of primordial fluctuations $P_\zeta(k)$, with $\alpha_s = -0.006 \pm 0.007$ at 68 % CL (Planck TT, TE, EE + lowP dataset). A more than ten-fold improvement in sensitivity is therefore needed to reach the typical slow-roll values with CMB experiments. However, CMB anisotropies can probe $P_\zeta(k)$ only up to $k \approx 0.1\,\mathrm{Mpc}^{-1}$, since at shorter scales primordial anisotropies are washed away by Silk damping [103–105] and foregrounds become dominant. There is, then, a limit in the range of multipoles that we can use to test the scale dependence of the power spectrum.[1] Moreover, CMB measurements will soon be limited by cosmic variance: recent analyses have shown that for upcoming experiments (COrE+ or CMB Stage IV), which are close to be CVL (Cosmic Variance Limited), one can expect $\sigma_{\alpha_s} \approx 10^{-3}$ [145–147].

As we have seen in Section 3.4, the CMB μ-type spectral distortion is sensitive to the amount of scalar power up to k of order $10^4\,\mathrm{Mpc}^{-1}$ because of the damping of acoustic modes. The strong lever arm makes this observable an ideal probe to improve the bounds on the running from large scale CMB anisotropies. In addition, the cosmic variance of the μ monopole and of the higher multipoles is minuscule (see [20] for a discussion). With a sufficiently broad frequency coverage, instrumental noise will be the main source of uncertainty for any foreseeable future, leaving ample room for improvements.

In this context, we address several questions:

1 For this reason, we expect that E-mode polarization will be better, in the long run, at constraining the scale dependence of $P_\zeta(k)$, since C_ℓ^{EE} starts to become damped around $\ell \approx 2500$ (see [144] for a discussion).

- is there a benchmark sensitivity for CMB spectrometry, i. e. which should be the target of the next generation experiments? How can we design an experiment to ensure a discovery even in the absence of a detection?

- what sensitivity to the spectrum is needed to detect μ-distortions when accounting for the prior knowledge from Planck?

- how much will a joint analysis of large scale CMB anisotropies and CMB spectral distortion strengthen the bounds on the running? How does this quantitatively depend on the improvement over PIXIE sensitivity?[2]

To articulate the answers to these questions, we consider the following three fiducial cosmologies:

- a ΛCDM cosmology with zero running: the best-fit for the μ-amplitude, in this case, is of order $\mu_8 = 1.6$. We stress that for the sensitivities considered in this and the following Chapters, this fiducial is indistinguishable from models with running of order $(1 - n_s)^2$, such as typical slow-roll models;

- a fiducial spectral distortion amplitude $\mu_8^{\rm fid}$ equal to the best-fit of the the Planck analysis for the $\Lambda\text{CDM} + \alpha_s$ model, i. e. $\mu_8^{\rm fid} = 1.06$. This value of μ is roughly correspondent to what one obtains for a running $\alpha_s = -0.01$ which is close to the mean value predicted by current Planck data;

- $\alpha_s^{\rm fid} = -0.02$ (corresponding to $\mu_8 = 0.73$), at the edge of the 2σ bounds of Planck. We note that it is possible to obtain such large negative runnings in some models of single-field inflation like, e. g., extra-dimensional versions of Natural Inflation [148, 149] or recent developments in axion monodromy inflation [150–152].

The rest of the Chapter is organized as follows: after a very brief review of photon thermodynamics in the early universe and of distortions from Silk damping (we refer to Sections 2.2, 2.3 and 3.4 for more details), we compute the μ-distortion parameter allowed by current Planck bounds for a ΛCDM and $\Lambda\text{CDM} + \alpha_s$ model (Section 5.3). We then analyze what a PIXIE-like mission will be able to say about the running, given these posteriors for μ. The discussion is divided in three Sections: we start with the predicted bounds on μ-distortions from current Planck data (Section 5.3). We proceed with a Fisher analysis (Section 5.4), discussing also the optimal choice of pivot scale for a combined study of CMB anisotropies and spectral distortions. The MCMC analysis and forecasts are carried out in Section 5.5. Finally, Section 5.6 studies the implications of these results for single-clock slow-roll inflation, and we draw our conclusions in Section 5.7.

2 For example the PRISM imager [125, 126] corresponds to approximately $10\times$ PIXIE.

5.2 PHOTON THERMODYNAMICS

At very early times, for redshifts larger than $z_{DC} \approx 2 \times 10^6$, processes like double Compton scattering and Bremsstrahlung are very efficient and maintain thermodynamic equilibrium: any perturbation to the system is thermalized and the spectrum of the CMB is given to very high accuracy by a black-body. At later times the photon number is effectively frozen, since photons can be created at low frequencies by elastic Compton scattering but their re-scattering at high frequencies via double Compton scattering and Bremsstrahlung is not efficient due to the expansion of the universe [7–10, 12, 13].

The end result is a Bose-Einstein distribution $1/(e^{x+\mu(x)} - 1)$ ($x \equiv h\nu/k_B T$) with chemical potential μ. Since photons can still be created at low frequencies, μ will not exactly be frequency independent: it can be approximated as $\mu_0 \exp(-x_c/x)$, with $x_c \approx 5 \times 10^{-3}$. However, no planned/proposed experiments will be able to probe such low frequencies: for this reason we will take the chemical potential to be a constant (and drop the subscript 0).

For a given energy release $d(Q/\rho_\gamma)/dz$, one can write the value of μ as (see Section 2.3.4)

$$\mu(z) = 1.4 \int_z^{z_{DC}} dz' \frac{d(Q/\rho_\gamma)}{dz'} e^{-\tau_\mu(z')} \Theta(z - z_K) \, , \tag{5.1}$$

where $z_K = 5 \times 10^4$ and $\tau_\mu(z)$ can be approximated as $(z/z_{DC})^{5/2}$ [7–10, 12, 13, 74].

Below redshifts around $z = z_{\mu\text{-}i} \approx 2 \times 10^5$, Compton scattering is not sufficient to maintain a Bose-Einstein spectrum in the presence of energy injection. The distortions generated will then be neither of the μ-type nor of the y-type: they will depend on the redshift at which energy injection occurs [12, 87, 138], and must be calculated numerically by solving the Boltzmann equation. Recently, in [87, 138], a set of Green's functions for the computation of these intermediate distortions has been provided:[3] they sample the intermediate photon spectrum $n^{(i)}$ for a energy release $Q_{ref}/\rho_\gamma = 4 \times 10^{-5}$ in $\mathcal{O}(10^3)$ redshift bins from $z \approx 2 \times 10^5$ to $z \approx 1.5 \times 10^4$. The i-type intensity, for a generic energy injection history $d(Q/\rho_\gamma)/dz$, will then be computed as [138]

$$\begin{aligned} I_\gamma^{(i)}(\nu) &= \frac{2h\nu^3}{c^2} \sum_{z_k} \frac{n_{z_k}^{(i)}(\nu)}{4 \times 10^{-5}} \left.\frac{d(Q/\rho_\gamma)}{dz}\right|_{z_k} \delta z_k \\ &\equiv \frac{2h\nu^3}{c^2} \sum_{z_k} \frac{n_{z_k}^{(i)}(\nu)}{4 \times 10^{-5}} \times \mu_{z_k}^{(i)} \, . \end{aligned} \tag{5.2}$$

At redshifts $z \lesssim 1.5 \times 10^4$ also elastic Compton scattering is not efficient enough: there is no kinetic equilibrium and the distortion is

3 We refer also to [88] for an alternative derivation.

of y-type. The transition between μ- and y-distortions can be modeled with a redshift dependent visibility function [88]. The information on the transition is encoded in the residual r-type distortions. Since r-distortions are not degenerate with μ- and y-type distortions (see Appendix D), they can be useful for probing the redshift dependence of different energy release histories [138, 153].[4]

The y-type distortions is expected to be dominated by astrophysics at low redshifts (created when the CMB photons are scattered in the clusters of galaxies by hot electrons, the thermal Sunyaev-Zeldovich effect). While this signal is very interesting by itself as a probe of the matter distribution in the universe [154–156], our goal is studying the contribution due to dissipation of acoustic waves, and so we will marginalize over it in our analysis (see Appendix D).[5]

Additional spectral distortions are the ones created during recombination [74, 75] and reionization [74, 158, 159]. Previous work on recombination spectra has been carried out in [160–165], and recently [75] has shown that spectral distortions from recombination can be computed with high precision. Therefore we are not going to include them in our analysis, assuming they can be subtracted when looking for the primordial signal.

In this and the following Chapters we will not consider these intermediate distortions, and take the transition between the μ- and y- era to be instantaneous at a redshift $z_K = 5 \times 10^4$ [90]: in the case of an energy release that does not vary abruptly with redshift, we do not expect the inclusion of r-distortions to alter significantly the constraints on the parameters describing $d(Q/\rho_\gamma)/dz$. We leave the analysis of their effect on combined CMB anisotropies - CMB distortions forecasts for cosmological parameters for future work (referring to [138, 153, 157] for forecasts involving CMB spectrometry alone).

While there are many non-standard potential sources of spectral distortions, e. g. decaying or annihilating Dark Matter particles [12, 87, 131], a source of heating that is present also in the standard picture is the dissipation of perturbations in the primordial plasma due to Silk damping. Even before recombination, when the tight-coupling approximation holds, photons are random-walking within the plasma with a mean free path $\lambda_{mfp} = (\sigma_T n_e)^{-1}$. In the fluid description, this amounts to anisotropic stresses that induce dissipation. One can compute the (integrated) fractional energy lost by these acoustic waves δ_γ: as we have seen in Section 3.4, in the tight-coupling approximation eq. (5.1) reduces to [78, 166]

$$\mu \approx 2.3 \int \frac{d\mathbf{k}_1 d\mathbf{k}_2}{(2\pi)^6} e^{i\mathbf{k}_+ \cdot \mathbf{x}} \zeta(\mathbf{k}_1)\zeta(\mathbf{k}_2) e^{-(k_1^2+k_2^2)/k_D^2} \Big|_{z_K}^{z_{DC}} , \tag{5.3}$$

4 As [12] shows, they can be used to put constraints on observables like the lifetime of decaying dark matter particles.

5 We note that in [157], the authors carried out this marginalization by taking into account also r-distortions: this results in a slightly higher μ detection limits, but does not affect the main results of this Chapter.

where $\mathbf{k}_+ \equiv \mathbf{k}_1 + \mathbf{k}_2$ and $\zeta(\mathbf{k}) = \zeta(k)$ are the Fourier modes of the primordial curvature perturbation. The diffusion damping length appearing in the above formula, instead, is given by [103–105]

$$k_D(z) = \sqrt{\int_z^{+\infty} dz \, \frac{1+z}{H\sigma_T n_e} \left[\frac{R^2 + \frac{16}{15}(1+R)}{6(1+R)^2}\right]} \, . \tag{5.4}$$

If we consider the ensemble average of μ, we see that it is equal to the log-integral of the primordial power spectrum multiplied by a window function

$$W_\mu(k) = 2.3 \, e^{-2k^2/k_D^2} \Big|_{z_K}^{z_{DC}} \, . \tag{5.5}$$

Since the tight-coupling approximation is very accurate at redshifts much before recombination we expect this to be a good approximation for the μ-distortion amplitude: this simplified picture allows us to obtain a qualitative understanding of the possible constraints coming from an experiment like PIXIE [22]. The window function of eq. (5.5) and the analogous one for y-distortions are shown in fig. 5.1. We also account for adiabatic cooling [12, 86], namely the fact that electrons and baryons alone would cool down faster than photons. Because of the continuous interactions, they effectively extract energy from the photons to maintain the same temperature, leading to an additional source of distortions of the CMB spectrum. During the μ-era, this energy extraction results in a negative μ-distortion of order $\mu_{BEC} \approx -2.7 \times 10^{-9}$ (for the Planck 2015 best-fit values of cosmological parameters).

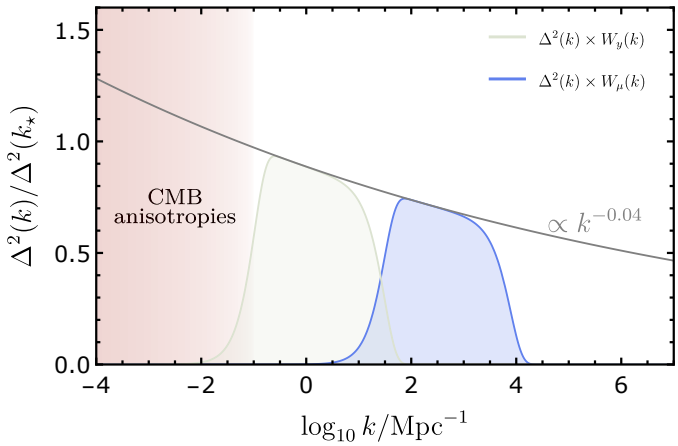

FIGURE 5.1: This cartoon plot shows the scales which are probed by μ- and y-type spectral distortions, using the "window function" approximation of eq. (5.5).

5.3 EXPECTATIONS FROM LARGE SCALES

As we discussed in the previous Section, the expected primordial spectral distortion μ is a function of cosmological parameters that play

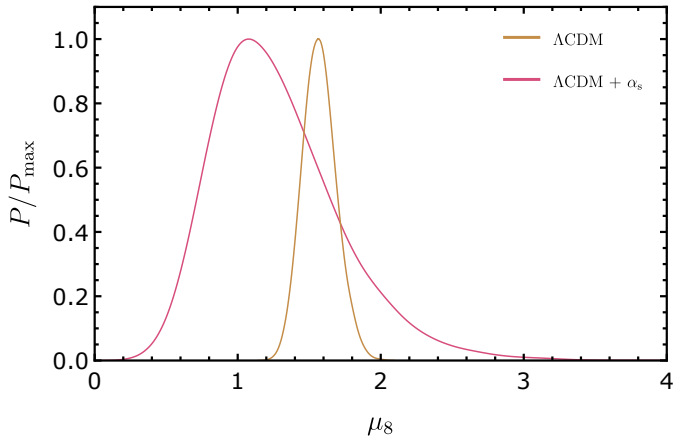

FIGURE 5.2: The figure shows the one-dimensional posteriors for μ_8 predicted by Planck TT, TE, EE + lowP data, for the ΛCDM model (orange curve) and the ΛCDM + α_s model (purple curve). The posteriors have been obtained through the `idistort` code developed by Khatri and Sunyaev [87, 138].

a role during the early universe epoch (like the scalar spectral index n_s, its running α_s, the cold dark matter energy density, etc.). Since most of these parameters are now well constrained by the recent measurements of CMB anisotropies (both in temperature an polarization) made by the Planck satellite, one could, albeit indirectly, constrain the expected value of μ assuming a ΛCDM model or one of its extensions (see also [140] for a recent analysis).

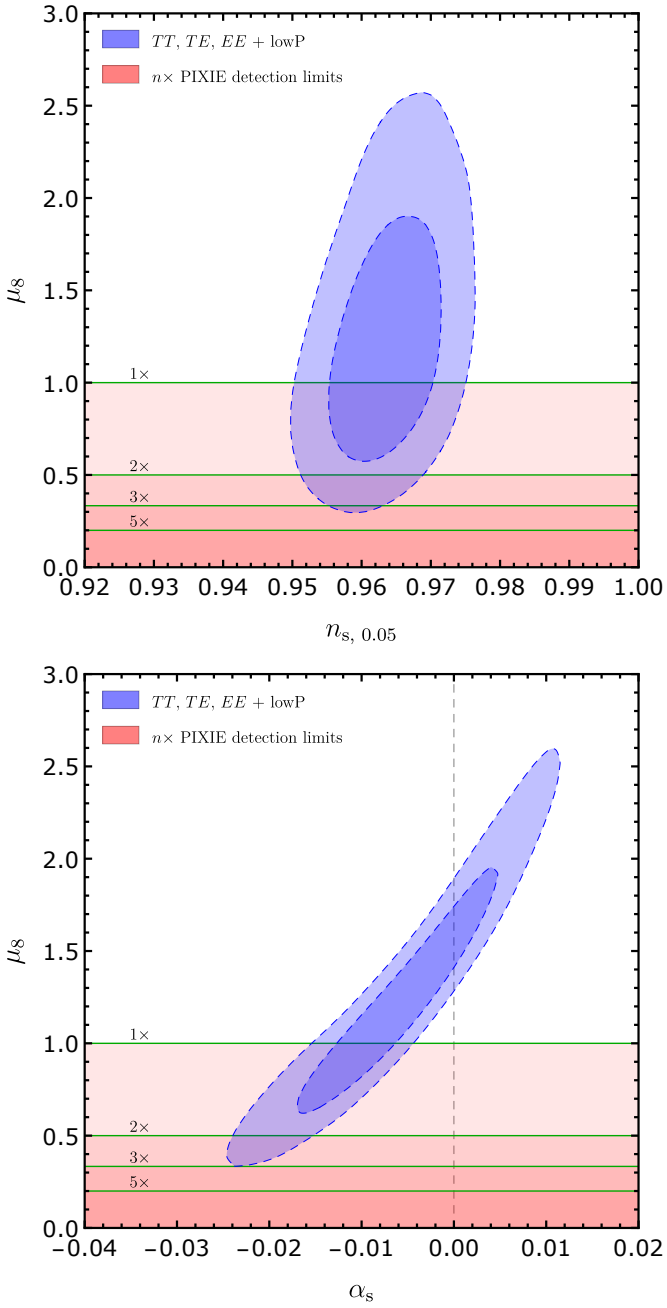

FIGURE 5.3: This figure shows the 68 % CL and 95 % CL contours in the n_s - μ (top panel) and the α_s - μ_8 plane (bottom panel) for the Planck TT, TE, EE + lowP dataset for ΛCDM + α_s, together with the 1σ detection limits for PIXIE and possible improvements.

Spectral distortions in the μ-era can be computed in terms of 6 - 7 parameters (which we will call $\boldsymbol{\theta}$):

- the baryon and cold dark matter density parameters $\Omega_b h^2 \equiv \omega_b$ and $\Omega_{cdm} h^2 \equiv \omega_{cdm}$, together with the number of effective relativistic degrees of freedom N_{eff}. These enter in the computation

of the expansion history: from them we compute the Hubble constant H_0 and the Helium mass fraction Y_P that enter in the computation of the dissipation scale k_D;

- the CMB temperature T_0;
- the parameters describing the primordial spectrum $P_\zeta(k)$, i. e.

$$P_\zeta(k) = \frac{2\pi^2}{k^3}\Delta_\zeta(k) = \frac{2\pi^2}{k^3} \times A_s \left(\frac{k}{k_\star}\right)^{n_s - 1 + \frac{\alpha_s}{2}\log\frac{k}{k_\star}} . \quad (5.6)$$

These are the amplitude $\log(10^{10}A_s)$ and tilt n_s for the ΛCDM case, with the addition of the running α_s for the $\Lambda\text{CDM} + \alpha_s$ case.

We performed an analysis of the recent Planck TT, TE, EE + lowP likelihood [167], which includes the (temperature and E-mode polarization) high-ℓ likelihood together with the TQU pixel-based low-ℓ likelihood, through Monte Carlo Markov Chain sampling, using the publicly available code `cosmomc` [168, 169]. We have varied the primordial parameters, along with ω_b, ω_{cdm}, the reionization optical depth τ,[6] and finally the ratio of the sound horizon to the angular diameter distance at decoupling $100\theta_{MC}$. For each model in the MCMC chain we compute, as derived parameter, the value of μ_8 using the `idistort` code developed by Khatri and Sunyaev [87, 138]. For this purpose we fix the CMB temperature to $T_0 = 2.7255\,K$, the neutrino effective number to the standard value $N_{eff} = 3.046$, and we evaluate the primordial Helium abundance Y_P assuming standard Big Bang Nucleosynthesis.

Processing the chains through the `getdist` routine (included in the `cosmomc` package), and marginalizing over all the nuisance parameters, we obtain for the ΛCDM case (no running) the indirect constraint $\mu_8 = 1.57^{+0.108}_{-0.127}$ at 68 % CL. Including the possibility of a running, the Planck constraint on μ is weakened to $\mu_8 = 1.28^{+0.299}_{-0.524}$ (68 % CL). The marginalized posterior distributions for μ_8 are shown in fig. 5.2. Notice that the "the balanced injection scenario", namely the possibility that the negative contribution to μ from adiabatic cooling cancels precisely the positive contribution from the dissipation of adiabatic modes [78, 86], leaving $\mu_8 = 0$, is excluded at extremely high significance (i. e. $\approx 15\sigma$) for the ΛCDM model, and at 97.4 % CL[7] if we allow the running to vary.

Fig. 5.3 shows the dependence of μ-distortion on the tilt n_s and the running α_s:

- in the top panel we see that μ_8 is not very degenerate with n_s. The reason is twofold. First and most importantly, for non-zero running of order 10^{-2}, as allowed by Planck, a change in the

6 We introduced this parameter in Section 3.3.2: we have called it τ_{rei} in eq. (3.80).

7 We quote the confidence level, in this case, because the posterior for μ_8 is non-Gaussian (as can be seen from fig. 5.2).

tilt of order 10^{-2} is a small correction to the power spectrum at the short scales that are responsible for μ-distortions (α_s appears in eq. (5.6) with a factor of $(\log k/k_\star)/2 \sim 5$ for $k \sim 10^3\,\mathrm{Mpc}^{-1}$). Secondly, Planck constraints on n_s are tighter than those on α_s by roughly a factor of two;

- the bottom panel, on the other hand, shows that μ_8 is strongly dependent on α_s (increasing α_s increases the power at short scales and hence leads to a larger μ_8, and viceversa). We also note that the two dimensional contour in the α_s - μ_8 plane is not ellipsoidal, but banana-shaped. The reason is that at large negative running, the contribution to spectral distortions from dissipation of acoustic waves will go to zero asymptotically, and the net μ amplitude will be the one from adiabatic cooling (which for the tightly constrained values of cosmological parameters can be practically considered a constant).

Having discussed the current (indirect) limits on μ-distortions from Planck measurements of CMB temperature and polarization anisotropies, we move to the forecasts for a PIXIE-like spectrometer.

5.4 FORECASTS FOR PIXIE: FISHER ANALYSIS

Considering only μ-distortions, and using the approximation in terms of a window function from $z_K = 5 \times 10^4$ to $z_{DC} = 2 \times 10^6$ (with the amplitude of the scalar spectrum fixed at $A_s \approx 2.2 \times 10^{-9}$), we can perform a simple Fisher forecast to see how the constraints on tilt and running are improved by combining PIXIE with the Planck prediction for μ_8.

This allows us also to discuss, mirroring what has been done for CMB anisotropies alone in [170], what is the optimal choice of pivot scale (that maximizes the detection power for these two parameters) for the combined analysis, as function of the sensitivity of a PIXIE-like mission. We stress that the choice of pivot has no impact on the detectability of μ-distortions themselves: it is just a particular way to parametrize the spectrum. Whether or not μ-distortions will be seen is only dependent on the amount of scalar power at small scales (which is captured by the fiducial μ_8 that we consider).

Finally, we also point out that this analysis already shows that an improvement of a factor of three over PIXIE implies a guaranteed discovery.

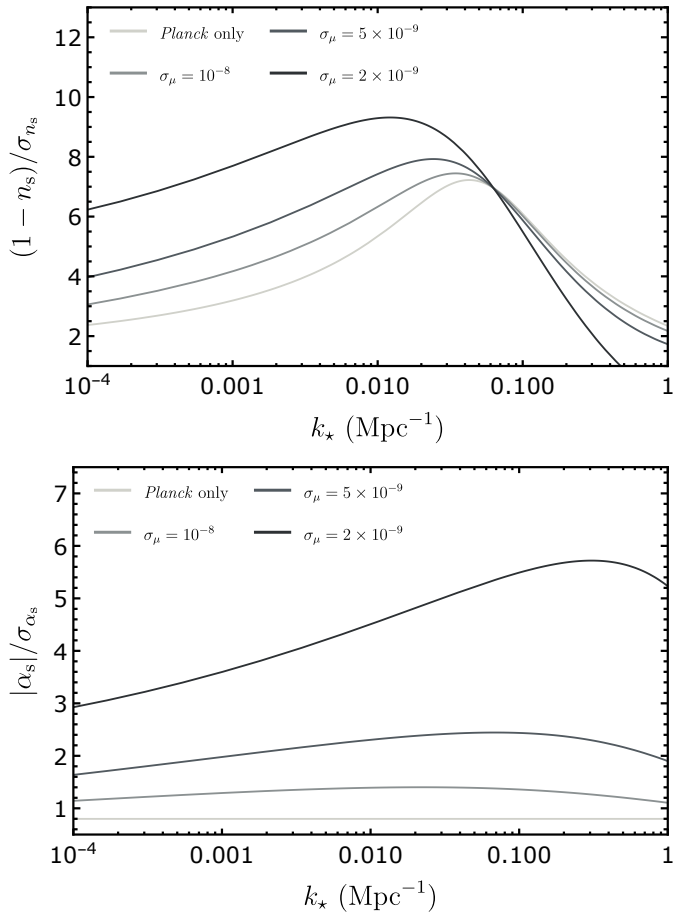

FIGURE 5.4: $(1-n_s)/\sigma_{n_s}$ (top panel) and $|\alpha_s|/\sigma_{\alpha_s}$ (bottom panel) as function of the pivot scale $k_\star$, for a vanishing fiducial distortions $\mu_8^{\rm fid} = 0$. A dependence on the pivot scale is always present for n_s (top panel), while for α_s the dependence becomes appreciable only for a significant improvements over PIXIE sensitivity. The optimal choice of $k_\star$ shifts towards $k < 0.05\,{\rm Mpc}^{-1}$ for n_s and $k > 0.05\,{\rm Mpc}^{-1}$ for α_s, when the information from spectral distortions is included.

We add to the Planck bounds the detection limits for μ-distortions from the PIXIE white paper [22], i. e.

$$\mathcal{L}(n_s, \alpha_s) \propto \mathcal{L}(n_s, \alpha_s)_{\rm Planck} \times \exp\left[-\frac{\left\{\mu_8(n_s, \alpha_s) + \mu_{8,\rm BEC} - \mu_8^{\rm fid}\right\}^2}{2\sigma_{\mu_8}^2}\right], \tag{5.7}$$

where σ_{μ_8} is equal to 1 (0.5 and 0.2) for ($2\times$ and $5\times$) PIXIE, and $\mu_8(n_s, \alpha_s)$ is given by

$$\mu_8(n_s, \alpha_s) = 2.3 \times 10^8 \times A_s \int_{k_D(z_K)}^{k_D(z_{DC})} \frac{dk}{k} \left(\frac{k}{k_\star}\right)^{n_s - 1 + \frac{\alpha_s}{2}\log\frac{k}{k_\star}}. \tag{5.8}$$

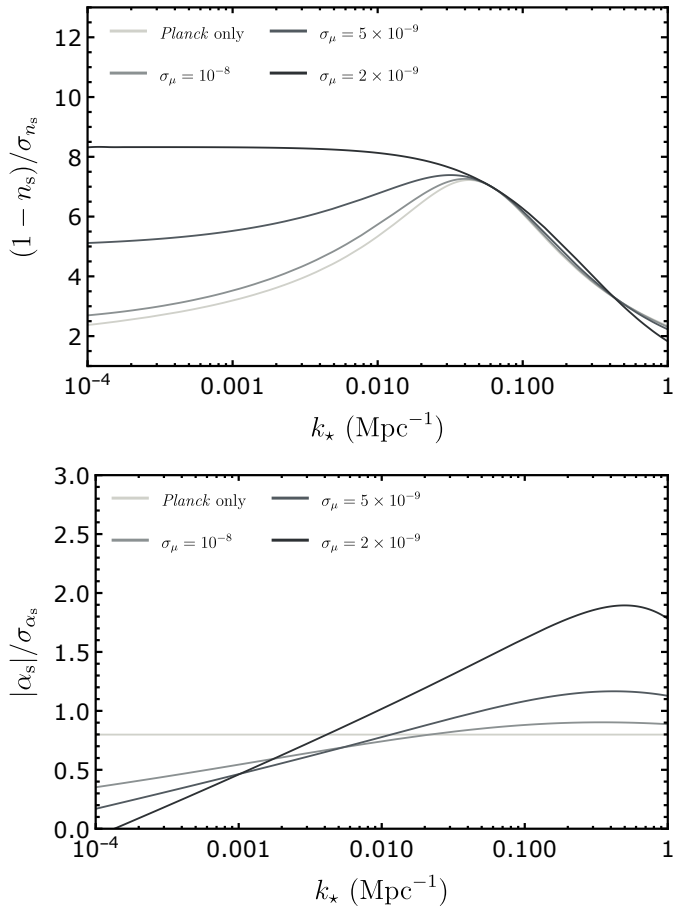

FIGURE 5.5: Same as fig. 5.4, but in this case we consider a fiducial μ_8 amplitude of 1.3 (see Section 5.4 for details). The behavior is qualitatively similar to the case of a vanishing fiducial μ_8.

The results of this Fisher analysis are just an approximation of the full MCMC sampling of the joint likelihood that we will present in the next Section. We can then safely consider only two fiducial values for μ_8, which approximate well the choices we will make later (see tab. 5.2):

- $\mu_8^{\rm fid} = 0$, i. e. a cosmology with zero μ-type distortions;
- $\mu_8^{\rm fid} = 1.3$, i. e. the mean-fit value from Planck data (for the ΛCDM + α_s case).

As Planck likelihood, we take (disregarding for simplicity the normalization)

$$\log \mathcal{L}(n_s, \alpha_s)_{\rm Planck} = -\frac{(\alpha_s - \bar{\alpha}_s)^2}{2\sigma^2_{\alpha_s}} - \frac{(n_s + \frac{\alpha_s}{2}\log(k_\star/k_\star^{(0)}) - \bar{n}_s)^2}{2\sigma^2_{n_s}}\,, \tag{5.9}$$

where:

- the tilt is written at an arbitrary pivot $k_\star$ in terms of the running and the reference scale $k_\star^{(0)}$ (note that the Jacobian of the transformation is 1 so it can be neglected);
- $k_\star^{(0)} = 0.05\,\mathrm{Mpc}^{-1}$ is the scale where n_s and α_s decorrelate: for this reason we take $\bar{n}_s$, $\bar{\alpha}_s$ to be the marginalized means from the Planck TT, TE, EE + lowP analysis. σ_{n_s} and σ_{α_s} are the corresponding marginalized standard deviations. The values are listed in tab. 5.1.

TABLE 5.1: Mean and standard deviation for spectral index and running used in eq. (5.9), from the Planck TT, TE, EE + lowP analysis.

$\bar{n}_s$	0.9639
$\bar{\alpha}_s$	−0.0057
σ_{n_s}	0.0050
σ_{α_s}	0.0071

Fig. 5.4 shows $(1-n_s)/\sigma_{n_s}$ and $|\alpha_s|/\sigma_{\alpha_s}$ as function of the pivot scale for vanishing μ_8^{fid}: we see that, as we increase the sensitivity of PIXIE, the $k_\star$ that maximizes the detection of the tilt is shifted towards values smaller than $k_\star^{(0)} = 0.05\,\mathrm{Mpc}^{-1}$. The best pivot for the running moves in the opposite direction, towards values larger than $0.05\,\mathrm{Mpc}^{-1}$. fig. 5.5 shows that the same qualitative behavior is reproduced in the case of a fiducial μ_8 different from zero.

These plots show that the effect of changing of pivot on the detection power for n_s and α_s is not very relevant, if we increase $1/\sigma_{\mu_8}$ up to $5\times$ PIXIE. At $10\times$ the choice of $k_\star$ can lead to a small improvement on σ_{α_s}: this is an interesting result, that could open up the possibility of choosing the pivot outside of the CMB window in the future, as σ_{μ_8} becomes even smaller.[8] However, since we will stop at $10\times$ PIXIE (i. e. the expected error on μ_8 achievable by PRISM) in this Chapter, we will keep $k_\star = 0.05\,\mathrm{Mpc}^{-1}$ in the following Sections.

For vanishing μ_8^{fid}, fig. 5.4 shows that the improvement for σ_{α_s} can be greater than the case with non-zero fiducial. However, it is important to stress that the assumption of having zero distortions starts to become incompatible with the Planck indirect constraints on μ_8 (as one can see, e. g., from fig. 5.2) for $\sigma_{\mu_8} \approx 0.3$, making a combination of the two likelihoods inadvisable (this is also the reason why we have decided to not consider, in Section 5.1, a fiducial running so small that spectral distortions from Silk damping are absent). For fiducial μ_8 different from zero we see that this does not happen: the

8 However, from the top panels of figs. 5.4, 5.5 we see how this improvement would be at the expense of an increased error on the tilt n_s.

combination of the likelihoods, which we will explore through MCMC sampling in the next Section, is therefore justified in this case.

Finally, it is interesting to ask whether there exist any threshold value for sensitivity to the μ amplitude such that, by reaching it, we are guaranteed to learn something about the early Universe, irrespectively of what the running might actually be. The bottom panel of fig. 5.4 suggests the answer to this question (which we will confirm in the next Section with a detailed calculation). Within the uncertainty of Planck, a vanishing running implies a distortion of order $\mu_8 \sim 1.4$, as we have seen in Section 5.3: therefore a measurement of the CMB spectrum at sensitivity of $\sigma_{\mu_8} \sim 1.4/4 = 0.35$, corresponding to about $3\times$ PIXIE, must lead to[9] a first detection of μ-distortions or a detection of negative running, or both. In fact, any central value $\mu_8 \lesssim 1.4/2 \sim 0.7$ at this resolution would exclude $\alpha_s \geqslant 0$, while any larger μ_8 would exclude $\mu_8 \leqslant 0$ at 95 % CL.

5.5 FORECASTS FOR PIXIE: MCMC

This Section contains the main results of the Chapter, summarized in tab. 5.2 and fig. 5.6 (which shows the contours in the α_s - μ_8 plane).

We start with a discussion of the detectability of μ-type distortions by PIXIE in the context of the ΛCDM model, i. e. with zero running of the spectral index. We stress that, in this case, Planck bounds imply that with only a small $2\times$ improvement over PIXIE noise, the exclusion of $\mu_8 \leqslant 0$ at $\approx 3\sigma$ is guaranteed, given the narrow posterior for μ_8. On the other hand, as we have seen in Section 5.3, for the $\Lambda\text{CDM} + \alpha_s$ case a value of $\mu_8 \sim 0.7$ is fully compatible with Planck data, and it will be only marginally detectable by PIXIE in the case of a minimal configuration. Assuming the Planck constraint on μ_8, the minimal value of μ_8 compatible with Planck in between two standard deviations is $\mu_8 \sim 0.25$. Clearly, given this value, a safe experimental direct detection of μ-type distortions can be obtained only with an experimental sensitivity of $\sigma_{\mu_8} \sim 0.2$, i. e. a $5\times$ improvement over PIXIE.

However, in the presence of running, the argument can be reversed: it becomes now interesting to see how precise should be the measurement performed by a PIXIE-like spectrometer to translate a non-detection of μ-distortions into a detection of $\alpha_s < 0$, pursuing the marginal (below one standard deviation) indication for negative running coming from Planck (whose posterior, while compatible with $\alpha_s = 0$, peaks at a negative value of $\alpha_s = -0.006$: see tab. 5.2). For this

9 This assumes that we interpret the data within ΛCDM plus running. Given our theoretical understanding of the early Universe, this is indeed perhaps the most natural choice.

TABLE 5.2: 68 % CL constraints on the scalar spectral index n_s, its running α_s and the μ-distortion amplitude from a future combined analysis of the Planck 2015 release in temperature and polarization (baseline: TT, TE, EE + lowP) and a PIXIE-like spectrometer as function of different experimental configurations and fiducial values for the running of the spectral index ($\alpha_s^{\rm fid} = -0.01$, corresponding to $\mu_8^{\rm fid} = 1.06$, and $\alpha_s^{\rm fid} = -0.02$, corresponding to $\mu_8^{\rm fid} = 0.73$). Notice that for $\alpha_s^{\rm fid} = -0.01$, $5\times$ PIXIE is needed to exclude $\alpha_s = 0$ at 95 % CL, while for $\alpha_s^{\rm fid} = -0.02$, $3\times$ PIXIE suffices.

baseline	n_s	α_s	μ_8
ΛCDM	$0.9645^{+0.0048}_{-0.0049}$	$\equiv 0$	$1.57^{+0.11}_{-0.13}$
ΛCDM + α_s	0.9639 ± 0.0050	$-0.0057^{+0.0071}_{-0.0070}$	$1.28^{+0.30}_{-0.52}$
"slow-roll"	$0.9644^{+0.0051}_{-0.0052}$	$\sim -(1-n_s)^2$	$1.49^{+0.12}_{-0.13}$
$\alpha_s^{\rm fid} = -0.01$	n_s	α_s	μ_8
+ $1\times$ PIXIE	$0.9637^{+0.0050}_{-0.0049}$	$-0.0064^{+0.0065}_{-0.0064}$	$1.22^{+0.28}_{-0.45}$
+ $2\times$ PIXIE	$0.9634^{+0.0049}_{-0.0048}$	$-0.0074^{+0.0061}_{-0.0053}$	$1.15^{+0.25}_{-0.34}$
+ $3\times$ PIXIE	0.9632 ± 0.0048	$-0.0079^{+0.0053}_{-0.0045}$	$1.11^{+0.22}_{-0.27}$
+ $5\times$ PIXIE	$0.9631^{+0.0048}_{-0.0047}$	$-0.0083^{+0.0040}_{-0.0035}$	$1.08^{+0.17}_{-0.18}$
+ $10\times$ PIXIE	0.9631 ± 0.0047	$-0.0085^{+0.0025}_{-0.0024}$	1.06 ± 0.09
$\alpha_s^{\rm fid} = -0.02$	n_s	α_s	μ_8
+ $1\times$ PIXIE	$0.9635^{+0.0050}_{-0.0049}$	$-0.0071^{+0.0065}_{-0.0063}$	$1.18^{+0.27}_{-0.43}$
+ $2\times$ PIXIE	$0.9628^{+0.0049}_{-0.0048}$	$-0.0094^{+0.0061}_{-0.0052}$	$1.04^{+0.23}_{-0.31}$
+ $3\times$ PIXIE	$0.9624^{+0.0049}_{-0.0048}$	$-0.0111^{+0.0055}_{-0.0045}$	$0.95^{+0.19}_{-0.24}$
+ $5\times$ PIXIE	$0.9618^{+0.0049}_{-0.0047}$	$-0.0131^{+0.0046}_{-0.0037}$	$0.85^{+0.16}_{-0.15}$
+ $10\times$ PIXIE	$0.9613^{+0.0048}_{-0.0047}$	$-0.0149^{+0.0033}_{-0.0029}$	0.77 ± 0.09

purpose, we reprocess the MCMC chains by importance sampling, multiplying the weight of each sample by (see also eq. (5.7))

$$\mathcal{L}_{\rm PIXIE} = \exp\left[-\frac{\left\{\mu_8(\boldsymbol{\theta}) + \mu_{8,\rm BEC}(\boldsymbol{\theta}) - \mu_8^{\rm fid}\right\}^2}{2\sigma^2_{\mu_8}}\right], \tag{5.10}$$

focussing on the two fiducial models for the running described in Section 5.1:

- $\alpha_s^{\rm fid} = -0.01$, corresponding to a spectral distortion $\mu_8 = 1.06$ (close to the Planck best-fit for μ_8);
- $\alpha_s^{\rm fid} = -0.02$ corresponding to a spectral distortion $\mu_8 = 0.73$, which is at the limit of two standard deviations from the Planck mean-fit.

As in Section 5.4, we take $\sigma_{\mu_8} = 1/n$ for a $n\times$ PIXIE experimental configuration. The results of this importance sampling are also reported in tab. 5.2.

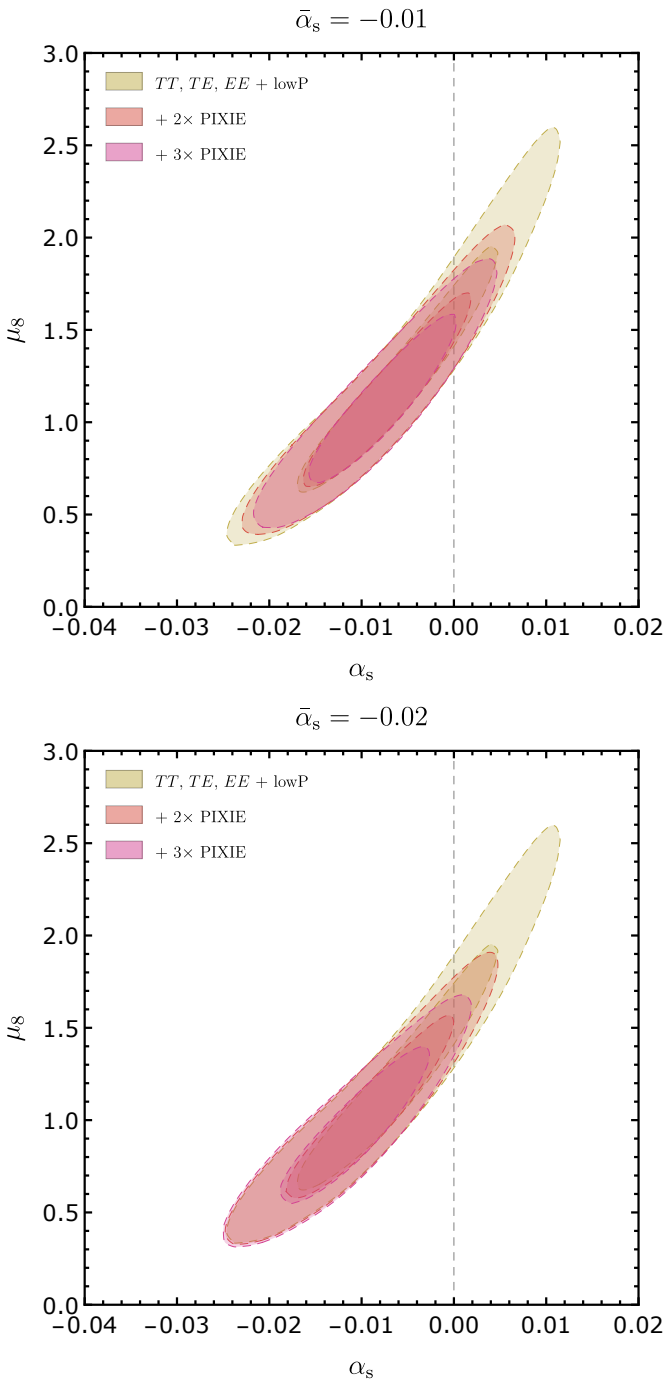

FIGURE 5.6: Top panel: 68 % CL and 95 % CL contours in the α_s - μ_8 plane, for Planck alone (yellow contour) and including in the analysis the likelihood with $\alpha_s^{fid} = -0.01$ (i. e. $\mu_8^{fid} = 1.06$) for a $2\times$ and $3\times$ improvement over PIXIE (orange and purple contours). Bottom panel: same as top panel, but with fiducial α_s equal to -0.02.

Considering that from the Planck dataset alone one obtains $\sigma_{n_s} \approx 0.005$ and $\sigma_{\alpha_s} \approx 0.007$, we see that the minimal configuration of $1\times$ PIXIE or the upgraded $2\times$ PIXIE will produce minimal effects on the Planck bounds, even when the fiducial model deviates significantly from the Planck best-fit.

If, instead, the experimental sensitivity will reach the level of $5\times$ PIXIE ($10\times$ PIXIE) then the constraints on the running of the spectral index can be improved by $\sim 30\%$ ($\sim 50\%$): this improvement could be extremely significant. More precisely, we see that if $\alpha_s^{\rm fid}$ is ~ -0.01, then the addition of $5\times$ PIXIE to Planck bounds could yield a detection of negative running at two standard deviations (three for $10\times$ PIXIE). If we allow an even more negative fiducial value for the running, i.e. $\alpha_s^{\rm fid} \sim -0.02$ then the negative running will be probed at two standard deviations by $3\times$ PIXIE (five standard deviations by $10\times$ PIXIE). tab. 5.2 also shows that the constraints on the tilt are left basically untouched, in agreement with the results of Section 5.3, where we have seen that μ_8 is only mildly dependent on it.

Finally, we comment on the possibility of discriminating between no-running ΛCDM and slow-roll inflation, where the running is second order in the slow-roll expansion. An order-of-magnitude prediction for α_s, that arises in many models, is $\alpha_s \sim -(1-n_s)^2$ [141–143]: tab. 5.2 shows that the predictions for μ_8 in these two cases are indistinguishable at PIXIE sensitivity, and that a massive improvement in sensitivity by a factor of order 10^2 is needed to probe the differences between them.

5.6 IMPLICATIONS FOR SLOW-ROLL INFLATION

In this Section, we discuss the implications of the value of the running within single-clock inflation. Observations tell us (see [14] and tab. 5.2)

$$1 - n_s(k_\star) \equiv -\frac{\partial \log \Delta^2_\zeta(k_\star)}{\partial \log k} \tag{5.11a}$$
$$= 0.0361 \pm 0.0050 \quad (68\,\%\,\mathrm{CL})\,,$$
$$\alpha_s = -n_{s,N} \tag{5.11b}$$
$$= -0.0057^{+0.0071}_{-0.0070} \quad (68\,\%\,\mathrm{CL})\,,$$
$$r < 0.08 \quad (95\,\%\,\mathrm{CL})\,, \tag{5.11c}$$

where $*_{,N}$ refers to a derivative with respect to the number of e-folds from the end of inflation, decreasing as time increases, namely $H dt = -dN$ (we refer to Section 4.7 for details). The standard slow-

roll solution for the primordial power spectrum gives (for an inflaton speed of sound $c_s \neq 0$)

$$1 - n_s = 2\varepsilon_H - \frac{(\varepsilon_H)_{,N}}{\varepsilon_H} - \frac{c_{s,N}}{c_s} \tag{5.12a}$$

$$= \frac{r}{8c_s} - \frac{r_{,N}}{r} , \tag{5.12b}$$

$$\alpha_s = 2(\varepsilon_H)_{,N} - \frac{r_{,NN}}{r} + \left(\frac{r_{,N}}{r}\right)^2 , \tag{5.12c}$$

where the tensor-to-scalar ratio is given approximately by $r = 16\varepsilon_H c_s$.

It is convenient to re-express the running by making explicit its dependence on the tilt, which is relatively well constrained, i. e.

$$\alpha_s = (1-n_s)^2 - 6\varepsilon_H(1-n_s) + 8\varepsilon_H^2 - \left(\frac{rs}{8c_s} + \frac{r_{,NN}}{r}\right) . \tag{5.13}$$

Here, ε_H can be extracted from r if we know the speed of sound c_s from the equilateral bispectrum, or if we assume standard slow-roll single-field inflation, namely $c_s = 1$. On the other hand, the last term $r_{,NN}/r$ makes its first appearance in the running α_s; also the penultimate term $s \equiv c_{s,N}/c_s$ is degenerate with $(\varepsilon_H)_{,N}/\varepsilon_H$ in n_s and so it is also considered unknown. In this precise sense, we can think of the running as a measurement of the yet unknown next-to-leading (NLO) order slow-roll parameters

$$\text{NLO} \equiv \frac{rs}{8c_s} + \frac{r_{,NN}}{r} \xrightarrow{c_s=1} \frac{(\varepsilon_H)_{,NN}}{\varepsilon_H} . \tag{5.14}$$

In fig. 5.7, we show a contour plot of α_s as function of ε_H for different values of the NLO slow-roll parameters. We point out that for $\text{NLO} = 0$ one finds $\alpha_s \geqslant -\frac{1}{8}(1-n_s)^2 \simeq -2 \times 10^{-4}$. Any evidence that the running is sizable and negative therefore implies $\text{NLO} > 0$, i. e. the discovery of a new higher order slow-roll parameter. In a typical slow-roll model, one indeed expects the NLO terms to be of the same order as $(1-n_s)^2$. For example, consider $c_s = 1$ and $\varepsilon_H = 3/(4N^2)$,[10] i. e. the Starobinsky model [171]. Then, we have

$$(1-n_s)^2 \simeq \frac{4}{N^2} , \tag{5.15a}$$

$$\frac{r_{,NN}}{r} = \frac{6}{N^2} . \tag{5.15b}$$

One hence finds

$$\alpha_s \simeq -\frac{2}{N^2} \simeq -\frac{1}{2}(1-n_s)^2 . \tag{5.16}$$

10 Note that the relation $\varepsilon_H = 3/(4N^2)$ holds at first order in slow-roll: it is accurate enough, however, for the values of N that reproduce a scalar spectral index n_s within the current Planck bounds.

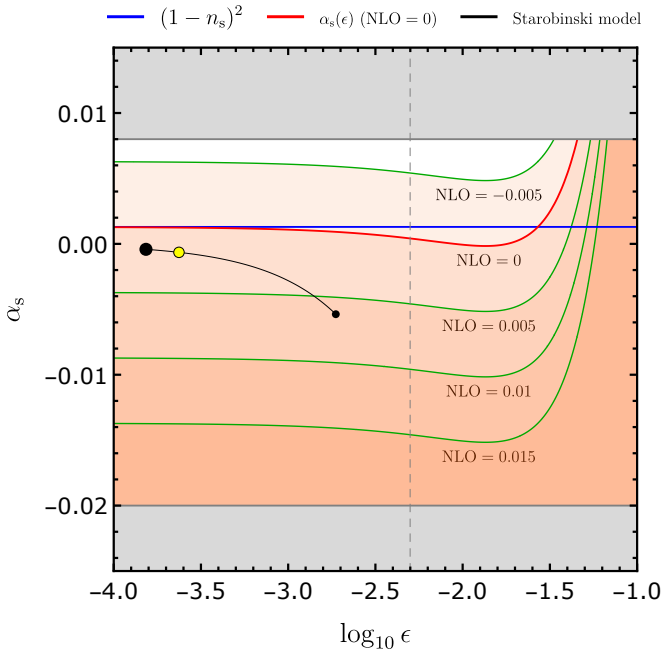

FIGURE 5.7: This contour plot shows α_s as function of ε_H (called ϵ in the figure) for different values of the NLO slow-roll parameters. Notice that the uncertainty in n_s is smaller than the thickness of the lines in the plot. In red we show $\alpha_s(\varepsilon_H)$ of eq. (5.13) for NLO $= 0$, while the blue line is its asymptotic value $(1-n_s)^2 \approx 0.0013$. The black line shows the predictions of the Starobinsky model [171] (with N going from 20 to 70), with the yellow dot being its prediction for $N = 56$ (chosen to reproduce the observed value of n_s). The gray bands show the values of α_s excluded (at 95 % CL) by Planck TT, TE, EE + lowP data, while the gray dashed vertical line shows the current bound on $\varepsilon_H = r/(16c_s)$ from eq. (5.11c), considering $c_s = 1$.

5.7 CONCLUSIONS

In this Chapter, we have considered how a measurement of the CMB spectrum by an experiment like PIXIE would extend our knowledge of the very early Universe. Using Planck data, we have derived the predicted likelihood for the size of the μ-type distortions generated by the dissipation of acoustic waves in the photon-baryon-electron plasma. As shown in fig. 5.2, both ΛCDM and ΛCDM + α_s predict $\mu_8 \simeq \mathcal{O}(1)$, and exclude $\mu_8 = 0$, a.k.a. the "the balanced injection scenario" [12, 78, 86] at high confidence (at 15σ for ΛCDM, at 97.4 % CL for ΛCDM + α_s). While this means that we will be eventually able to measure μ-distortions, it is important to determine whether this will already be possible with the next satellite experiment. Here we point out that, irrespectively of the actual value of α_s (and its respective μ_8, according to eq. (5.8)), a meaningful sensitivity target is $\sigma_{\mu_8} \simeq 0.35$, namely about a three times improvement over the current PIXIE

design (but still less sensitive than the proposed PRISM). This is in fact the threshold for a guaranteed discovery: either μ_8 is large enough that it will be detected (at 95 % CL), or else $\alpha_s \geqslant 0$ will be excluded (at 95 % CL) and with it our current standard model, namely the 6-parameter ΛCDM. The absence of a detection of μ_8 for a $3\times$ PIXIE improvement would exclude most slow-roll models as well, since typically $|\alpha_s| \sim (1 - n_s)^2$, which is indistinguishable from $\alpha_s = 0$ at these sensitivities.

We have further considered the constraining power of CMB spectral distortions combined with the current Planck data. We have discussed how to optimize this analysis by choosing an appropriate pivot for the parameterization of the primordial power spectrum (see fig. 5.5 and fig. 5.5). In tab. 5.2, we present the improved constraints on the spectral tilt and its running from Planck plus an n-fold improvement over PIXIE sensitivity. For a fiducial $\alpha_s = -0.01$, close to the fit for Planck, one expects a detection of μ_8 at 95 % CL already with $2\times$ PIXIE. Conversely, for a fiducial $\alpha_s = -0.02$ (which is at the low 95 % CL end of the Planck constraint), $3\times$ PIXIE will already provide evidence (at 2σ) of a sizable negative running. This would put pressure on the standard slow-roll paradigm, which leads to the typical expectation $\alpha_s \simeq -(1 - n_s)^2$ (see, e. g., eq. (5.13)). Finally, we proposed fig. 5.7 as a convenient and compact way to visualize the improving constraints on the tilt, running and tensor-to-scalar ratio.

6

RUNNING THE RUNNING

CONTENTS

In this Chapter we discuss what are the current constraints on the running of the running β_s from Planck data. Besides, we see what are the possible improvements on these constraints that a PIXIE-like experiment could provide. The Chapter is based on the work Phys. Rev. D **94**, no. 2, 023523 (2016).

6.1 INTRODUCTION

The recent measurement of the Cosmic Microwave Background (CMB) anisotropies provided by the Planck satellite mission (see [6, 14], for example) have provided a wonderful confirmation of the standard ΛCDM cosmological model. However, when the base model is extended and other cosmological parameters are let free to vary, a few "anomalies" are present in the parameter values that, even if their significance is only at the level of two standard deviations, deserve further investigation.

First of all, the parameter A_L, that measures the amplitude of the lensing signal in the CMB angular spectra [172], has been found larger than the standard value with $A_L = 1.22 \pm 0.10$ at 68 % CL ($A_L = 1$ being the expected value in ΛCDM) from Planck temperature and polarization angular spectra [6]. A value of A_L larger than one is difficult to accommodate in ΛCDM, and several solutions have been proposed as modified gravity [173, 174], neutrino anisotropies [175], and compensated isocurvature perturbations [176]. Combining Planck with data from the Atacama Cosmology Telescope (ACT) and the South Pole Telescope (SPT) to better constrain the foregrounds, Couchot et al. [177], found a consistency with $A_L = 1$. However the compatibility of the CMB datasets used is unclear. More recently Addison et al. [178] have found that including the A_L parameter solves the tension between Planck and WMAP9 on the value of the derived cosmological parameters.

As shown in [6], the A_L anomaly persists when the Planck data is combined with Baryonic Acoustic Oscillation surveys (BAO), it is enhanced when the CFHTLenS shear lensing survey is included, but it practically disappears when CMB lensing from Planck trispectrum observations are considered. The A_L anomaly is also still present in a 12-parameter extended ΛCDM analysis of the Planck dataset (see [60]), showing no significant correlation with extra parameters such as the dark energy equation of state w, the neutrino mass, and the neutrino effective number N_{eff}.

Second, the Planck dataset prefers a positively curved universe, again at about two standard deviations with $\Omega_k = -0.040 \pm 0.020$ at 68 % CL (Ω_k being the parameter defined in eq. (1.41), evaluated at the present time). This "anomaly" is not due to an increased parameter volume effect but, as stated in [14], curvature provides a genuine better fit to the data with an improved fit of $\Delta\chi^2 \sim 6$. When BAO data is included, however, the curvature of the universe is again compatible with zero with the stringent constraint $\Omega_k = -0.000 \pm 0.005$ at 95 % CL.

The fact that both the A_L and Ω_k anomalies disappear when reliable external datasets are included suggests that their origin might be a systematic or that they are produced by a different physical effect than lensing or curvature.

In this respect it is interesting to note that a third parameter is constrained to anomalous values from the Planck data. The primordial scalar spectral index n_s of scalar perturbations is often assumed to be independent of scale. However, since some small scale-dependence is expected, we can expand the dimensionless scalar power spectrum $\Delta^2_\zeta(k) = k^3 P_\zeta(k)/2\pi^2$ as in eq. (4.40), i. e.

$$\Delta^2_\zeta(k) = A_s \left(\frac{k}{k_\star}\right)^{n_s - 1 + \frac{\alpha_s}{2}\log\frac{k}{k_\star} + \frac{\beta_s}{6}\log^2\frac{k}{k_\star}}, \tag{6.1}$$

where α_s is the running of the spectral index, β_s is the running of the running, and $k_\star = 0.05\,\mathrm{Mpc}^{-1}$.

The Planck temperature and polarization data analysis presented in [14], while providing a small indication for a *positive* running different from zero ($\alpha_s = 0.009 \pm 0.010$ at 68 % CL), suggests also the presence of a running of the running at the level of two standard deviations ($\beta_s = 0.025 \pm 0.013$ at 68 % CL). The inclusion of a running of the running improves the fit to the Planck temperature and polarization data by $\Delta\chi^2 \sim 5$. This third anomaly is therefore robust and hints for possible new physics beyond the standard model. A discussion of the impact of this anomaly on inflationary models has been presented in [179].

What this Chapter aims to do, then, is to discuss the possible correlations between these three anomalies, β_s, A_L and Ω_k and see, for example, if one of them vanishes if a second one is considered at the

same time in the analysis. Moreover, we will see if the indication for the running of the running survives when additional datasets as BAO or lensing (CMB and shear) are considered.

This Chapter is structured as follows. In the next Section we will describe the analysis method and the cosmological datasets used. In Section 6.3 we present our results and discuss possible correlations between β_s, A_L and Ω_k. We also investigate the possibility that a running of the running affects current and future measurements of CMB spectral distortions. Finally, in Section 6.6 we derive our conclusions.

6.2 METHOD

We perform a Monte Carlo Markov Chain (MCMC) analysis of the most recent cosmological datasets using the publicly available code `cosmomc` [168, 169]. We consider the 6 parameters of the standard ΛCDM model, i.e. the baryon $\omega_b \equiv \Omega_b h^2$ and cold dark matter $\omega_{cdm} \equiv \Omega_{cdm} h^2$ energy densities (we will use the subscript c instead of "cdm" in the following), the angular size of the horizon at the last scattering surface θ_{MC}, the optical depth τ (called τ_{rei} in eq. (3.80)), the amplitude of primordial scalar perturbations $\log(10^{10} A_s)$ and the scalar spectral index n_s. We extend this scenario by including the running of the scalar spectral index α_s and the running of the running β_s. We fix the pivot scale at $k_\star = 0.05\,\mathrm{Mpc}^{-1}$. This is our baseline cosmological model, that we will call "base" in the following. Moreover, as discussed in the introduction, we also consider separate variation in the lensing amplitude A_L, in the curvature density Ω_k and in the sum of neutrino masses $\sum m_\nu$.

The main dataset we consider, to which we refer as "*Planck*", is based on CMB temperature and polarization anisotropies. We analyze the temperature and polarization Planck likelihood [167]: more precisely, we make use of the TT, TE, EE high-ℓ likelihood together with the TEB pixel-based low-ℓ likelihood. The additional datasets we consider are the following:

- Planck measurements of the lensing potential power spectrum $C_\ell^{\phi\phi}$ [180];
- weak gravitational lensing data of the CFHTLenS survey [181, 182], taking only wavenumbers $k \leqslant 1.5h\,\mathrm{Mpc}^{-1}$ [6, 183];
- Baryon Acoustic Oscillations (BAO): the surveys included are 6dFGS [184], SDSS-MGS [185], BOSS LOWZ [186] and CMASS-DR11 [186]. This dataset will help to break geometrical degeneracies when we let Ω_k free to vary.

TABLE 6.1: 68 %CL bounds on $\Omega_b h^2$, $\Omega_c h^2$, $100\theta_{MC}$, τ, H_0, $\log(10^{10} A_s)$, n_s, α_s, β_s, for the listed datasets: the model is $\Lambda CDM + \alpha_s + \beta_s$, $k_\star = 0.05\,\mathrm{Mpc}^{-1}$.

base	*Planck*	+ lensing	+ WL	+ BAO
$\Omega_b h^2$	0.02216 ± 0.00017	0.02215 ± 0.00017	0.02221 ± 0.00017	0.02224 ± 0.00015
$\Omega_c h^2$	0.1207 ± 0.0015	0.1199 ± 0.0015	0.1197 ± 0.0014	0.1196 ± 0.0011
$100\theta_{MC}$	1.04070 ± 0.00032	1.04080 ± 0.00032	1.04078 ± 0.00032	$1.04082^{+0.00029}_{-0.00030}$
τ	0.091 ± 0.019	0.064 ± 0.014	0.086 ± 0.019	0.096 ± 0.018
H_0	66.88 ± 0.68	67.16 ± 0.67	$67.29^{+0.66}_{-0.65}$	$67.36^{+0.49}_{-0.48}$
$\log(10^{10} A_s)$	3.118 ± 0.037	3.061 ± 0.026	$3.104^{+0.038}_{-0.037}$	3.125 ± 0.036
n_s	$0.9582^{+0.0055}_{-0.0054}$	0.9607 ± 0.0054	0.9608 ± 0.0055	$0.9613^{+0.0046}_{-0.0047}$
α_s	0.011 ± 0.010	0.012 ± 0.010	0.012 ± 0.010	0.010 ± 0.010
β_s	0.027 ± 0.013	0.022 ± 0.013	0.026 ± 0.013	0.025 ± 0.013

6.3 RESULTS

In tab. 6.1 we present the constraints on n_s, α_s and β_s from the Planck 2015 temperature and polarization data and in combination with BAO, cosmic shear and CMB lensing. As we can see, the *Planck* dataset alone provides an indication for $\beta_s > 0$ at more than two standard deviations with $\beta_s = 0.027 \pm 0.013$ at 68 % CL.

It is interesting to investigate the impact of the inclusion of α_s and β_s on the remaining 6 parameters of the ΛCDM model. Comparing our results with those reported in tab. 3 of [14], we see that there are no major shifts on the parameters. The largest shifts are present for the scalar spectral index n_s, that is ~ 0.9 standard deviations *lower* when β_s is included, and for the reionization optical depth τ that is ~ 0.9 standard deviations *higher* with respect to the standard ΛCDM scenario. A similar shift is also present for the value of the root mean square density fluctuations on scales of $8h\,\mathrm{Mpc}^{-1}$ (the σ_8 derived parameter), which is higher by about one standard deviation when β_s is considered. In Fig. 6.1 we plot the probability contour at 68 % CL and 95 % CL for the several combinations of datasets in the β_s - σ_8 and β_s - τ planes respectively. Clearly, a new determination of τ from future large scale polarization data as those expected from the Planck HFI experiment could have an impact on the value of β_s. On the other hand, this one sigma shift in τ with respect to ΛCDM shows that a large scale measurement of CMB polarization does not fully provide a direct determination of τ but that some model dependence is present.

Moreover, as expected, there is a strong correlation between α_s and β_s. Thanks to this correlation, the running α_s is constrained to be positive, with $\alpha_s > 0$ at more than 68 % CL when β_s is considered. This is a ~ 1.3 standard deviations shift on α_s if we compare this result with the value obtained using the same dataset but fixing $\beta_s = 0$ in tab. 5 of [14]. In fig. 6.2 we plot the two dimensional likelihood constraints in the β_s - n_s and β_s - α_s planes respectively. As we can see, a correlation between the parameters is clearly present.

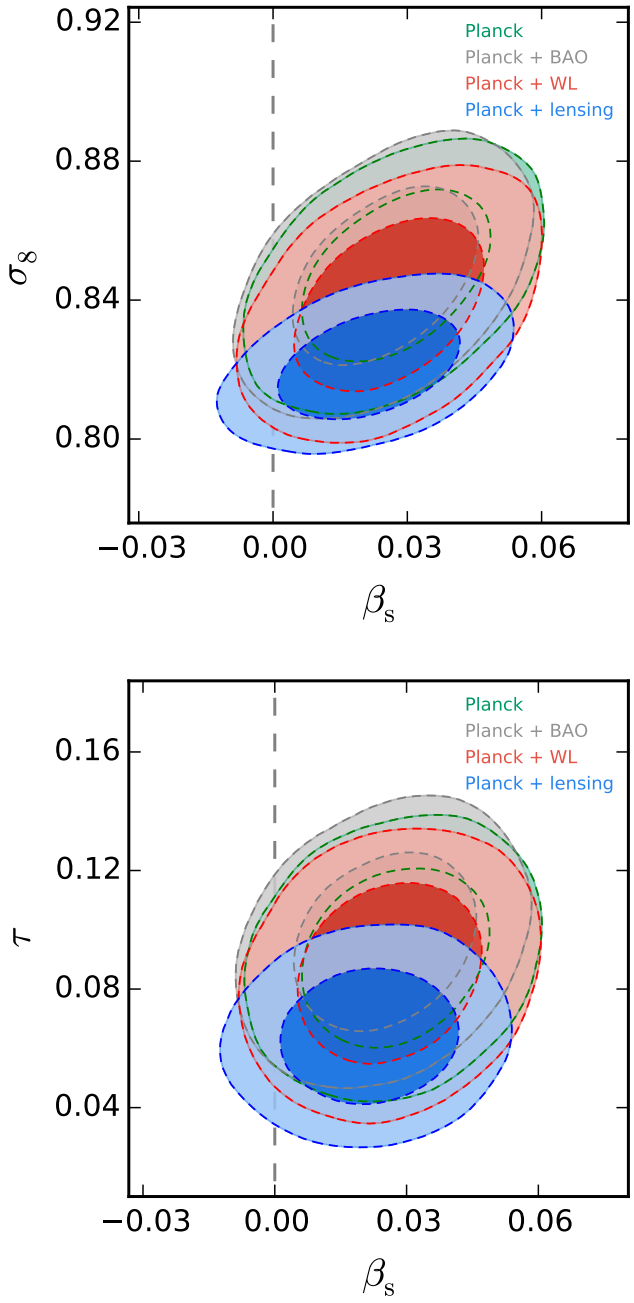

FIGURE 6.1: Constraints at 68 % CL and 95 % CL in the β_s - σ_8 plane (top panel) and in the β_s - τ plane (bottom panel).

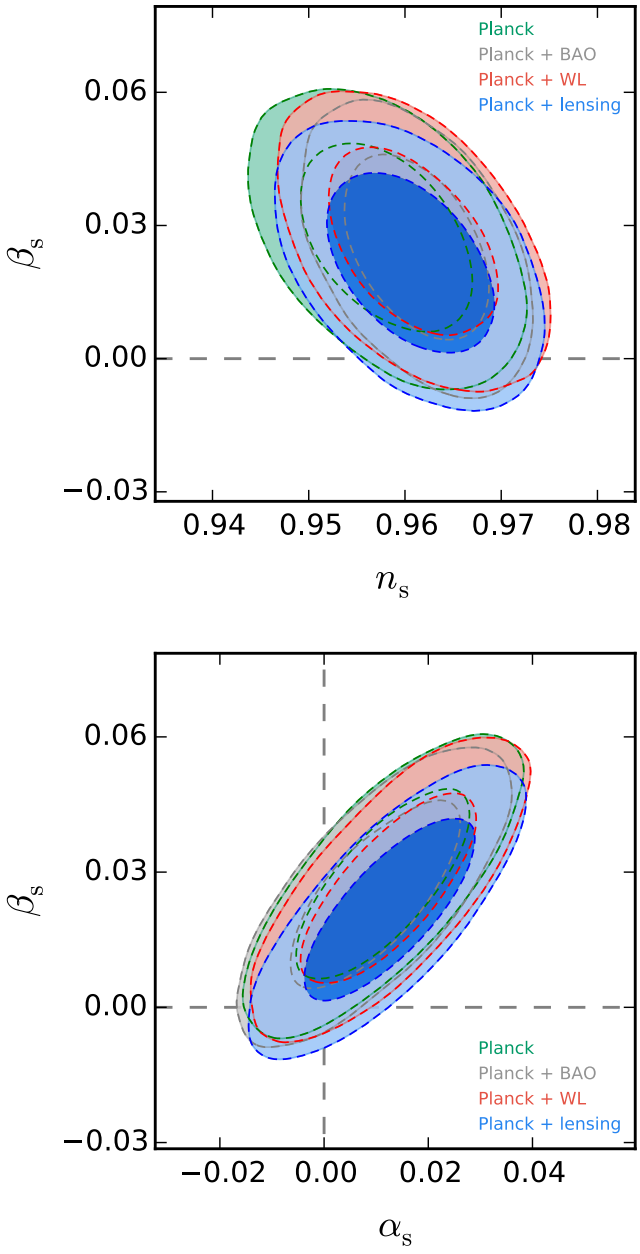

FIGURE 6.2: Likelihood constraints in the β_s - n_s (top panel) and β_s - α_s (bottom panel) planes for different combination of datasets, as discussed in the text.

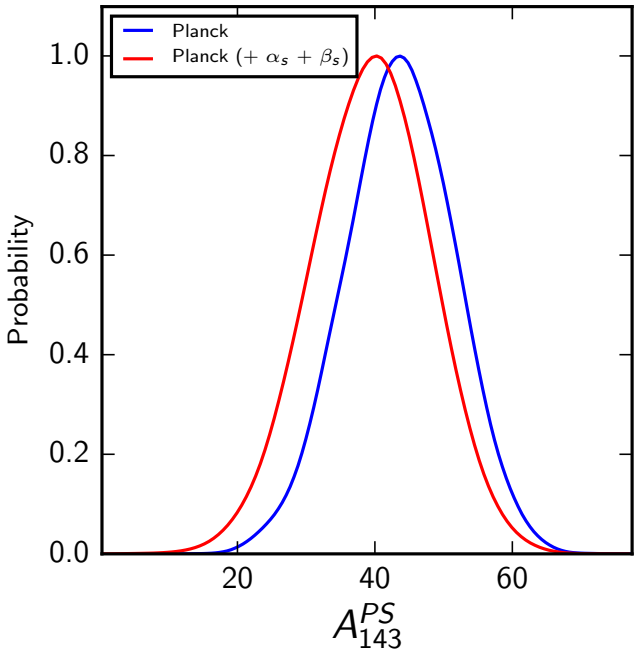

FIGURE 6.3: Shift in the amplitude of unresolved foreground point sources at 143 GHz between the ΛCDM case and the case when variation in α_s and β_s are considered, for the *Planck* dataset.

The Planck likelihood consists essentially of three terms: a low-ℓ ($\ell = 2 \div 29$) TEB likelihood based on the Planck LFI 70 GHz channel full mission dataset, an high-ℓ likelihood based on Planck HFI 100 GHz, 143 GHz and 217 GHz channels half mission dataset and, finally, an additional χ^2 term that comes from the external priors assumed on foregrounds (see [167]). By looking at the mean $\chi^2_{\rm eff}$ values from these three terms we can better understand from where (low ℓ, high ℓ, foregrounds) the indication for β_s is coming. Comparing with the χ^2 values obtained under standard ΛCDM with $\alpha_s = 0$ and $\beta_s = 0$, we have found that while the high-ℓ likelihood remains unchanged, there is an improvement in the low-ℓ likelihood of $\Delta\chi^2_{\rm eff} \sim 2.5$ and in the foregrounds term with $\Delta\chi^2_{\rm eff} \sim 1$. The inclusion of β_s provides therefore a better fit to the low-ℓ part of the CMB spectrum and to the foregrounds prior. While the better fit to the low-ℓ part of the CMB spectrum can be easily explained by the low quadrupole TT anomaly and by the dip at $\ell \sim 20 \div 30$, the change due to foregrounds is somewhat unexpected since, in general, foregrounds do not correlate with cosmological parameters. We have found a significant correlation between β_s and the point source amplitude at 143 GHz, A^{PS}_{143}. The posterior of A^{PS}_{143} shifts indeed by half sigma towards lower values with respect to the standard ΛCDM case (see fig. 6.3) from $A^{PS}_{143} = 43 \pm 8$ to $A^{PS}_{143} = 39 \pm 8$ at 68 % CL. This shift could also explain the small difference between the constraints reported here and those reported

in [14], that uses the *Pliklite* likelihood code where foregrounds are marginalized at their ΛCDM values.

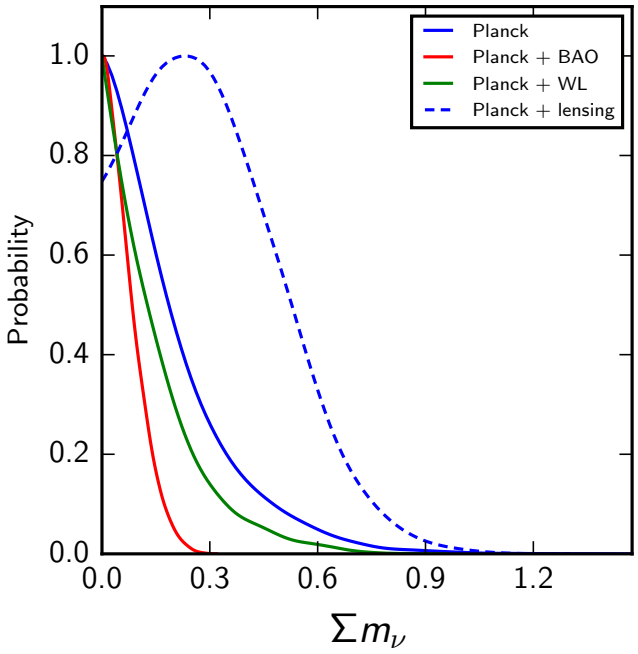

FIGURE 6.4: One-dimensional posterior distributions for the sum of neutrino masses $\sum m_\nu$, for the indicated datasets. The model considered is $\Lambda\text{CDM} + \alpha_s + \beta_s + \sum m_\nu$.

Going back to tab. 6.1, we can see that the indication for $\beta_s > 0$ is slightly weakened but still present also when external datasets are considered. Adding CMB lensing gives $\beta_s = 0.022 \pm 0.013$, i. e. reducing the tension at about 1.7 standard deviations, while the inclusion of weak lensing and BAO data does not lead to an appreciable decrease in the statistical significance of α_s and β_s.

In tab. 6.2 we report similar constraints but including also variations in the neutrino mass absolute scale $\sum m_\nu$. The constraints obtained from the Planck 2015 data release on the neutrino masses are indeed very strong, especially when combined with BAO data, ruling out the possibility of a direct detection from current and future beta and double beta decay experiments (see, e. g., [187]). Since Planck data show a preference for $\beta_s > 0$, it is clearly interesting to investigate if the inclusion of running has some impact on the cosmological constraints on $\sum m_\nu$. Comparing the results of tab. 6.2 with those in [14], which were obtained assuming $\alpha_s = \beta_s = 0$, we see that the constraints on $\sum m_\nu$ are only slightly weakened, moving from $\sum m_\nu < 0.490\,\text{eV}$ to $\sum m_\nu < 0.530\,\text{eV}$ at 95 % CL for the *Planck* dataset alone and from $\sum m_\nu < 0.590\,\text{eV}$ to $\sum m_\nu < 0.644\,\text{eV}$ at 95 % CL when also lensing is considered. The constraints on $\sum m_\nu$ including the WL

and BAO datasets are essentially unaffected by β_s. We can therefore conclude that there is no significant correlation between β_s and $\sum m_\nu$.

In fig. 6.4 we plot the posterior distributions for $\sum m_\nu$, while in fig. 6.5 we plot the probability contour at 68 % CL and 95 % CL for the several combinations of datasets in the β_s - $\sum m_\nu$ plane, respectively.

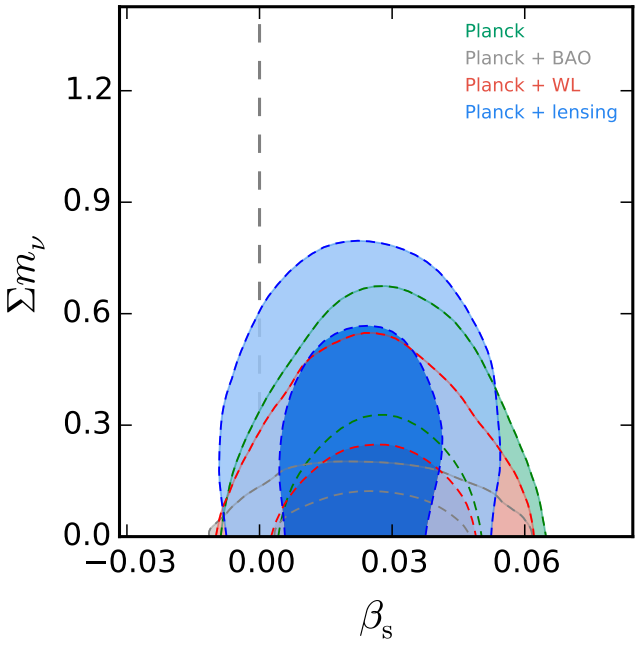

FIGURE 6.5: Two-dimensional posteriors in the β_s - $\sum m_\nu$ plane, for the indicated datasets. We see that there is no correlation between $\sum m_\nu$ and β_s.

In tab. 6.3 we report the constraints from the same datasets but letting also the lensing amplitude A_L free to vary. As discussed in Section 6.1, Planck data are also suggesting a value for $A_L > 1$ and is therefore interesting to check if there is a correlation with β_s. As we can see there is a correlation between the two parameters but not extremely significant. Even with a lower statistical significance, at about $\sim 1.2 \div 1.5$ standard deviations for A_L and β_s respectively (that could be also explained by the increased volume of parameter space), data seem to suggest the presence of *both* anomalies. When the CMB lensing data are included, A_L goes back to its standard value while the indication for β_s increases. When the WL shear data are included the A_L anomaly is present while the indication for β_s is weakened.

We also consider variation in the curvature of the universe and we report the constraints in tab. 6.4. As we can see, also in this case we have a correlation between β_s and Ω_k but not significant enough to completely cancel any indication for these anomalies from Planck data. Indeed, when Ω_k is considered, we have still a preference for $\Omega_k < 0$ and $\beta_s > 0$ at more than one standard deviation. More

TABLE 6.2: 68 % CL bounds and 95 % CL upper limits on $\Omega_b h^2$, $\Omega_c h^2$, $100\theta_{MC}$, τ, $\sum m_\nu$, H_0, $\log(10^{10} A_s)$, n_s, α_s, β_s, for the listed datasets: the model is $\Lambda\text{CDM} + \alpha_s + \beta_s + \sum m_\nu$, $k_\star = 0.05\,\text{Mpc}^{-1}$.

base $+ \sum m_\nu$	*Planck*	+ lensing	+ WL	+ BAO
$\Omega_b h^2$	0.02213 ± 0.00018	0.02207 ± 0.00019	0.02219 ± 0.00018	0.02224 ± 0.00015
$\Omega_c h^2$	0.1208 ± 0.0016	0.1206 ± 0.0016	0.1199 ± 0.0015	0.1196 ± 0.0011
$100\theta_{MC}$	$1.04062^{+0.00033}_{-0.00034}$	1.04060 ± 0.00035	1.04072 ± 0.00033	1.04082 ± 0.00030
τ	$0.095^{+0.019}_{-0.020}$	0.080 ± 0.019	0.088 ± 0.020	$0.095^{+0.020}_{-0.019}$
$\left(\sum m_\nu\right)/\text{eV}$	< 0.530	< 0.644	< 0.437	< 0.159
H_0	$65.76^{+2.12}_{-0.99}$	$64.76^{+2.49}_{-1.70}$	$66.46^{+1.76}_{-0.91}$	67.38 ± 0.56
$\log(10^{10} A_s)$	$3.127^{+0.038}_{-0.039}$	$3.093^{+0.037}_{-0.036}$	3.109 ± 0.038	$3.124^{+0.037}_{-0.038}$
n_s	$0.9576^{+0.0056}_{-0.0057}$	0.9583 ± 0.0057	$0.9601^{+0.0055}_{-0.0054}$	$0.9612^{+0.0047}_{-0.0048}$
α_s	0.011 ± 0.010	0.011 ± 0.010	0.012 ± 0.010	$0.010^{+0.010}_{-0.011}$
β_s	0.028 ± 0.013	0.023 ± 0.013	0.026 ± 0.013	0.025 ± 0.013

TABLE 6.3: 68 % CL bounds and 95 % CL upper limits on $\Omega_b h^2$, $\Omega_c h^2$, $100\theta_{MC}$, τ, A_L, H_0, $\log(10^{10} A_s)$, n_s, α_s, β_s, for the listed datasets: the model is $\Lambda CDM + \alpha_s + \beta_s + A_L$, $k_\star = 0.05\,Mpc^{-1}$.

base + A_L	*Planck*	+ lensing	+ WL	+ BAO
$\Omega_b h^2$	0.02227 ± 0.00019	0.02214 ± 0.00018	0.02235 ± 0.00019	0.02232 ± 0.00016
$\Omega_c h^2$	0.1196 ± 0.0017	0.1202 ± 0.0017	0.1185 ± 0.0016	0.1190 ± 0.0011
$100\theta_{MC}$	1.04081 ± 0.00033	1.04076 ± 0.00033	1.04093 ± 0.00033	1.04089 ± 0.00030
τ	0.070 ± 0.025	0.070 ± 0.025	< 0.095	$0.070^{+0.024}_{-0.026}$
A_L	$1.106^{+0.079}_{-0.090}$	$0.984^{+0.058}_{-0.064}$	$1.157^{+0.077}_{-0.086}$	$1.118^{+0.075}_{-0.084}$
H_0	67.38 ± 0.77	$67.04^{+0.75}_{-0.76}$	67.88 ± 0.73	$67.64^{+0.52}_{-0.53}$
$\log(10^{10} A_s)$	$3.073^{+0.050}_{-0.051}$	$3.074^{+0.050}_{-0.051}$	$3.044^{+0.044}_{-0.051}$	3.072 ± 0.049
n_s	0.9621 ± 0.0062	0.9597 ± 0.0061	$0.9652^{+0.0059}_{-0.0060}$	0.9637 ± 0.0049
α_s	0.010 ± 0.010	0.012 ± 0.010	0.010 ± 0.010	0.009 ± 0.010
β_s	0.021 ± 0.014	0.024 ± 0.014	0.018 ± 0.013	0.019 ± 0.013

TABLE 6.4: 68 % CL bounds on $\Omega_b h^2$, $\Omega_c h^2$, $100\theta_{MC}$, τ, Ω_k, H_0, σ_8, $\log(10^{10} A_s)$, n_s, α_s, β_s, for the listed datasets: the model is $\Lambda CDM + \alpha_s + \beta_s + \Omega_k$, $k_\star = 0.05\,Mpc^{-1}$.

base + Ω_k	*Planck*	+ lensing	+ WL	+ BAO
$\Omega_b h^2$	0.02230 ± 0.00019	0.02213 ± 0.00018	0.02214 ± 0.00019	0.02218 ± 0.00018
$\Omega_c h^2$	$0.1192^{+0.0017}_{-0.0018}$	0.1204 ± 0.0017	0.1206 ± 0.0017	0.1205 ± 0.0016
$100\theta_{MC}$	1.04086 ± 0.00034	1.04074 ± 0.00033	$1.04068^{+0.00035}_{-0.00034}$	$1.04072^{+0.00033}_{-0.00034}$
τ	$0.062^{+0.024}_{-0.028}$	0.076 ± 0.026	$0.099^{+0.023}_{-0.024}$	0.094 ± 0.018
Ω_k	$-0.0302^{+0.0250}_{-0.0173}$	$0.0045^{+0.0096}_{-0.0076}$	$0.0082^{+0.0091}_{-0.0071}$	0.0015 ± 0.0021
H_0	$57.75^{+4.81}_{-6.34}$	$69.71^{+4.11}_{-4.62}$	$71.70^{+3.91}_{-5.02}$	$67.72^{+0.71}_{-0.72}$
σ_8	$0.799^{+0.033}_{-0.036}$	0.837 ± 0.029	$0.860^{+0.026}_{-0.027}$	0.850 ± 0.016
$\log(10^{10} A_s)$	$3.057^{+0.048}_{-0.058}$	3.087 ± 0.052	$3.133^{+0.047}_{-0.049}$	$3.124^{+0.036}_{-0.037}$
n_s	$0.9642^{+0.0064}_{-0.0065}$	$0.9589^{+0.0064}_{-0.0063}$	0.9574 ± 0.0063	0.9587 ± 0.0057
α_s	$0.008^{+0.010}_{-0.011}$	0.013 ± 0.010	0.014 ± 0.011	0.011 ± 0.010
β_s	0.013 ± 0.014	$0.027^{+0.015}_{-0.017}$	$0.035^{+0.015}_{-0.017}$	0.027 ± 0.014

interestingly, when external datasets are included, the indication for a positive curvature simply vanishes, while we get $\beta_s > 0$ slightly below 95 % CL.

In fig. 6.6 we show the constraints at 68 % CL and 95 % CL in the β_s - A_L plane (top panel) and in the β_s - Ω_k plane (bottom panel).

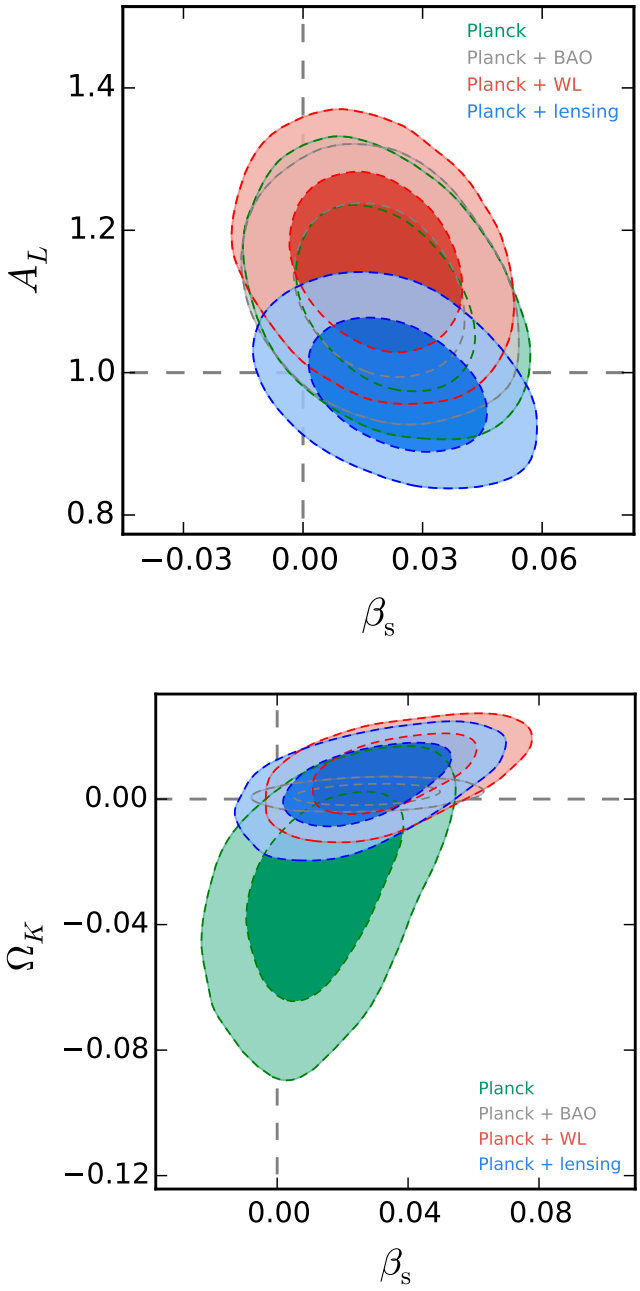

FIGURE 6.6: Constraints at 68 % CL and 95 % CL in the β_s - A_L plane (top panel) and in the β_s - Ω_k plane (bottom panel).

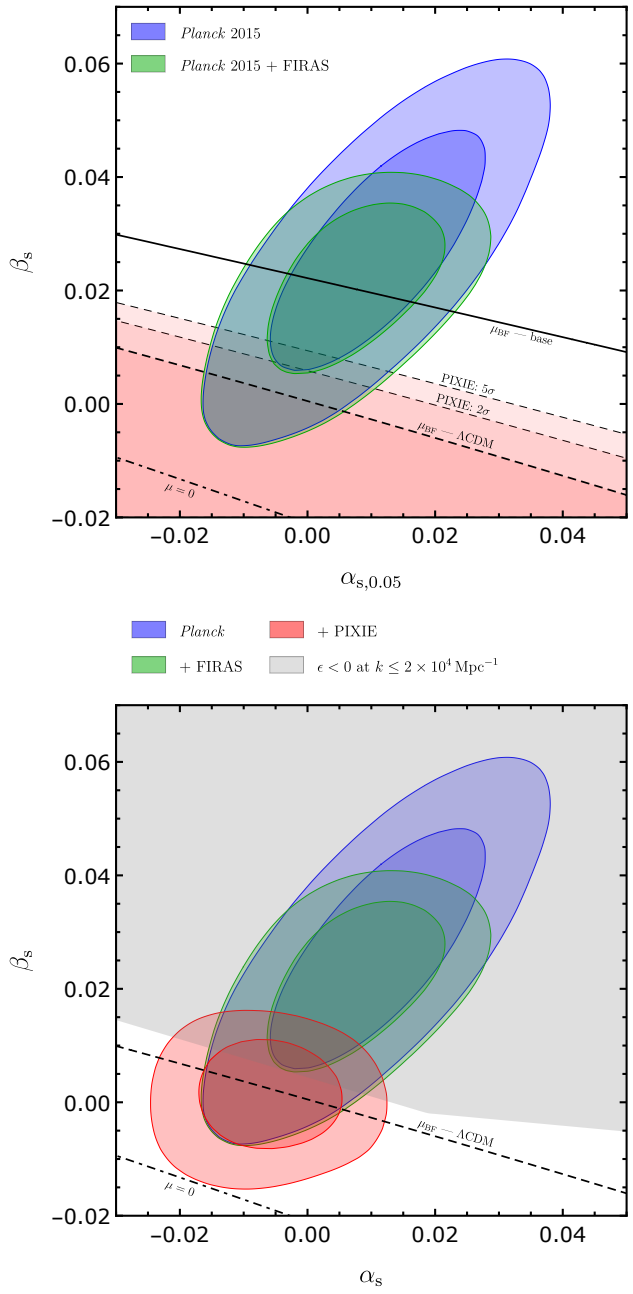

FIGURE 6.7: Top panel: 68 % CL and 95 % CL contours in the α_s - β_s plane, for the *Planck* (blue) and *Planck* + FIRAS (green) datasets (base model). The red regions represent the 2σ and 5σ limits from PIXIE around the *Planck* dataset best-fit for the ΛCDM model, i. e. $\mu = 1.57 \times 10^{-8}$ [49]. Bottom panel: same as top panel, with the red contours represent the 68 % CL and 95 % CL limits from PIXIE, obtained by post-processing the Markov chains with a Gaussian likelihood $\mu = (1.57 \pm 1.00) \times 10^{-8}$. The grey region represents the values of α_s and β_s that lead to a slow-roll parameter $\varepsilon_H(k)$ (called ϵ in the figure), computed via the Taylor expansion of eq. (4.42), less than zero before or at $k = 2 \times 10^4\ \mathrm{Mpc}^{-1}$.

6.4 CONSTRAINTS FROM μ-DISTORTIONS

As we have seen in Section 3.4, CMB μ-type spectral distortions from the dissipation of acoustic waves at redshifts between $z = 2 \times 10^6$ and $z = 5 \times 10^4$ offer a window on the primordial power spectrum at very small scales, ranging from 50 to $10^4\,\mathrm{Mpc}^{-1}$ (for recent works on this topic see [49, 91] and references therein). The impact of a PIXIE-like mission on the constraints on the running α_s has been analyzed in [49], while [91] investigated the variety of signals (and corresponding forecasts) that are expected in the ΛCDM model (not limited to a μ-type distortion).

In this Section, we briefly investigate the constraining power of μ-distortions on β_s, given the *Planck* constraints on α_s and β_s of Section 6.3. We compute the contribution to the μ-monopole from Silk damping of acoustic waves in the photon-baryon plasma [90, 103–105], using the expression for the distortion visibility function presented in [138] and discussed in Section 2.3. The resulting formula for μ is the same as the one used in Chapter 5, namely eqs. (5.3), (5.4), (5.5).

TABLE 6.5: 95 % CL bounds on α_s and β_s from the *Planck* (TT, TE, EE + lowP), *Planck* + FIRAS and *Planck* + PIXIE datasets, for the $\Lambda\mathrm{CDM} + \alpha_s + \beta_s$ (i. e. "base") model. The results have been obtained by post-processing with a Gaussian likelihood the Markov chains considering $\mu = (1.0 \pm 4.0) \times 10^{-5}$ [11] for FIRAS, and $\mu = (1.57 \pm 1.00) \times 10^{-8}$ for PIXIE. See the main text for a discussion of the bounds on the μ-amplitude.

base	α_s	β_s	μ
Planck	0.011 ± 0.021	0.027 ± 0.027	/
+ FIRAS	$0.006^{+0.017}_{-0.018}$	$0.020^{+0.016}_{-0.019}$	$(0.77^{+3.10}_{-0.77}) \times 10^{-6}$
+ PIXIE	$-0.007^{+0.012}_{-0.013}$	$0.001^{+0.008}_{-0.009}$	$(1.59^{+1.75}_{-1.52}) \times 10^{-8}$

Tab. 6.5 shows how, already with the current limit on the μ-distortion amplitude from the FIRAS instrument on the COBE satellite, namely $\mu = (1 \pm 4) \times 10^{-5}$ at 68 % CL [11], we can get a 28 % increase in the 95 % CL upper limits on α_s, and a 33 % increase in those on β_s. In fig. 6.7, we also report a forecast for PIXIE, whose expected error on μ is 10^{-8} [22]. Actually, in [157] it was shown that, when also r-distortions are considered,[1] the expected error should be larger (about $\sigma_\mu = 1.4 \times 10^{-8}$): however, for the large values of α_s and β_s allowed by the *Planck* dataset, the forecasts of tab. 6.5 are not significantly affected. Besides, we see that:

1 r-distortions are the residual distortions that encode the information on the transition between the μ-era and the y-era, where the CMB is not in kinetic equilibrium and energy injections result in distortions of the y-type [88].

- for the best-fit values of cosmological parameters in the ΛCDM + $\alpha_s + \beta_s$ model, which leads to $\mu = 1.09 \times 10^{-6}$, PIXIE will be able to detect spectral distortions from Silk damping at extremely high significance (fig. 6.7). Besides, we see that a statistically significant detection of β_s is expected, along with a sizable shrinking of the available parameter space (fig. 6.7). As we discuss later, any detection of such values of μ-distortions will rule out single-field slow-roll inflation (we did not investigate whether it could be possible to have models of multi-field inflation, or models where the slow-roll assumption is relaxed [188], that can predict such values for the μ-distortion amplitude);
- for a fiducial value of μ corresponding to the ΛCDM best-fit i. e. $\mu = 1.57 \times 10^{-8}$ [49], we see that we get a 84 % increase in the 95 % CL upper limits on α_s, and a 83 % increase in those on β_s. More precisely, values of β_s larger than 0.02 will be excluded at $\sim 5\sigma$.

We conclude this Section with a comment on the validity of a Taylor expansion (in $\log k/k_\star$) of the power spectrum down to scales probed by spectral distortions. We can estimate the terms in the expansion of $n_s(k)$ by choosing $k = 10^4\,\mathrm{Mpc}^{-1}$, corresponding to k_D at $z = z_{DC}$: for values of β_s of order 0.06 (which are still allowed at 95 % CL, as shown in fig. 6.7), the term $\frac{\beta_s}{6}(\log k/k_\star)^2$ in eq. (6.1) becomes of order 1. For this reason, tab. 6.5 does not report the limits on μ coming from the current Planck constraints on the scale dependence of the spectrum. When existing limits on μ from FIRAS are instead added, an extrapolation of $\Delta^2_\zeta(k)$ at the scales probed by μ-distortions starts to become meaningful, and when also PIXIE is included in our forecast around the ΛCDM prediction, the upper bounds on α_s and β_s are lowered enough that a perturbative expansion becomes viable, making our forecast valid.

6.5 LARGE β_s AND SLOW-ROLL INFLATION

In this Section we discuss briefly the implications that values of α_s and β_s of order 10^{-2} have for slow-roll inflation. We can compute the running of the slow-roll parameter ε_H in terms of n_s, α_s and β_s using the procedure described in Section 4.7, namely in eqs. (4.41), (4.42), (4.43), (4.44). From those results, we see that at scales around $k_\star$, n_s dominates, so that ε_H is increasing and a red spectrum is obtained. However, in presence of positive α_s and β_s, at small scales ε_H becomes smaller, until it becomes zero at $k \approx 39.7\,\mathrm{Mpc}^{-1}$ for $\alpha_s = 0.01$ and $\beta_s = 0.02$ (taking $\varepsilon_H|_\star = 0.002$, i. e. the maximum value allowed by current bounds on r, when the inflaton speed of sound c_s is fixed to 1). If we impose that ε_H stays positive down to $k \approx 2 \times 10^4\,\mathrm{Mpc}^{-1}$, which is of the same order of magnitude of the maximum k probed by

μ-distortions (as we have seen Section 2.3), we can obtain a theoretical bound on α_s and β_s. We show this bound in fig. 6.7: this plot tells us that a large part of the contours from the *Planck* + FIRAS and *Planck* + PIXIE datasets cannot be interpreted in the context of slow-roll inflation extrapolated to μ-distortion scales, because ε_H becomes negative before reaching $k \approx k_D(z_{DC})$.

These kind of bounds tell us that the Taylor expansion is not suitable for extrapolating the inflationary spectrum far away from the CMB window, in presence of the values of α_s and β_s that are currently allowed by Planck, since ε_H becomes zero already ~ 7 *e*-folds after the horizon exit of $k_\star$. To avoid this problem, one could consider a series expansion that takes into account the theoretical bounds on ε_H, i. e. $\varepsilon_H(N = 0) = 1$ and $0 < \varepsilon_H < 1$: the Taylor series does not respect these requirements, so it does *not* in general represent a possible power spectrum from inflation, over the whole range of scales. Only when the values of the phenomenological parameters describing the scale dependence of the spectrum are small, the Taylor expansion can be a good approximation of a realistic power spectrum over a range of scales much larger than those probed by the CMB.

Another possibility is to consider bounds on the primordial power spectrum coming from observables that lie outside the CMB scales, but are still at small enough k that the Taylor series applies. In this regard, constraints on the scale dependence of the primordial power spectrum from observations of the Ly-α forest could be very powerful (the forest constrains wavenumbers $k \approx 1 h\,\mathrm{Mpc}^{-1}$),[2] In [191], an analysis of the the one-dimensional Ly-α forest power spectrum measured in [192] was carried out, showing that it provides also small-scale constraints on the tilt n_s and the running α_s: more precisely, for a $\Lambda\mathrm{CDM} + \alpha_s + \sum m_\nu$ model, a detection at approximately 3σ of α_s ($\alpha_s = -0.00135^{+0.0046}_{-0.0050}$ at 68 % CL) is obtained. It would be interesting to carry out this analysis including the running of the running, to see if the bounds on β_s are also lowered.

6.6 CONCLUSIONS

In this Chapter we have studied the constraints on the running of the running of the scalar spectral index β_s and discussed in more detail the 2σ indication for $\beta_s > 0$ that comes from the analysis of CMB anisotropies data from the Planck satellite.

We have considered simultaneous variations in the lensing amplitude parameter A_L and the curvature of the universe Ω_k. We have found that, while a correlation does exist between these parameters, Planck data still hint for non-standard values in the extended

2 Even if modeling the ionization state and thermodynamic properties of the intergalactic medium to convert flux measurements into a density power spectrum is very challenging (see [189] and [190] for a discussion).

ΛCDM $+ \alpha_s + \beta_s + A_L$ and ΛCDM $+ \alpha_s + \beta_s + \Omega_k$ model, only partially suggesting a common origin for their anomalous signal related to the low CMB quadrupole. We have found that the Planck constraints on neutrino masses $\sum m_\nu$ are essentially stable under the inclusion of β_s.

We have shown how future measurements of CMB μ-type spectral distortions from the dissipation of acoustic waves, such as those expected by PIXIE, could severely constrain both the running and the running of the running. More precisely we have found that an improvement on Planck bounds by a factor of $\sim 80\,\%$ is expected. Finally, we discussed the conditions under which the phenomenological expansion of the primordial power spectrum in eq. (6.1) can be extended to scales much shorter that those probed by CMB anisotropies and can provide a good approximation to the predictions of inflationary models.

7

NON-GAUSSIANITY AND SPECTRAL DISTORTIONS

CONTENTS

In this Chapter we will discuss why we expect deviations from Gaussianity in the statistic of cosmological correlation functions, and how the $C_\ell^{\mu T}$ angular cross spectrum is a probe of the three-point function of the primordial curvature perturbation generated by inflation. The Chapter is based mainly on [20, 25, 31].

7.1 WHY NON-GAUSSIANITY?

So far, we have considered only two-point functions of cosmological perturbations. Indeed, in a Gaussian theory the power spectrum completely characterizes the statistics of perturbations. However, gravitational evolution and the collision terms in the Boltzmann equation are non-linear (i. e. we have an interacting theory), and will lead to a coupling between modes with different wavenumber. This will lead to deviations from Gaussian statistics, that we call "non-Gaussianity".

In this and the following Chapters we will focus mainly on non-Gaussianity coming from inflationary physics: this is encoded in the higher-order correlation functions of the scalar and tensor perturbations (ζ and γ_{ij}) of Chapter 4. Any interaction present during inflation will generate these n-point functions:

- for single-field inflation, these can come from the scalar sector. For example, in single-field slow-roll inflation there will be contribution to the cubic Lagrangian for perturbations coming from the potential $V(\phi)$. In theories where the inflaton Lagrangian is a function $P(X, \phi)$, with $X \equiv g^{\mu\nu}\partial_\mu\phi\partial_\nu\phi$, there will be higher-derivative interactions [62, 119, 193];
- if other fields besides the inflaton are active during inflation, interactions between the inflaton and these fields will also lead to non-Gaussianities [194];
- finally, gravity itself is a non-linear theory. We then expect some amount of non-Gaussianity due to gravitational interactions.

Derivative interactions and multi-field inflation can lead to sizable n-point functions: the minimal amount of non-Gaussianity, however, come from gravitational interactions, and is of order of the slow-roll parameters. To see this, we can go to the so-called "flat gauge", where we restore the field perturbation $\delta\phi$ from the unitary gauge (and remove ζ) with a time redefinition. The cubic scalar Lagrangian will have a contribution $\mathcal{L}_{(3)} \supset V'''(\bar{\phi})\delta\phi^3$: however, it is straightforward to show that $V'''(\bar{\phi})$ is second-order in slow-roll (indeed, it is of the same order of the running of the spectral index). The only remaining $\delta\phi$ interaction terms can come only from gravity, i.e. from the solution of the constraint equations (since in this gauge there are no scalar modes in the three-dimensional metric h_{ij}). As we will see in more detail in the next Chapter, the solution of δN and $N^I = \partial_i\psi$ in terms of $\delta\phi$ is of order ε_H, so that the interaction Lagrangian for $\delta\Phi$ will be of order ε_H.

7.2 SQUEEZED LIMIT AND $f_{NL}^{loc.}$

In the following we will focus only on non-Gaussianity in the scalar sector, i.e. we will focus only on (super-horizon) n-point functions of the comoving curvature perturbation ζ (or, equivalently, of the perturbation $\delta\phi$ to the inflaton v.e.v.).

The simplest observable that we can think of when talking about deviations from Gaussian statistics is the three-point function. Indeed, $\langle\zeta(\mathbf{k}_1)\zeta(\mathbf{k}_2)\zeta(\mathbf{k}_3)\rangle$ vanishes for a Gaussian theory, so it is a direct probe of the interactions of ζ. Due to translational and rotational invariance, $\langle\zeta(\mathbf{k}_1)\zeta(\mathbf{k}_2)\zeta(\mathbf{k}_3)\rangle$ can be written as

$$\boxed{\begin{aligned}\langle\zeta(\mathbf{k}_1)\zeta(\mathbf{k}_2)\zeta(\mathbf{k}_3)\rangle = (2\pi)^3\delta^{(3)}(\mathbf{k}_1+\mathbf{k}_2+\mathbf{k}_3)\\ \times B_\zeta(k_1,k_2,k_3)\ ,\end{aligned}} \tag{7.1}$$

where the *bispectrum* $B_\zeta(k_1,k_2,k_3)$ can depend only on the moduli k_i of the three momenta $\mathbf{k}_i$. The freedom in the choice of the momenta k_i means that we can look at the bispectrum in different configurations. Two of the most common are:

EQUILATERAL CONFIGURATION It corresponds to looking at modes of similar size, i.e. $k_1 \sim k_2 \sim k_3$.

SQUEEZED CONFIGURATION It considers one mode to be much longer than the other two, i.e. $k_3 \sim k_\ell \ll k_1 \sim k_2 \sim k_s$.

The overall strength of non-Gaussianities is parameterized by f_{NL}, which is the overall amplitude of the bispectrum. The shape of non-Gaussianities, instead, is usually parameterized as

$$B_\zeta(k_1,k_2,k_3) \propto \frac{S(k_1,k_2,k_3)}{(k_1k_2k_3)^2}(\Delta_\zeta^2)^2\ , \tag{7.2}$$

for scale-invariant power spectra $P_\zeta(k) = \frac{2\pi^2}{k^3}\Delta_\zeta^2$. Depending on the shape of the bispectrum, one defines different f_{NL} parameters. Two common shapes are the equilateral and the local shape (with their corresponding $f_{NL}^{equil.}$ and $f_{NL}^{loc.}$ amplitudes): the equilateral shape peaks in the equilateral configuration, while the local shape peaks in the squeezed configuration (see fig. 7.1). The constraints on $f_{NL}^{equil.}$ and $f_{NL}^{loc.}$ from Planck are [195]

$$f_{NL}^{equil.} = -3.7 \pm 43 \quad (68\,\%\,\mathrm{CL})\,, \tag{7.3a}$$

$$f_{NL}^{loc.} = 0.8 \pm 5.0 \quad (68\,\%\,\mathrm{CL})\,. \tag{7.3b}$$

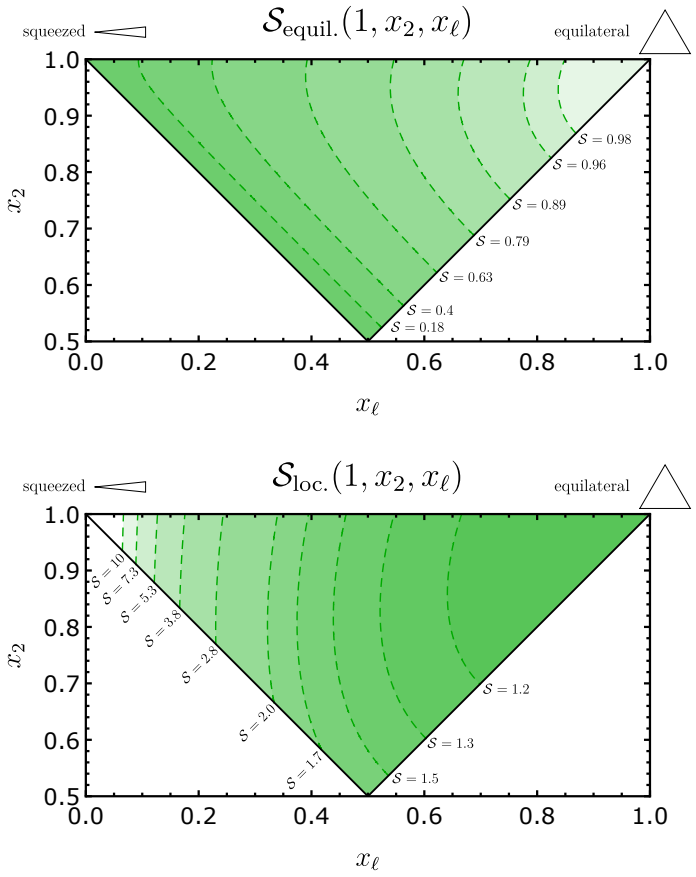

FIGURE 7.1: Top panel: contour plot of the equilateral shape $\mathcal{S}_{equil.}$, normalized such that $\mathcal{S}_{equil.}(1,1,1) = 1$. The axes x_ℓ and x_2 are the rescaled momenta k_ℓ/k_1 and k_2/k_1, respectively (choosing $k_3 \equiv k_\ell$). Momenta are ordered such that $x_\ell < x_2 < 1$, and satisfy the triangle inequality $x_2 + x_\ell > 1$. $\mathcal{S}_{equil.}$ goes to zero as k_ℓ/k_1 in the squeezed limit $x_\ell \ll 1$. Bottom panel: contour plot of the local shape $\mathcal{S}_{loc.}$. We see that it increases rapidly (as k_1/k_ℓ) in the squeezed limit.

Multi-field inflation can give sizable $f_{NL}^{loc.}$, while derivative interactions can give sizable $f_{NL}^{equil.}$. What about single-field slow-roll inflation? The bispectrum in this case is given by [17, 18]

$$\boxed{\mathcal{S}_{s.f.s.r.} = (1-n_s)\mathcal{S}_{loc.} + \frac{5}{3}\varepsilon\mathcal{S}_{equil.}\ ,} \tag{7.4}$$

where from now on we will drop the subscripts H on the Hubble slow-roll parameters. Eq. (7.4) shows that both ε and η appear in the amplitude in the three-point function. To gain some intuition on what this means, we can go to the squeezed limit. The bispectrum has a simple physical interpretation in this configuration (see fig. 7.2 for details): as we will see in more detail in the next Chapter, it corresponds to looking at how the power spectrum of a short-scale perturbation ζ_s defined in a region of size $R \gtrsim k_s^{-1}$ is correlated with a long-wavelength mode ζ_ℓ which is almost constant over that region ($k_\ell^{-1} \gg R$). eq. (7.4) says that, at leading order in gradients of ζ_ℓ (i. e. for a constant ζ_ℓ), the coupling between $P_\zeta(k_s)$ and ζ_ℓ is given by (minus) the tilt of the power spectrum.

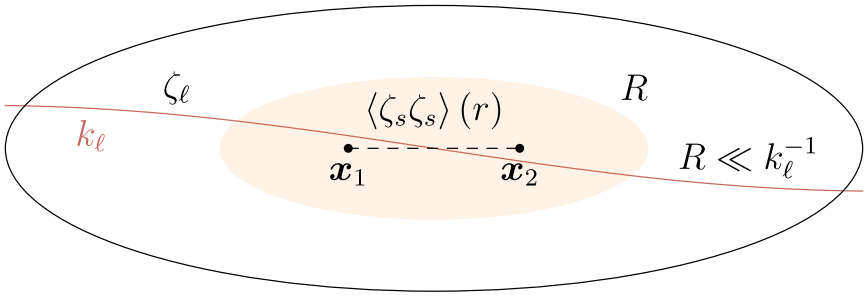

FIGURE 7.2: Squeezed limit of $\zeta = \zeta_\ell + \zeta_s$ in real space: we compute how the correlation function of ζ_s (which we call $\langle\zeta_s\zeta_s\rangle(r)$, where $r \equiv |\mathbf{x}_1 - \mathbf{x}_2|$) depends on the long-wavelength fluctuation ζ_ℓ. We can expand ζ_ℓ in a Taylor series, since it is slowly varying inside R: any point inside of R is as good as the other for the expansion [24, 196], so we will choose the middle point $\mathbf{x}_c \equiv (\mathbf{x}_1 + \mathbf{x}_2)/2$ for simplicity. We also stress that the choice of R is immaterial in the squeezed limit, the only real requirement being that $k_\ell \ll k_s$ [197].

If we work in real space, and stop at zeroth order in gradients of the long mode ζ_ℓ, this translates into

$$\langle\zeta_s\zeta_s\rangle(r)|_{\zeta_\ell} = \{1 + (1-n_s)\zeta_\ell(\mathbf{x}_c)\}\langle\zeta_s\zeta_s\rangle(r)\ , \tag{7.5}$$

where $r \equiv |\mathbf{x}_1 - \mathbf{x}_2|$ and $\mathbf{x}_c \equiv (\mathbf{x}_1 + \mathbf{x}_2)/2$ (see fig. 7.2). This seems to suggest that $f_{NL}^{loc.}$ is equal to $1 - n_s$: however, there are some subtleties. Indeed, consider an observer living in the region R, as depicted in fig. 7.2. She is living in a "separate universe" perturbed by the

(constant) long mode $\zeta_\ell(\mathbf{x}_c)$, so that the spatial background metric is given by

$$\bar{g}_{ij} = a^2\{1 + 2\zeta_\ell(\mathbf{x}_c)\}\delta_{ij} \ . \tag{7.6}$$

The observer can look at correlations of the short-scale perturbations with the long mode, and she would do it by measuring the short-scale power spectrum in terms of the physical distance d_p between $\mathbf{x}_1$ and $\mathbf{x}_2$. Now, we can see that given the metric of eq. (7.6), d_p is not equal to $a \times r$, but it is given by

$$d_p = a \times \{1 + \zeta_\ell(\mathbf{x}_c)\} \times r \equiv a \times r_p \ . \tag{7.7}$$

When eq. (7.5) is rewritten in terms of r_p, we see that the term $\propto (1 - n_s)$ cancels, i. e.

$$\boxed{\begin{aligned}\langle\zeta_s\zeta_s\rangle\,(r(r_p))|_{\zeta_\ell} &= \{1 + (1-n_s)\zeta_\ell(\mathbf{x}_c)\}\,\langle\zeta_s\zeta_s\rangle\,(r_p) \\ &\quad - \zeta_\ell(\mathbf{x}_c)\frac{d\,\langle\zeta_s\zeta_s\rangle\,(r_p)}{d\log r_p} \\ &= \langle\zeta_s\zeta_s\rangle\,(r_p) \ .\end{aligned}} \tag{7.8}$$

Therefore, for a local observer, there is no coupling between long and short modes at leading order in k_ℓ/k_s in single-field inflation: corrections will enter at second order in derivatives of ζ_ℓ, i. e. at $\mathcal{O}(r^2\partial^2\zeta_\ell)$. We will see in the next Section an example of an observable where we can apply this argument, i. e. the correlation between CMB temperature and μ-distortion anisotropies.

7.3 μT ANGULAR CORRELATIONS

As we have shown in Section 3.4, the heating rate from Silk damping is proportional to the power spectrum on very short scales (from $\approx 50\,\mathrm{Mpc}^{-1}$ to $\approx 10^4\,\mathrm{Mpc}^{-1}$). In presence of a $f_{NL}^{loc.}$ different from zero, and then of a coupling between long and short modes, we see that the heating rate becomes spatially dependent (see fig. 7.3). Therefore, we expect to see anisotropies of μ in the sky. More precisely, if we parameterize the long-short mode coupling in real space as[1]

$$\zeta = \zeta_s + \zeta_\ell - \frac{6}{5}f_{NL}^{loc.}\zeta_s\zeta_\ell \ , \tag{7.9}$$

and use eq. (3.101), we see that at the observation point the average chemical potential will be modulated by ζ_ℓ, its fractional variation being [20, 25]

$$\frac{\Delta\mu}{\mu} \approx \frac{\delta\,\langle\zeta_s^2\rangle\,|_{\zeta_\ell}}{\langle\zeta_s^2\rangle} = -\frac{12}{5}f_{NL}^{loc.}\zeta_\ell \ , \tag{7.10}$$

1 The factor of $-\frac{6}{5}$ is conventional: with this factor the Newtonian potential in matter domination has a bispectrum of the local shape with amplitude $f_{NL}^{loc.}$. We refer to [25] for details.

where $\delta\langle\zeta_s^2\rangle|_{\zeta_\ell} \equiv \langle\zeta_s^2\rangle|_{\zeta_\ell} - \langle\zeta_s^2\rangle$. Therefore, we see that, with local-model non-Gaussianity, the fractional chemical potential fluctuation in a given region of the sky is given simply by the long-wavelength curvature perturbation in that region at the surface of last scatter. The same is true for the large-angle temperature fluctuation: as we have seen in Section 3.3.2, it is determined primarily by the curvature fluctuation at the surface of last scatter and has magnitude $\frac{\Delta T}{T} \approx -\frac{\zeta_\ell}{5}$, as we can see by combining eqs. (3.73), (3.75). Therefore, for multipole moments $\ell \lesssim 100$, that probe causally disconnected regions at the surface of last scattering, the cross-correlation between the fractional chemical potential fluctuation $\frac{\Delta\mu}{\mu}$ and the temperature fluctuation $\frac{\Delta T}{T}$ has an angular power spectrum equal $C_\ell^{\mu T}$ to

$$\boxed{C_\ell^{\mu T} = 12 f_{NL}^{loc.} C_\ell^{TT}} \,. \tag{7.11}$$

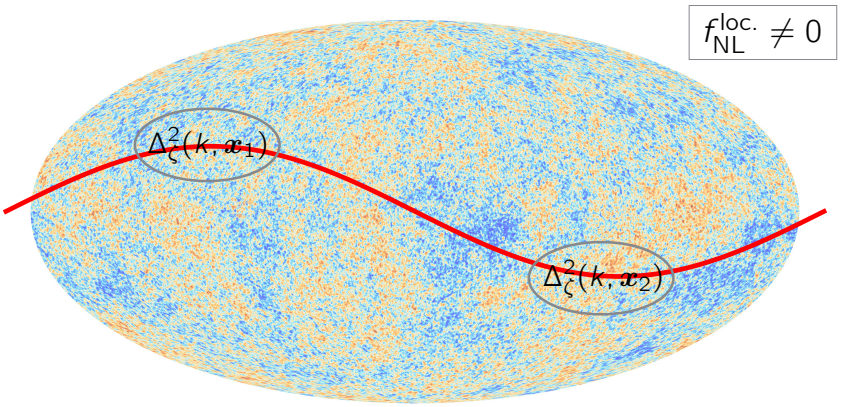

FIGURE 7.3: Modulation of the average chemical potential in the sky by a long wavelength mode: for non-zero $f_{NL}^{loc.}$, the coupling between long and short modes leads to a modulation of the amplitude of the spectral distortion.

Now, we have seen in Section 7.2 that the *physical* coupling between the long and short modes, in any of the regions at last scattering that subtend an angle $\sim \ell^{-1}$ in the sky, is zero in single-field inflation. Therefore, there will be no contribution from primordial physics to the correlation between temperature and μ-distortion anisotropies. Does this mean that $C_\ell^{\mu T}$ identically vanishes? We are currently investigating this [31]. There will be projection effects as photons travel from each of these regions to us: since they will travel in a universe perturbed by the long-wavelength mode, this can lead to additional correlations with ζ_ℓ that can mimic a non-zero $f_{NL}^{loc.}$. For example, this happens for the CMB bispectrum. Consider the squeezed limit of the three-point function of $\frac{\Delta T}{T}$ in the sky: this corresponds to looking at how the power spectrum of $\frac{\Delta T}{T}$ on small angular scales is correlated with a large-angle temperature fluctuation. We can do this by measuring the power spectrum in small patches in the sky, and then seeing if

such power spectrum varies from patch to patch (and if the change is correlated with a long temperature perturbation). We recognize that there are at least three effects that can generate such changes:

- there can be a change in the angular size of the short-scale anisotropies from patch to patch;
- in every patch, the local temperature will have experienced a different redshift;
- finally, the definition itself of local temperature in every patch will be changed by the presence of a long-wavelength perturbation at recombination. That is, we have to define the short-scale temperature anisotropies with respect to the average temperature in every patch, which is a direct tracer of ζ_ℓ.

However, we now also see that these three effects will be absent in the case of μT correlations:

- when we compute $C_\ell^{\mu T}$, we are not looking at how the *power spectrum* of μ varies from patch to patch, but we are considering the *average* μ. Therefore, there is no "angular size" of short-scale μ that could change from patch to patch;
- differently from T, μ does not redshift after the end of the μ-era, but it is frozen;
- once we define the average temperature in the patch, we are automatically able to extract the average μ. This follows directly from the form of the Bose-Einstein frequency spectrum.

Therefore, we expect that in single-field inflation we expect *exactly zero* μT correlations, up to corrections suppressed by $(k_\ell/k_s)^2$ (where k_ℓ is of the order of the comoving horizon at recombination and k_s is of the order of the damping scale at the end of the μ-era). The goal of [31] is to investigate this in more detail. However, one can also ask oneself what happens to the primordial contribution at second order in gradients of ζ_ℓ. We have seen in Section 7.2 that the contribution proportional to the tilt cancels from local observables at leading order in gradients: does this happen at $\mathcal{O}(k_\ell/k_s)^2$ too? The goal of the next Chapter is to answer this question.

8

HOW GAUSSIAN CAN OUR UNIVERSE BE?

CONTENTS

In this Chapter we will study what is the minimal amount of primordial non-Gaussianity that can be observed today in n-point functions of cosmological perturbations. The Chapter is based on the work JCAP **1701**, no. 01, 003 (2017).

8.1 INTRODUCTION

As cosmological observations show no evidence of departures from Gaussian primordial perturbations, it is natural to ask: How Gaussian can our Universe be? If we assume primordial perturbations to be generated during inflation, we know that multi-field and higher derivative interactions typically enhance primordial non-Gaussianity. Setting aside these more general scenarios, we focus on the simplest model, which leads to the least amount of non-Gaussianity: canonical single-field slow-roll inflation. We know that inflaton self-interactions are subleading in the slow-roll expansion (see [18, 65, 198, 199] for explicit calculations), so we are led to ask how small gravitational non-

linearities can be. Maldacena answered this question in [18] computing the primordial bispectrum in comoving coordinates

$$B_\zeta(k_1,k_2,k_3) \propto \frac{(\Delta^2_\zeta)^2}{(k_1k_2k_3)^2}\Big[(1-n_s)\,\mathcal{S}_{\text{loc.}}(k_1,k_2,k_3) + \frac{5}{3}\varepsilon\,\mathcal{S}_{\text{equil.}}(k_1,k_2,k_3)\Big]\,, \tag{8.1}$$

where $P_\zeta(k) = k^3\Delta^2_\zeta/2\pi^2$ is the power spectrum of curvature perturbations, $\mathcal{S}_{\text{loc.}}$ and $\mathcal{S}_{\text{equil.}}$ are the shape functions of local and equilateral non-Gaussianity, and $n_s - 1$ is the scalar spectral tilt, which is given in terms of the Hubble slow-roll parameters by

$$n_s - 1 = -\eta - 2\varepsilon, \text{ with } \varepsilon \equiv -\frac{\dot H}{H^2}, \eta \equiv \frac{\dot\varepsilon}{H\varepsilon}\,. \tag{8.2}$$

The minimum size of non-Gaussianity is therefore determined by ε and the spectral tilt $n_s - 1$. Although these two contributions are "of order slow-roll", there is a dramatic difference between the two. The spectral tilt is relatively well known, $n_s - 1 = -0.0355 \pm 0.005$ (95 % CL) [14]. On the other hand, ε is uncertain by more than 50 orders of magnitude: an upper bound comes from the tensor-to-scalar ratio bound $16\varepsilon = r < 0.07$ (95 % CL) [47], while a lower bound comes from conservatively assuming a reheating scale larger than a TeV, leading to $5\times10^{-3} \gtrsim \varepsilon \gtrsim 10^{-54}$. So the answer to the title of this Chapter can be hugely different, depending on whether it is ε or $n_s - 1$ that control the minimum amount of primordial non-Gaussianity.

It was shown in [24] that, to leading order in derivatives, the contribution from the local shape, of size $n_s - 1$, cancels exactly for any local measurement. In particular, it does not contribute to the scale-dependent bias [200–202], to the CMB bispectrum in the squeezed limit [203, 204], and to the cross-correlation between CMB temperature anisotropies and spectral distortions [20]. It is therefore natural to ask whether $n_s - 1$ survives at some subleading order in derivatives or if it cancels to all orders, allowing primordial non-Gaussianity to be, for all practical purposes, arbitrarily small. The goal of this Chapter is to answer this question. Using Conformal Fermi Coordinates (CFC) [24, 200, 201], we will show that a term which involves two spatial derivatives of ζ and is proportional to $n_s - 1$ survives in local observables and therefore appears in the appropriately defined curvature bispectrum.

To put our result into context, we stress two main points. First, the original motivation for our investigation was the widespread suspicion, put forward in [205], that some general argument might exist to guarantee the complete cancellation of any term proportional to η (and therefore to the tilt). After all, it is ε that controls the departure from an exact de Sitter spacetime (see eq. (8.85)), in which case, following the argument sketched in [205], non-Gaussianity should vanish. Our

explicit calculation shows that this suspicion is unfounded. We also clarify how the survival of $n_s - 1$ is indeed expected when considering the de Sitter limit. Second, even though we compute the bispectrum of primordial curvature perturbations on a constant-proper-time hypersurface at the end of inflation, as opposed to some late-time observable such as the CMB or galaxy bispectrum, our result has a direct and transparent physical implication.

Recall that curvature perturbations, and hence their correlators, are conserved until they re-enter the (largest) sound horizon of any relevant component (matter, radiation, etc.). As an example, consider then matter domination, when the sound horizon is parametrically smaller than the Hubble radius. Two short and one long mode that enter the Hubble horizon during this epoch still possess the primordial correlation we compute here as long as they are larger than the sound horizon, and this coupling is in principle observable, as we will discuss in Section 8.6. In practice of course we are interested in modes that enter also during radiation domination and we observe non-conserved density perturbations as opposed to conserved curvature perturbations. Many evolution and projection effects then need to be added to our result. Nevertheless, the example above highlights that our result describes a physical and in principle measurable late-time correlation. Connection to observations will be further discussed in Section 8.6.

The rest of the Chapter is organized as follows. In Section 8.2 we construct the CFC frame for single-field slow-roll inflation; in Section 8.3 and Section 8.4 we compute the local bispectrum in CFC; in Section 8.5 we discuss why we expect η to also be locally observable, in contrast to what was argued in [205], and briefly describe the case where the inflaton speed of sound c_s is different from 1. Finally, we derive our conclusions in Section 8.7. We collect the technical details in Appendix E (about the CFC construction), Appendix F (about the transformation of the curvature perturbation ζ from comoving coordinates to CFC), and Appendix G (about the bispectrum in Fourier space). In Appendix H we briefly describe the simplifications in the calculation of the CFC bispectrum when $c_s \ll 1$.

Notation and conventions As we are doing throughout this thesis, we use ζ (not $\mathcal{R}$) to define the comoving curvature perturbation, following [18]. In the remainder of the Chapter, we work in units where the reduced Planck mass $M_P^2 \equiv 1/8\pi G_N = 1$, unless it is explicitly said otherwise. It can be reintroduced easily with dimensional analysis in the final results, if needed. In this Chapter (and in the Appendices E, F, G and H), we are going to use τ in place of η as conformal time. We will also drop the superscript (3) on the three-dimensional Dirac delta functions, and we will often denote derivatives with respect to τ with ∂_0.

8.2 CFC COORDINATES IN SINGLE-FIELD INFLATION

When we referred to "local measurements" in the introduction above, we meant in particular the response of short-wavelength perturbations ($k_1 \sim k_2 \sim k_s$) to the presence of long-wavelength ones $k_3 \sim k_\ell \ll k_s$ (squeezed limit). As shown, e. g., in [206],[1] the squeezed limit of correlation functions of ζ in Fourier space corresponds to looking at how perturbations ζ_s which are defined in a region of size $R \gtrsim k_s^{-1}$ are correlated with perturbations ζ_ℓ of wavelength $k_\ell^{-1} \gg R$, i. e. that are almost constant in the region R (see fig. 7.2). This correlation between long and short modes is expected, since the long modes will affect the dynamics of the short modes, modifying the background over which they evolve: up to second order in gradients, the long-wavelength perturbation can be reabsorbed in the FLRW background, while at $\mathcal{O}(k_\ell^2)$ it adds curvature to the "separate universe" of size $\sim k_\ell^{-1}$ and modifies its expansion history [207, 208]. Maldacena's consistency relation is just a statement of the fact that these effects are suppressed by how much the long mode is outside the horizon at a given time (for primordial correlations this saturates at k_ℓ^2/k_s^2, $k_s \sim aH \equiv \mathcal{H}$ being the moment when short modes freeze out).

We can see this in the following way. We start by asking ourselves what a local observer with proper 4-velocity U^μ in the separate universe of fig. 7.2, freely falling in the background perturbed by the long-wavelength mode ζ_ℓ, can measure during inflation. First, she naturally sets the time coordinate to match what is measured by her clock (i. e. by her proper time $\equiv t_F$) and uses it to define surfaces of constant time. The (non-rotating) spatial coordinate axes of her local laboratory frame emanate from her worldline along geodesics. The resulting coordinate system (x_F^μ) depends on the worldline of U^μ: timelike and spacelike coordinates are defined in such a way that the distance of a point from the worldline is given by $\eta_{\mu\nu}\Delta x_F^\mu \Delta x_F^\nu$, with higher order corrections in $\Delta \mathbf{x}_F$ that encode how spacetime deviates from flatness. This local coordinate system is known as Fermi Normal Coordinates (FNC) [206, 207, 209–211].

However, space is also expanding, as determined locally by how a small sphere of test particles carried on the worldline changes in volume. This change is encoded by the geodesic expansion $\nabla_\mu U^\mu$. By introducing a local FLRW scale factor a_F, the spatial coordinates can account for the fact that $\nabla_\mu U^\mu \neq 0$: the distance of a point from the worldline is then given by $-\Delta t_F^2 + a_F^2 |\Delta \mathbf{x}_F|^2$, where a_F is the integral over the local expansion rate $\nabla_\mu U^\mu = 3H_F$. The important point is that spatial geodesics are *still* used to define spatial distances, the only difference with the previous case being the fact that the overall expansion of space has now been factored out. Higher-order

1 See its Sec. 2.

corrections in $\Delta\mathbf{x}_F$ to the distance between points would now encode the intrinsic curvature of spatial slices.

This generalization of the FNC is called Conformal Fermi Coordinates (CFC) [24, 200, 201]: they are the coordinates that a local observer uses to describe physics in an *expanding* universe. They are naturally suited to the case where there is a separation of scales, such as the one described in fig. 7.2: an observer who has access only to scales $\sim 1/k_s$ treats the long mode as an effective background within which the short modes evolve,[2] and then looks at what is the power spectrum of the latter in this background, which she describes through CFC. This coordinate system makes explicit that the separate universe is an unperturbed FLRW universe (the corrections to the expansion history coming from $H_F \neq H$ are of order of the time dependence of ζ_ℓ, which starts at order $\partial^2\zeta_\ell$ in single-field inflation): deviations from this picture enter only at second order in spatial gradients of ζ_ℓ. Hence, the first non-zero, physical coupling between short and long modes that a local observer can measure appears at quadratic order in the momentum of the long mode. At this order, if the CFC power spectrum of ζ_s in presence of ζ_ℓ does not vanish for $\varepsilon \to 0$ on super-Hubble scales (we will show later that the difference between constant t surfaces and constant t_F surfaces goes to zero as the Hubble radius decreases), we conclude that the "gravitational floor" of non-Gaussianities from inflation is of order of the tilt $n_s - 1$.

8.2.1 *Construction of CFC*

As we explained above, CFC coordinates $x_F = (\tau_F, \mathbf{x}_F)$ for a geodesic observer $U^\mu \equiv (e_0)^\mu$ are constructed in a similar way to Fermi Normal Coordinates, the difference being that around the observer's geodesic the metric looks approximately as FLRW (not Minkowski). The deviations from FLRW are of order $|\mathbf{x}_F|^2 k_\ell^2 \zeta_\ell$, instead of $|\mathbf{x}_F|^2 H^2$ as in the FNC case. The construction goes as follows:

1. we construct an orthonormal tetrad $(e_\nu)^\mu$, parallel transported along the central geodesic $P(t_F)$ of the observer $(e_0)^\mu$ (t_F being the observer's proper time);

2. given a spacetime scalar $a_F(x)$, we define a conformal proper time τ_F by

$$d\tau_F = a_F^{-1}(P(t_F))dt_F \,, \tag{8.3}$$

and we choose τ_F as time coordinate (often replacing $P(t_F(\tau_F))$ with just P to simplify the notation). This allows us to define sur-

2 It is clear that this picture, during inflation, can hold only if we stop at quadratic order in gradients of the long mode: at higher order we cannot neglect the quantum nature of perturbations and treat them as a classical background. To see this, it is enough to think about the de Sitter mode functions $\zeta(\tau, k) = \zeta(0, k)(1 + ik\tau)e^{-ik\tau}$: for $k \to 0$, the term of $\mathcal{O}(k^3)$ picks up a factor of i.

faces of constant τ_F, spanned by space-like conformal geodesics (i. e. geodesics of the conformal metric $\tilde{g}_{\mu\nu}(x) \equiv a_F^{-2}(x) g_{\mu\nu}(x)$) originating from the central geodesic;

3. this construction of surfaces of constant τ_F also gives us spatial coordinates x_F^i. More precisely:
   - one defines the central geodesic to have coordinates $x_F = (\tau_F, \mathbf{0})$;
   - one takes the family $\gamma(\tau_F; \alpha^i, \lambda)$ of geodesics of the conformal metric with affine parameter $\lambda = 0$ at P, and tangent vector given by $\alpha^i (e_i)^\mu_P$;
   - the point Q with coordinates $(\tau_F, \mathbf{x}_F)$ is then identified with $\gamma(\tau_F; \beta^i, \lambda_Q)$, where

$$\lambda_Q = \delta_{ij} x_F^i x_F^j \,, \tag{8.4a}$$

$$\beta^i = \frac{a_F(P) x_F^i}{\sqrt{\delta_{ij} x_F^i x_F^j}} \,; \tag{8.4b}$$

   - with the exponential map we can then construct the coordinate transformation from global coordinates (x) to CFC coordinates (x_F) as a power series in x_F^i. Rescaling λ so that it runs from 0 to 1, i. e. $\beta^i = a_F(P) x_F^i$, this power series reads as

$$x^\mu(x_F) = c_0^\mu(\tau_F) + \sum_{n=1}^{+\infty} c_n^\mu(\tau_F, \mathbf{x}_F) \,, \tag{8.5}$$

   with

$$c_n^\mu(x_F) = \mathcal{O}[(x_F^i)^n] \text{ for } n \geqslant 1 \,. \tag{8.6}$$

   We see that $c_0^\mu(\tau_F)$ is simply given by $x^\mu(P)$, the coordinates of the central geodesic evaluated at $t_F(\tau_F)$, and can be computed once one knows a_F and $(e_0)^\mu$. The tangent vector on P, i. e. $c_1^\mu(\tau_F, \mathbf{x}_F)$, is then given by

$$c_1^\mu(\tau_F, \mathbf{x}_F) = a_F(P) (e_i)^\mu_P x_F^i \,. \tag{8.7}$$

   Higher order coefficients are computed recursively by solving the geodesic equation for the conformal metric: we refer to [200, 201] and to Appendix E for details.

The resulting metric has the form

$$g^F_{\mu\nu}(x_F) = a_F^2(\tau_F)[\eta_{\mu\nu} + h^F_{\mu\nu}(x_F)], \text{ with } h^F_{\mu\nu}(x_F) = \mathcal{O}[(x_F^i)^2] \,. \tag{8.8}$$

More precisely, stopping at order $(x_F^i)^2$, we have [200, 201]

$$h^F_{00}(x_F) = -\tilde{R}^F_{0k0l}|_P x_F^k x_F^l \,, \tag{8.9a}$$

$$h^F_{0i}(x_F) = -\frac{2}{3}\tilde{R}^F_{0kil}|_P x_F^k x_F^l \,, \tag{8.9b}$$

$$h^F_{ij}(x_F) = -\frac{1}{3}\tilde{R}^F_{ikjl}|_P x_F^k x_F^l \,, \tag{8.9c}$$

where $\tilde{R}^F_{\mu\rho\nu\sigma}$ is the Riemann tensor of the conformal metric in CFC coordinates, and indices have been lowered with the conformal metric. In terms of global coordinates, $\tilde{R}^F_{\mu\rho\nu\sigma}|_P$ is

$$\tilde{R}^F_{\mu\rho\nu\sigma}|_P = \tilde{R}_{\alpha\beta\gamma\delta}|_P (\tilde{e}_\mu)^\alpha_P (\tilde{e}_\rho)^\beta_P (\tilde{e}_\nu)^\gamma_P (\tilde{e}_\sigma)^\delta_P \,, \tag{8.10}$$

where on the central geodesic the CFC coordinate vectors are given by $(\tilde{e}_\nu)^\mu_P = a_F(P)(e_\nu)^\mu_P$.

When compared to the Fermi Normal Coordinates construction, CFC need one additional ingredient to determine the metric perturbations $h^F_{\mu\nu}$, i. e. the scalar $a_F(x)$ computed along the central geodesic.[3] The idea is to absorb the leading contributions to the spacetime curvature in this scale factor a_F, and make then the Riemann tensor of $\tilde{g}_{\mu\nu}$ as simple as possible. In [200] it is shown how this is achieved by defining $a_F(x)$ from the local expansion rate

$$\frac{d\log a_F(P)}{dt_F} = \frac{1}{a_F(\tau_F)}\frac{d\log a_F(P)}{d\tau_F} = \frac{\nabla_\mu U^\mu|_P}{3} \,. \tag{8.11}$$

8.2.2 *Residual coordinate freedom*

This construction, even after having fixed the geodesic $U^\mu(t_F)$ and the choice of a_F, has two residual "gauge" freedoms that leave h^F_{00} and h^F_{0i} invariant at $\mathcal{O}[(x_F^i)^2]$:

- it is possible to perform a coordinate transformation

$$\tau_F \to \tau_F \,, \tag{8.12a}$$

$$x_F^i \to x_F^i(y_F) = y_F^i + \frac{A^i_{jkl}(\tau_F)}{6} y_F^j y_F^k y_F^l \,, \tag{8.12b}$$

  where $A^i_{jkl}(\tau_F)$ is fully symmetric with respect to j, k, l. This transformation does not affect a_F, but changes $h^F_{\mu\nu}$ via

$$h^F_{00}(x_F) \to h^F_{00}(y_F) \,, \tag{8.13a}$$

$$h^F_{0i}(x_F) \to h^F_{0i}(y_F) \,, \tag{8.13b}$$

$$h^F_{ij}(x_F) \to h^F_{ij}(y_F) + A_{(ij)kl}(\tau_F)\, y_F^k y_F^l \,, \tag{8.13c}$$

3 We also need its derivatives along the central geodesic, since these will enter in $\tilde{R}^F_{\mu\rho\nu\sigma}|_P$: we refer to [200, 201] for a more detailed review.

where the indices of $A^i_{jkl}(\tau_F)$ are lowered with the conformal metric. It is important to stress that, up to including order $(y^i_F)^2$, coordinate lines $\mathbf{y}_F = \lambda_{,F}$ are *still* geodesics of the conformal metric;

- one can rescale a_F by a constant $a_F(\tau) \to c\, a_F(\tau)$: it comes from the fact that we defined it through the local Hubble rate for the observer U^μ, so we still have the freedom of choosing the integration constant when we integrate eq. (8.11) along the central geodesic.

This construction holds for any spacetime: there is no need of expanding the metric in perturbations around a given background. However, we will specialize to the case of a perturbed FLRW spacetime in the following Sections. For this reason, we defer the discussion of these two residual transformations to the next Sections, where working in perturbation theory will allow us to fix them in a much easier way.

8.2.3 *From comoving to CFC coordinates*

The main goal of this and the following Sections is to construct explicitly the change from the global to the CFC frame, constructed for the long-wavelength part of the metric: this will allow us to find the effect that a long-wavelength perturbation ζ_ℓ has on short modes ζ_s. The construction will follow closely the one presented in [24], the main difference being the fact that we will go up to order k_ℓ^2/k_s^2 in the gradient expansion. Here we provide the outline of the calculation, while the details are collected in Appendix E.

We work in a perturbed FLRW spacetime $g_{\mu\nu} = a^2(\eta_{\mu\nu} + h_{\mu\nu})$: more precisely we consider the comoving gauge [18], where the inflaton perturbations $\delta\phi$ are set to zero and the metric is given by (neglecting tensor modes)

$$g_{00} = a^2(-1 - 2N_1), \text{ with } N_1 = \frac{\partial_0 \zeta}{\mathcal{H}} , \tag{8.14a}$$

$$g_{0i} = a^2 N_i = a^2 \partial_i \psi, \text{ with } \psi = -\frac{\zeta}{\mathcal{H}} + \varepsilon \partial^{-2} \partial_0 \zeta , \tag{8.14b}$$

$$g_{ij} = a^2 e^{2\zeta} \delta_{ij} \approx a^2 (1 + 2\zeta)\delta_{ij} . \tag{8.14c}$$

Since we are interested in three-point functions, we restricted to linear order in the lapse and shift constraints [18, 65, 119]. We can now split ζ in a long- and short-wavelength part, $\zeta(x) = \zeta_s(x) + \zeta_\ell(x)$: because we are interested in the bispectrum only, it will be sufficient to consider the linear response of the short-scale modes to the coordinate transformation (that is, we can work at linear order in ζ_ℓ). Now, given that the background is FLRW, we can straightforwardly write down the (normalized) time-like geodesic congruence U^μ as [200, 201]

$$U^\mu = (e_0)^\mu = a^{-1}\left(1 + \frac{h_{00}}{2}, V^i\right) = a^{-1}(1 - N_1, V^i) , \tag{8.15}$$

where the first order perturbations V^i are the peculiar velocities of the observers U^μ. Neglecting vorticity (which is not sourced in single-field models), the corresponding spatial vectors of the tetrad are [200, 201]

$$(e_i)^\mu = a^{-1}\left(V_i + h_{0i}, \delta^j_i - \frac{h^j_i}{2}\right) = a^{-1}\left(V_i + N_i, \left[1-\zeta\right]\delta^j_i\right) \,, \tag{8.16}$$

where we raise and lower latin indices with δ^j_i. Since the tetrad $(e_\nu)^\mu$ is parallel transported along the central geodesic, one can show that the peculiar velocities must obey the equation

$$\partial_0 V^i + \mathcal{H} V^i = -\partial^i N_1 - \partial_0 N^i - \mathcal{H} N^i \,. \tag{8.17}$$

Finally, one can use the relation $H_F = \nabla_\mu U^\mu/3$ to find the expression for the CFC scale factor a_F: at linear order in perturbations, one has that (see, e. g., Section E.1)

$$\begin{aligned}\frac{a_F(P)}{a(P)} &= 1 + C_{a_F}(\tau_*, \mathbf{x}_c(\tau_*)) \\ &\quad + \int_{\tau_*}^{\tau} ds \left(\partial_0\zeta(s, \mathbf{x}_c(s)) + \frac{1}{3}\partial_i V^i(s, \mathbf{x}_c(s))\right) \,,\end{aligned} \tag{8.18}$$

where both left-hand side and right-hand side of this equation are computed in global coordinates along the central geodesic $(\mathbf{x}_c(\tau))$. We have defined τ_* as the initial time in the integration of eq. (8.11), while $C_{a_F}(\tau_*, \mathbf{x}_c(\tau_*))$ is an arbitrary constant which we treat as first order in perturbations. This corresponds to the freedom to rescale a_F by a constant, as mentioned in the previous Section. The last step is to solve the geodesic equation for the peculiar velocities. We can do it by defining $F^i \equiv V^i + N^i$: the solution for $F_i = \partial_i \mathcal{F}$ then reads as

$$\begin{aligned}\mathcal{F}(x) = e^{-\int_{\tau_*}^{\tau} ds\, \mathcal{H}(s)} \Bigg[&\tau_* C_{\mathcal{F}}(\tau_*, \mathbf{x}) \\ &- \int_{\tau_*}^{\tau} ds\, e^{\int_{\tau_*}^{s} dw\, \mathcal{H}(w)} N_1(s, \mathbf{x})\Bigg] \,,\end{aligned} \tag{8.19}$$

where $C_{\mathcal{F}}(\tau_*, \mathbf{x})$ is a second integration constant (which we multiply by τ_* for convenience). $C_{\mathcal{F}}$ corresponds to an initial relative velocity of the geodesic (which, as we can see, decays on super-Hubble scales) considered with respect to comoving observers.

It is now straightforward to show that on the central geodesic (i. e. for $\mathbf{x}_F = \mathbf{0}$) we have

$$x^\mu(\tau_F, \mathbf{0}) = x^\mu_F + \xi^\mu(\tau_F, \mathbf{0}), \text{ with } \xi^\mu(\tau_F, \mathbf{0}) = \mathcal{O}(\zeta_\ell) \,, \tag{8.20}$$

so in Eqs. (8.18), (8.19) we can neglect the shift in the arguments of first order perturbations (i. e. we can take $\mathbf{x}_c(\tau) = \mathbf{0}$, $\tau = \tau_F$). This allows to write down the full exponential map at first order in the long-wavelength perturbations. If we denote by $\tilde{\Gamma}$ the Christoffel coefficients

of the conformal metric (collected in tab. E.1), and by $(a_F/a)|_\ell$ the terms of order ζ_ℓ in eq. (8.18), the final result at $\mathcal{O}[(x_F^i)^3]$ is equal to

$$\begin{aligned} x^\mu(\tau_F, \mathbf{x}_F) = x_F^\mu + \xi^\mu(\tau_F, \mathbf{0}) + A_i^\mu(\tau_F)\, x_F^i \\ + B_{ij}^\mu(\tau_F)\, x_F^i x_F^j + C_{kij}^\mu(\tau_F)\, x_F^i x_F^j x_F^k \ , \end{aligned} \tag{8.21}$$

where the coefficients of the expansion are given by

$$\xi^\mu(\tau_F, \mathbf{0}) = \begin{cases} \int_{\tau_*}^{\tau_F} ds \left[(a_F/a)(\tau_F, \mathbf{0})|_\ell - N_1(s, \mathbf{0})\right] & \mu = 0 \ , \\ \int_{\tau_*}^{\tau_F} ds\, V^l(s, \mathbf{0}) & \mu = l \ , \end{cases} \tag{8.22a}$$

$$A_i^\mu(\tau_F) = \begin{cases} F_i(\tau_F, \mathbf{0}) & \mu = 0 \ , \\ \left[(a_F/a)(\tau_F, \mathbf{0})|_\ell - \zeta(\tau_F, \mathbf{0})\right]\delta_i^l & \mu = l \ , \end{cases} \tag{8.22b}$$

$$B_{ij}^\mu(\tau_F) = -\frac{1}{2}\tilde{\Gamma}_{ij}^\mu(\tau_F, \mathbf{0}) \ , \tag{8.22c}$$

$$C_{kij}^\mu(\tau_F) = -\frac{1}{6}\partial_k \tilde{\Gamma}_{ij}^\mu(\tau_F, \mathbf{0}) \ . \tag{8.22d}$$

Notice that a_F never appears by itself. Only $\xi^0(\tau_F, \mathbf{0})$ and $(a_F/a)|_\ell$ appear.

We can now fix the additional freedoms in the CFC construction (namely, the choice of τ_*, the constants C_{a_F} and C_F, and the possibility of changing spatial coordinates without changing the time-time and time-space components of the metric). We start with the choice of initial time (noting that the initial time appears always in quantities that are already first order in the long mode): we are trying to absorb the effect that long-wavelength modes ζ_ℓ have on short modes ζ_s through a change of coordinates. In order to do this, we must be able to treat them as classical, so we have to start defining the CFC after they have long exited the horizon. Then, we could choose τ_* such that $\mathcal{H}(\tau_*) = k_s$, where k_s is the typical wavelength of the short-scale ζ_s. However, it is much simpler to choose as "initial" time $\tau_* \to 0^-$ (the end of inflation), when all modes of interest have left the horizon and ζ has become constant, mirroring what has been done in [201]. This fixes the lower limit in the various integrals that define $(a_F/a)|_\ell$, the peculiar velocity potential F, and time shift along the central geodesic $\xi^0(\tau_F, \mathbf{0})$. Now, the upper limit will also be taken to be $\tau_F \to 0^-$, since we are interested in the super-Hubble limit of correlation functions. This will simplify a lot the calculation, since many time integrals will not contribute.

Then, as shown in Section E.2, this CFC construction gives

$$h_{00}^F = -x_F^k x_F^l \left(\partial_k \partial_l - \frac{\delta_{kl}}{3}\partial^2\right)(N_1 + \partial_0 \psi + \mathcal{H}\psi) \ , \tag{8.23a}$$

$$h_{0i}^F = \frac{2}{3} x_F^k x_F^l \left[\varepsilon \mathcal{H}^2 (\delta_{kl} F_i - \delta_{ki} F_l)\right] \ , \tag{8.23b}$$

$$h_{ij}^F = -\frac{1}{3} x_F^k x_F^l \left[\frac{2}{3}\mathcal{H}(\partial_m V^m) T_{ijkl} + S_{ijkl}(\zeta + \mathcal{H}\psi)\right] \ , \tag{8.23c}$$

where all terms on the right-hand side are evaluated on the central geodesic (i. e. at $(\tau_F, \mathbf{0})$), and the tensors T_{ijkl}, S_{ijkl} are given by

$$T_{ijkl} = \delta_{il}\delta_{kj} - \delta_{ij}\delta_{kl} \,, \tag{8.24a}$$

$$S_{ijkl} = \delta_{il}\partial_j\partial_k - \delta_{kl}\partial_i\partial_j + \delta_{kj}\partial_i\partial_l - \delta_{ij}\partial_l\partial_k \,. \tag{8.24b}$$

We can then use the additional freedom in the definition of spatial coordinates to bring the spatial part h^F_{ij} in conformal Newtonian form, following [201]. In Section E.3 we show that, at linear order in perturbations, the coordinate transformation of eqs. (8.12) amounts to subtracting the tensor $A^l_{kij}(\tau_F, \mathbf{0})$ from $\partial_k \tilde{\Gamma}^l_{ij}$ in eq. (8.22d). h^F_{ij}, correspondingly, transforms as in eq. (8.13c). We perform this coordinate change with

$$\begin{aligned} A^l_{kij} = &-\frac{1}{6}K_F(\delta^l_k\delta_{ij} + \delta^l_i\delta_{jk} + \delta^l_j\delta_{ki}) \\ &+ \frac{1}{9}(\delta^l_k\delta_{ij} + \delta^l_i\delta_{jk} + \delta^l_j\delta_{ki})\partial^2(\zeta + \mathcal{H}\psi) \\ &- \frac{2}{3}(\delta^l_k\partial_i\partial_j + \delta^l_i\partial_j\partial_k + \delta^l_j\partial_k\partial_i)(\zeta + \mathcal{H}\psi) \\ &+ \frac{1}{3}(\delta_{ij}\partial^l\partial_k + \delta_{jk}\partial^l\partial_i + \delta_{ki}\partial^l\partial_j)(\zeta + \mathcal{H}\psi) \,, \end{aligned} \tag{8.25}$$

where we have defined K_F as

$$K_F = -\frac{2}{3}\left[\partial^2(\zeta + \mathcal{H}\psi) + \mathcal{H}\partial_m V^m\right] = -\frac{2}{3}(\partial^2\zeta + \mathcal{H}\partial^2 F) \,. \tag{8.26}$$

After this final change of coordinates, the spatial metric g_{ij} becomes

$$g^F_{ij} = a_F^2\left(\frac{1 + x^k_F x^l_F \mathcal{D}_{kl}(\zeta + \mathcal{H}\psi)}{\left(1 + \frac{K_F|\mathbf{x}_F|^2}{4}\right)^2}\right)\delta_{ij} \,, \tag{8.27}$$

with

$$\mathcal{D}_{kl} \equiv \partial_k\partial_l - \frac{\delta_{kl}}{3}\partial^2 \,. \tag{8.28}$$

Eq. (8.27), combined with eqs. (8.23a), (8.23b), shows that the final result for the spatial metric is that of a curved FLRW metric plus tidal corrections. This form of the metric makes it clear that the scalar curvature of constant-proper-time slices of the observer is $\propto K_F/a_F^2$ and, as we will see in Section 8.4, can be used to calculate the CFC bispectrum directly at the level of the action. Besides, as we will discuss in more detail in Section 8.6, it will allow us to connect our result to the late-time evolution.

Finally, we can fix the constants C_{a_F} and C_F. We start from C_{a_F}: following [200, 201], we fix it by imposing that, at $\tau_F \to \tau_*$, the local scale factor-proper time relation is the same as that of the unperturbed background cosmology, i. e. we require that

$$\lim_{\tau_F \to \tau_*} a_F(\tau_F) = a(\tau_*) \,. \tag{8.29}$$

In Section E.3 we prove that taking $C_{a_F} = 0$ satisfies this equality. We then move to C_F, whose gradient is the initial peculiar velocity of the CFC observers. From eq. (8.19), we see that such initial velocity will decay as $1/\mathcal{H}$: therefore, we can put it to zero in our treatment, since we neglect decaying modes throughout. In this way, we also see from eq. (8.23b) that the effect of a long ζ_ℓ on the difference between hypersurfaces of constant τ and constant τ_F (encoded in the difference between τ and τ_F away from the central geodesic, which generates a non-zero h^F_{0i}) is of order k_ℓ^3.

With these choices for C_{a_F} and C_F, and straightforward manipulation of the lapse and shift constraints N_1 and ψ, the metric perturbations $h^F_{\mu\nu}$ become

$$h^F_{00}(\tau_F, \mathbf{x}_F) = -x^k_F x^l_F \mathcal{D}_{kl}\big[\varepsilon\mathcal{H}(1+\eta)\partial^{-2}\partial_0\zeta - \varepsilon\zeta + \varepsilon\partial^{-2}\partial_0^2\zeta\big] \,, \tag{8.30a}$$

$$h^F_{0i}(\tau_F, \mathbf{x}_F) = \mathcal{O}(k_\ell^3) \,, \tag{8.30b}$$

$$h^F_{ij}(\tau_F, \mathbf{x}_F) = \left[x^k_F x^l_F \mathcal{D}_{kl}(\varepsilon\mathcal{H}\partial^{-2}\partial_0\zeta) - \frac{K_F|\mathbf{x}_F|^2}{2}\right]\delta_{ij} \,, \tag{8.30c}$$

i. e. a curved FLRW metric with $K_F \propto \partial^2\zeta$ and (slow-roll suppressed) tidal corrections. We can also write down the correction $(a_F/a)|_\ell$ to the scale factor, i. e. eq. (8.18), at linear order in perturbations (as we are doing throughout this Section). We find

$$\begin{aligned}\frac{a_F(P)}{a(P)} &= 1 + \int_{\tau_*}^{\tau_F} ds \left(\partial_0\zeta(s,\mathbf{o}) + \frac{1}{3}\partial_i V^i(s,\mathbf{o})\right) \\ &= 1 + \int_{\tau_*}^{\tau_F} ds \left(\partial_0\zeta(s,\mathbf{o}) - \frac{1}{3}\partial^2\psi(s,\mathbf{o})\right) + \mathcal{O}(k_\ell^4) \,.\end{aligned} \tag{8.31}$$

We will use this metric in Section 8.4, where we will compute the full CFC bispectrum by working directly at the level of the action.

8.3 BISPECTRUM TRANSFORMATION

In this Section, we transform Maldacena's bispectrum to the conformal Fermi frame, following the approach of [24], to obtain our main result, i. e. the bispectrum $B^F_\zeta(\mathbf{k}_s, \mathbf{k}_\ell)$. We split the computation into three steps:

- in Section 8.3.1 and Section 8.3.2, respectively, we derive the transformation rules for the short-scale curvature perturbation and its power spectrum under the CFC change of coordinates;
- Section 8.3.3 contains the derivation of the bispectrum $B^F_\zeta(\mathbf{k}_s, \mathbf{k}_\ell)$ up to and including second order in gradients of the long mode.

8.3.1 *Transformation of ζ*

We start from the transformation of the curvature perturbation ζ: we consider a coordinate transformation from x to $\bar{x}$ that does not change the hypersurfaces of constant τ, i. e.

$$\tau = \tau(\bar{x}) = \bar{\tau} \,, \tag{8.32a}$$
$$x^i = x^i(\bar{x}) = \bar{x}^i + \xi^i(\bar{x}) \,. \tag{8.32b}$$

Since $\tau = \bar{\tau}$, the metric on surfaces on constant time will now be given by

$$\begin{aligned} \bar{g}_{ij}(\bar{x}) = g_{ij}(x(\bar{x})) + g_{il}(x(\bar{x}))\partial_j \xi^l(\bar{x}) \\ + g_{kj}(x(\bar{x}))\partial_i \xi^k(\bar{x}) + \mathcal{O}(\xi^2) \,, \end{aligned} \tag{8.33}$$

where derivatives are understood to be with respect to $\bar{x}$. Now, the curvature perturbation on surfaces of constant time is defined by [18, 212–217]

$$\bar{\zeta}(\bar{x}) = \frac{\log\det(\bar{g}_{ij}(\bar{x})/a^2(\tau))}{6} \,, \tag{8.34}$$

where a is not changed since we are not transforming the time coordinate. If we work in the comoving gauge, we can write down $\bar{g}_{ij}(\bar{x})$ as (lowering spatial indices with δ_{ij})

$$\begin{aligned} \bar{g}_{ij}(\bar{x})/a^2 = \delta_{ij} + \partial_i \xi_j(\bar{x}) + \partial_j \xi_i(\bar{x}) + (\underbrace{e^{2\zeta(x(\bar{x}))} - 1}_{=\Delta g(\bar{x})})\delta_{ij} \\ + \Delta g(\bar{x})\big[\partial_i \xi_j(\bar{x}) + \partial_j \xi_i(\bar{x})\big] + \mathcal{O}(\xi^2) \,. \end{aligned} \tag{8.35}$$

Dropping terms cubic in perturbations (which we denote by "…" below), we arrive at

$$\begin{aligned} \log(\bar{g}_{ij}(\bar{x})/a^2) &= \partial_i \xi_j(\bar{x}) + \partial_j \xi_i(\bar{x}) + \Delta g(\bar{x})\delta_{ij} \\ &\quad + \Delta g(\bar{x})\big[\partial_i \xi_j(\bar{x}) + \partial_j \xi_i(\bar{x})\big] - \frac{1}{2}\big[\Delta g(\bar{x})\big]^2 \delta_{ij} \\ &\quad - \Delta g(\bar{x})\big[\partial_i \xi_j(\bar{x}) + \partial_j \xi_i(\bar{x})\big] + \dots \\ &= \partial_i \xi_j(\bar{x}) + \partial_j \xi_i(\bar{x}) + 2\zeta(x(\bar{x}))\delta_{ij} + \dots \,. \end{aligned} \tag{8.36}$$

Taking the trace of the above equation, we find

$$\bar{\zeta}(\bar{x}) = \frac{\partial_i \xi^i(\bar{x})}{3} + \zeta(x(\bar{x})) \,. \tag{8.37}$$

Now, we are interested in long-wavelength transformations, i. e. $\xi^\mu = \xi^\mu_\ell$ will contain only long modes. Therefore, if we split also $\bar{\zeta}$ in long and short modes, we find that its short-scale part transforms as a scalar: $\bar{\zeta}_s(\bar{x}) = \zeta_s(x(\bar{x}))$.

This derivation does not hold if we change also the time coordinate. If one is interested in working at zeroth and linear order in gradients,

as it was done in [24], this is not a problem since the change to CFC affects τ only at order k_ℓ^2. However, for our purposes we will need to consider also the fact that surfaces of constant conformal time are not surfaces of constant CFC time. In Appendix F we show that in this case the transformation rule for ζ_s is nontrivial, namely it acquires a shift

$$\bar{\zeta}_s(\bar{x}) = \zeta_s(x(\bar{x})) + \frac{N_s^i(\bar{x})\partial_i\xi_\ell^0(\bar{x})}{3} \,. \tag{8.38}$$

Since $N_i = \partial_i\psi$, with ψ a function of ζ, this additional shift will generate other terms proportional to (spatial derivatives) of the short-scale power spectrum $\langle\zeta_s\zeta_s\rangle$.

8.3.2 *Transformation of the power spectrum*

We can now see how the short-scale power spectrum $\langle\zeta_s\zeta_s\rangle$ of the curvature perturbation ζ is transformed when moving to the CFC frame. The overall transformation of $\langle\zeta_s\zeta_s\rangle$ will follow closely the one presented in [24], the main difference being the fact that we will go up to order k_ℓ^2 in the gradient expansion. This implies that, in principle, we would need to take the transformation of conformal time (i. e. the contribution of ξ^0) into account. However, it is straightforward to see that these terms will not matter on super-Hubble scales:

- the first contribution is

$$\zeta_s^F(x_F) \supset \frac{N_s^i(x_F)\partial_i\xi_\ell^0(x_F)}{3} \,. \tag{8.39}$$

  Since $N_s^i \sim -\partial_i(\zeta_s/\mathcal{H})$ and $\partial_i\xi_\ell^0$ go to zero for $-k_s\tau_F \ll 1$, $-k_\ell\tau_F \ll 1$, these terms in the transformation of the short-scale curvature perturbation can be dropped;

- the second contribution is, instead, given by

$$\zeta_s^F(x_F) \supset \xi_\ell^0(x_F)\partial_0\zeta_s(x_F) \,. \tag{8.40}$$

  Since ζ_s freezes on super-Hubble scales, we see that also this part of the transformation will not be relevant for $B_\zeta^F(\mathbf{k}_s, \mathbf{k}_\ell)$.

Then, for $\tau_F \to 0^-$, we can write the equal-time power spectrum of short modes in CFC as

$$\langle\zeta_s^F(\mathbf{x}_1^F)\zeta_s^F(\mathbf{x}_2^F)\rangle = \langle\zeta_s(\mathbf{x}_1)\zeta_s(\mathbf{x}_2)\rangle \,, \tag{8.41}$$

where we have defined $x_{1,2}^i \equiv x^i(\mathbf{x}_{1,2}^F)$, and we have dropped all time dependences for simplicity of notation. Now, thanks to translation invariance, we can write the short-scale power spectrum in real space as

$$\langle\zeta_s(\mathbf{x}_1)\zeta_s(\mathbf{x}_2)\rangle = \langle\zeta_s\zeta_s\rangle(r) \,, \tag{8.42}$$

where $\mathcal{R} \equiv \mathbf{x}_1 - \mathbf{x}_2$, and $r \equiv |\mathcal{R}|$. We can now expand this at $\mathcal{O}[(r_F^i)^3]$ and to first order in long-wavelength perturbations: it is straightforward to see that

$$r_F^l = r_F^l + A_i^l(\mathbf{x}_c^F)\, r_F^i + \frac{1}{4} C_{kij}^l(\mathbf{x}_c^F)\, r_F^i r_F^j r_F^k \,, \tag{8.43}$$

since we construct the CFC frame around $\mathbf{x}_c^F = (\mathbf{x}_1^F + \mathbf{x}_2^F)/2$. The exact position of the central geodesic does not matter in the squeezed limit. This has been proven up to order k_ℓ in [24], and here we see that this is true also at order k_ℓ^2: indeed, choosing the middle point gets rid of $B_{ij}^l(\mathbf{x}_c^F)$ only, which is of order k_ℓ (in fact, it is $\sim \delta_{ij}\partial^l \zeta_\ell(\mathbf{x}_c^F)$), and no terms of order k_ℓ^2 are cancelled. That is, any additional correction to our result coming from the change in the position of the central geodesic enters at order k_ℓ^3. The final expression for the power spectrum of the short modes in CFC, then, is given by

$$\begin{aligned} \langle \zeta_s^F \zeta_s^F \rangle (r_F) = \langle \zeta_s \zeta_s \rangle (r_F) + A_i^l(\mathbf{x}_c^F)\, r_F^i \partial_l \langle \zeta_s \zeta_s \rangle (r_F) \\ + \frac{1}{4} C_{kij}^l(\mathbf{x}_c^F)\, r_F^i r_F^j r_F^k \partial_l \langle \zeta_s \zeta_s \rangle (r_F) \,. \end{aligned} \tag{8.44}$$

8.3.3 *Squeezed limit bispectrum – 1st method*

The Maldacena consistency relation [18, 23, 196, 210, 218] in global coordinates, i. e.

$$B_\zeta(\mathbf{k}_s, \mathbf{k}_\ell) = -(n_s - 1) P_\zeta(k_s) P_\zeta(k_\ell) + \mathcal{O}\left(\frac{k_\ell^2}{k_s^2}\right) , \tag{8.45}$$

is equivalent to saying that a long-wavelength mode modulates the small-scale power as

$$P_\zeta(k_s)|_{\zeta(k_\ell)} = [1 - (n_s - 1)\zeta(k_\ell)] P_\zeta(k_s) \,. \tag{8.46}$$

The transformation to CFC, up to linear order in k_ℓ/k_s, cancels exactly the term $\propto (n_s - 1)$ in the previous equation. We want to see, now, what are the terms that survive if we carry the CFC construction up to order k_ℓ^2/k_s^2. Schematically, working in real space, we can write the transformation to CFC of the short-scale power spectrum as (we drop all "F"s on coordinates for simplicity of notation)

$$\langle \zeta_s \zeta_s \rangle (r)|_{\zeta_\ell(\mathbf{x}_c)} \to \langle \zeta_s \zeta_s \rangle (r)|_{\zeta_\ell(\mathbf{x}_c)} + \Xi(\zeta_\ell(\mathbf{x}_c)) \langle \zeta_s \zeta_s \rangle (r) \,, \tag{8.47}$$

where Ξ stands for the various terms, including derivatives with respect to $\mathbf{r}$, of eq. (8.44). If we multiply the right-hand side of the above equation by $\zeta_\ell(\mathbf{x}_3)$, and then average over long modes, we can see what part of the long-short coupling is cancelled when we move to the CFC frame. Following [24], we can compute what is the contribution of these terms when we go in Fourier space $\mathbf{x}_1 \leftrightarrow \mathbf{k}_1$, $\mathbf{x}_2 \leftrightarrow \mathbf{k}_2$ and $\mathbf{x}_3 \leftrightarrow \mathbf{k}_\ell$:

- the first term on the right-hand side of the above equation will give the single-field slow-roll bispectrum in global coordinates of [18], i. e.

$$B_\zeta(\mathbf{k}_s,\mathbf{k}_\ell) = P_\zeta(k_s)P_\zeta(k_\ell)\Bigg\{(1-n_s)+\frac{k_\ell^2}{k_s^2}\Bigg[\left(\frac{29}{6}\varepsilon+\frac{1}{4}\eta\right) - \left(\frac{1}{12}\varepsilon+\frac{5}{8}\eta\right)(1-3\mu^2)\Bigg]\Bigg\}\,, \tag{8.48}$$

  where we have split the part $\propto k_\ell^2/k_s^2$ into a monopole and a quadrupole part. This shows how, for an isotropic long mode, the contribution of ε to the bispectrum of Maldacena at order k_ℓ^2/k_s^2 is ≈ 20 times larger than the one proportional to η;

- in [24] it is shown how, thanks to translational invariance, the term coming from the coordinate transformation can be written in Fourier space as

$$\langle\zeta_\ell(\mathbf{x}_3)\Xi(\zeta_\ell(\mathbf{x}_c))\rangle\,\langle\zeta_s\zeta_s\rangle\,(r) \to \underbrace{P_{\zeta\Xi}(k_\ell)P_\zeta(k_s)|_{\mathbf{k}_s=\mathbf{k}_1+\mathbf{k}_\ell/2}}_{\equiv\Delta B_\zeta(\mathbf{k}_s,\mathbf{k}_\ell)}\,, \tag{8.49}$$

  where we have omitted an overall $(2\pi)^3\delta(\mathbf{k}_1+\mathbf{k}_2+\mathbf{k}_\ell)$ of momentum conservation.

This result allows us to compute separately the long- and short-wavelength power spectra. More precisely, when we go to Fourier space, we include directly in $\langle\zeta_s\zeta_s\rangle\,(r)$ the powers of r^i and derivatives ∂_i contained in Ξ. The full calculation is carried out in Appendix G; here we cite the only result that we are going to need, that is

$$(r^i r^j r^k\dots)\partial_l\,\langle\zeta_s\zeta_s\rangle\,(r) \to i^{N+1}\frac{\partial^N}{\partial k_s^i\partial k_s^j\partial k_s^k\dots}\left[k_s^l P_\zeta(k_s)\right]\,. \tag{8.50}$$

In $\langle\zeta_\ell(\mathbf{x}_3)\Xi(\zeta_\ell(\mathbf{x}_c))\rangle \equiv P_{\zeta_\ell\Xi}(|\mathbf{x}_3-\mathbf{x}_c|)$, now, we will only have contributions like

$$P_{\zeta_\ell\Xi}(|\mathbf{x}_3-\mathbf{x}_c|) \supset \langle\zeta_\ell(\mathbf{x}_3)\partial_{ijk\dots}\zeta_\ell(\mathbf{x}_c)\rangle\,, \tag{8.51}$$

that in Fourier space will read as

$$\langle\zeta_\ell(\mathbf{x}_3)\partial_{ijk\dots}\zeta_\ell(\mathbf{x}_c)\rangle \to \left[(-ik_\ell^i)(-ik_\ell^j)(-ik_\ell^k)\dots\right]P_\zeta(k_\ell)\,. \tag{8.52}$$

The two contributions that we have to consider are $A_i^l(\mathbf{x}_c)$ and $C_{kij}^l(\mathbf{x}_c)$. Before embarking on the calculation, we note that ΔB_ζ will be of order n_s-1: in fact, since we are basically just changing the way in which we measure distance, we will have an effect only if the short-scale power spectrum is not scale invariant. This tells us three things:

- we can use the de Sitter mode functions [18, 43, 119, 219], i. e., dropping irrelevant phases,

$$\zeta(\tau, k) = \zeta(0, k)(1 + ik\tau)e^{-ik\tau} = \sqrt{P_\zeta(k)}\,(1 + ik\tau)e^{-ik\tau} \ , \tag{8.53}$$

  to compute $(a_F/a)|_\ell$, that will enter in $A_i^l(\mathbf{x}_c)$. This is analogous to what is done in Maldacena's calculation of the bispectrum in global coordinates: once the cubic Lagrangian for ζ is found to be of second order in slow-roll (the quadratic one being of first order), the in-in computation of the leading order contribution to the three-point function can be carried out using just the de Sitter modes;

- we can drop the slow-roll suppressed part of the shift constraint when we compute $(a_F/a)|_\ell$. That is, we can take ψ_ℓ to be just $-\zeta_\ell/\mathcal{H}$ and drop $\varepsilon\partial^{-2}\partial_0\zeta_\ell$, when we use the expression for $(a_F/a)|_\ell$ given in eq. (8.31);

- when we consider $C_{kij}^l(\mathbf{x}_c)$, we can drop the ε-suppressed part of the stereographic projection, i. e. the last three lines of eq. (8.25): the only contribution that we need to consider is the isotropic one, which involves the curvature K_F.

However, we note that there will be no need of actually computing $(a_F/a)|_\ell$: in fact, from its definition of Section 8.2.3 and our choice of initial time for the definition of Conformal Fermi Coordinates, we have that

$$(a_F/a)|_\ell \xrightarrow{-k_\ell\tau \ll 1} C_{a_F} + \mathcal{O}(k_\ell^3) \ . \tag{8.54}$$

Since we take C_{a_F} to be zero, we can forget about this contribution. Then,

- we start from $A_i^l(\mathbf{x}_c)$, which gives

$$\Delta B_\zeta^{(1)}(\mathbf{k}_s, \mathbf{k}_\ell) = P_\zeta(k_\ell)\frac{\partial}{\partial k_s^i}[k_s^i P_\zeta(k_s)] \ , \tag{8.55}$$

  where

$$\frac{\partial}{\partial k_s^i}[k_s^i P_\zeta(k_s)] = \left(3 + \frac{d}{d\log k_s}\right)P_\zeta(k_s) = (n_s - 1)P_\zeta(k_s) \ . \tag{8.56}$$

  So we have

$$\Delta B_\zeta^{(1)}(\mathbf{k}_s, \mathbf{k}_\ell) = (n_s - 1)P_\zeta(k_\ell)P_\zeta(k_s) \ ; \tag{8.57}$$

- the second (and last) term we have to consider is $C_{kij}^l(\mathbf{x}_c)$. It contains two contributions. One from $\sim \partial_i\partial_j\zeta$, and one from $\sim \mathcal{H}\partial_i\partial_j F$ (as we see from tab. E.1): since F is already of order

k_ℓ^2, it is sufficient to include the former. At leading order in slow-roll, then, we have

$$\begin{aligned} C^l_{kij}(k_\ell) = -\frac{1}{6}\Big[&\delta_{ij}k^k_\ell k^l_\ell \zeta(k_\ell) \\ &- \delta^l_j k^k_\ell k^i_\ell \zeta(k_\ell) - \delta^l_i k^k_\ell k^j_\ell \zeta(k_\ell) \\ &+ \frac{1}{9}(\delta^l_k\delta_{ij} + \delta^l_i\delta_{jk} + \delta^l_j\delta_{ki})k^2_\ell\zeta(k_\ell)\Big] \,. \end{aligned} \tag{8.58}$$

In the above equation, if we isolate a tensor $\mathcal{L}^l_{kij} \propto k^2_\ell \zeta(k_\ell)$, we can write

$$\begin{aligned} \Delta B^{(2)}_\zeta(\mathbf{k}_s, \mathbf{k}_\ell) &= \frac{1}{4}P_\zeta(k_\ell)\mathcal{L}^l_{kij}\left[i^4 \frac{\partial^3}{\partial k^i_s \partial k^j_s \partial k^k_s}\left[k^l_s P_\zeta(k_s)\right]\right] \\ &\equiv \frac{1}{4}P_\zeta(k_\ell)\mathcal{L}^l_{kij}\mathcal{S}^l_{ijk}P_\zeta(k_s) \,. \end{aligned} \tag{8.59}$$

We compute this quantity in Appendix G and cite here only the final result, i. e.[4]

$$\Delta B^{(2)}_\zeta(\mathbf{k}_s, \mathbf{k}_\ell) = (n_s - 1)\frac{k^2_\ell}{k^2_s}\left(-\frac{5}{24} + \frac{5}{8}\mu^2\right)P_\zeta(k_\ell)P_\zeta(k_s) \,. \tag{8.60}$$

Summing these two contributions to the Maldacena bispectrum of eq. (8.48), we see that in the CFC frame the long-short coupling still retains terms $\propto \eta$: more precisely, we have

$$\begin{aligned} B^F_\zeta(\mathbf{k}_s, \mathbf{k}_\ell) &= \frac{k^2_\ell}{k^2_s}P_\zeta(k_s)P_\zeta(k_\ell)\left[\left(\frac{29}{6}\varepsilon + \frac{1}{4}\eta\right)\right. \\ &\qquad \left. + \left(\frac{1}{3}\varepsilon - \frac{5}{12}\eta\right)(1 - 3\mu^2)\right] \\ &= \frac{k^2_\ell}{k^2_s}P_\zeta(k_s)P_\zeta(k_\ell)\left[\left(\frac{13}{3}\varepsilon - \frac{1}{4}(n_s - 1)\right)\right. \\ &\qquad + \left(\frac{7}{6}\varepsilon + \frac{5}{12}(n_s - 1)\right) \\ &\qquad \left. \times (1 - 3\mu^2)\right] \,, \end{aligned} \tag{8.61}$$

where, in the second equality, we have highlighted the tilt of the scalar spectrum $n_s - 1$ instead of η. We see that, as in Maldacena's squeezed bispectrum at order k^2_ℓ/k^2_s, the contribution to the physical isotropic mode coupling $\propto \varepsilon$ is larger than the one $\propto \eta$ by a factor of ≈ 20.

4 This contribution vanishes for an isotropic long mode (i. e. $\mu^2 = 1/3$). Indeed, in this case it is easy to see that to go from the metric in global coordinates to the CFC metric described in Section 8.2.3 it is enough to remove the constant and constant gradient parts of metric perturbations. In fact, g_{0i} is already zero in the isotropic case and the curvature part of g_{ij} (i. e. the one proportional to $|\mathbf{x}|^2$) is already of the right form.

For reference, we can match the result eq. (8.61) to the squeezed limit of the equilateral shape $\mathcal{S}_{\text{equil.}}(k_1, k_2, k_3)$. Using Eq. (52) from [40], we have

$$B_\zeta^{\text{equil.}}(\mathbf{k}_s, \mathbf{k}_\ell) = \frac{k_\ell^2}{k_s^2} P_\zeta(k_s) P_\zeta(k_\ell)\, 4 f_{\text{NL}}^{\text{equil.}} \left[2 + (1 - 3\mu^2)\right] . \tag{8.62}$$

Clearly, eq. (8.61) cannot be matched to the equilateral shape, since the relative isotropic and anisotropic contributions are different. Moreover, we have only calculated the $\mathcal{O}(k_\ell^2/k_s^2)$ contribution in the squeezed limit, and different shapes $\mathcal{S}(k_1, k_2, k_3)$ can have the same squeezed-limit scaling $\propto k_\ell^2/k_s^2$. Hence, we caution against associating eq. (8.61) with the equilateral template. Roughly, however, eq. (8.61) corresponds to $f_{\text{NL}}^{\text{equil.}} \sim 0.1 \times (n_s - 1)$.

8.4 CALCULATION AT THE LEVEL OF THE ACTION

In this Section we derive the CFC bispectrum in the limit $\varepsilon \to 0$ directly, without recurring to a transformation of Maldacena's result.

8.4.1 *Short modes in CFC*

We start by defining the short modes in CFC: keeping the "F" label on coordinates and components to parallel the first part of our previous calculation, we write the line element in CFC coordinates as

$$\begin{aligned} ds_F^2 = &-a^2\left[1 + 2(N_1^F)_\ell + 2(N_1^F)_s\right] d\tau_F^2 \\ &+ a^2 (N_i^F)_s (d\tau_F dx_F^i + dx_F^i d\tau_F) \\ &+ a^2 e^{2\zeta_\ell^F} e^{2\zeta_s^F} \delta_{ij} dx_F^i dx_F^j , \end{aligned} \tag{8.63}$$

where:

- we have put to zero $(N_i^F)_\ell$, since we have seen that the time-space components of the long-wavelength metric in CFC are of order k_ℓ^3;
- working at linear order in the long mode (as we are doing throughout the Chapter), the long-wavelength part of the metric can be related, by direct comparison, to the results of Section 8.2. For example, the anisotropic part of ζ_ℓ^F will be

  $$(\zeta_\ell^F)(x_F)^{\text{anis.}} = \frac{1}{2} x_F^i x_F^j \mathcal{D}_{ij} \left[\varepsilon \mathcal{H} \partial^{-2} \partial_0 \zeta_\ell(\tau, \mathbf{0})\right] , \tag{8.64}$$

  where ζ_ℓ is the long-wavelength curvature perturbation in global coordinates;
- we have included the modification to the scale factor, i. e.

  $$a_F(\tau_F) = a(\tau_F)\left[1 + (a_F/a)(\tau_F)|_\ell + \mathcal{H}\xi^0(\tau_F, \mathbf{0})\right] , \tag{8.65}$$

directly into ζ^F_ℓ and $(N^F_1)_\ell$: by doing so we can keep track more easily of both the order in perturbations and the order in the slow-roll expansion;

- ζ^F_s, $(N^F_1)_s$ and $(N^F_i)_s = \partial_i \psi^F_s$ (whose indices will be raised and lowered with δ^j_i) are the short modes. As before, we stopped at first order in perturbations in the small-scale lapse and shift constraints, which will be solved linearly in terms of ζ_s.

At this point, one can write down the action for ζ^F_s: the lapse and shift constraints will have the usual expression, and the quadratic action $S_{(2)}$ will be given by [18]

$$S_{(2)} = \int d^4x_F \, a^2 \varepsilon \left[(\partial_0 \zeta^F_s)^2 - (\partial_i \zeta^F_s)^2 \right] . \tag{8.66}$$

Then, the goal is to compute the power spectrum of ζ^F_s in the background of the CFC long-wavelength metric: since the latter is explicitly of order k^2_ℓ, it is clear that the CFC bispectrum will vanish at zeroth and first order in gradients of the long mode. Now, in order to calculate the $\mathcal{O}(k^2_\ell)$ contribution, one needs the cubic action with one long leg and two short legs. This can be computed with the standard methods (see [18, 119], for example) and, as in the standard case, the "brute-force" computation gives an action which is of order zero in slow-roll (compared with the quadratic action of eq. (8.66), which is slow-roll suppressed): however, due to the complicated relation between ζ^F_ℓ and $(N^F_1)_\ell$,[5] integrating by parts to remain with $\mathcal{O}(\varepsilon)$ terms that can be removed with a field redefinition is more difficult than in Maldacena's calculation.

A possible alternative approach is to work in ϕ gauge for the short modes, while keeping the long-wavelength metric as in eq. (8.63). In this case, the quadratic action for the small-scale field fluctuations $\delta\phi_s$ would be of order zero in slow-roll [18, 119], but this would still not help because the cubic action will again, naively, not be slow-roll suppressed (we refer also to Appendix H for a more detailed discussion about these issues). In both these cases, then, we could not do an in-in calculation using the de Sitter modes $\propto e^{-ik\tau}(1 + ik\tau)$, since we would be missing terms due to slow-roll corrections to the mode functions: we would need to use the full solution of the classical equations of motion for the short modes in terms of Hankel functions, complicating the in-in integral considerably. For this reason, we will employ a different method, that is explained in the following Section.

5 This relation can be found by solving at linear order the lapse constraint for $(N^F_1)_\ell$ with the metric of eq. (8.63). The result is not particularly illuminating, so we will not write it down.

8.4.2 *From flat gauge to CFC*

This second method is based on the observation that, in flat gauge, all interactions are suppressed by $\sqrt{\varepsilon}$. Therefore, if we are interested only in the contribution to the CFC bispectrum proportional to η (which is the focus of this Chapter), we expect that it will not be necessary to do any in-in calculation. We will explain how this comes about in the following.

To simplify notation, in this Section we will use $x = (x^0, \mathbf{x})$ for global coordinates, $x_F = (x_F^0, \mathbf{x}_F)$ for CFC. We use a "tilde" and a "hat" for coordinate changes, and a "prime" for time derivatives of the background inflaton $\bar{\phi}$). We then proceed in the following way:

- we start from the long-wavelength metric in global coordinates x, in ζ gauge. At linear order in the long mode, we can go to flat gauge with a simple time shift, i. e.

$$x^0 = \tilde{x}^0 - \frac{\zeta_\ell}{\mathcal{H}} \,. \tag{8.67}$$

  This coordinate change will originate an inflaton perturbation $\delta\phi_\ell = -\sqrt{2\varepsilon}\,\zeta_\ell$, which is of order zero in slow-roll since a factor of $1/\sqrt{\varepsilon}$ is "hidden" in ζ_ℓ;

- to this $\delta\phi_\ell$ we add a short $\delta\phi_s$, solve the constraints, and compute both the quadratic action for $\delta\phi_s$ and the interaction terms at cubic order (see also [65] for details):
  - $S_{(2)}$ is given by

$$S_{(2)} = \int d^4\tilde{x}\, a^2 \left[(\partial_0\delta\phi_s)^2 - (\partial_i\delta\phi_s)^2 + \mathcal{H}^2\eta\,\delta\phi_s^2\right] \,. \tag{8.68}$$

    So, we see that η provides a mass for $\delta\phi_s$, which tells us that $\delta\phi_s$ will not be conserved on super-Hubble scales;
  - the result for the cubic terms will be Maldacena's cubic Lagrangian in flat gauge, with one long leg and two short legs. It is then easy to see from Eq. (3.8) of [18] that, at leading order in slow-roll, interactions will be suppressed by a factor $\sqrt{\varepsilon}$: therefore in the limit $\varepsilon \to 0$ there is no coupling between the long mode and short modes, i. e. we can schematically write

$$P_{\delta\phi_s|\delta\phi_\ell} = P_{\delta\phi_s} \,, \tag{8.69}$$

    where $P_{\delta\phi_s}$ is the usual power spectrum of $\delta\phi_s$ in an unperturbed FLRW background that one computes from eq. (8.68), while $P_{\delta\phi_s|\delta\phi_\ell}$ is the power spectrum of $\delta\phi_s$ in the background of a long-wavelength mode (i. e. considering the coupling with $\delta\phi_\ell$);

- then, we transform from the flat gauge in global coordinates to CFC. At linear order, the transformation is simply given by

$$\tilde{x}^{\mu} = x_F^{\mu} + \underbrace{\frac{\zeta_\ell}{\mathcal{H}}\delta_0^{\mu} + \xi_\ell^{\mu}}_{\equiv \Delta_\ell^{\mu}} , \tag{8.70}$$

where ξ_ℓ^{μ} is the vector field given in eqs. (8.22) in terms of ζ_ℓ. Now, after this change of coordinates, the spatial part of the metric at quadratic order in perturbations but at linear order in the long mode,[6] will be given by

$$\begin{aligned} g_{ij}^F &= -a^2 \frac{\partial \Delta_\ell^0}{\partial x_F^i}\frac{\partial \Delta_\ell^0}{\partial x_F^j} + \frac{\partial \Delta_\ell^0}{\partial x_F^i}\tilde{g}_{0j} + \frac{\partial \Delta_\ell^0}{\partial x_F^j}\tilde{g}_{i0} + a^2 e^{2\zeta_\ell^F}\delta_{ij} \\ &= a^2 \frac{\partial \Delta_\ell^0}{\partial x_F^i}\partial_j\tilde{\psi}_s + a^2 \frac{\partial \Delta_\ell^0}{\partial x_F^j}\partial_i\tilde{\psi}_s + a^2 e^{2\zeta_\ell^F}\delta_{ij} + \mathcal{O}[(\zeta_\ell)^2] , \end{aligned} \tag{8.71}$$

where $\tilde{\psi}_s$ is the short-scale shift constraint in flat gauge, i. e.

$$\tilde{\psi}_s = -\varepsilon \partial^{-2}\partial_0(\mathcal{H}\delta\phi_s/\bar{\phi}') , \tag{8.72}$$

and we dropped terms quadratic in ζ_ℓ. Correspondingly, the inflaton will transform as

$$\phi = \bar{\phi} + \sqrt{2\varepsilon}\,\mathcal{H}\xi_\ell^0 + \delta\phi_s + \Delta_\ell^{\mu}\partial_\mu\delta\phi_s , \tag{8.73}$$

where we used $\bar{\phi}' = \sqrt{2\varepsilon}\,\mathcal{H}$;

- then: we want to find the relation between $\delta\phi_s$ and ζ_s^F, defined as in eq. (8.63). In order to do this, we first do a time translation $x_F^0 = \hat{x}_F^0 + T$ (with T starting linear in short modes, and having a quadratic long-short coupling) that brings ϕ to $\bar{\phi} + \sqrt{2\varepsilon}\,\mathcal{H}\xi_\ell^0$. It is easy to see that T is given by

$$\begin{aligned} T &= -\frac{1}{\sqrt{2\varepsilon}\,\mathcal{H}}\Bigg[\delta\phi_s + \Delta_\ell^{\mu}\partial_\mu\delta\phi_s \\ &\qquad - \frac{\bar{\phi}''}{\bar{\phi}'}\xi_\ell^0\delta\phi_s - \partial_0\xi_\ell^0\delta\phi_s\Bigg] \\ &= -\frac{1}{\sqrt{2\varepsilon}\,\mathcal{H}}\Bigg[\delta\phi_s + \Delta_\ell^{\mu}\partial_\mu\delta\phi_s \\ &\qquad - \mathcal{H}\left(1 - \varepsilon + \frac{\eta}{2}\right)\xi_\ell^0\delta\phi_s - \partial_0\xi_\ell^0\delta\phi_s\Bigg] . \end{aligned} \tag{8.74}$$

Now, we focus on the spatial metric $\hat{g}_{ij}$ after this time translation, working at quadratic order in perturbations but dropping terms involving two short modes. It will be given by

$$\hat{g}_{ij}^F = a^2 \frac{\partial \Delta_\ell^0}{\partial \hat{x}_F^i}\partial_j\tilde{\psi}_s + a^2 \frac{\partial \Delta_\ell^0}{\partial \hat{x}_F^j}\partial_i\tilde{\psi}_s + a^2 e^{\zeta_\ell^F} e^{\zeta_s^F}\delta_{ij} , \tag{8.75}$$

6 That is, we consider only quadratic terms that mix long and short modes: therefore, we do not consider the long part of $\tilde{g}_{0i}$ (which will not be of order k_ℓ^3 yet) since it will give rise to terms quadratic in the long mode in the transformed spatial metric.

where we have used the fact that the long-wavelength part of g^F_{0i} is $\mathcal{O}(k_\ell^3)$ (so that we can safely neglect its contribution to the transformation at the order we are working at), and we have defined ζ_s as

$$\zeta_s^F = \mathcal{H}T + T\partial_0\zeta_\ell = \mathcal{H}T - \frac{\delta\phi_s}{\sqrt{2\varepsilon}}\partial_0\zeta_\ell \ . \tag{8.76}$$

With some hindsight, then, we can also define ζ_s as

$$\zeta_s = -\frac{\mathcal{H}}{\bar{\phi}'}\delta\phi_s = -\frac{\delta\phi_s}{\sqrt{2\varepsilon}} \ , \tag{8.77}$$

so that ζ_s^F becomes

$$\zeta_s^F = \mathcal{H}T + \zeta_s\partial_0\zeta_\ell \ . \tag{8.78}$$

We note that $\hat{g}^F_{ij}$ is not yet of the form of eq. (8.63) because of the terms in eq. (8.75) involving the short-scale shift constraint in flat gauge, which is given by

$$\tilde{\psi}_s = -\varepsilon\partial^{-2}\partial_0\left(\frac{\mathcal{H}}{\bar{\phi}'}\delta\phi_s\right) = \varepsilon\partial^{-2}\partial_0\zeta_s \ . \tag{8.79}$$

However, we can see that these terms will not matter on super-Hubble scales. We can follow the approach of Maldacena: with a second order long-short spatial transformation (which does not modify the field perturbations at the order we are working at) we can remove these terms at the price of new second order contributions to ζ_s^F. From [18] we can see that all the new terms that ζ_s^F gains will contain $\tilde{\psi}_s$, that is proportional to $\partial^{-2}\partial_0\zeta_s$. However, we know that ζ_s must freeze on super-Hubble scales (this can be seen also at the level of the quadratic action, that can be derived from the action for $\delta\phi_s$ with the changes of coordinates discussed above). This tells us that we can safely neglect the contributions from this second order spatial transformations in the relation between $\delta\phi_s$ and ζ_s^F;

- then, we can focus just on eq. (8.77). We consider only terms that are either of order zero in slow-roll, or suppressed by η, dropping all terms $\propto \varepsilon$. With these assumptions, ζ_s^F becomes equal to

$$\begin{aligned}\zeta_s^F = \zeta_s + \xi^i_\ell\partial_i\zeta_s + \xi^0_\ell\partial_0\zeta_s + \frac{1}{\mathcal{H}}\zeta_\ell\partial_0\zeta_s \\ + \frac{\eta}{2}\zeta_\ell\zeta_s - \zeta_s\partial_0\xi^0_\ell - \mathcal{H}\xi^0_\ell\zeta_s + \zeta_s\partial_0\zeta^F_\ell \ .\end{aligned} \tag{8.80}$$

In the above equation we recognize the term $\xi^i_\ell\partial_i\zeta_s$ from Section 8.3.3. We also see that both terms containing $\partial_0\zeta_s$ will not contribute on super-Hubble scales, so they can be dropped. We deal with the remaining terms separately by considering that ξ^0_ℓ and ζ_ℓ can be split in a uniform (which encodes the modified expansion history), isotropic and anisotropic part:

– we start from the isotropic part. For ξ^0_ℓ it is zero, while for $\partial_0\zeta^F_\ell$ it is proportional to $|\mathbf{x}_F|^2\partial_0 K_F$, which in turn is $\propto k^4_\ell$;
– the uniform part of $\partial_0\zeta^F_\ell$ is, dropping ε-suppressed terms, equal to $\partial_0\xi^0_\ell + \mathcal{H}\xi^0_\ell + \partial_0(a_F/a)|_\ell$. The first two terms exactly cancel with those in eq. (8.80), while from the definition of $(a_F/a)|_\ell$ discussed in Section 8.2.3 we see that the last one vanishes on super-Hubble scales;
– finally, we can easily see from the results of Section 8.2.3 that the anisotropic part of $\partial_0\zeta^F_\ell$ is of order ε (or higher), while that of $\partial_0\xi^0_\ell + \mathcal{H}\xi^0_\ell$ contains either ε-suppressed terms, or terms that go to zero as fast as $\mathcal{H}^{-2}$.

So we conclude that the only relevant terms in eq. (8.78) will be

$$\zeta^F_s = \zeta_s + \xi^i_\ell\partial_i\zeta_s + \frac{\eta}{2}\zeta_\ell\zeta_s \ . \tag{8.81}$$

8.4.3 *Squeezed limit bispectrum – 2nd method*

We are now in a position to compute the squeezed limit bispectrum in the conformal Fermi frame. Since we have the power spectrum of $\delta\phi_s$, we can compute the power spectrum of ζ^F_s in the background of the long modes. Schematically, since ζ^F_s is ζ_s plus a long-short coupling, we would have

$$\langle\zeta^F_s\zeta^F_s\rangle|_{\zeta_\ell} = \langle\zeta_s\zeta_s\rangle|_{\zeta_\ell} + \mathcal{O}(\zeta_\ell)\langle\zeta_s\zeta_s\rangle \ . \tag{8.82}$$

Had we kept also ε-suppressed interactions in our flat gauge calculation of Section 8.4.2, the first term on the right-hand side of the above equation would actually also contain a coupling with long modes: however, we do not care about this term (since we are trying to capture only the part of the bispectrum proportional to η). Then, $\langle\zeta_s\zeta_s\rangle|_{\zeta_\ell}$ will just be the power spectrum of ζ_s computed from the quadratic Lagrangian of $\delta\phi_s$, i. e. what we called $\langle\zeta_s\zeta_s\rangle$ in the previous Section. The second term on the right-hand side of eq. (8.82) contains both the contribution of $\xi^i_\ell\partial_i\zeta_s$, which reproduces exactly what we have computed in Section 8.3.3, and a second term $\propto\eta$. We can deal with the latter by expanding ζ_ℓ in a Taylor series around $\mathbf{x}^F_c \equiv (\mathbf{x}^F_1 + \mathbf{x}^F_2)/2$, so that

$$\begin{aligned}\langle\zeta^F_s(\mathbf{x}^F_1)\zeta^F_s(\mathbf{x}^F_2)\rangle|_{\zeta_\ell(\mathbf{x}^F_c)} \supset \frac{\eta}{2}\left[2\zeta_\ell(\mathbf{x}^F_c) + \frac{r^i_F r^j_F}{4}\partial_i\partial_j\zeta_\ell(\mathbf{x}^F_c)\right] \\ \times\langle\zeta_s\zeta_s\rangle(r_F) + \mathcal{O}(k^3_\ell) \ .\end{aligned} \tag{8.83}$$

Going to Fourier space using the results of Appendix G, more precisely the fact that

$$\frac{\partial^2}{\partial k^i_s\partial k^j_s}P_\zeta(k_s) = -3\frac{\delta_{ij}}{k^2_s}P_\zeta(k_s) + 15\frac{k^i_s k^j_s}{k^4_s}P_\zeta(k_s) + \mathcal{O}(n_s - 1) \ , \tag{8.84}$$

and averaging over the long-wavelength perturbations, we reproduce the η part of Maldacena's bispectrum in the squeezed limit, up to and including $\mathcal{O}(k_\ell^2/k_s^2)$. Summing this to the other contribution (noting that the first term in eq. (8.82) will not matter once we average over long modes, since it has no coupling to them that are proportional to η), we reproduce our final result of eq. (8.61) for $\varepsilon \to 0$. This concludes our analysis: we stress that this method is not completely independent from that of Section 8.3, since we still need to compute what is the effect of the shift $\xi_\ell^i \partial_i \zeta_s$, but we consider it different enough to provide a consistency check.

8.5 INTERACTIONS DURING INFLATION

In this Section we discuss an argument, put forward in [205], to estimate the size of (gravitational) interactions between long and short modes. More generally, we review how the contribution $\propto \eta$ arises in Maldacena's bispectrum, and argue that η must be locally observable, as shown through the direct calculation in Section 8.3 and Section 8.4.

8.5.1 *Where does η come from?*

Let us start by considering short-scale scalar field perturbations $\delta\phi_s$ in the separate universe (similarly to the setup described in fig. 7.2). Naively, one might think that a coupling to ζ_ℓ enters at order ε^0 [207, 208]: for example, the Ricci three-scalar on constant time hypersurfaces, which measures the spatial curvature, is ${}^{(3)}R \propto \partial^2 \zeta_\ell$; that is, it is not slow-roll suppressed. Indeed, if one were to do a brute-force computation of the action for $\delta\phi_s$ in the long-wavelength background modified by ζ_ℓ (i. e. the cubic action with two short legs $\delta\phi_s$ and one long leg ζ_ℓ, which controls the interactions between the long and short modes), the result would naively appear to be of such order. However, one can compute the full spacetime Riemann tensor $R_{\mu\nu\rho\sigma}$ of the background (in any gauge[7])

$$R_{\mu\nu\rho\sigma} = H^2(g_{\mu\rho}g_{\nu\sigma} - g_{\mu\sigma}g_{\nu\rho}) + \mathcal{O}(\varepsilon \times \partial^2\zeta_\ell) \,, \tag{8.85}$$

where we stopped at quadratic order in gradients of ζ_ℓ, and used the fact that time derivatives of ζ_ℓ are also $\propto \partial^2\zeta_\ell$. In a general set of coordinates, $g_{\mu\nu}$ might contain unsuppressed terms of order $\varepsilon^0\zeta_\ell$. We notice though that the leading term is the Riemann tensor for a maximally symmetric spacetime with Ricci scalar $\propto H^2$, namely de Sitter spacetime. Therefore, up to terms of order ε, there must exist a change of coordinates that removes *completely* the long mode from the right

7 This expression is covariant, but not *manifestly* covariant because we are trying to make explicit the dependence on ε and ζ_ℓ, which are defined in global FLRW coordinates.

hand side.[8] Then, the coupling between $\delta\phi_s$ and ζ_ℓ is suppressed by ε, and no term $\propto \eta$ only appears. We also know that these small-scale inflaton fluctuations have non-zero mass. eq. (8.68) tells us that this mass is $\propto \eta$. Therefore, $\delta\phi_s$ evolves on super-Hubble scales. Switching from inflaton perturbations to curvature perturbations cancels this time dependence, and induces an additional term $\propto \eta$ in the long-short mode coupling, since the relation between $\delta\phi$ and ζ is non-linear. For this reason, we can regard η as measuring a *physical* effect, i. e. the time evolution of inflaton correlators on super-Hubble scales, and we do not expect η to vanish in the CFC bispectrum at order k_ℓ^2/k_s^2.

Another way to look at this is to work directly with short-scale curvature perturbations ζ_s: as Maldacena has shown, a straightforward computation of the cubic action of ζ with ζ_ℓ in one leg and ζ_s in the other two leads to $S_{(3)} \sim \varepsilon^0 \times \zeta_\ell \times \zeta_s^2$. However, one can do a sequence of integration by parts to rewrite this as $S_{(3)} \sim \varepsilon(1+\varepsilon+\eta) \times \zeta_\ell \times \zeta_s^2$, with the term proportional to $\varepsilon\eta$ arising when one integrates by parts terms such as $a^2\varepsilon\,\zeta(\partial_0\zeta)^2$. This shows that also $S_{(3)}$ goes to zero when ε goes to zero. However, what matters is the relative order in slow-roll between the quadratic action $S_{(2)} \sim \varepsilon \times \zeta_s^2$ and this cubic action. The quadratic action for ζ_s is also suppressed by ε, so the size of interactions is $\sim (1+\varepsilon+\eta)$: η and ε are *both* a measure of the coupling between long- and short-wavelength modes of ζ. The fact that the background spacetime is de Sitter in the $\varepsilon \to 0$ limit, even in presence of ζ_ℓ, does *not* allow us to conclude that such long-wavelength perturbations have no effect on the short modes ζ_s.[9] Notice that the terms of order $\varepsilon \times 1$ in $S_{(3)}$ do not contribute to correlation functions on super-Hubble scales (their contribution in the in-in calculation of the bispectrum decays). In fact, we know that the final result for the 2-point function of ζ_s in presence of ζ_ℓ must satisfy the consistency relation in the squeezed limit, i. e. at leading order in derivatives of ζ_ℓ we have

$$\langle \zeta_s \zeta_s \rangle (r)|_{\zeta_\ell(\mathbf{x}_c)} = [1 + (1-n_s)\zeta_\ell(\mathbf{x}_c)]\, \langle \zeta_s \zeta_s \rangle (r) \,. \tag{8.86}$$

Then, one can do a counting of factors of ε and η to see what is the order in slow-roll of the above expression. The tilt contains both ε and η, while the three perturbations of ζ each contain $1/\sqrt{\varepsilon}$ (recall that $\langle\zeta\zeta\rangle \sim H^2/\varepsilon$). Therefore the overall order of eq. (8.86) is $\sim (\varepsilon, \eta) \times \varepsilon^{-3/2}$. One can then repeat the same argument for the full in-in calculation of this position-dependent power spectrum. From two powers of the

8 In passing, we also note that this is the reason why in Section 8.2.3 we have seen that the anisotropic part of the long-wavelength metric in CFC is slow-roll suppressed. Indeed, de Sitter is an isotropic spacetime.

9 The argument we made for scalar perturbations, using eq. (8.85), does not apply to curvature perturbations. In fact, ζ_s is not a (perturbation of a) scalar field: it is a component of the metric which is non-linearly related to the inflaton $\delta\phi_s$ and has a non-minimal coupling with the Riemann tensor of the long-wavelength background.

short modes, of which we compute the 2-point function in presence of ζ_ℓ, we have $(1/\sqrt{\varepsilon})^2$, while $S_{(3)}$ would give

$$S_{(3)} \sim \varepsilon(1+\varepsilon+\eta) \times \zeta_\ell \times \zeta_s^2 \sim \varepsilon(1+\varepsilon+\eta) \times \varepsilon^{-3/2} \,. \tag{8.87}$$

Overall, we have $(1+\varepsilon+\eta) \times \varepsilon^{-3/2}$: to agree with the result in the squeezed limit, then, the terms of order $\varepsilon \times 1$ in $S_{(3)}$ must not contribute on super-Hubble scales. By continuity, the same applies to other momentum configurations away from the squeezed limit.

Finally, there is yet another way to see why we must expect η to be present in physical observables. Recall the discussion of Section 7.2. We have seen that any uniform ζ_ℓ disappears from local observables when correlators are re-written in terms of the physical distance between $\mathbf{x}_1$ and $\mathbf{x}_2$. The reason is that the consistency relation is, at this order, completely equivalent to a constant rescaling of the scale factor, and then of the distance on constant-time hypersurfaces. However, this ceases to be true at second order in gradients of ζ_ℓ: while the primordial coupling is still of the local type, i. e. it corresponds to a spatially-dependent rescaling of volumes, the physical distance and the coordinate distance will not be simply proportional to each other (as it can be checked straightforwardly by computing the distance between $\mathbf{x}_1$ and $\mathbf{x}_2$ with a curved FLRW metric).

8.5.2 *Non-trivial speed of sound*

We conclude this Section by briefly discussing the case where the inflaton speed of sound c_s is different from 1. In this case, we know that the operator giving $c_s \neq 1$ also induces cubic couplings for the inflaton [62], leading to enhanced non-Gaussianities. Indeed, while the three-point function from these inflaton self-interactions still satisfies the consistency relation in the squeezed limit, the term proportional to k_ℓ^2/k_s^2 is of order $(1-c_s^2)/c_s^2$ [119, 208, 220], which can be much larger than the one coming from gravitational interactions for $c_s < 1$. It is then easy to see how this still holds in the conformal Fermi frame: the corrections to the bispectrum coming from the transformation to CFC are of order of the scale dependence of the power spectrum, namely

$$\Delta B_\zeta(\mathbf{k}_s, \mathbf{k}_\ell) \sim \frac{k_\ell^2}{k_s^2} \times \frac{d\log[k_s^3 P_\zeta(k_s)]}{d\log k_s} \,, \tag{8.88}$$

For $c_s \neq 1$, we have [62, 119, 219]

$$P_\zeta(k_s) \propto \frac{H^2}{\varepsilon c_s} \,, \tag{8.89}$$

so that

$$\frac{d\log[k_s^3 P_\zeta(k_s)]}{d\log k_s} = \mathcal{O}(\varepsilon, \eta, s), \text{ with } s \equiv \frac{\dot{c}_s}{H c_s} \,. \tag{8.90}$$

Approximate time translation invariance requires $s \ll 1$, i. e. that the inflaton sound speed does not evolve quickly in one Hubble time [62]. Therefore, ΔB_ζ is subleading with respect to the bispectrum in global coordinates when $c_s \ll 1$, and the $1/c_s^2$-enhanced non-Gaussianity is locally observable.

8.6 CONNECTION TO OBSERVATIONS

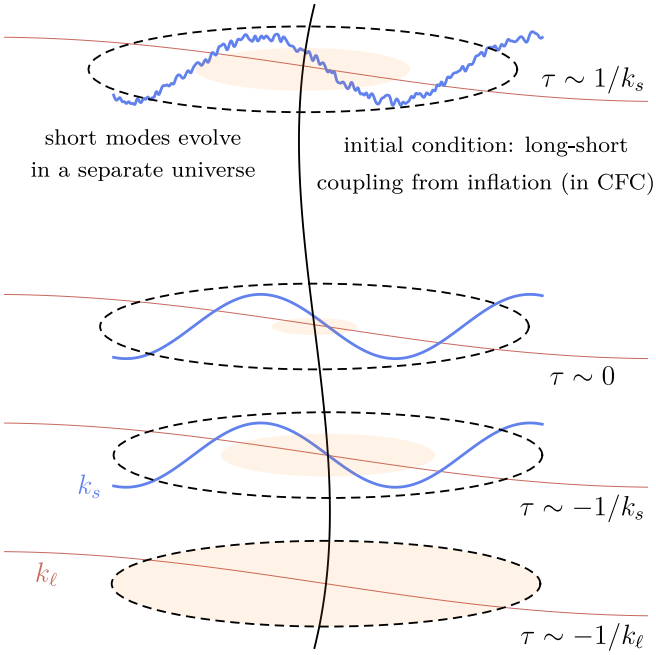

FIGURE 8.1: For a local observer U^μ, the effect of a long mode k_ℓ is that of making the short modes evolve in a separate universe of size $\sim 1/k_\ell$, described by a curved FLRW metric with time-dependent tidal corrections [200, 201]. Long modes become classical on super-Hubble scales, and we can describe their effect on small-scale perturbations by going to CFC. We carry on our construction to the end of inflation, when all relevant modes are super-Hubble and time-independent. This gives the coupling between long- and short-scale perturbations measured by the observer U^μ, that can be used as initial condition for the evolution of short modes as they re-enter the Hubble radius during the Hot Big Bang.

The result that we have found in Section 8.3 and Section 8.4 can be used as initial condition for the study of the dynamics of small-scale perturbations in the CFC frame when they re-enter the horizon, which has been carried out in [200, 201]. In this Section we sketch how this can be done, leaving the details for future work.

First, note that in order to achieve this (i. e. to be able to use the inflationary prediction as initial condition for the late-time gravita-

tional dynamics, while working in this local CFC frame throughout the whole history of short modes), the "factoring out" of the background expansion in the definition of CFC coordinates is crucial, as was already emphasized in [24]. In fact, if we wanted to do the same calculation, but working in FNC, we could not have followed the small-scale perturbations from horizon exit to horizon re-entry: the reason is that FNC are valid on a physical scale $d^{\text{phys.}}$ which is either the physical Hubble radius H^{-1}, or the scale of variation a/k_ℓ of long modes, whichever is smaller. During inflation all modes of interest exit the horizon, i. e. we have $a/k_\ell \gg H^{-1}$ (see fig. 8.1). Hence, we have for the range of validity of FNC $d^{\text{phys.}} \lesssim H^{-1} \ll a/k$, and FNC are therefore unable to cover the small-scale mode of interest with wavelength $\sim 1/k_s$.

We begin with laying out a simple procedure for how eq. (8.61) could in principle be measured. For this, we focus on the isotropic part of the long-short coupling, and assume that the long-wavelength perturbation ζ_ℓ considered is outside the sound horizon of all fluid components. Then, the locally observable effects of ζ_ℓ are exactly described by the separate-universe picture [201]. Suppose now that at some time during matter domination there is a collection of comoving observers distributed throughout the Universe (e. g., at $z \sim 10$). Each observer measures the amplitude of large-scale (linear) density perturbations on a fixed physical scale a_F/k_s in their local Universe, as well as their local cosmology: proper time since the Big Bang, Hubble rate, and spatial curvature $K = K_F$. Using this information and linear perturbation theory, they can immediately infer the amplitude $\mathcal{A}_s$ of the super-horizon curvature perturbations at the end of inflation at the same fixed physical scale. Specifically, choosing comoving gauge, they calculate the super-horizon amplitude of the perturbations ζ_s to their local CFC-frame metric, which, through eq. (8.63), precisely correspond to our ζ_s^F:

$$g_{ij}^F = \frac{a_F^2(1+2\zeta_s^F)}{\left(1+\frac{K_F}{4}|\mathbf{x}_F|^2\right)^2}\delta_{ij} \,. \tag{8.91}$$

They then communicate their local cosmology including $\mathcal{A}_s$ to a distant observer on their future light cone (e. g., at $z \sim 0$). This distant observer, now, has access to the locally measurable (in a spatial sense) amplitude of small-scale curvature perturbations $\mathcal{A}_s$ at the end of inflation, at a number of Lagrangian locations corresponding to Eulerian locations throughout his Hubble volume. He also knows what the local curvature is at each of these locations, and can use this to reconstruct the large-scale curvature perturbations ζ_ℓ. Correlating $\zeta_\ell(\mathbf{k}_\ell)$ with $\mathcal{A}_s(\mathbf{k}_\ell)$, he then obtains precisely eq. (8.61), if the initial conditions are set by single-field slow-roll inflation.

Let us now briefly discuss more realistic observables, such as the CMB temperature bispectrum [19], or the scale-dependent bias of

halos [221]. The contributions to any late-time observable can be split into three physically distinct contributions, as illustrated in fig. 8.1:

- **Primordial contribution:** this is defined as the contribution from eq. (8.61) in single-field slow-roll inflation, whose physical interpretation is given above. The leading contribution is $\propto k_\ell^2/k_s^2$, with a coefficient of order ε, η, and of order $1/c_s^2$ for $c_s \ll 1$. Using the rough matching made after eq. (8.61), we can approximate this as $f_{NL}^{equil.} \sim \varepsilon, \eta$, and $\sim 1/c_s^2$, respectively.

- **Gravitational evolution:** the gravitational dynamics that become active when the short modes re-enter the horizon contribute to the mode coupling at order $f_{NL}^{equil.} \sim 1$ (see also [222–225] for a discussion). Consider again an isotropic long mode for simplicity. Then, by way of the separate-universe picture, the leading long-short coupling can be calculated exactly by running a Boltzmann code with modified cosmological parameters [226]. This contribution to the mode coupling is enhanced with respect to the primordial contribution for sub-horizon modes $k_s \gg \mathcal{H}$, as [201] has shown. During matter domination, the equation for the second order (i. e. containing the long-short coupling) density contrast $\delta_{(2)}$ in CFC, for an isotropic long mode, reads (Eq. (5.28) of [201])

$$\delta''_{(2)} + \mathcal{H}\delta'_{(2)} - \frac{3}{2}\mathcal{H}^2\delta_{(2)} = \frac{26}{27}\frac{1}{\mathcal{H}^2}\partial^2\Phi\partial^2\phi \ , \tag{8.92}$$

where Φ and ϕ are, respectively, the long- and short-scale Newtonian potentials, and we have used the linear (sub-Hubble) solution for $\delta_{(1)}$, that is

$$\delta_{(1)} = \frac{2}{3\mathcal{H}^2}\partial^2\phi \ . \tag{8.93}$$

The initial condition from the primordial contribution, eq. (8.61), for $\delta^{(2)}$, defined when the short modes re-enter the horizon ($k_s \sim \mathcal{H}_{ini}$), scales as

$$\delta''_{(2),ini} \sim \mathcal{O}(\varepsilon, \eta) \times \partial^2\Phi_{ini}\frac{\partial^2\phi_{ini}}{\mathcal{H}_{ini}^2} \ . \tag{8.94}$$

The late-time evolution is hence enhanced by a factor of $k_s^2/\mathcal{H}^2$, which is much larger than 1 for sub-horizon small-scale modes. The sum of the two yields the late-time small-scale perturbations in the presence of the long mode in the local CFC frame.

- **Projection effects:** In order to connect to observations made on Earth, we have to map the CFC-frame quantities to the frame of a distant observer. These projection effects are calculated by following photon geodesics from the different CFC patches to

the distant observer. Importantly, the projection effects scale as $k_\ell^2/\mathcal{H}_0^2$, where $\mathcal{H}_0^{-1}$ is the observer's comoving horizon. If $\mathcal{H}_0^{-1} \gg \mathcal{H}^{-1}$ like in our thought experiment above, where $\mathcal{H}^{-1}$ is the comoving horizon at the time of light emission, then there is an interesting regime where $k_\ell \gtrsim \mathcal{H}_0$ but $k_\ell \ll \mathcal{H} \lesssim k_s$. Unlike the first two contributions above, which are suppressed by k_ℓ^2/k_s^2 and $k_\ell^2/\mathcal{H}^2$, respectively, the projection effects are not suppressed in this regime. They are thus the only contribution that can mimic non-Gaussianity of the local type. However, it is important to stress that these contributions are completely independent of the long-short coupling generated from inflation. They can be easily computed at linear order with the so-called ruler perturbations of [227–229] (see also [230–232] for similar approaches). An example is provided by the squeezed-limit CMB bispectrum [203, 204, 233–235]. If we restrict to multipoles $\ell_\ell \lesssim \mathcal{O}(100)$, the long-wavelength mode is outside the horizon at recombination, so that any effect that it can have on the dynamics of short modes during recombination is suppressed, and the largest contribution comes from projection effects [24, 203].

8.7 CONCLUSIONS

Our main result, eq. (8.61), is the three-point correlation between the large-scale curvature perturbation and the short-scale curvature power spectrum in Conformal Fermi Coordinates. This coordinate system allows us to follow the evolution of short modes in the background perturbed by the long-wavelength mode from the end of inflation until the long mode starts evolving again. eq. (8.61) encodes the primordial mode coupling that a local observer measures before it is reprocessed by the late-time non-linear gravitational evolution. We find that the magnitude of the physically relevant part of the curvature bispectrum in models of canonical single-field inflation is controlled by both ε and η so, barring cancellations, the minimal amount of primordial non-Gaussianity which arises from gravitational interactions during inflation is bounded from below by the measured tilt of the power spectrum $n_s - 1$.

As a byproduct of the calculation, we show explicitly that for $c_s < 1$ the size of non-Gaussianity is of order $(1 - c_s^2)/c_s^2$ [119, 208], as expected. The transformation to the conformal Fermi frame is proportional to ε, η, and $\dot{c}_s/Hc_s$, and can be neglected for a slowly varying c_s. For a very small speed of sound, in fact, we do not expect gravity to play a role: the equivalence principle still demands that the bispectrum starts $\propto (k_\ell^2/k_s^2) P_\zeta(k_s) P_\zeta(k_\ell)$ in the squeezed limit, but the overall amplitude is fixed by inflaton derivative self-interactions.

We trace the presence of η in our final result to the fact that it is also appearing in the cubic action $S_{(3)}$ of curvature perturbations [18], i. e. η is *also* a measure of the gravitational interactions of ζ during inflation. When $S_{(3)}$ is integrated by parts to show that it must have at least a factor of ε suppressing the interactions, a term $\propto \varepsilon\eta$ is also introduced.

Concerning the measurability of this effect, we see that single-field slow-roll inflation does not produce any f_{NL} of the local type, but is guaranteed to produce non-Gaussianity roughly corresponding to an equilateral amplitude of $f_{NL}^{equil.} \sim 0.1 \times (n_s - 1)$. Notice that, as discussed after eq. (8.61), our results strictly apply to the $\mathcal{O}(k_\ell^2/k_s^2)$ part of the locally observable mode coupling, and hence cannot be matched unambiguously to equilateral non-Gaussianity. As discussed in Section 8.6, this effect is swamped by late-time gravitational non-linearities, which give $f_{NL}^{equil.}$ of order 1. It would be interesting to study models that exhibit a peculiar behavior in the squeezed limit, such as resonant non-Gaussianity [41], to see if they predict signatures that can be distinguished more easily from the gravitational ones. We leave this, along with the details of the connection to observations, to a future work.

CONCLUSIONS

The goal of my Ph.D. thesis was to study how the temperature anisotropies of the Cosmic Microwave Background and the distortions of its frequency spectrum can constrain the physics of inflation.

μ-distortions of the CMB from Silk damping measure the primordial power spectrum on scales between $50\,\mathrm{Mpc}^{-1}$ and $10^4\,\mathrm{Mpc}^{-1}$: they are, then, an exceptional tool for constraining its scale scale dependence. In [49] I have considered the running of the spectral index $\alpha_s = \frac{dn_s}{d\log k}$, and I have shown that a PIXIE-like mission [22] that will measure the CMB frequency spectrum with sensitivity of ~ 3 times the original mission design [22] is guaranteed to make a discovery:

- if μ is detected, we can start constraining cosmology at $z > 10^4$;
- the absence of a detection, instead, means that the running α_s is too large and negative to be consistent with the predictions of single-field slow-roll inflation (i. e., $\alpha_s^{SR} \sim -(1-n_s)^2$). The slow-roll paradigm is then ruled out.

In [50], instead, I have included the running of the running $\beta_s = \frac{d\alpha_s}{d\log k}$ to the analysis. I have shown that, in this case, a $\sim 35\,\%$ improvement on the bounds from Planck can be achieved already with the FIRAS constraints on μ [11]. PIXIE, instead, can bring this improvement to $\sim 85\,\%$.

There can be other sources of energy injection in the plasma: e. g. DM annihilation and DM decay [12]. During the completion of these works, I developed a modified version of the `idistort` code [138], that allows to include bounds on these processes from measurements of the CMB spectrum: one of my goals is to continue its development, with the purpose of a joint analysis of the constraints on dark matter annihilation from Planck [6, 236–240] together with possible future constraints from PIXIE.

While this work was being completed, [42] has shown that including the uncertainties in the frequency dependence of foregrounds (like thermal and spinning dust, synchrotron emission, etc.) will worsen the constraints that PIXIE can provide on μ by $\sim 5\times$ with respect to the forecasts of [22]. As a consequence, a $\sim 3\times$ only improvement over the design of [22] will not be enough to exclude slow-roll inflation (even if it is important to stress that this is just a limitation due to the sensitivity of the experiment, not a conceptual one). Regarding the running of the running β_s, instead, we have seen that the large uncertainties on this parameter coming from current data mean that, even when the foregrounds are correctly accounted for, PIXIE would still provide a $\sim 80\,\%$ improvement over Planck.

The second part of the thesis deals with primordial non-Gaussianity. From the point of view of inflationary physics, deviations from Gaussian statistics in observed correlation functions contain information about the whole spectrum of the theory (inflaton self-interactions, presence of other particles, etc.). The simplest observable that one can consider when investigating non-Gaussianity is the three-point function (bispectrum). Translational and rotational invariance imply that in Fourier space it will depend on the amplitude of three momenta. When comparing theoretical predictions to observations, the focus is mainly on two momentum configurations:

- "equilateral", which looks at the coupling between three modes of comparable size;
- "squeezed", which instead considers a long (k_ℓ) and two short (k_s) modes.

Since improving the constraints on equilateral non-Gaussianity beyond those coming from the CMB will be challenging [241], I decided to focus on the squeezed limit $k_\ell \ll k_s$.

The strength of the mode coupling is measured by the f_{NL} parameter. In [51] I studied what is the physical f_{NL} in single-field inflation. "Physical" because of the following fact: a local observer who has access only to short comoving distances $\sim 1/k_s$ would interpret local physics as taking place in a "separate universe" of size k_ℓ^{-1} and the non-Gaussianity she would measure would be suppressed by $(k_\ell/k_s)^2$ (because of the equivalence principle). The goal of [51] was to see if, in single-field inflation (where any coupling between long and short modes is dominated by gravitational interactions, and so it is slow-roll suppressed), the physical f_{NL} is proportional to $(1-n_s)\times(k_\ell/k_s)^2$, or if it vanishes. The final result is that $(1-n_s)$ survives: in single-field inflation, a local observer on scales $\sim k_s^{-1}$ *is guaranteed* to see a coupling with the long modes.

While it is important to show that there is this definite target, it would be interesting to study cases where the behavior in the squeezed limit is different from the single-field consistency relation: this happens in models that predict a fractional scaling in the squeezed limit $(k_\ell/k_s)^\nu$ (ν being related to the mass of heavy particles present during inflation) [242], or models like resonant non-Gaussianity [41].

It is important to stress, however, that interactions during inflation are not the only (and not even the most important) source of non-Gaussianity. Indeed, there are contributions to cosmological three-point functions from late-time evolution that will add to the primordial ones. These are both gravitational non-linearities that are generated once perturbations re-enter the horizon, and projection effects due to photon propagation in a perturbed background [227–232]. A systematic treatment is needed to disentangle them from the primordial bispectrum. This can be done using "Conformal Fermi Coordinates"

[201], which are the coordinates that the local observer uses to describe her separate universe. In [31] we plan to do this for the correlation of temperature anisotropies and spectral distortions: Silk damping of acoustic waves heats the photons in the photon-electron-baryon fluid, so that distortions in the CMB spectrum are generated. In presence of non-Gaussianity, and then of long-short mode coupling, the heating rate acquires a spatial dependence on large scales, and becomes correlated with large-scale temperature anisotropies. This effect can be used to constrain primordial non-Gaussianity [20]: however, as in the case of the CMB temperature bispectrum [203, 204, 234, 243, 244], we expect that the above mentioned projection effects will again add up to the primordial contribution.

Another related question that I intend to investigate is whether it is possible to extend the separate universe picture to theories of gravity different from General Relativity. This would prove invaluable in light of the planned large-scale structure surveys, since it would allow to study in an analytical way how the growth of structure in the late-time universe is affected by modifications of gravity. Besides, it would be possible to extend this approach to N-body simulations: currently, simulations are already implementing the separate universe picture with standard General Relativity [207, 226, 245], but are not considering the possibility of doing the same with another theory of gravity.

Part IV

APPENDIX

A

CMB LIKELIHOODS

In this short Appendix we describe how the likelihood for the Cosmic Microwave Background angular power spectra is constructed, referring to [96, §11] for a more detailed discussion. For simplicity, we focus on a single anisotropy spectrum of the CMB: the generalization to the full T, E, B spectra is straightforward [246]. We start from the expression for the likelihood of a full-sky experiment, i. e. (disregarding factors of 2π)

$$\mathcal{L} = \frac{1}{\sqrt{\det(C_S + C_N)}} e^{-\frac{1}{2}\Delta^T \cdot (C_S + C_N)^{-1} \cdot \Delta} , \tag{A.1}$$

with data points $\Delta^i_{\ell m} = s^i_{\ell m} + n^i_{\ell m}$ at each pixel (labelled by ℓm since we work in harmonic space) and each frequency channel i. The signal $s^i_{\ell m}$ is given by $\hat{W}^i_c \hat{a}^c_{\ell m}$, where the $\hat{a}_{\ell m}$ are the harmonic coefficients of the (beam-smoothed) temperature anisotropy for each component c (i. e. CMB + foregrounds such as dust, synchrotron, etc.), and the shape vector $\hat{W}^i_c$ provides the frequency dependence of each component.[1] These are constructed from the frequency spectra of fig. 2.3, so that besides a standard temperature shift Θ (corresponding to the CMB anisotropies studied in Section 3.3), we can allow for distortions from a black-body spectrum. The spectral shape of the foregrounds must be provided, as well. In these formulas we have used a "hat" symbol to denote that the W_c and $a^c_{\ell m}$ are those of the specific realization we observe, following [247].

We will assume isotropic white noise in each channel, i. e.

$$\langle n^i_{\ell m} (n^j_{\ell' m'})^* \rangle = w^{-1}_{(i)} \delta^{ij} \delta_{\ell\ell'} \delta_{mm'} . \tag{A.2}$$

Assuming statistical isotropy, the signal covariance matrix will be block diagonal in harmonic space: therefore the expression for the log-likelihood $L \equiv -2 \log \mathcal{L}$ becomes

$$\begin{aligned} L = \sum_\ell (2\ell+1) \Bigg\{ \mathrm{Tr} \left[\frac{\sum_{m=-\ell}^{\ell} \Delta^i_{\ell m} (\Delta^j_{\ell m})^*}{W^i_c C^{cc'}_\ell W^j_{c'} + N^{ij}_\ell} \right] \\ + \log\det \left[W^i_c C^{cc'}_\ell W^j_{c'} + N^{ij}_\ell \right] \Bigg\} . \end{aligned} \tag{A.3}$$

In this equation we denote by Tr the trace over the frequency channels, and all terms with i, j indices are understood as matrices. Besides we have defined the noise bias as

$$N^{ij}_\ell \equiv N^{(i)}_\ell \delta^{ij} = w^{-1}_{(i)} e^{\sigma^2_{(i)} \ell(\ell+1)} \delta^{ij} , \tag{A.4}$$

1 Note that in writing eq. (A.1) we assume that each component is Gaussian.

for a gaussian beam of beam-size variance $\sigma_{(i)}$. Eq. (A.3) is the expression of the CMB likelihood, once we are given a map $\Delta^i_{\ell m}$ from an experiment. Let us see, instead, what is the procedure to follow if one wants to carry out forecasts for a CMB mission. In this case, we do not have the map $\Delta^i_{\ell m}$ itself, but we can use the estimator that would be made from such a map, i. e. (see also the caption of fig. 3.3)

$$\hat{D}^{ij}_\ell = \sum_{m=-\ell}^{\ell} \Delta^i_{\ell m}(\Delta^j_{\ell m})^* \equiv \hat{W}^i_c \hat{C}^{cc'}_\ell \hat{W}^j_{c'} + N^{ij}_\ell \ , \tag{A.5}$$

where the hats denote the fact that the cosmological parameters are fixed to their "true" values. Therefore our expression for L becomes

$$L = \sum_\ell (2\ell+1)\left\{ \mathrm{Tr}\left[\frac{\hat{W}^i_c \hat{C}^{cc'}_\ell \hat{W}^j_{c'} + N^{ij}_\ell}{W^i_c C^{cc'}_\ell W^j_{c'} + N^{ij}_\ell}\right] + \log\det\left[W^i_c C^{cc'}_\ell W^j_{c'} + N^{ij}_\ell\right]\right\} . \tag{A.6}$$

Given fiducial cosmological parameters (which we assume are the ones describing our Universe) and the beam and noise specifications of the experiment, one can construct the likelihood for CMB anisotropies, and then use it in a Monte Carlo Markov Chain exploration of parameter space.

Eq. (A.6) simplifies a little if we can consider the case of only one component (the CMB) and forget about foregrounds: however, one has still to take into account both auto- and cross-channel power spectra. For N_c channels with the same noise level, considering both auto and cross power spectra is equivalent to have one frequency channel with an effective noise power spectrum lower by a factor N_c. One can generalize these considerations to the case of channels with different noise levels. The optimal channel combination results in having an effective noise bias N_ℓ given by [248–250]

$$N_\ell = \left(\sum_i \frac{1}{N^{(i)}_\ell}\right)^{-1} = \left(\sum_i w_{(i)} e^{-\sigma^2_{(i)}\ell(\ell+1)}\right)^{-1} . \tag{A.7}$$

In reality the presence of foregrounds limits our ability of extracting the CMB signal from the data, and a full likelihood analysis should take them into account. Fortunately, each component scales differently in frequency (i. e., every foreground has a different shape W_c): therefore it is possible to separate them using maps at different frequencies [251, 252]. This foreground subtraction will be the source of additional noise, depending on the level of foreground removal, which will contribute to the noise bias N_ℓ (we refer to [250] for a more detailed analysis). In the case where this additional noise is much smaller than the instrumental noise of eq. (A.4), eq. (A.7) is recovered.

Therefore, normalizing the likelihood such that $L = 0$ at the fiducial values of the cosmological parameters, we have that (for TT spectra only)

$$L = \sum_{\ell} (2\ell + 1) \left[-1 + \frac{\hat{C}_\ell^{TT} + N_\ell}{C_\ell^{TT} + N_\ell} + \log \left(\frac{C_\ell^{TT} + N_\ell}{\hat{C}_\ell^{TT} + N_\ell} \right) \right] . \tag{A.8}$$

Finally, there is one additional caveat: in the case of a non full-sky experiment (where only part of the sky is observed or can be used for cosmology) not all modes are available for the analysis, and eq. (A.6) does not hold. One can capture this effect by introducing the f_{sky} parameter, which reduces the available modes by (we refer the reader to [253] for better approximations)

$$\sum_{\ell} (2\ell + 1) \to \sum_{\ell} (2\ell + 1) \times f_{sky} . \tag{A.9}$$

B

ADM FORMALISM

CONTENTS

In this Appendix we collect some results regarding the $3+1$ decomposition of the Einstein, fluid and (collision-less) Boltzmann equations. Section B.1 will deal with the first two, while Section B.2 will focus on the latter.

B.1 EINSTEIN AND FLUID EQUATIONS

As explained in the main text, given an observer n^μ we can decompose tensorial quantities along the wordline of n^μ or on the local subspace orthogonal to it by using the projector $h^\mu{}_\nu$. If, furthermore, the observer is hypersurface-orthogonal we can define a time coordinate t such that $n_\mu \propto \partial_\mu t$ (the proportionality factor being defined by $n^\mu \partial_\mu t = n^0 = N^{-1}$, where N is the lapse function). This, in turn, implies that the three-tensor $K_{\mu\nu}$, defined by

$$K_{\mu\nu} \equiv h_\mu{}^\rho \nabla_\rho n_\nu \ , \tag{B.1}$$

is symmetric. $K_{\mu\nu}$, then, is the extrinsic curvature of the constant-t hypersurfaces.

B.1.1 *Einstein tensor decomposition*

Assuming the observer n^μ to be hypersurface-orthogonal, we can proceed to a decomposition of the Einstein tensor $G_{\mu\nu} = R_{\mu\nu} - \frac{R}{2} g_{\mu\nu}$:

- the $\|\|$ contraction gives

$$G_{\mu\nu} n^\mu n^\nu = \frac{1}{2}({}^{(3)}R + K^2 - K_{\mu\nu}K^{\mu\nu}) \ ; \tag{B.2}$$

- the $\|\perp$ contraction, instead, gives

$$h^{\mu\rho} n^\sigma G_{\rho\sigma} = {}^{(3)}\nabla_\nu K^{\mu\nu} - {}^{(3)}\nabla^\mu K \ ; \tag{B.3}$$

- finally, the $\perp\perp$ contraction gives

$$\begin{aligned} h_\mu{}^\rho h_\nu{}^\sigma G_{\rho\sigma} = {}^{(3)}R_{\mu\nu} + KK_{\mu\nu} - {}^{(3)}\nabla_\mu A_\nu + n^\rho \nabla_\rho K_{\mu\nu} \\ - 2n_{(\mu}A_{|\rho|}K_{\nu)}{}^\rho - A_\mu A_\nu - \frac{{}^{(3)}R}{2} h_{\mu\nu} \\ + \frac{K^2}{2} h_{\mu\nu} - \frac{K_{\rho\sigma}K^{\rho\sigma}}{2} h_{\mu\nu} \\ - \{\nabla_\rho (Kn^\rho - A^\rho)\} h_{\mu\nu} \ , \end{aligned} \tag{B.4}$$

  where $A_\mu = n^\nu \nabla_\nu n_\mu = {}^{(3)}\nabla_\mu \log N$, and an useful relation to keep in mind when dealing with derivatives of three-tensors like $K_{\mu\nu}$ is

$$n^\rho \nabla_\rho T_{\mu\nu} = \frac{1}{N}(\mathcal{L}_t T_{\mu\nu} - \mathcal{L}_{\mathbf{N}} T_{\mu\nu}) \ , \tag{B.5}$$

  where $h_\mu{}^\rho h_\nu{}^\sigma T_{\rho\sigma} = T_{\mu\nu}$, and $\mathcal{L}_t$, $\mathcal{L}_{\mathbf{N}}$ denote a Lie derivative along the time direction and the shift vector, respectively. By tracing eq. (B.4) with $h^{\mu\nu}$, or by considering its trace-free part, one can obtain the results of Section 3.2.3.

B.1.2 *Fluid equations*

As discussed in the main text, given a perfect fluid with four-velocity U^μ, we can decompose U^μ in a part parallel and one orthogonal to n^μ, i. e.

$$U^\mu = \gamma(n^\mu + v^\mu) = \frac{n^\mu + v^\mu}{\sqrt{1 - h_{\rho\sigma} v^\rho v^\sigma}} \ , \tag{B.6}$$

with $n_\mu v^\mu = 0$. Then, it is possible to project the conservation equations of $T_{\mu\nu} = (\rho + p)U_\mu U_\nu + p g_{\mu\nu}$ and $N_\mu = n U_\mu$ along n^μ or orthogonal to it:

- the number current conservation equation becomes

$$0 = n^\mu \nabla_\mu(\gamma n) + v^\mu {}^{(3)}\nabla_\mu(\gamma n) + \gamma n K + \gamma n {}^{(3)}\nabla_\mu v^\mu + \gamma n A_\mu v^\mu \ ; \tag{B.7}$$

- the projection of $\nabla_\nu T^{\nu\mu} = 0$ parallel to n^μ is equal to

$$\begin{aligned} 0 = n^\mu \nabla_\mu(\gamma^2 M) + v^\mu {}^{(3)}\nabla_\mu(\gamma^2 M) + \gamma^2 M K \\ + \gamma^2 M {}^{(3)}\nabla_\mu v^\mu + 2\gamma^2 M A_\mu v^\mu + \gamma^2 M K_{\mu\nu} v^\mu v^\nu - n^\mu \nabla_\mu p \ , \end{aligned} \tag{B.8}$$

  where $M \equiv \rho + p$;

- the projection of $\nabla_\nu T^{\nu\mu} = 0$ orthogonal to n^μ, instead, is

$$0 = \gamma^2 v^\mu n^\nu \nabla_\nu M + \gamma^2 v^\mu v^{\nu\,(3)}\nabla_\nu M + \gamma M \theta v^\mu + M\theta^\mu_\perp + {}^{(3)}\nabla^\mu p \,, \tag{B.9}$$

  where we defined θ (not to be confused with the variable appearing in eqs. (3.28), (3.29) and similar), $\theta^\mu_\perp$ as

$$\theta = \nabla_\mu U^\mu = \gamma K + \gamma^{(3)}\nabla_\mu v^\mu + \gamma A_\mu v^\mu + n^\mu \nabla_\mu \gamma + v^{\mu\,(3)}\nabla_\mu \gamma \,, \tag{B.10a}$$

$$\theta^\mu_\perp = h^\mu{}_\rho \underbrace{U^\nu \nabla_\nu U^\rho}_{\equiv \theta^\rho} = \frac{v^\mu}{2}(n^\nu \nabla_\nu \gamma^2 + v^{\nu\,(3)}\nabla_\nu \gamma^2) + \gamma^2 A^\mu + \gamma^2 h^\mu{}_\rho n^\nu \nabla_\nu v^\rho \tag{B.10b}$$

$$+ \gamma^2 v^\nu K_\nu{}^\mu + \gamma^2 h^\mu{}_\rho v^\nu \nabla_\nu v^\rho \,. \tag{B.10c}$$

  It is possible, then, to take the three-divergence of eq. (B.9): this results in eq. (3.29) that, as discussed in the main text, assumes t to be the time coordinate in Newtonian gauge, considers only scalar modes, and stops at leading order in perturbations.

We conclude this Section by listing the relevant projections of the stress-energy tensor, that would go together with eqs. (B.2), (B.3), (B.4):

- the $\|\|$ projection is

$$T_{\mu\nu} n^\mu n^\nu = \gamma^2 M - p \,; \tag{B.11}$$

- the $\|\perp$ one, instead, is

$$h^{\mu\rho} n^\sigma T_{\rho\sigma} = -\gamma^2 M v^\mu \,; \tag{B.12}$$

- finally, since we have zero anisotropic stress, the only remaining relevant contraction is the trace of $T^{\perp\perp}_{\mu\nu}$, i. e.

$$T_{\mu\nu} h^{\mu\nu} = 3p + M(\gamma^2 - 1) \,. \tag{B.13}$$

B.2 BOLTZMANN EQUATION

The same machinery can be used to do a $3+1$ decomposition of the Boltzmann equation for photons. In this Section we are going to consider the collision-less Boltzmann equation, i. e.

$$0 = \frac{Df}{d\lambda} = P^\mu \frac{\partial f}{\partial x^\mu} + \frac{DE}{d\lambda}\frac{\partial f}{\partial E} + \frac{Dl^\mu}{d\lambda}\frac{\partial f}{\partial l^\mu} \,, \tag{B.14}$$

where λ is an affine parameter along the photon worldline. The photon four-momentum is decomposed as

$$P^\mu = E(n^\mu + l^\mu) \,, \tag{B.15}$$

where the three-vector l^μ has unit norm, since $P^\mu P_\mu = 0$ for photons. In the following, we will drop the assumption of an hypersurface-orthogonal n^μ, but we still denote the three-tensor $h_\mu{}^\rho \nabla_\rho n_\nu$ as $K_{\mu\nu}$. Since $K_{\mu\nu}$ can possibly be non-vanishing, we decompose it as

$$K_{\mu\nu} = \frac{K}{3} h_{\mu\nu} + \sigma_{\mu\nu} + \omega_{\mu\nu} \,, \tag{B.16}$$

where

$$K = h^{\mu\nu} K_{\mu\nu} = \nabla_\mu n^\mu \,, \tag{B.17a}$$

$$\sigma_{\mu\nu} = h_\mu{}^\rho h_\nu{}^\sigma K_{\rho\sigma} - \frac{K}{3} h_{\mu\nu} = K_{(\mu\nu)} - \frac{K}{3} h_{\mu\nu} \,, \tag{B.17b}$$

$$\omega_{\mu\nu} = K_{[\mu\nu]} \,. \tag{B.17c}$$

Now, if $C[f] = 0$ the photons follow geodesics, i. e.

$$P^\nu \nabla_\nu P^\mu = 0 \,. \tag{B.18}$$

Projecting this equation along the worldline of the observer n^μ and in the hyperplane orthogonal to it allows to derive the evolution equations for E (redshift) and l^μ (lensing), that can be plugged in eq. (B.14). More precisely, one has that

$$\frac{DE}{d\lambda} = -E^2 \left(A_\mu l^\mu + l^\mu l^\nu \sigma_{\mu\nu} + \frac{K}{3} \right) \,, \tag{B.19a}$$

$$\frac{Dl^\mu}{d\lambda} = h^\mu{}_\rho \frac{Dl^\rho}{d\lambda} + E n^\mu l^\nu A_\nu + E n^\mu l^\rho l^\sigma K_{\rho\sigma} \,, \tag{B.19b}$$

where

$$h^\mu{}_\rho \frac{Dl^\rho}{d\lambda} = E(A_\nu l^\nu + l^\rho l^\sigma K_{\rho\sigma}) l^\mu - E A^\mu - E l^\rho K_\rho{}^\mu \,. \tag{B.20}$$

It is important to stress that only the projection of eq. (B.20) can enter in the contraction with $\frac{\partial f}{\partial l^\mu}$, since the latter cannot have a non-zero projection along n^μ. Therefore, we can just focus on $h^\mu{}_\rho \frac{Dl^\rho}{d\lambda}$, that can be rewritten as

$$h^\mu{}_\rho \frac{Dl^\rho}{d\lambda} = -E s^\mu{}_\nu A^\nu - E \omega^\mu{}_\nu l^\nu - E s^{\mu\nu} \sigma_{\nu\rho} l^\rho \,, \tag{B.21}$$

where the screen projector $s_{\mu\nu} \equiv h_{\mu\nu} - l_\mu l_\nu$ projects a three-tensor in the plane orthogonal to l^μ, i. e. orthogonal to the line of sight. Finally, we notice that eq. (B.21) implies that the normalization $l_\mu l^\mu = 1$ is conserved along the photon path, since

$$P^\nu \nabla_\nu (l_\mu l^\mu) = 2 l_\mu h^\mu{}_\nu \frac{Dl^\nu}{d\lambda} = 0 \,. \tag{B.22}$$

C

TWO-FLUID APPROXIMATION – NUMERICS

In this Appendix we review the two-fluid approximation and how fig. 3.2 was obtained. As discussed in Section 3.3.1, the system of equations that we need to solve is

$$\delta'_{cdm} = -k u_{cdm} + 3\Phi' \,, \tag{C.1a}$$
$$u'_{cdm} = -\mathcal{H} u_{cdm} + k\Phi \,, \tag{C.1b}$$
$$\delta'_{\gamma} = -\frac{4}{3} k u_{\gamma} + 4\Phi' \,, \tag{C.1c}$$
$$(1+R) u'_{\gamma} = -R\mathcal{H} u_{\gamma} + \frac{1}{4} k \delta_{\gamma} + (1+R) k\Phi \,, \tag{C.1d}$$
$$-\frac{k^2}{\mathcal{H}^2}\Phi - \frac{3\Phi'}{\mathcal{H}} - 3\Phi = \frac{a^2}{\mathcal{H}^2} \sum_{\substack{i = \\ \{cdm, b\gamma\}}} \frac{\bar{\rho}_i \delta_i}{2M_P^2} \,, \tag{C.1e}$$

where the baryon loading is defined as $R \equiv \frac{3\bar{\rho}_b}{4\bar{\rho}_\gamma}$, and we used the lapse constraint eq. (3.25) to close the system, instead of the shift constraint eq. (3.36e). The initial conditions for the equations are set for $\eta \to 0$, and are equal to

$$\delta_{\gamma} = -2\Phi \,, \tag{C.2a}$$
$$\delta_{cdm} = \frac{3}{4}\delta_{\gamma} \,, \tag{C.2b}$$
$$u_{\gamma} = -\frac{1}{4}\frac{k}{\mathcal{H}}\delta_{\gamma} \,. \tag{C.2c}$$
$$u_{cdm} = u_{\gamma} \,, \tag{C.2d}$$

where the initial value of Φ will be set to 1 (as discussed in the main text, its expression in terms of ζ can be reinserted easily at the end of the calculation). The last ingredient is the Friedmann equation for the background, i. e.

$$\mathcal{H}^2 = \left(\frac{a'}{a}\right)^2 = \frac{a^2}{3M_P^2} \sum_{\substack{i = \\ \{cdm, b\gamma\}}} \bar{\rho}_i \,. \tag{C.3}$$

It is straightforward to see that if we define $y \equiv \frac{a}{a_{m\text{-}r}}$, where the matter-radiation equality redshift is given by

$$1 + z_{m\text{-}r} = \frac{a_0}{a_{m\text{-}r}} = \frac{\Omega_m}{\Omega_r} \approx 3500 \,, \tag{C.4}$$

we can rewrite eq. (C.3) as

$$\mathcal{H}^2 = \mathcal{H}_0^2 \frac{\Omega_m^2}{\Omega_r}\left(\frac{1}{y} + \frac{1}{y^2}\right) \,. \tag{C.5}$$

The above equation is solved by

$$y = 2\alpha x + \alpha^2 x^2 \,, \tag{C.6}$$

where we defined (taking $a_0 = 1$)

$$x \equiv \frac{\eta}{\eta_r} \,, \tag{C.7a}$$

$$\eta_r \equiv 2\sqrt{\frac{a_{rec}}{\Omega_m H_0^2}} \,, \tag{C.7b}$$

$$\alpha^2 \equiv \frac{a_{rec}}{a_{m\text{-}r}} \,. \tag{C.7c}$$

If further define $\kappa \equiv k\eta_r$ and the reduced Hubble parameter

$$\mathcal{H}_r \equiv \eta_r \mathcal{H} = \frac{2\alpha(1+\alpha x)}{2\alpha x + \alpha^2 x^2} \,, \tag{C.8}$$

eqs. (C.1) take the form

$$\frac{d\delta_{cdm}}{dx} = -\kappa u_{cdm} + 3\frac{d\Phi}{dx} \,, \tag{C.9a}$$

$$\frac{du_{cdm}}{dx} = -\mathcal{H}_r u_{cdm} + \kappa\Phi \,, \tag{C.9b}$$

$$\frac{d\delta_\gamma}{dx} = -\frac{4}{3}\kappa u_\gamma + 4\frac{d\Phi}{dx} \,, \tag{C.9c}$$

$$\frac{du_\gamma}{dx} = \left(1 + \frac{3R_b y}{4}\right)^{-1}\left(-\frac{3R_b y}{4}\mathcal{H}_r u_\gamma + \frac{\kappa}{4}\delta_\gamma\right) + \kappa\Phi \,, \tag{C.9d}$$

$$-\frac{\kappa^2}{\mathcal{H}_r^2}\Phi - \frac{3}{\mathcal{H}_r}\frac{d\Phi}{dx} - 3\Phi = \frac{3}{2}\frac{\delta_\gamma + y R_{cdm}\delta_{cdm}}{1+y} \,, \tag{C.9e}$$

where $R_{cdm} \equiv \frac{\Omega_{cdm}}{\Omega_m}$, $R_b \equiv \frac{\Omega_b}{\Omega_m} = 1 - R_{cdm}$.

To obtain fig. 3.2, we have solved eqs. (C.9) in x^{-1} from $x_i = 10^{-3}$ to x_{rec}, which is equal to

$$x_{rec} = \frac{\sqrt{\alpha^2+1} - 1}{\alpha} \,, \tag{C.10}$$

sampling κ from 10^{-2} to 300 (logarithmically from 10^{-2} to 1, linearly from 1 to 300), and choosing $\Omega_m h^2 = 0.13$, $\Omega_b h^2 = 0.02$. Finally, following [92], we have multiplied $\Phi + \frac{\delta_\gamma}{4}$ and u_γ at x_{rec} with a factor $D(\kappa)$, to account for Silk damping and the finite thickness of the last-scattering surface. $D(\kappa)$ is given by [92]

$$D(\kappa) = e^{-\frac{\kappa^2}{2\kappa_D^2}} \,, \tag{C.11}$$

where

$$\kappa_D^{-2} = 2x_S^2 + \sigma^2 x_{rec}^2 \,, \tag{C.12a}$$

$$x_S = 0.6(\Omega_m h^2)^{\frac{1}{4}}(\Omega_b h^2)^{-\frac{1}{2}} a_{rec}^{\frac{3}{4}} \,, \tag{C.12b}$$

$$\sigma = 0.03 \,. \tag{C.12c}$$

D

SPECTRAL SHAPES AND S/N FOR PIXIE

In this short Appendix we are going to show how one can obtain the $1\,\sigma$ error on the μ-distortion amplitude for PIXIE, that we used in Chapters 5 and 6. This Appendix follows the notation of Chapter 5.

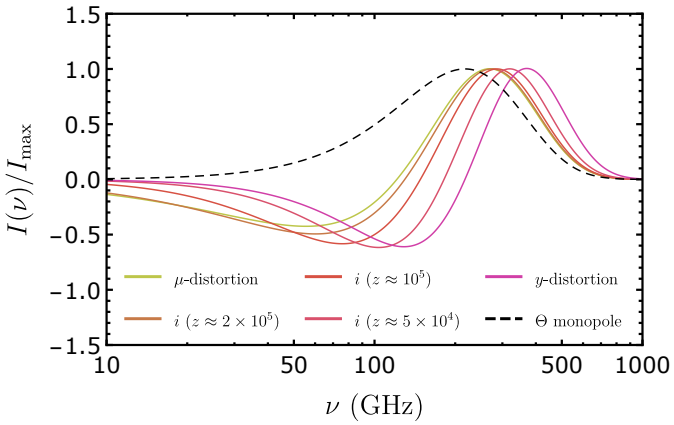

FIGURE D.1: This plot shows the spectral shapes (normalized at the maximum) for μ- and y-distortions, together with the spectra for i-type distortions at redshifts $z = \mathcal{O}(2\times10^5)$, $z = \mathcal{O}(1\times10^5)$ and $z = \mathcal{O}(5\times10^4)$ and the spectral shape of the monopole of temperature anisotropies Θ. We see that for increasing redshift, the maximum, minimum and zero of the occupation numbers are moved towards lower frequencies.

If we consider eq. (5.2) and the results of Section 2.3, we see that we can write down the observed photon spectrum in terms of shapes $\mathcal{I}_a$ and corresponding amplitudes μ_a where, for example [7, 80]:

- $a = 1$ corresponds to μ-type occupation number, i. e. (recalling that $x \equiv h\nu/k_B T$)

$$\mathcal{I}_1 = \frac{2h\nu^3}{c^2}\frac{e^x}{(e^x-1)^2}\left(\frac{x}{2.19}-1\right) \equiv \frac{2h\nu^3}{c^2}\times n^{(\mu)}(\nu)\;; \quad \text{(D.1)}$$

- $a = 2$ corresponds to y-type occupation number, i. e.

$$\mathcal{I}_2 = \frac{2h\nu^3}{c^2}\frac{xe^x}{(e^x-1)^2}\left[x\left(\frac{e^x+1}{e^x-1}\right)-4\right] \equiv \frac{2h\nu^3}{c^2}\times n^{(y)}(\nu)\;; \quad \text{(D.2)}$$

and so on. Besides μ-, i- and y-type distortions, that we have discussed in Section 5.2, one must also consider the fact that the uniform part of temperature perturbations Θ is not known a priori and must be fit

simultaneously with the spectral distortions: for this reason we also consider the t-type occupation number, i. e. [138]

$$\mathcal{I}_t = \frac{2h\nu^3}{c^2}\frac{xe^x}{(e^x-1)^2} \equiv \frac{2h\nu^3}{c^2} \times n^{(t)}(\nu) \ . \tag{D.3}$$

We do not include foregrounds in our analysis since, for PIXIE, the noise penalty for rejecting foregrounds is only 2 %, and this noise penalty has been included in all the estimates of CMB sensitivity by the PIXIE collaboration [22].

We can then write down the signal-to-noise, in terms of amplitudes μ_a and spectra $\mathcal{I}_a$ as (dropping factors of 2 for simplicity)

$$\left(\frac{S}{N}\right)^2 = \sum_c \frac{\left[\sum_a \mathcal{I}_a(\nu_c) \times (\mu_a - \bar{\mu}_a)\right]^2}{\delta I^2(\nu_c)} \ , \tag{D.4}$$

where $\bar{\mu}_a$ are the fiducial values of the amplitudes, and $\delta I(\nu_c)$ is the noise at each frequency channel c:

- PIXIE will have 400 channels (15 GHz-wide) from 30 GHz to 6 THz: however, we see from fig. D.1 that the signals that we consider go quickly to zero beyond $\nu \approx 1000$ GHz (see fig. D.1), so the sum over channels in eq. (D.4) will stop there;
- δI for PIXIE, as from Fig. 12 of [22], is expected to be

$$\delta I^{\text{PIXIE}} = 5 \times 10^{-26}\,\text{W}\,\text{m}^{-2}\,\text{Hz}^{-1}\,\text{sr}^{-1} \ . \tag{D.5}$$

If we want to marginalize over some of the amplitudes μ_a (see [254], for example), we can use the fact that for a Gaussian with inverse covariance matrix (Fisher matrix) F given by

$$F = \begin{pmatrix} \tilde{F} & S \\ S^T & M \end{pmatrix} \ , \tag{D.6}$$

where $\tilde{F}$ is the sub-matrix that spans the parameters that we are interested in, the marginalized Fisher matrix will be equal to

$$F_{\text{marg}} = \tilde{F} - SM^{-1}S^T \ . \tag{D.7}$$

For eq. (D.4), we will want to marginalize over t and y, so M will be the 2×2 matrix

$$M_{ab} = \sum_c \frac{\mathcal{I}_a(\nu_c)}{\delta I(\nu_c)}\frac{\mathcal{I}_b(\nu_c)}{\delta I(\nu_c)} \ , \tag{D.8}$$

with $a, b = y, t$. Similar expressions can be derived for S and its transpose, while $\tilde{F}$ is simply given by eq. (D.4) with a running on all components except y and t. If we had instead supposed that the two

y and t amplitudes were known, we could just have taken $\tilde{F}$ as Fisher matrix for eq. (D.4).

In this work we have not considered i-distortions, so F will be a 3×3 matrix with $a, b, c = \mu, y, t$: marginalizing over y and t amplitudes, as described in Eqs. (D.7) and (D.8), we obtain $\sigma_{\mu_8} = 1$ for the standard PIXIE configuration. The increments in PIXIE sensitivity that we considered in Chapters 5 and 6, then, can be interpreted as either an increase in the number N of frequency channels (that would decrease σ_{μ_8} by a factor $\sqrt{N^{\rm PIXIE}/N^{\rm new}}$), or a decrease in the instrumental noise δI (which instead gives a linear improvement $\delta I^{\rm new}/\delta I^{\rm PIXIE}$).

E

DETAILS OF THE TRANSFORMATION TO CFC

CONTENTS

In this Appendix we review in more detail the transformation from global coordinates to CFC, following closely the results of [200, 201] but focusing on the comoving gauge for single-field slow-roll inflation:

- we explicitly compute the coefficients $c_n^\mu(P)$ of eq. (8.5), highlighting the simplifications that occur when working at linear order in perturbations. We focus particularly on $c_0^\mu(P) = x^\mu(P)$, i. e. the CFC coordinates of the central observer's worldline;
- we use the results of the previous point to compute the Riemann tensor of the conformal metric on the central geodesic, and then arrive at the expression for the long-wavelength CFC metric. We also list the various residual gauge freedoms that are present after this step of the CFC construction;
- we fix the freedom in the initial time used to define the CFC and the arbitrary constant that comes from the integration of the local Hubble rate;
- finally, we discuss the possibility of changing spatial coordinates without changing the time-time and time-space components of $g^F_{\mu\nu}(x_F)$: following [201], we fix this ambiguity by choosing a frame where the effect of a long-wavelength ζ on the curvature of spatial slices is explicit (we basically use the stereographic parameterization of a curved, homogeneous space). The freedom in the definition of the space-like vectors of the tetrad, $(e_i)^\mu$, i. e. the choice of the integration constant in eq. (8.19), is discussed in detail in Section 8.2.3.

Before proceeding, notice that in this Appendix we will use $\bar{x}$ and not x_F to define the CFC coordinates: this is done to simplify the notation (apart from this change, the notation follows the one of Chapter 8). We will also take the CFC spatial coordinates of the central geodesic to be, generically, $\bar{\mathbf{x}}_c$ (instead of $\mathbf{0}$).

E.1 CFC EXPONENTIAL MAP AT LINEAR ORDER

Dai, Pajer and Schmidt derived the general expression for the coefficients $c^{\mu}_{n}(P)$ of eq. (8.5) in terms of the Christoffel symbols $\tilde{\Gamma}^{\rho}_{\mu\nu}$ of the conformal metric $\tilde{g}_{\mu\nu}(x) = a_F^{-2}(x) g_{\mu\nu}(x)$ evaluated on the central geodesic [200]. Up to third order in powers of $\bar{\mathbf{x}}$, the transformation is

$$\begin{aligned} x^{\mu}(\bar{\tau}, \bar{\mathbf{x}}) = x^{\mu}(P) &+ a_F(P)(e_i)^{\mu}_{P} \Delta\bar{x}^i \\ &- \frac{a_F^2(P)}{2} \tilde{\Gamma}^{\mu}_{\alpha\beta}|_P (e_i)^{\alpha}_{P} (e_j)^{\beta}_{P} \Delta\bar{x}^i \Delta\bar{x}^j \\ &- \frac{a_F^3(P)}{6} (\partial_\gamma \tilde{\Gamma}^{\mu}_{\alpha\beta} - 2\tilde{\Gamma}^{\mu}_{\sigma\alpha}\tilde{\Gamma}^{\sigma}_{\beta\gamma})|_P \\ &\qquad \times (e_i)^{\alpha}_{P} (e_j)^{\beta}_{P} (e_k)^{\gamma}_{P} \Delta\bar{x}^i \Delta\bar{x}^j \Delta\bar{x}^k \ . \end{aligned} \tag{E.1}$$

In this equation, we have denoted $\bar{\mathbf{x}} - \bar{\mathbf{x}}_c$ as $\Delta\bar{\mathbf{x}}$, where $\bar{\mathbf{x}}_c$ is the CFC position of the central geodesic. Besides, we stress that all quantities are evaluated in the global coordinate system, on the central geodesic. For example, we have

$$(e_i)^{\mu}_{P} \equiv (e_i)^{\mu}(x(P)), \text{ where } x^{\mu}(P) = x^{\mu}(\bar{\tau}, \bar{\mathbf{x}}_c) \ . \tag{E.2}$$

For this reason, in order to express everything in terms of barred coordinates $\bar{x}$, we need to compute $x^{\mu}(P)$ in terms of $\bar{\tau}$ (and $\bar{\mathbf{x}}_c$). In [200] it is shown that $x^{\mu}(\bar{\tau}, \bar{\mathbf{x}}_c)$ satisfies the equations

$$\frac{\partial x^{\mu}(\bar{\tau}, \bar{\mathbf{x}}_c)}{\partial \bar{\tau}} = a_F(P)(e_0)^{\mu}_{P} \ , \tag{E.3}$$

which can be easily solved if we work in perturbation theory. We start from $\mu = i$: from eq. (8.15) we see that (keeping the notation a bit heavy for the moment)

$$(e_0)^{i}_{P} = a^{-1}(\tau(\bar{\tau}, \bar{\mathbf{x}}_c)) V^i(x(\bar{\tau}, \bar{\mathbf{x}}_c)) \ , \tag{E.4}$$

while eq. (8.18) reads as

$$\begin{aligned} \frac{a_F(P)}{a(P)} &= 1 + C_{a_F}(\tau_*, \mathbf{x}_c(\tau_*)) \\ &\quad + \int_{\tau_*}^{\tau} ds \left(\partial_0 \zeta(s, \mathbf{x}_c(s)) + \frac{1}{3} \partial_i V^i(s, \mathbf{x}_c(s)) \right) \ . \end{aligned} \tag{E.5}$$

As explained in Section 8.2.3, both l.h.s. and r.h.s. of this equation are understood to be computed in global coordinates along the central geodesic (i. e. on $\mathbf{x} = \mathbf{x}_c(\tau)$: we parameterize the central geodesic with τ). Besides, we also recall that:

- the first order perturbation C_{a_F} is the constant coming from the integration of eq. (8.11);
- τ_* is the initial time for the definition of CFC.

Before inserting this relation for the $\mu = i$ component of eq. (E.3), we need to express the r.h.s. in barred coordinates: however, we note that $(e_0)^i_P$ is already first order in perturbations, so that the zeroth order of a_F/a (which is $\equiv 1$) suffices. Therefore, we find

$$a_F(P)(e_0)^i_P = V^i(x(\bar{\tau}, \bar{\mathbf{x}}_c)) \,, \tag{E.6}$$

so that

$$x^i(\bar{\tau}, \bar{\mathbf{x}}_c) = \bar{\mathbf{x}}_c + \int_{\bar{\tau}_*}^{\bar{\tau}} d\bar{s}\, V^i(\tau(\bar{s}, \bar{\mathbf{x}}_c), \bar{\mathbf{x}}_c) \,, \tag{E.7}$$

where we used the fact that $\mathbf{x}_c = \bar{\mathbf{x}}_c$ at zeroth order in perturbations. We now move to $\mu = 0$ in eq. (E.3): using eq. (8.15) (that defines the components of U^μ in global coordinates) we arrive at

$$a_F(P)(e_0)^0_P = \frac{a_F(P)}{a(P)}\big[1 - N_1(x(P))\big] = 1 - N_1(x(P)) + \frac{a_F(P)}{a(P)}\bigg|_\ell \,, \tag{E.8}$$

where we called $a_F(P)/a(P)|_\ell$ the first order term in eq. (E.5). Inserting this into eq. (E.3) and integrating in $\bar{\tau}$ (choosing $\bar{\tau}_* = \tau_*$), we see that along the central geodesic τ is equal to $\bar{\tau} + \Delta\tau$, where $\Delta\tau$ is first order in perturbations. Therefore, we can simplify eq. (E.8) into

$$x^i(\bar{\tau}, \bar{\mathbf{x}}_c) = \bar{\mathbf{x}}_c + \int_{\bar{\tau}_*}^{\bar{\tau}} d\bar{s}\, V^i(\bar{s}, \bar{\mathbf{x}}_c) \,, \tag{E.9}$$

and we can write eq. (E.5) in CFC coordinates as

$$\frac{a_F(P)}{a(P)} = 1 + C_{a_F}(\bar{\tau}_*, \bar{\mathbf{x}}_c) + \int_{\bar{\tau}_*}^{\bar{\tau}} d\bar{s} \left(\partial_0 \zeta(\bar{s}, \bar{\mathbf{x}}_c) + \frac{1}{3}\partial_i V^i(\bar{s}, \bar{\mathbf{x}}_c) \right) . \tag{E.10}$$

Finally, we write the time shift $\Delta\tau$ as

$$\Delta\tau(\bar{\tau}, \bar{\mathbf{x}}_c) = \int_{\bar{\tau}_*}^{\bar{\tau}} d\bar{s} \big[(a_F/a)(\bar{s}, \bar{\mathbf{x}}_c)|_\ell - N_1(\bar{s}, \bar{\mathbf{x}}_c) \big] \,. \tag{E.11}$$

Having found the expression of $x^\mu(P)$, we can move to the additional terms in eq. (E.1), i. e. the ones away from the central geodesic. We see that they all involve the connection coefficients (in global coordinates) of the conformal metric $\tilde{\Gamma}$, evaluated on the central geodesic. An important simplification, then, arises: since a_F is equal to a at zeroth order in perturbations, the conformal metric $\tilde{g}_{\mu\nu}(x) = a_F^{-2}(x) g_{\mu\nu}(x)$ will be equal to $\eta_{\mu\nu}$ at zeroth order in perturbations. Then, the Christoffel symbols will be already first order in perturbations, and eq. (E.1) simplifies into

$$\begin{aligned} x^\mu(\bar{\tau}, \bar{\mathbf{x}}) = {} & x^\mu(P) + a_F(P)(e_i)^\mu_P \, \Delta\bar{x}^i \\ & - \frac{1}{2}\tilde{\Gamma}^\mu_{ij}|_P \, \Delta\bar{x}^i \Delta\bar{x}^j - \frac{1}{6}(\partial_k \tilde{\Gamma}^\mu_{ij})|_P \, \Delta\bar{x}^i \Delta\bar{x}^j \Delta\bar{x}^k \,, \end{aligned} \tag{E.12}$$

where we used $a_F = a$ and $(e_i)^\mu = a^{-1}\delta_i^\mu$ at zeroth order. The quickest way to compute the connection coefficients of $\tilde{g}_{\mu\nu}$ is to use the relation

$$\tilde{\Gamma}^\rho_{\mu\nu} = \Gamma^\rho_{\mu\nu} + \delta^\rho{}_\mu \nabla_\nu \log\omega + \delta^\rho{}_\nu \nabla_\mu \log\omega - g_{\mu\nu} g^{\rho\sigma} \nabla_\sigma \log\omega \ , \tag{E.13}$$

for $\tilde{g}_{\mu\nu} = \omega^2 g_{\mu\nu}$.[1] For $\omega = a_F^{-1}$, we can use of the results of [200] for the derivatives of a_F along the central geodesic, i. e.

$$(\nabla_\mu \log a_F)|_P = -\frac{\mathcal{H}_F(P)}{a_F(P)}(e_0)_{\mu,P}, \text{ with } (e_0)_{\mu,P} = (g_{\mu\nu}(e_0)^\nu)_P \ . \tag{E.14}$$

In this expression, the local comoving expansion rate $\mathcal{H}_F$ is given by (again, we refer to [200] for details)

$$\begin{aligned}\frac{\mathcal{H}_F(P)}{a_F(P)} = \frac{1}{a(\tau)}\Big(&\mathcal{H}(\tau) - \mathcal{H}(\tau) N_1(s, \mathbf{x}_c(s)) \\ &+ \partial_0 \zeta(s, \mathbf{x}_c(s)) + \frac{1}{3}\partial_i V^i(s, \mathbf{x}_c(s))\Big) \ ,\end{aligned} \tag{E.15}$$

where, as in eq. (E.5) above, both sides of the equation are computed in global coordinates along the central geodesic. From these equations, we see that $(\nabla_\mu \log a_F)|_P$ contains also terms that are of zeroth order in perturbations. However, these terms will identically cancel with the zeroth order ones of $\Gamma^\rho_{\mu\nu}$: therefore we can safely drop the first order time shift and the first order shift of the position of the central geodesic in the argument of the Christoffel symbols $\tilde{\Gamma}^\rho_{\mu\nu}$. We have collected these coefficients in tab. E.1: we note that no time derivative of the Christoffel symbols appear in eq. (E.12), so we can just take their spatial derivatives in global coordinates and compute them at $(\bar{\tau}, \bar{\mathbf{x}}_c)$. In the end, the full transformation at order $(\bar{x}^i)^3$ reads

$$\begin{aligned}\tau(\bar{\tau}, \bar{\mathbf{x}}) = \bar{\tau} &+ \Delta\tau(\bar{\tau}, \bar{\mathbf{x}}_c) + F_i(\bar{\tau}, \bar{\mathbf{x}}_c)\,\Delta\bar{x}^i \\ &- \frac{1}{2}\tilde{\Gamma}^0_{ij}(\bar{\tau}, \bar{\mathbf{x}}_c)\,\Delta\bar{x}^i\Delta\bar{x}^j \\ &- \frac{1}{6}\partial_k\tilde{\Gamma}^0_{ij}(\bar{\tau}, \bar{\mathbf{x}}_c)\,\Delta\bar{x}^i\Delta\bar{x}^j\Delta\bar{x}^k \ ,\end{aligned} \tag{E.16a}$$

$$\begin{aligned}x^l(\bar{\tau}, \bar{\mathbf{x}}) = \bar{x}^l &+ \int_{\bar{\tau}_*}^{\bar{\tau}} d\bar{s}\, V^l(\bar{s}, \bar{\mathbf{x}}_c) \\ &+ \big[(a_F/a)(\bar{\tau}, \bar{\mathbf{x}}_c)|_\ell - \zeta_\ell(\bar{\tau}, \bar{\mathbf{x}}_c)\big]\Delta\bar{x}^l \\ &- \frac{1}{2}\tilde{\Gamma}^l_{ij}(\bar{\tau}, \bar{\mathbf{x}}_c)\,\Delta\bar{x}^i\Delta\bar{x}^j \\ &- \frac{1}{6}\partial_k\tilde{\Gamma}^l_{ij}(\bar{\tau}, \bar{\mathbf{x}}_c)\,\Delta\bar{x}^i\Delta\bar{x}^j\Delta\bar{x}^k \ .\end{aligned} \tag{E.16b}$$

where we have used the fact that e^l_i is equal to $a^{-1}(1-\zeta_\ell)\delta^l_i$ to cancel the $\bar{\mathbf{x}}_c$ coming from eq. (E.9). In eq. (E.16a), we denote the sum $V_i + N_i$

1 See, e. g., [46].

as F_i. This definition is particularly convenient: in fact the parallel transport equation for V^i in global coordinates reads as

$$\partial_0 V^i + \mathcal{H} V^i = -\partial^i N_1 - \partial_0 N^i - \mathcal{H} N^i \,. \tag{E.17}$$

So, if we take V^i to be $-N^i + \partial_i F$, eq. (E.17) is solved if $\partial_0 F + \mathcal{H} F = -N_1$, i. e.

$$\begin{aligned} F(x) = e^{-\int_{\tau_*}^{\tau} ds\, \mathcal{H}(s)} \Bigg[& \tau_* C_F(\tau_*, \mathbf{x}) \\ & - \int_{\tau_*}^{\tau} ds\, e^{\int_{\tau_*}^{s} dw\, \mathcal{H}(w)} N_1(s, \mathbf{x}) \Bigg] \,, \end{aligned} \tag{E.18}$$

where the integration constant C_F is first order in perturbations.

Now, to avoid having to carry around signs and factorials, and to simplify a little bit the notation, we rewrite Eqs. (E.16) as

$$\begin{aligned} x^\mu(\bar\tau, \bar{\mathbf{x}}) &= \bar x^\mu + \xi^\mu(\bar\tau, \bar{\mathbf{x}}) \\ &= \bar x^\mu + \xi^\mu(\bar\tau, \bar{\mathbf{x}}_c) + A^\mu_i(\bar\tau, \bar{\mathbf{x}}_c)\, \Delta\bar x^i \\ &\quad + B^\mu_{ij}(\bar\tau, \bar{\mathbf{x}}_c)\, \Delta\bar x^i \Delta\bar x^j + C^\mu_{kij}(\bar\tau, \bar{\mathbf{x}}_c)\, \Delta\bar x^i \Delta\bar x^j \Delta\bar x^k \,. \end{aligned} \tag{E.19}$$

TABLE E.1: In this table we collect the Christoffel coefficients of the conformal metric along the central geodesic in global coordinates, that we computed making use of eq. (E.14). We separate them into the contributions from $\eta_{\mu\nu} + h_{\mu\nu}$ and those from the conformal factor a^2/a_F^2. As explained in the main text, there is no need to consider the time shift and the shift of the position of the central geodesic in their argument, so we omitted them. $F^i = \partial^i F$ is defined in eq. (E.18): since it is a first order perturbation, we can neglect the shift in its argument as well.

	$\Gamma(\eta_{\mu\nu} + h_{\mu\nu})$	$C(a_F^{-1}) + C(a)$
Γ^0_{00}	$\partial_0 N_1$	$-\partial_0\zeta - \partial_m V^m/3$
Γ^0_{0i}	$\partial_i N_1$	$\mathcal{H} F_i$
Γ^0_{ij}	$\partial_0\zeta\delta_{ij} - \partial_{(i} N_{j)}$	$-(\partial_0\zeta + \partial_m V^m/3)\delta_{ij}$
Γ^k_{00}	$\partial_0 N^k + \partial^k N_1$	$\mathcal{H} F^k$
Γ^k_{0i}	$\partial_0\zeta\delta_{ik} + \partial_{[i} N_{k]}$	$-(\partial_0\zeta + \partial_m V^m/3)\delta^k_i$
Γ^k_{ij}	$-\partial^k\zeta\delta_{ij} + \partial_i\zeta\delta^k_j + \partial_j\zeta\delta^k_i$	$\mathcal{H}(-F^k\delta_{ij} + F_i\delta^k_j + F_j\delta^k_i)$

E.2 CONFORMAL RIEMANN TENSOR

We are now ready to compute the long-wavelength metric in the conformal Fermi frame, for which we need the conformal Riemann tensor in CFC coordinates. Since this will be already first order in perturbations, it is sufficient to calculate it in global coordinates on

the central geodesic.[2] The calculation goes as follows: we use the properties of the Riemann tensor under a conformal transformation, i. e. [46]

$$\begin{aligned}\tilde{R}^{\rho}{}_{\sigma\mu\nu} = R^{\rho}{}_{\sigma\mu\nu} &- 2(\delta^{\rho}{}_{[\mu}\delta^{\alpha}{}_{\nu]}\delta^{\beta}{}_{\sigma} - g_{\sigma[\mu}\delta^{\alpha}{}_{\nu]}g^{\rho\beta})\nabla_{\alpha}\nabla_{\beta}\log\omega \\ &+ 2(\delta^{\rho}{}_{[\mu}\delta^{\alpha}{}_{\nu]}\delta^{\beta}{}_{\sigma} - g_{\sigma[\mu}\delta^{\alpha}{}_{\nu]}g^{\rho\beta} + g_{\sigma[\mu}\delta^{\rho}{}_{\nu]}g^{\alpha\beta}) \\ &\times \nabla_{\alpha}\log\omega\nabla_{\beta}\log\omega\ ,\end{aligned} \tag{E.20}$$

where we will take again $\omega = a_F^{-1}$. It is clear that if we want to compute $\tilde{R}^{\rho}_{\sigma\mu\nu}$ we need to know also the second (covariant) derivatives $(\nabla_\mu\nabla_\nu \log a_F)|_P$ on the central geodesic (whose zeroth order will exactly cancel the corresponding contribution from the background scale factor a). The coordinate-free expression for these derivatives of the local scale factor has been derived in [200], and reads as

$$\begin{aligned}(\nabla_\mu\nabla_\nu \log a_F)|_P = &-\left(\frac{\mathcal{H}_F(P)}{a_F(P)}\right)^2 g_{\mu\nu}|_P \\ &+ \left[\frac{1}{a_F^2(P)}\frac{d\mathcal{H}_F(P)}{d\bar{\tau}} - 2\left(\frac{\mathcal{H}_F(P)}{a_F(P)}\right)^2\right](e_0)_{\mu,P}(e_0)_{\nu,P}\ ,\end{aligned} \tag{E.21}$$

where the "local cosmic acceleration" is given by (like in Eqs. (E.5), (E.15), both sides are understood as computed in global coordinates along the central geodesic)

$$\frac{1}{a_F^2(P)}\frac{d\mathcal{H}_F(P)}{d\bar{\tau}} = \left(\frac{\mathcal{H}_F(P)}{a_F(P)}\right)^2 + (e_0)^{\mu}_P\partial_\mu\left(\frac{\mathcal{H}_F(P)}{a_F^2(P)}\right)\ . \tag{E.22}$$

Now, as explained in Section 8.2.3, we split the curvature perturbation ζ into a long- and short-wavelength part: $\zeta(x) = \zeta_s(x) + \zeta_\ell(x)$. Then, at leading order in ζ, the metric $g_{\mu\nu}$ in global coordinates becomes

$$\left.\begin{aligned} g_{00} &= a^2(-1 - 2(N_1)_s - 2(N_1)_\ell) \\ g_{0i} &= a^2\partial_i\psi_s + a^2\partial_i\psi_\ell \\ g_{ij} &= a^2(1 + 2\zeta_s + 2\zeta_\ell)\delta_{ij}\end{aligned}\right\} \Rightarrow g_{\mu\nu} = (g_{\mu\nu})_s + (g_{\mu\nu})_\ell\ . \tag{E.23}$$

The goal is to absorb the effect of ζ_ℓ by changing coordinates to CFC: therefore, we will construct the CFC metric w.r.t. $(g_{\mu\nu})_\ell$. All Christoffel symbols of tab. E.1, the derivatives of the local scale factor of eq. (E.21), and the conformal Riemann tensor can be computed in terms of ζ_ℓ:

2 That is, in the definition of eq. (8.10) one can take the CFC coordinate basis along the central geodesic, $(\tilde{e}_\nu)^\mu_P = a_F(P)(e_\nu)^\mu_P$, at zeroth order. Using $a_F = a$ one remains with $(\tilde{e}_\nu)^\mu_P = \delta^\mu_\nu$. $\tilde{R}_{\mu\rho\nu\sigma}$ will not carry any power of the background scale factor by itself.

putting all together, and using Eqs. (8.9), we arrive at the expression for the long-wavelength metric perturbations in CFC coordinates[3]

$$\bar{h}_{00}(\bar{\tau},\bar{\mathbf{x}}) = -\Delta\bar{x}^k\Delta\bar{x}^l\left(\partial_k\partial_l - \frac{\delta_{kl}}{3}\partial^2\right)(N_1 + \partial_0\psi + \mathcal{H}\psi)\ , \tag{E.24a}$$

$$\bar{h}_{0i}(\bar{\tau},\bar{\mathbf{x}}) = \frac{2}{3}\Delta\bar{x}^k\Delta\bar{x}^l\Bigg[\underbrace{(\partial_0\mathcal{H} - \mathcal{H}^2)}_{=\varepsilon\mathcal{H}^2}\left[\delta_{kl}F_i - \delta_{ki}F_l\right] - (\delta_{kl}\partial_i - \delta_{ki}\partial_l)\underbrace{(\mathcal{H}N_1 - \partial_0\zeta)}_{=0}\Bigg]\ , \tag{E.24b}$$

$$\bar{h}_{ij}(\bar{\tau},\bar{\mathbf{x}}) = -\frac{1}{3}\Delta\bar{x}^k\Delta\bar{x}^l\left[\frac{2}{3}\mathcal{H}(\partial_m V^m)T_{ijkl} + S_{ijkl}(\zeta + \mathcal{H}\psi)\right]\ , \tag{E.24c}$$

where

$$T_{ijkl} = \delta_{il}\delta_{kj} - \delta_{ij}\delta_{kl}\ , \tag{E.25a}$$

$$S_{ijkl} = \delta_{il}\partial_j\partial_k - \delta_{kl}\partial_i\partial_j + \delta_{kj}\partial_i\partial_l - \delta_{ij}\partial_l\partial_k\ . \tag{E.25b}$$

The last ingredient is the local scale factor $a_F(P)$: it is given by eq. (E.10), i. e.

$$a_F(\bar{\tau}) = a(\bar{\tau} + \Delta\tau(\bar{\tau}))\left(1 + C_{a_F}(\bar{\tau}_*) + \int_{\bar{\tau}_*}^{\bar{\tau}} d\bar{s}\left(\partial_0\zeta(\bar{s}) + \frac{1}{3}\partial_i V^i(\bar{s})\right)\right)\ , \tag{E.26}$$

where we suppressed the label $\bar{\mathbf{x}}_c$ for simplicity.

E.3 FIXING THE RESIDUAL FREEDOM

In this Section we discuss the additional "gauge" degrees of freedom present in the construction of the CFC metric. We start from the choice of initial time $\bar{\tau}_*$, and the constant C_{a_F} in the definition of a_F. We will be interested in computing equal-time correlation functions as $\bar{\tau} \to 0^-$ (that is, on super-Hubble scales: in this way, the long modes will have have already exited the horizon, and will be classical variables that we can use in a coordinate transformation). Now, as discussed in Section 8.2.3, we choose also the initial time to be $\bar{\tau}_* \to 0^-$. If we decide to fix the constant following [200, 201], that is by requiring that at $\bar{\tau}_*$ the local scale factor-proper time relation is the same as that of the unperturbed background cosmology, i. e.

$$\lim_{\bar{\tau}\to\bar{\tau}_*} a_F(\bar{\tau}) = a(\bar{\tau}_*)\ , \tag{E.27}$$

3 As discussed above, we suppress the argument $(\bar{\tau}, \bar{\mathbf{x}}_c)$ on the r.h.s. of these equations.

then we see that C_{a_F} can be safely taken equal to zero. In fact, expanding eq. (E.26) at first order in perturbations, we see that (dropping the label $\bar{\mathbf{x}}_c$)

$$a_F(\bar{\tau}) = a(\bar{\tau})\left[1 + (a_F/a)(\bar{\tau})|_\ell + \mathcal{H}\Delta\tau(\bar{\tau})\right] . \tag{E.28}$$

For $\bar{\tau}$ going to zero we have that:

- the integral in the definition of $\Delta\tau = \xi^0(\bar{\tau}, \bar{\mathbf{x}}_c)$ is killed (basically one has the limit of $x^{-1}\int_0^x dy\, f(y)$ for $x \to 0$), and $\mathcal{H}\Delta\tau(\bar{\tau})$ becomes $-C_{a_F}(\bar{\tau}_*)$;
- $(a_F/a)(\bar{\tau})|_\ell$, instead, simply becomes $C_{a_F}(\bar{\tau}_*)$.

This tells us that for this choice of initial time a_F goes to a for any choice of C_{a_F}. Therefore we fix this constant to be zero in the following, for simplicity. This choice is such that $(a_F/a)(P)$, that is the difference between a_F and a along the central geodesic (i. e. with both a_F and a being evaluated at the same spacetime point), goes to 1 for $\bar{\tau} \to \bar{\tau}_*$.[4]

The second gauge freedom that we discuss in this Section is the possibility of changing the spatial coordinates as

$$\bar{x}^l \to \bar{x}^l(\bar{y}) = \bar{y}^l + \frac{A^l_{kij}(\bar{\tau}, \bar{\mathbf{x}}_c)}{6}\Delta\bar{y}^i\Delta\bar{y}^j\Delta\bar{y}^k , \tag{E.29}$$

where the first order perturbation $A^l_{kij}(\bar{\tau}, \bar{\mathbf{x}}_c)$ is fully symmetric w.r.t. its three lower indices. Going back to $\bar{x}$ as the label for the coordinates, we see how this additional gauge freedom simply means that we can take C^l_{kij} in eq. (E.19) to be not only $-\partial_k\tilde{\Gamma}^l_{ij}(\bar{\tau}, \bar{\mathbf{x}}_c)/6$, but

$$C^l_{kij}(\bar{\tau}, \bar{\mathbf{x}}_c) = -\frac{1}{6}\left[\partial_k\tilde{\Gamma}^l_{ij}(\bar{\tau}, \bar{\mathbf{x}}_c) - A^l_{kij}(\bar{\tau}, \bar{\mathbf{x}}_c)\right] . \tag{E.30}$$

One can show that, under this transformation, the CFC metric perturbations $\bar{h}_{ij}$ transform as

$$\bar{h}_{ij}(\bar{\tau}, \bar{\mathbf{x}}) \to \bar{h}_{ij}(\bar{\tau}, \bar{\mathbf{x}}) + A_{(ij)kl}(\bar{\tau}, \bar{\mathbf{x}}_c)\Delta\bar{x}^k\Delta\bar{x}^l , \tag{E.31}$$

where we have lowered spatial indices with δ_{ij}. One can use this additional freedom to put the spatial part of the metric in the desired shape, without altering h_{00} and h_{0i}.[5] More precisely, we use this

4 This choice makes clear that there is no contribution from primordial physics which is not suppressed by two spatial derivatives of long-wavelength perturbations. Notice that in a curved universe the normalization of the scale factor cannot be reabsorbed by a simple rescaling of spatial coordinates. However, since K_F is already first order in the long-wavelength modes, at this order any rescaling of a_F can be mimicked by a coordinate transformation, and then cannot have any effect on physical observables.

5 Notice that, since $\bar{h}_{\mu\nu}$ is already first order in perturbations, there is no need to consider the change of its argument. a_F will not be touched either, since it depends only on $\bar{\tau}$ which is not changed.

freedom to put the metric of Eqs. (E.24) in conformal Newtonian form, following [201]: we add two tensors $A^l_{kij}(\bar{\tau}, \bar{\mathbf{x}})$, given by

$$
\begin{aligned}
{}_{(1)}A^l_{kij} &= -\frac{1}{6}K_F(\delta^l_k\delta_{ij} + \delta^l_i\delta_{jk} + \delta^l_j\delta_{ki}) \,, && \text{(E.32a)}\\
{}_{(2)}A^l_{kij} &= \frac{1}{9}(\delta^l_k\delta_{ij} + \delta^l_i\delta_{jk} + \delta^l_j\delta_{ki})\partial^2(\zeta + \mathcal{H}\psi) \\
&\quad - \frac{2}{3}(\delta^l_k\partial_i\partial_j + \delta^l_i\partial_j\partial_k + \delta^l_j\partial_k\partial_i)(\zeta + \mathcal{H}\psi) \\
&\quad + \frac{1}{3}(\delta_{ij}\partial^l\partial_k + \delta_{jk}\partial^l\partial_i + \delta_{ki}\partial^l\partial_j)(\zeta + \mathcal{H}\psi) \,, && \text{(E.32b)}
\end{aligned}
$$

where we defined $K_F(\bar{\tau}, \bar{\mathbf{x}})$ as

$$
K_F = -\frac{2}{3}\left[\partial^2(\zeta + \mathcal{H}\psi) + \mathcal{H}\partial_m V^m\right] = -\frac{2}{3}(\partial^2\zeta + \mathcal{H}\partial^2 F) \,. \qquad \text{(E.33)}
$$

After this transformation, the spatial part of the metric becomes (where both l.h.s. and r.h.s. are intended as functions of $\bar{\mathbf{x}}$)

$$
\bar{g}_{ij} = a_F^2\left(\frac{1 + \Delta\bar{x}^k\Delta\bar{x}^l\mathcal{D}_{kl}(\zeta + \mathcal{H}\psi)}{\left(1 + \frac{K_F|\Delta\bar{\mathbf{x}}|^2}{4}\right)^2}\right)\delta_{ij}, \text{ with } \mathcal{D}_{kl} = \partial_k\partial_l - \frac{\delta_{kl}}{3}\partial^2 \,. \qquad \text{(E.34)}
$$

F

TRANSFORMING THE CURVATURE PERTURBATION

In this Appendix we provide the transformation rules for the long- and short-wavelength curvature perturbations ζ. As we have seen in Section 8.3.1, when the change of coordinates does not touch time, we can derive its effect easily with a passive approach. However, when also the time coordinate changes it is more straightforward to use an active approach. One starts from the definition of ζ given a slicing of spacetime by surfaces Σ_τ, i. e. [18, 212–217]

$$\zeta = \frac{\log\det(g_{ij}/a^2)}{6} \,, \tag{F.1}$$

where g_{ij} is the induced metric on Σ_τ. This is nothing else but the local number of e-folds definition, that relates the curvature perturbation ζ to the volume element on the Σ_τ surfaces. We can then use this definition to see how ζ transforms under a long-wavelength transformation $x^\mu \to \bar{x}^\mu = x^\mu - \xi^\mu$, $\xi^\mu = \xi^\mu_\ell$: as usual, we will stay linear in ξ^μ, but we will go up to second order in perturbations (since in the end we will want to find the induced coupling between long and short modes). Denoting with a bar the transformed metric, at leading order in ξ we have [101]

$$\begin{aligned} g_{\mu\nu} \to \bar{g}_{\mu\nu} &= g_{\mu\nu} + 2\nabla_{(\mu}\xi_{\nu)} \\ &= g_{\mu\nu} + g_{\nu\rho}\nabla_\mu\xi^\rho + g_{\mu\rho}\nabla_\nu\xi^\rho + \mathcal{O}(\xi^2) \,, \end{aligned} \tag{F.2}$$

so that

$$\bar{g}_{ij}/a^2 = \delta_{ij} + (\underbrace{e^{2\zeta} - 1}_{\equiv \Delta g})\delta_{ij} + 2\nabla_{(i}\xi_{j)}/a^2 + \mathcal{O}(\xi^2) \,. \tag{F.3}$$

Using the relation $\log\det = \mathrm{Tr}\log$, and working at quadratic order in perturbations (linear in ξ), we obtain (the ellipsis indicates that we have dropped terms of higher order in perturbations)

$$\begin{aligned} \log(\bar{g}_{ij}/a^2) &= \Delta g\delta_{ij} + 2\nabla_{(i}\xi_{j)}/a^2 \\ &\quad - \frac{1}{2}\Delta g^2\delta_{ij} - 2\Delta g\nabla_{(i}\xi_{j)}/a^2 + \mathcal{O}(\xi^2) \\ &= 2\zeta\delta_{ij} + 2\nabla_{(i}\xi_{j)}/a^2 \\ &\quad - 2\zeta(\partial_i\xi_j + \partial_j\xi_i + 2\mathcal{H}\xi^0\delta_{ij}) + \dots \,. \end{aligned} \tag{F.4}$$

What we need now is the expression for $\nabla_{(i}\xi_{j)}/a^2$. First of all we have that

$$\begin{aligned} \nabla_i\xi_j/a^2 = g_{j\rho}\nabla_i\xi^\rho/a^2 &= g_{j\rho}\partial_i\xi^\rho/a^2 + g_{j\rho}\Gamma^\rho_{i\sigma}\xi^\sigma/a^2 \\ &= \partial_i\xi_j + 2\zeta\partial_i\xi_j + N_j\partial_i\xi^0 + g_{j\rho}\Gamma^\rho_{i\sigma}\xi^\sigma/a^2 \,, \end{aligned} \tag{F.5}$$

where, staying linear in ξ and quadratic in perturbations, $g_{j\rho}\Gamma^{\rho}_{i\sigma}\xi^{\sigma}/a^2$ is given by (see tab. F.1)

$$g_{jk}\Gamma^{k}_{il}\xi^{l}/a^2 = \delta_{jk}\Gamma^{k}_{il}\xi^{l} = -\mathcal{H}N_j\xi_i + \delta_{ij}\xi^{l}\partial_l\zeta - 2\xi_{[i}\partial_{j]}\zeta \ , \tag{F.6a}$$

$$\begin{aligned} g_{jk}\Gamma^{k}_{i0}\xi^{0}/a^2 &= e^{2\zeta}\delta_{jk}\Gamma^{k}_{i0}\xi^{0} \\ &= \mathcal{H}\delta_{ij}\xi^{0} + 2\mathcal{H}\zeta\xi^{0}\delta_{ij} + \xi^{0}\partial_0\zeta\delta_{ij} - \partial_{[i}N_{j]}\xi^{0} \ , \end{aligned} \tag{F.6b}$$

$$g_{j0}\Gamma^{0}_{i\sigma}\xi^{\sigma}/a^2 = N_j\Gamma^{0}_{i\sigma}\xi^{\sigma} = N_j\Gamma^{0}_{ik}\xi^{k} = N_j\mathcal{H}\delta_{ik}\xi^{k} = \mathcal{H}\xi_i N_j \ . \tag{F.6c}$$

With this, eq. (F.4) becomes

$$\begin{aligned} \log(\bar{g}_{ij}/a^2) &= 2\zeta\delta_{ij} + 2\nabla_{(i}\xi_{j)}/a^2 - 2\zeta(\partial_i\xi_j + \partial_j\xi_i + 2\mathcal{H}\xi^{0}\delta_{ij}) + \dots \\ &= 2\zeta\delta_{ij} + 2\partial_{(i}\xi_{j)} + 2\mathcal{H}\xi^{0}\delta_{ij} \\ &\quad + 2N_{(i}\partial_{j)}\xi^{0} + 2\xi^{\mu}\partial_{\mu}\zeta\delta_{ij} + \dots \ . \end{aligned} \tag{F.7}$$

Taking the trace, we obtain

$$\bar{\zeta} = \frac{\mathrm{Tr}\log(\bar{g}_{ij}/a^2)}{6} = \zeta + \frac{\partial_i\xi^{i}}{3} + \mathcal{H}\xi^{0} + \frac{N^{i}\partial_i\xi^{0}}{3} + \xi^{\mu}\partial_{\mu}\zeta \ . \tag{F.8}$$

TABLE F.1: In this table we collect the Christoffel coefficients of $g_{\mu\nu}$, separating the contribution of the conformal factor a^2 from the full result: Δ is defined as $2\zeta - N_1$. We refer to tab. E.1 for the contribution from $\eta_{\mu\nu} + h_{\mu\nu}$.

	$C(a)$	Γ
Γ^{0}_{00}	$\mathcal{H}$	$\mathcal{H} + \partial_0 N_1$
Γ^{0}_{0i}	$\mathcal{H}N_i$	$\partial_i N_1 + \mathcal{H}N_i$
Γ^{0}_{ij}	$\mathcal{H}\delta_{ij} + \mathcal{H}\Delta\delta_{ij}$	$\mathcal{H}\delta_{ij} + \mathcal{H}\Delta\delta_{ij} + \partial_0\zeta\delta_{ij} - \partial_{(i}N_{j)}$
Γ^{k}_{00}	$\mathcal{H}N^{k}$	$\partial_0 N^{k} + \mathcal{H}N^{k} + \partial^{k}N_1$
Γ^{k}_{0i}	$\mathcal{H}\delta^{k}_{i}$	$\mathcal{H}\delta^{k}_{i} + \partial_0\zeta\delta^{k}_{i} + \frac{1}{2}(\partial_i N^{k} - \partial^{k}N_i)$
Γ^{k}_{ij}	$-\mathcal{H}\delta_{ij}N^{k}$	$\partial_i\zeta\delta^{k}_{j} + \partial_j\zeta\delta^{k}_{i} - \partial^{k}\zeta\delta_{ij} - \mathcal{H}\delta_{ij}N^{k}$

Now, recall that we are interested in a long-wavelength transformation $\xi^{\mu} = \xi^{\mu}_{\ell}$, and that we want to remain linear in the long mode. Then, splitting both ζ and $\bar{\zeta}$ in long- and short-wavelength parts, we obtain

$$\bar{\zeta}_{\ell} = \zeta_{\ell} + \frac{\partial_i\xi^{i}_{\ell}}{3} + \mathcal{H}\xi^{0}_{\ell} \ , \tag{F.9a}$$

$$\bar{\zeta}_{s} = \zeta_{s} + \frac{N^{i}_{s}\partial_i\xi^{0}_{\ell}}{3} + \xi^{\mu}_{\ell}\partial_{\mu}\zeta_{s} \ , \tag{F.9b}$$

where $N_i = N_i(\zeta)$ is the shift constraint at linear order in ζ. This shows that the short-wavelength ζ transforms as a scalar, with an additional shift if ξ^0 is $\mathbf{x}$-dependent (as it is in our case). This shift will be of no consequence for the final bispectrum transformation, in fact it is straightforward to see that both N_s^i and $\partial_i \xi_\ell^0$ go to zero on super-Hubble scales (we refer to Section 8.3.3 for more details).

G

BISPECTRUM IN FOURIER SPACE

We follow closely [24] to derive the transformation of the bispectrum from global coordinates to CFC. In Section 8.3.2 we have seen that the change to CFC gives rise to the following terms (where we have dropped the label "F" for simplicity and we have taken $\mathbf{x}_c \equiv (\mathbf{x}_1 + \mathbf{x}_2)/2$). As explained in Section 8.3.2, only the contributions from the change in the spatial coordinates need to be considered. If we call $\mathbf{r} \equiv \mathbf{x}_1 - \mathbf{x}_2$ and $r \equiv |\mathcal{R}|$, they are given by

$$\begin{aligned}\Delta B_\zeta = {} & P_{\zeta_\ell A}(|\mathbf{x}_3 - \mathbf{x}_c|)\, r^i \partial_l \langle \zeta_s \zeta_s \rangle (r) \\ & + \frac{1}{4} P_{\zeta_\ell C}(|\mathbf{x}_3 - \mathbf{x}_c|)\, r^i r^j r^k \partial_l \langle \zeta_s \zeta_s \rangle (r) \ ,\end{aligned} \tag{G.1}$$

where with $P_{\zeta_\ell X}$ we denote the cross-spectrum between the long-wavelength curvature perturbation and X, which denotes the two tensors A^l_i and C^l_{kij}.

We can now compute what is the contribution of these terms when we go in Fourier space $\mathcal{R} \leftrightarrow \mathbf{k}_S$ and $\mathbf{x}_3 - \mathbf{x}_c \leftrightarrow \mathbf{k}_L$. As shown in [24], translational invariance allows to focus separately on the long- and short-wavelength power spectra:

- a generic $P_{\zeta_\ell X_{ijk\ldots}}(|\mathbf{x}_3 - \mathbf{x}_c|)$ will be of the form

$$P_{\zeta_\ell X_{ijk\ldots}}(|\mathbf{x}_3 - \mathbf{x}_c|) = \langle \zeta_\ell(\mathbf{x}_3) \partial_{ijk\ldots} \zeta_\ell(\mathbf{x}_c) \rangle \ , \tag{G.2}$$

  so that, going to Fourier space, we get

$$\int \frac{d\mathbf{k}_\ell}{(2\pi)^3} P_\zeta(k_\ell) \frac{\partial^N}{\partial x_c^i \partial x_c^j \partial x_c^k \ldots} e^{i\mathbf{k}_\ell \cdot (\mathbf{x}_3 - \mathbf{x}_c)} \ , \tag{G.3}$$

  where N is the number of derivatives we are considering. We see that each of these derivatives $\partial/\partial x_c^n$ brings down $-ik_\ell^n$: collecting these terms together with $P_\zeta(k_\ell)$ gives

$$P_{\zeta_\ell X_{ijk\ldots}}(|\mathbf{x}_3 - \mathbf{x}_c|) \to \left[(-ik_\ell^i)(-ik_\ell^j)(-ik_\ell^k)\ldots\right] P_\zeta(k_\ell) \ ; \tag{G.4}$$

- the short-scale spectra can be dealt with in a similar way. More precisely, a generic term that one needs to compute is of the form

$$(r^i r^j r^k \ldots)\partial_l \langle \zeta_s \zeta_s \rangle (r) = \int \frac{d\mathbf{k}_s}{(2\pi)^3} P_\zeta(k_s) (r^i r^j r^k \ldots) \partial_l e^{i\mathbf{k}_s \cdot \mathbf{r}} \ , \tag{G.5}$$

that can be rewritten as

$$\begin{aligned}
&\int \frac{d\mathbf{k}_s}{(2\pi)^3} P_\zeta(k_s)(r^i r^j r^k \dots)\partial_l e^{i\mathbf{k}_s\cdot\mathbf{r}} = \\
&i(-i)^N \int \frac{d\mathbf{k}_s}{(2\pi)^3} \left[k_s^l P_\zeta(k_s)\right] \left(\frac{\partial^N}{\partial k_s^i \partial k_s^j \partial k_s^k \dots} e^{i\mathbf{k}_s\cdot\mathbf{r}}\right) = \\
&i(-i)^N (-1)^N \int \frac{d\mathbf{k}_s}{(2\pi)^3} \left(\frac{\partial^N}{\partial k_s^i \partial k_s^j \partial k_s^k \dots} \left[k_s^l P_\zeta(k_s)\right]\right) e^{i\mathbf{k}_s\cdot\mathbf{r}} ,
\end{aligned} \tag{G.6}$$

where N is the number of powers of $\mathbf{r}$ that we are considering. We have moved the derivatives from the exponential to the power spectrum integrating by parts N times. This generates an overall $(-1)^N$ factor. Then, the Fourier transform of $(r^i r^j r^k \dots)\partial_l \langle \zeta_s \zeta_s \rangle (r)$ is given by

$$(r^i r^j r^k \dots)\partial_l \langle \zeta_s \zeta_s \rangle (r) \to i^{N+1} \frac{\partial^N}{\partial k_s^i \partial k_s^j \partial k_s^k \dots} \left[k_s^l P_\zeta(k_s)\right] . \tag{G.7}$$

For our applications, we will need to take N up to 3. The expressions can quickly become cumbersome, so we proceed step by step and collect the intermediate results for convenience of the reader. Since all derivatives $\partial/\partial k_s^i$ are acting on a function of k_s only, some simplifications will arise:

- we start from the simple $\partial/\partial k_s^i$, that we rewrite as

$$\frac{\partial}{\partial k_s^i} = \frac{k_s^i}{k_s^2} \frac{d}{d\log k_s} . \tag{G.8}$$

  This directly leads to

$$\frac{\partial}{\partial k_s^i} k_s^j = \delta_i^j + k_s^j \frac{\partial}{\partial k_s^i} = \delta_i^j + \frac{k_s^i k_s^j}{k_s^2} \frac{d}{d\log k_s} ; \tag{G.9}$$

- then we will encounter terms like $\partial^2/\partial k_s^i \partial k_s^j$. With simple manipulations one arrives at

$$\frac{\partial^2}{\partial k_s^i \partial k_s^j} = \frac{\delta_{ij}}{k_s^2} \frac{d}{d\log k_s} + \frac{k_s^i k_s^j}{k_s^4} \left(\frac{d^2}{d\log k_s^2} - 2\frac{d}{d\log k_s}\right) ; \tag{G.10}$$

- finally, we will have terms with three derivatives and one power of $\mathbf{k}_s$, i. e.

$$\mathcal{S}_{ijk}^l = \frac{\partial^3}{\partial k_s^i \partial k_s^j \partial k_s^k} k_s^l . \tag{G.11}$$

If we define

$$\mathcal{D}_1 = \frac{d}{d\log k_s} \,, \tag{G.12a}$$

$$\mathcal{D}_2 = \frac{d^2}{d\log k_s^2} - 2\frac{d}{d\log k_s} \,, \tag{G.12b}$$

$$\mathcal{D}_3 = \frac{d^3}{d\log k_s^3} - 6\frac{d^2}{d\log k_s^2} + 8\frac{d}{d\log k_s} \,, \tag{G.12c}$$

we can write this term as a sum of various pieces (all symmetric in i, j, k)

$$\begin{aligned} \mathcal{S}^l_{ijk} = \frac{\delta_{ij}\delta_{kl}}{k_s^2}\mathcal{D}_1 + 2 \text{ perms.} + \frac{\delta_{ij}k_s^k k_s^l}{k_s^4}\mathcal{D}_2 + 2 \text{ perms.} \\ + \frac{\delta_{li}k_s^j k_s^k}{k_s^4}\mathcal{D}_2 + 2 \text{ perms.} + \frac{k_s^i k_s^j k_s^k k_s^l}{k_s^6}\mathcal{D}_3 \,. \end{aligned} \tag{G.13}$$

With some simple algebra, one can now write the expression for the action of $\mathcal{S}^l_{ijk}$ on the small-scale power spectrum at leading order in slow-roll, recalling that if we neglect any running of the spectral index we can write derivatives of $P_\zeta(k_s)$ as

$$\begin{aligned} \frac{d^m P_\zeta(k_s)}{d\log k_s^m} &= (n_s - 4)^m P_\zeta(k_s) \\ &= (-3)^m \left[1 + \frac{m}{3}(n_s - 1)\right] P_\zeta(k_s) \,. \end{aligned} \tag{G.14}$$

H

SMALL SPEED OF SOUND: OVERVIEW

In this Appendix we investigate briefly the simplifications that arise when one is interested in the limit of a small inflaton speed of sound ($c_s \ll 1$). In passing, we collect some results that can be useful if one wants to compute the CFC bispectrum directly from the action, with the long-wavelength metric given by eqs. (8.30). This approach is different from the one we have followed in Section 8.4, where we obtained the η contribution to the CFC bispectrum by mirroring Maldacena's calculation in flat gauge [18].

We will take the Goldstone boson of time diffeomorphisms (that we will call π) as short-wavelength variable [62, 219]. Before proceeding, let us see how the metric in the conformal Fermi frame looks like when working in the π gauge for the short modes: dropping for simplicity the "F" label not only on coordinates, but also on all the components of the metric (for simplicity of notation), we have that

$$\begin{aligned} ds^2 = &- \underbrace{a^2(1 + 2(N_1)_\ell + 2(N_1)_s)}_{=N^2} d\tau^2 \\ &+ a^2 N_s^i (d\tau dx^i + dx^i d\tau) + \underbrace{a^2 e^{2\zeta_\ell} \delta_{ij}}_{=h_{ij}} dx^i dx^j \ , \end{aligned} \tag{H.1}$$

where:

- we have taken $a_F = a$ in g_{0i}. The reason is that we can remain at linear order in perturbations when we deal with the time-time and time-space components of the metric;
- we have put to zero the long-wavelength shift constraint, because we have seen in Section 8.2.3 that it is of order k_ℓ^3. Besides, the short-scale shift constraint N_s^i can be written as $\partial_i \psi$, as usual: we will omit the "s" subscript in the following for simplicity of notation. We note that this definition (i. e. without including the factor of a^2) agrees with the ADM parameterization of g_{0i} (which is $h_{ij} N^j$), because we are working at linear order in the constraints. Therefore, in the following we will raise and lower the indices of N^i with δ^j_i;
- both $(N_1)_s$ and ψ will be linearly solved in terms of π [62, 219]. In single-field slow-roll inflation, the leading interaction (cubic) Lagrangian comes from the mixing with gravity, so it is not

possible to neglect these terms (i. e., the decoupling limit would not capture the relevant physics);[1]

- the long-wavelength contribution to a_F, which is equal to (we refer to Section E.2 for details)

$$a_F(\tau) = a(\tau)\left[1 + (a_F/a)(\tau)|_\ell + \mathcal{H}\xi^0(\tau, \mathbf{0})\right] , \tag{H.2}$$

is included in $(N_1)_\ell$ and ζ_ℓ (the subscript "ℓ" is dropped on ξ^μ for simplicity). That is, we add it to the perturbations h_{00} and $h_{ij} \propto \delta_{ij}$ that make up the long-wavelength CFC metric of eqs. (8.30). In this way it is easier to keep track of both the order in perturbations and the order in the slow-roll expansion.

In this gauge, the action is equal to

$$S = S_{EH} + \int d^4x\, N\sqrt{h}\left[\frac{(\partial_0\phi - N^i\partial_i\phi)^2}{N^2} - h^{ij}\partial_i\phi\partial_j\phi - 2V(\phi)\right] , \tag{H.3}$$

where we have that:

- the inflaton ϕ, whose background value we write as $\bar{\phi}$, is given by (in the following, we will often denote derivatives w.r.t. τ with a "prime")

$$\begin{aligned}\phi &= \bar{\phi}(\tau+\pi) + \underbrace{\bar{\phi}'(\tau+\pi)\xi^0(\tau+\pi)}_{\equiv \delta\phi_\ell(\tau+\pi)} + \mathcal{O}[(\xi^0)^2] \\ &= \sqrt{2\varepsilon}\,\mathcal{H}\left[\xi^0 + \pi + \partial_0\xi^0\pi + \frac{\mathcal{H}}{2}\left(1 - \varepsilon + \frac{\eta}{2}\right)(\pi^2 + 2\xi^0\pi)\right] + \dots ,\end{aligned} \tag{H.4}$$

where we have dropped terms cubic in perturbations (staying linear in the long-wavelength ξ^0) and we have used the slow-roll relations

$$\bar{\phi}' = \sqrt{2\varepsilon}\,\mathcal{H} , \tag{H.5a}$$

$$\mathcal{H}' = \mathcal{H}^2(1-\varepsilon) , \tag{H.5b}$$

$$\varepsilon' = \mathcal{H}\varepsilon\eta . \tag{H.5c}$$

The presence of $\bar{\phi}'\xi^0 \equiv \delta\phi_\ell$ is due to the transformation to CFC, and the fact that at second order in k_ℓ we cannot neglect the change in the time coordinate;

- the potential $V(\phi)$ can likewise be expanded in perturbations, using the above result for ϕ and the fact that $V(\bar{\phi}) = H^2(3-\varepsilon)$. We will not write down the expansion here, since it is very easy to obtain it with simple algebra. We note that useful relations between $V(\bar{\phi})$ (and its derivatives) and the Hubble slow-roll parameters are also listed in Sec. B of [65];

1 Even if, as we have seen in Section 8.4, there are a lot of simplifications that arise if we are interested only in contributions to the bispectrum that are $\propto \eta$.

- the Einstein-Hilbert action S_{EH}, i. e.

$$S_{EH} = \frac{1}{2}\int d^4x\, N\sqrt{h}\left[R^{(3)}(h) + \frac{E^{ij}E_{ij} - E^2}{N^2}\right] , \tag{H.6}$$

with

$$E_{ij} \equiv \frac{1}{2}\left[\partial_0 h_{ij} - 2\nabla_{(i}N_{j)}\right] , \tag{H.7a}$$

$$E = h^{ij}E_{ij} , \tag{H.7b}$$

is computed in terms of the metric of eq. (H.1).

It is now straightforward to solve the constraints in terms of π: at linear order in perturbations they are given by [219]

$$(N_1)_s = \varepsilon\mathcal{H}\pi , \tag{H.8a}$$

$$\psi = -\varepsilon\mathcal{H}\partial^{-2}\partial_0\pi . \tag{H.8b}$$

From this one can find the quadratic action for the Goldstone boson π. At leading order in slow-roll it is equal to [62, 219]

$$S_{\pi\pi} = \int d^4x\, a^2\mathcal{H}^2\varepsilon\left[(\partial_0\pi)^2 - (\partial_i\pi)^2\right] . \tag{H.9}$$

Now, what we are looking for is the coupling between long and short modes, so what we need is the interaction Lagrangian at cubic order in perturbations with one long leg and two short ones (we focus only on scalar degrees of freedom, i. e. we discard the graviton). Adding this to the quadratic action for π, one can compute the power spectrum of π in the background of a long-wavelength classical curvature perturbation: we will denote this two-point function $\langle\pi\pi\rangle|_\ell$ by $P_\pi|_\ell$ (we use the subscript "ℓ" to indicate that the power spectrum of π will depend on the whole long-wavelength part of the metric in eq. (H.1), i. e. on a_F, K_F, etc.). Once the cubic action $S_{\pi\pi}|_\ell$ has been found, one can use the in-in formalism [18, 119, 255–258], which guarantees the correct choice of normalization and vacuum for the modes, to calculate $P_\pi|_\ell$. Since we are computing a two-point function in a perturbed background FLRW, and not a full three-point function, there is a simplification [208]: the cubic Lagrangian will depend explicitly on the spatial coordinates, since the long-wavelength metric in CFC does. However, the terms coming from the correction to the scale factor are evaluated only on the central geodesic, and do not depend on $\mathbf{x}$: schematically, we denote these terms by $S_{\pi\pi}|_{\ell,\mathbf{x}=\mathbf{0}}$. Therefore, it is possible (but not necessary) to deal with them by taking as free action not only the one of eq. (H.9), but $S_{\pi\pi} + S_{\pi\pi}|_{\ell,\mathbf{x}=\mathbf{0}}$. The resulting equation of motion can be solved perturbatively with Green's function methods (see [65], for example), and the normalization of the modes (necessary to have the correct commutation relations) and the choice of vacuum (i. e. the Bunch-Davies vacuum) can be carried out in the usual way.[2] At this point, $P_\pi|_\ell$

2 For example, for the normalization of the modes it will be necessary to impose that the Wronskian of the mode functions of the canonically normalized variable is equal to 1 [18, 43, 119, 219, 259].

is $P_\pi + P_\pi|_{\ell,\mathbf{x}=\mathbf{0}}$. To find the final contribution $P_\pi|_{\ell,\mathbf{x}\neq\mathbf{0}}$, which comes from the $\mathbf{x}$-dependent terms in the cubic action, one can do a tree-level in-in calculation. Denoting by $\mathcal{L}_{\pi\pi}|_{\ell,\mathbf{x}\neq\mathbf{0}}$ the corresponding cubic Lagrangian, and using the fact that at third order in perturbations the interaction Hamiltonian density is $-\mathcal{L}_{\text{int.}}$, one can write this power spectrum on super-Hubble scales ($\tau \to 0^-$) as [18, 43, 119, 208, 219, 259]

$$\begin{aligned}\langle \pi(0,\mathbf{x}_1)\pi(0,\mathbf{x}_2)\rangle\,|_{\ell,\mathbf{x}\neq\mathbf{0}} = (2\pi)^3 \int \frac{d\mathbf{k}_1 d\mathbf{k}_2}{(2\pi)^6} \mathcal{P}_{ij}(\tau,\mathbf{k}_1,\mathbf{k}_2) \\ \times \left[\frac{\partial^2}{\partial k_1^i \partial k_1^j}\delta(\mathbf{k}_1+\mathbf{k}_2)\right] \\ \times e^{i\mathbf{k}_1\cdot\mathbf{x}_1 + i\mathbf{k}_2\cdot\mathbf{x}_2}\,.\end{aligned} \tag{H.10}$$

In the above equation, the function $\mathcal{P}_{ij}$ is defined as [208]

$$\mathcal{P}_{ij}(\tau,\mathbf{k}_1,\mathbf{k}_2) = -4\,\mathrm{Re}\left[i\pi(\tau,\mathbf{k}_1)\pi(\tau,\mathbf{k}_2)\int_{-\infty^+}^{0} ds\, \mathcal{L}^*_{ij}(s,\mathbf{k}_1,\mathbf{k}_2)\right], \tag{H.11}$$

where the boundary condition $-\infty^+ \equiv -\infty(1-i\epsilon)$ picks out the interacting vacuum. With $\mathcal{L}^*_{ij}$ we denote the (complex conjugate of the) Fourier transform of $\mathcal{L}_{\pi\pi}|_{\ell,\mathbf{x}\neq\mathbf{0}}$ evaluated on the mode functions of π, that we will denote by $\pi_{\text{cl.}}$. The i, j indices mean that every explicit power of $\mathbf{x}$ that is carried by the long legs (which are all quadratic in x^i, e. g. $\propto K_F|\mathbf{x}|^2$) is taken care of by the derivatives of $\delta(\mathbf{k}_1+\mathbf{k}_2)$ in eq. (H.10). More precisely:

- suppose that $\mathcal{L}_{\pi\pi}|_{\ell,\mathbf{x}\neq\mathbf{0}}$ contains a term of the form

$$\mathcal{L}_{\pi\pi}|_{\ell,\mathbf{x}\neq\mathbf{0}} \supset a_1\, a^2\mathcal{H}^2\varepsilon\, K_F|\mathbf{x}|^2\,(\partial_i\pi)^2\,, \tag{H.12}$$

  where a_1 is a numerical factor. In this case, $\mathcal{L}_{ij}$ would be equal to

$$\begin{aligned}\mathcal{L}_{ij}(\tau,\mathbf{k}_1,\mathbf{k}_2) \supset -a_1 \times a^2\mathcal{H}^2\varepsilon \times \underbrace{K_F\delta_{ij}}_{K_F|\mathbf{x}|^2} \\ \times \underbrace{(i\mathbf{k}_1)\cdot(i\mathbf{k}_2)\,\pi_{\text{cl.}}(\tau,k_1)\pi_{\text{cl.}}(\tau,k_2)}_{(\partial_i\pi)^2}\,.\end{aligned} \tag{H.13}$$

  We stress that K_F is just a real, classical, $\mathbf{x}$-independent number (it is evaluated on the central geodesic), therefore it is on the same footing as $a^2\mathcal{H}^2\varepsilon$, i. e. it is not touched by the Fourier transform (and it is already evaluated on the classical mode functions). We note that the time dependence of K_F starts at $\mathcal{O}(k_\ell^4)$, so it can be considered a constant at the order in the gradient expansion that we are working;

- one can also consider the case where that $\mathcal{L}_{\pi\pi}|_{\ell,\mathbf{x}\neq\mathbf{0}}$ contains an anisotropic term. From eq. (8.30c), we have that the anisotropic part of ζ_ℓ is (in terms of the long-wavelength curvature perturbation in global coordinates $\zeta_{\rm gl.}$)

$$\zeta_\ell^{\rm anis.}(x) = \frac{1}{2}x^i x^j \mathcal{D}_{ij}\left[\varepsilon\mathcal{H}\partial^{-2}\partial_0\zeta_{\rm gl.}(\tau,\mathbf{0})\right] \equiv x^i x^j Z_{ij}(\tau,\mathbf{0}) \ , \tag{H.14}$$

with $\mathcal{D}_{ij} = \partial_i\partial_j - \partial^2\delta_{ij}/3$. Then the cubic Lagrangian will contain a term of the form (a_2 is again a numerical factor)

$$\mathcal{L}_{\pi\pi}|_{\ell,\mathbf{x}\neq\mathbf{0}} \supset a_2\, a^2\mathcal{H}^2\varepsilon\, x^i x^j Z_{ij}\,(\partial_0\pi)^2 \ , \tag{H.15}$$

and $\mathcal{L}_{ij}$ would, similarly to eq. (H.13), be given by

$$\mathcal{L}_{ij}(\tau,\mathbf{k}_1,\mathbf{k}_2) \supset -a_1 \times a^2\mathcal{H}^2\varepsilon \times Z_{ij} \times \partial_0\pi_{\rm cl.}(\tau,k_1)\partial_0\pi_{\rm cl.}(\tau,k_2) \ . \tag{H.16}$$

As before, Z_{ij} is a real number: however, in this case one cannot neglect its time dependence when computing the corresponding $\mathcal{P}_{ij}$, since it starts at order k_ℓ^2.

We note that an overall -1 in the definition of $\mathcal{P}_{ij}$ is due to the fact that

$$x^i x^j = -\int\frac{d\mathbf{k}}{(2\pi)^3}\left[\frac{\partial^2}{\partial k^i\partial k^j}\delta(\mathbf{k})\right]e^{i\mathbf{k}\cdot\mathbf{x}} \ , \tag{H.17}$$

while an overall factor of 2 comes from the two different contractions that we need to consider when we use Wick's theorem. Now, integrating by parts eq. (H.10) to isolate a $(2\pi)^3\delta(\mathbf{k}_1+\mathbf{k}_2)$, it is possible to extract the expression for $P_\pi|_{\ell,\mathbf{x}\neq\mathbf{0}}$. Multiplying it with a second long mode, and taking the average, gives then the squeezed limit bispectrum in CFC.

Eventually, one is interested in the short-wavelength ζ_s and its coupling with the long mode. In unitary gauge $\pi = 0$, the perturbation ζ_s is defined by

$$h_{ij} = a^2 e^{2\zeta_\ell} e^{2\zeta_s}\delta_{ij} \ , \tag{H.18}$$

so what one needs to do is find the relation between ζ_s and the Goldstone boson π. We see from eq. (H.4) that a time shift $\tau = \tilde{\tau} - \pi$ would take care of the inflaton perturbation, that would go back to $\phi = \bar{\phi} + \delta\phi_\ell$ (as it was after the transformation from global coordinates in ζ gauge to CFC) at linear order in π. This is enough for our purposes, since we are interested only in the long-short coupling and therefore we can drop all terms that are quadratic (or higher) in π. Correspondingly, at quadratic order in perturbations, the spatial metric would transform as (see also Section 8.4 for more details)

$$\begin{aligned}\hat{\tilde{g}}_{ij} = &-a^2\frac{\partial\pi}{\partial\tilde{x}^i}\frac{\partial\pi}{\partial\tilde{x}^j} - a^2\frac{\partial\pi}{\partial\tilde{x}^i}\partial_j\psi \\ &- a^2\frac{\partial\pi}{\partial\tilde{x}^j}\partial_i\psi + a^2 e^{2\zeta_\ell}e^{-\mathcal{H}\pi}e^{-\pi\partial_0\zeta_\ell}\delta_{ij} \ ,\end{aligned} \tag{H.19}$$

where in the expansion of h_{ij} (i. e. the last term on the r.h.s.) we have stopped at linear order in the short mode, for the same reason discussed above. We see that the metric, after this time shift, is not of the form of eq. (H.18), because of the first two terms that involve spatial derivatives of π. It is possible to remove them with a second order spatial coordinate transformation: however, since the terms we have to remove are of quadratic order in the short modes, their contribution to ζ_s would be negligible for our purposes. From this, comparing with eq. (H.18), we conclude that the relation between ζ_s and π is given by

$$\zeta_s = -\mathcal{H}\pi - \pi\partial_0\zeta_\ell \ . \tag{H.20}$$

After the in-in calculation of $P_\pi|_\ell$ that we have briefly discussed above has been carried out, one can use eq. (H.20) to compute the power spectrum of the short-scale ζ_s in the background of the long modes: in addition to the coupling coming from the interactions (i. e. the contribution coming from replacing π with $-\zeta_s/\mathcal{H}$ in $P_\pi|_\ell$), there will be additional terms coming from the second order (long-short) term $\zeta_s \supset -\partial_0\zeta_\ell\pi$.

At this point, one must compute the cubic Lagrangian, and for each term derive the corresponding $\mathcal{P}_{ij}$. However, since we are working in a "mixed ζ - π gauge", it is clear that there will be some complications due to the fact that the interaction Lagrangian will not be slow-roll suppressed w.r.t. the quadratic Lagrangian for the pion. For example, there will be interactions of the form

$$\begin{aligned}\mathcal{L}_{\pi\pi}|_\ell \supset \big\{ & a_1\, a^2\mathcal{H}^2\varepsilon\, \zeta_\ell\, (\partial_0\pi)^2,\, a_2\, a^2\mathcal{H}^2\varepsilon\, \zeta_\ell\, (\partial_i\pi)^2, \\ & a_3\, a^2\mathcal{H}^4\varepsilon\, \partial_0\xi^0\, \pi^2,\, a_4\, a^2\mathcal{H}^2\varepsilon\, \partial_i\xi^0\partial_i\pi\,\pi, \dots \big\} \ ,\end{aligned} \tag{H.21}$$

coming from both the EH action (once we plug in it the constraints solved in terms of π) and the inflaton action. Since the mode functions $\pi_{cl.}$, $(\zeta_\ell)_{cl.}$ and $\xi^0_{cl.}$ are $\propto 1/\sqrt{\varepsilon}$ at leading order in slow-roll, the cubic Lagrangian should be at least of order $\varepsilon^{3/2}$ to be able to capture the leading part of the bispectrum (which we know is slow-roll suppressed, i. e. it is of order $(\varepsilon^2, \varepsilon\eta) \times (1/\sqrt{\varepsilon}\,)^6$) by using the de Sitter modes alone. In other words, if we were to compute the bispectrum using the in-in formalism discussed above, we would indeed see that at zeroth order in slow-roll (that is, at order $(1/\sqrt{\varepsilon}\,)^6$) it is zero, and that the leading order result is $\mathcal{O}(\varepsilon, \eta)$. However, we could not trust the slow-roll-suppressed part of the result because we would be neglecting contributions coming from corrections to the mode functions: to capture all the effects it would be necessary to use the full classical solutions in terms of Hankel functions, which complicate considerably the time integrals of eq. (H.11).

We are now in the position to discuss briefly the case of an inflaton speed of sound c_s different from 1. We know that for $c_s \neq 1$, the contribution to the bispectrum which is not slow-roll suppressed will

be different from zero: namely, it will be proportional to $(1-c_s^2)/c_s^2$ [119, 208, 219]. Therefore, the de Sitter modes would be able to fully capture the leading order bispectrum (which would be much larger than its slow-roll suppressed part if c_s is not too close to 1) in this case. Besides, a further simplification arises if $c_s \ll 1$: in fact, in this non-relativistic limit we do not expect the short modes π to feel the spatial curvature of the universe induced by the long mode,[3] but to be sensitive only to the effect it has on the expansion history $a_F \neq a$ [208]. Translated at the level of the interaction Lagrangian, this statement means that it is possible to drop all the long legs that are not (functions of) a_F, because only these will affect the bispectrum at order $(k_\ell^2/k_s^2)/c_s^2$ [208]. Then, powers of x^i will not appear explicitly in $\mathcal{L}_{\pi\pi}|_\ell$ and it will not be necessary to compute $\mathcal{P}_{ij}$ using the method of eq. (H.11), greatly simplifying the calculation.

3 The same argument can be used for the anisotropic part of the long-wavelength metric (which we also know has an additional slow-roll suppression w.r.t. the other parts).

BIBLIOGRAPHY

[1] S. W. Hawking, I. G. Moss, and J. M. Stewart. "Bubble collisions in the very early universe." *Phys. Rev.* D26, 2681 (1982).

[2] A. H. Guth and E. J. Weinberg. "Could the Universe Have Recovered from a Slow First Order Phase Transition?" *Nucl. Phys.* B212, 321 (1983).

[3] A. Albrecht and P. J. Steinhardt. "Cosmology for grand unified theories with radiatively induced symmetry breaking." *Phys. Rev. Lett.* 48, 1220 (1982).

[4] A. D. Linde. "A new inflationary universe scenario: A possible solution of the horizon, flatness, homogeneity, isotropy and primordial monopole problems." *Phys. Lett.* B108, 389 (1982).

[5] G. Hinshaw et al. "Nine-Year Wilkinson Microwave Anisotropy Probe (WMAP) Observations: Cosmological Parameter Results." *Astrophys. J. Suppl.* 208 (2013), p. 19. arXiv: 1212.5226 [astro-ph.CO].

[6] P. A. R. Ade et al. "Planck 2015 results. XIII. Cosmological parameters." *Astron. Astrophys.* 594 (2016), A13. arXiv: 1502.01589 [astro-ph.CO].

[7] R. A. Sunyaev and Ya. B. Zeldovich. "The Interaction of matter and radiation in the hot model of the universe." *Astrophys. Space Sci.* 7 (1970), pp. 20–30.

[8] A. F. Illarionov and R. A. Sunyaev. *Soviet Astronomy* 18 (1975), pp. 691–699.

[9] L. Danese and G. De Zotti. *A&A* f107 (39 1982).

[10] C. Burigana, L. Danese, and G. De Zotti. *A&A* 246 (49 1991).

[11] D. J. Fixsen, E. S. Cheng, J. M. Gales, J. C. Mather, R. A. Shafer, and E. L. Wright. "The Cosmic Microwave Background spectrum from the full COBE FIRAS data set." *Astrophys. J.* 473 (1996), p. 576. arXiv: astro-ph/9605054 [astro-ph].

[12] J. Chluba and R. A. Sunyaev. "The evolution of CMB spectral distortions in the early Universe." *Mon. Not. Roy. Astron. Soc.* 419 (2012), pp. 1294–1314. arXiv: 1109.6552 [astro-ph.CO].

[13] R. Khatri and R. A. Sunyaev. "Creation of the CMB spectrum: precise analytic solutions for the blackbody photosphere." *JCAP* 1206 (2012), p. 038. arXiv: 1203.2601 [astro-ph.CO].

[14] P. A. R. Ade et al. "Planck 2015 results. XX. Constraints on inflation." *Astron. Astrophys.* 594 (2016), A20. arXiv: 1502.02114 [astro-ph.CO].

[15] S. Hannestad, S. H. Hansen, F. L. Villante, and A. J. S. Hamilton. "Constraints on inflation from CMB and Lyman alpha forest." *Astropart. Phys.* 17 (2002), pp. 375–382. arXiv: astro-ph/0103047 [astro-ph].

[16] U. Seljak, A. Slosar, and P. McDonald. "Cosmological parameters from combining the Lyman-alpha forest with CMB, galaxy clustering and SN constraints." *JCAP* 0610 (2006), p. 014. arXiv: astro-ph/0604335 [astro-ph].

[17] V. Acquaviva, N. Bartolo, S. Matarrese, and A. Riotto. "Second-Order Cosmological Perturbations from Inflation." *Nucl. Phys.* B667 (2003), pp. 119–148. arXiv: astro-ph/0209156v3.

[18] J. Maldacena. "Non-Gaussian features of primordial fluctuations in single field inflationary models." *JHEP* 013 (May 2003). arXiv: astro-ph/0210603v5.

[19] N. Bartolo, E. Komatsu, S. Matarrese, and A. Riotto. "Non-Gaussianity from Inflation: Theory and Observations." *Phys. Rept.* 402 (2004), pp. 103–266. arXiv: astro-ph/0406398v2.

[20] E. Pajer and M. Zaldarriaga. "A New Window on Primordial non-Gaussianity." *Phys. Rev. Lett.* 109 (2012), p. 021302. arXiv: 1201.5375 [astro-ph.CO].

[21] J. Chluba, E. Dimastrogiovanni, M. A. Amin, and M. Kamionkowski. "Evolution of CMB spectral distortion anisotropies and tests of primordial non-Gaussianity." *Mon. Not. Roy. Astron. Soc.* 466.2 (2017), pp. 2390–2401. arXiv: 1610.08711 [astro-ph.CO].

[22] A. Kogut et al. "The Primordial Inflation Explorer (PIXIE): A Nulling Polarimeter for Cosmic Microwave Background Observations." *JCAP* 1107 (2011), p. 025. arXiv: 1105.2044 [astro-ph.CO].

[23] P. Creminelli and M. Zaldarriaga. "Single field consistency relation for the 3-point function." *JCAP* 0410 (2004), p. 006. arXiv: astro-ph/0407059 [astro-ph].

[24] E. Pajer, F. Schmidt, and M. Zaldarriaga. "The Observed Squeezed Limit of Cosmological Three-Point Functions." *Phys. Rev.* D88.8 (2013), p. 083502. arXiv: 1305.0824 [astro-ph.CO].

[25] R. Emami, E. Dimastrogiovanni, J. Chluba, and M. Kamionkowski. "Probing the scale dependence of non-Gaussianity with spectral distortions of the cosmic microwave background." *Phys. Rev.* D91.12 (2015), p. 123531. arXiv: 1504.00675 [astro-ph.CO].

[26] M. Shiraishi, M. Liguori, N. Bartolo, and S. Matarrese. "Measuring primordial anisotropic correlators with CMB spectral distortions." *Phys. Rev.* D92 (2015), p. 083502. arXiv: 1506.06670 [astro-ph.CO].

[27] N. Bartolo, M. Liguori, and M. Shiraishi. "Primordial trispectra and CMB spectral distortions." *JCAP* 1603.03 (2016), p. 029. arXiv: 1511.01474 [astro-ph.CO].

[28] A. Ota. "Cosmological constraints from μE cross-correlations." *Phys. Rev.* D94.10 (2016), p. 103520. arXiv: 1607.00212 [astro-ph.CO].

[29] M. Shiraishi, N. Bartolo, and M. Liguori. "Angular dependence of primordial trispectra and CMB spectral distortions." *JCAP* 1610.10 (2016), p. 015. arXiv: 1607.01363 [astro-ph.CO].

[30] A. Ravenni, M. Liguori, N. Bartolo, and M. Shiraishi. "Primordial non-Gaussianity with μ-type and y-type spectral distortions: exploiting Cosmic Microwave Background polarization and dealing with secondary sources" (2017). arXiv: 1707.04759 [astro-ph.CO].

[31] G. Cabass, E. Pajer, and D. van der Woude. *In preparation*.

[32] G. Cabass, E. Pajer, and F. Schmidt. *In preparation*.

[33] E. Silverstein and A. Westphal. "Monodromy in the CMB: Gravity Waves and String Inflation." *Phys. Rev.* D78 (2008), p. 106003. arXiv: 0803.3085 [hep-th].

[34] L. McAllister, E. Silverstein, and A. Westphal. "Gravity Waves and Linear Inflation from Axion Monodromy." *Phys. Rev.* D82 (2010), p. 046003. arXiv: 0808.0706 [hep-th].

[35] R. Flauger, L. McAllister, E. Pajer, A. Westphal, and G. Xu. "Oscillations in the CMB from Axion Monodromy Inflation." *JCAP* 1006 (2010), p. 009. arXiv: 0907.2916 [hep-th].

[36] N. Dalal, O. Doré, D. Huterer, and A. Shirokov. "The imprints of primordial non-gaussianities on large-scale structure: scale dependent bias and abundance of virialized objects." *Phys. Rev.* D77 (2008), p. 123514. arXiv: 0710.4560 [astro-ph].

[37] S. Matarrese and L. Verde. "The effect of primordial non-Gaussianity on halo bias." *Astrophys. J.* 677 (2008), pp. L77–L80. arXiv: 0801.4826 [astro-ph].

[38] A. Slosar, C. Hirata, U. Seljak, S. Ho, and N. Padmanabhan. "Constraints on local primordial non-Gaussianity from large scale structure." *JCAP* 0808 (2008), p. 031. arXiv: 0805.3580 [astro-ph].

[39] C. Carbone, L. Verde, and S. Matarrese. "Non-Gaussian halo bias and future galaxy surveys." *Astrophys. J.* 684 (2008), pp. L1–L4. arXiv: 0806.1950 [astro-ph].

[40] F. Schmidt and M. Kamionkowski. "Halo Clustering with Non-Local Non-Gaussianity." *Phys. Rev.* D82 (2010), p. 103002. arXiv: 1008.0638 [astro-ph.CO].

[41] R. Flauger and E. Pajer. "Resonant Non-Gaussianity." *JCAP* 1101 (2011), p. 017. arXiv: 1002.0833 [hep-th].

[42] M. H. Abitbol, J. Chluba, J. C. Hill, and B. R. Johnson. "Prospects for Measuring Cosmic Microwave Background Spectral Distortions in the Presence of Foregrounds." *Mon. Not. Roy. Astron. Soc.* 471 (2017), pp. 1126–1140. arXiv: 1705.01534 [astro-ph.CO].

[43] D. Baumann. "TASI Lectures on Inflation." *TASI 2009: Physics of the Large and the Small*. 2012. arXiv: 0907.5424v2 [hep-th].

[44] D. Baumann. *Cosmology*. URL: http://www.damtp.cam.ac.uk/user/db275/Cosmology/Lectures.pdf.

[45] J. Chluba. *CUSO Lectures*. URL: http://www.jb.man.ac.uk/~jchluba/Science/.

[46] S. Carroll. *Spacetime and Geometry: An Introduction to General Relativity*. 2003.

[47] P. A. R. Ade et al. "Improved Constraints on Cosmology and Foregrounds from BICEP2 and Keck Array Cosmic Microwave Background Data with Inclusion of 95 GHz Band." *Phys. Rev. Lett.* 116 (2016), p. 031302. arXiv: 1510.09217 [astro-ph.CO].

[48] K. N. Abazajian et al. "CMB-S4 Science Book, First Edition" (2016). arXiv: 1610.02743 [astro-ph.CO].

[49] G. Cabass, A. Melchiorri, and E. Pajer. "μ-distortions or running: A guaranteed discovery from CMB spectrometry." *Phys. Rev.* D93.8 (2016), p. 083515. arXiv: 1602.05578 [astro-ph.CO].

[50] G. Cabass, E. Di Valentino, A. Melchiorri, E. Pajer, and J. Silk. "Constraints on the running of the running of the scalar tilt from CMB anisotropies and spectral distortions." *Phys. Rev.* D94.2 (2016), p. 023523. arXiv: 1605.00209 [astro-ph.CO].

[51] G. Cabass, E. Pajer, and F. Schmidt. "How Gaussian can our Universe be?" *JCAP* 1701.01 (2017), p. 003. arXiv: 1612.00033 [hep-th].

[52] R. Durrer. "The cosmic microwave background: the history of its experimental investigation and its significance for cosmology." *Class. Quant. Grav.* 32.12 (2015), p. 124007. arXiv: 1506.01907 [astro-ph.CO].

[53] V. Springel, C. S. Frenk, and S. D. M. White. "The large-scale structure of the Universe." *Nature* 440 (2006), p. 1137. arXiv: astro-ph/0604561 [astro-ph].

[54] A. Goobar and B. Leibundgut. "Supernova cosmology: legacy and future." *Ann. Rev. Nucl. Part. Sci.* 61 (2011), pp. 251–279. arXiv: 1102.1431 [astro-ph.CO].

[55] R. M. Wald. *General Relativity*. 1984.

[56] C. W. Misner, K. S. Thorne, and J. A. Wheeler. *Gravitation*. 1973.

[57] E. Bertschinger. *Cosmological Dynamics*. URL: https://ned.ipac.caltech.edu/level5/March02/Bertschinger/paper.pdf.

[58] C. G. Tsagas, A. Challinor, and R. Maartens. "Relativistic cosmology and large-scale structure." *Phys. Rept.* 465 (2008), pp. 61–147. arXiv: 0705.4397 [astro-ph].

[59] *Planck* collaboration. "*Planck* 2013 results. XVI. Cosmological parameters." *A&A* (2013). arXiv: 1303.5076v3 [astro-ph.CO]. In press.

[60] E. Di Valentino, A. Melchiorri, and J. Silk. "Beyond six parameters: extending ΛCDM." *Phys. Rev.* D92.12 (2015), p. 121302. arXiv: 1507.06646 [astro-ph.CO].

[61] P. Creminelli, M. A. Luty, A. Nicolis, and L. Senatore. "Starting the Universe: Stable Violation of the Null Energy Condition and Non-standard Cosmologies." *JHEP* 12 (2006), p. 080. arXiv: hep-th/0606090 [hep-th].

[62] C. Cheung, P. Creminelli, A. L. Fitzpatrick, J. Kaplan, and L. Senatore. "The Effective Field Theory of Inflation." *JHEP* 014 (Mar. 2008). arXiv: 0709.0293v2 [hep-th].

[63] A. H. Guth. "The Inflationary Universe: A Possible Solution to the Horizon and Flatness Problems." *Phys. Rev.* D23, 347 (1981).

[64] A. R. Liddle, P. Parsons, and J. D. Barrow. "Formalising the Slow-Roll Approximation in Inflation." *Phys. Rev.* D50, 7222 (1994). arXiv: astro-ph/9408015v1.

[65] E. Pajer, G. L. Pimentel, and J. V. S. Van Wijck. "The Conformal Limit of Inflation in the Era of CMB Polarimetry." *JCAP* 1706.06 (2017), p. 009. arXiv: 1609.06993 [hep-th].

[66] J. Martin, C. Ringeval, and V. Vennin. "Encyclopædia Inflationaris." *Phys. Dark Univ.* 5-6 (2014), pp. 75–235. arXiv: 1303.3787 [astro-ph.CO].

[67] D. S. Gorbunov and V. A. Rubakov. *Introduction to the Theory of the Early Universe: Hot Big Bang Theory*. 2011.

[68] G. Mangano, G. Miele, S. Pastor, and M. Peloso. "A Precision calculation of the effective number of cosmological neutrinos." *Phys. Lett.* B534 (2002), pp. 8–16. arXiv: astro-ph/0111408 [astro-ph].

[69] G. Mangano, G. Miele, S. Pastor, T. Pinto, O. Pisanti, and P. D. Serpico. "Relic neutrino decoupling including flavor oscillations." *Nucl. Phys.* B729 (2005), pp. 221–234. arXiv: hep-ph/0506164 [hep-ph].

[70] M. Kawasaki, K. Kohri, and N. Sugiyama. "Cosmological constraints on late time entropy production." *Phys. Rev. Lett.* 82 (1999), p. 4168. arXiv: astro-ph/9811437 [astro-ph].

[71] M. Kawasaki, K. Kohri, and N. Sugiyama. "MeV scale reheating temperature and thermalization of neutrino background." *Phys. Rev.* D62 (2000), p. 023506. arXiv: astro-ph/0002127 [astro-ph].

[72] P. F. de Salas, M. Lattanzi, G. Mangano, G. Miele, S. Pastor, and O. Pisanti. "Bounds on very low reheating scenarios after Planck." *Phys. Rev.* D92.12 (2015), p. 123534. arXiv: 1511.00672 [astro-ph.CO].

[73] D. S. Gorbunov and V. A. Rubakov. *Introduction to the Theory of the Early Universe: Cosmological Perturbations and Inflationary Theory*. 2011.

[74] R. A. Sunyaev and R. Khatri. "Unavoidable CMB spectral features and blackbody photosphere of our Universe." *Int. J. Mod. Phys.* D22 (2013), p. 1330014. arXiv: 1302.6553 [astro-ph.CO].

[75] J. Chluba and Y. Ali-Haïmoud. "CosmoSpec: Fast and detailed computation of the cosmological recombination radiation from hydrogen and helium." *Mon. Not. Roy. Astron. Soc.* 456.4 (2016), pp. 3494–3508. arXiv: 1510.03877 [astro-ph.CO].

[76] L. Spitzer. *Physics of Fully Ionized Gases*. 1956.

[77] S. Stepney. "Two-body relaxation in relativistic thermal plasmas." *Monthly Notices of the Royal Astronomical Society* 202 (Feb. 1983), pp. 467–481.

[78] J. Chluba, R. Khatri, and R. A. Sunyaev. "CMB at 2x2 order: The dissipation of primordial acoustic waves and the observable part of the associated energy release." *Mon. Not. Roy. Astron. Soc.* 425 (2012), pp. 1129–1169. arXiv: 1202.0057 [astro-ph.CO].

[79] A. Kompaneests. *Sov. Phys. JETP* 31 (876 1956).

[80] Ya. B. Zeldovich and R. A. Sunyaev. "The Interaction of Matter and Radiation in a Hot-Model Universe." *Astrophys. Space Sci.* 4 (1969), pp. 301–316.

[81] S. Y. Sazonov and R. A. Sunyaev. "The Profile of a narrow line after single scattering by maxwellian electrons: Relativistic corrections to the kernel of the integral kinetic equation." *Astrophys. J.* 543 (2000), pp. 28–55. arXiv: astro-ph/9910280 [astro-ph].

[82] R. Svensson. *Monthly Notices of the Royal Astronomical Society* 209 (175 1984).

[83] N. Itoh, T. Sakamoto, S. Kusano, S. Nozawa, and Y. Kohyama. "Relativistic thermal bremsstrahlung gaunt factor for the intracluster plasma. 2. Analytic fitting formulae." *Astrophys. J. Suppl.* 128 (2000), pp. 125–138. arXiv: astro-ph/9906342 [astro-ph].

[84] Ya. B. Zeldovich and L. E. V. *SJETP* 28 (1287 1969).

[85] Ya. B. Zeldovich and R. A. Sunyaev. *Zhurnal Eksperimentalnoi i Teoreticheskoi Fiziki* 62 (153 1972).

[86] R. Khatri, R. A. Sunyaev, and J. Chluba. "Does Bose-Einstein condensation of CMB photons cancel μ-distortions created by dissipation of sound waves in the early Universe?" *Astron. Astrophys.* 540 (2012), A124. arXiv: 1110.0475 [astro-ph.CO].

[87] R. Khatri and R. A. Sunyaev. "Beyond y and μ: the shape of the CMB spectral distortions in the intermediate epoch, $1.5 \times 10^4 < z < 2 \times 10^5$." *JCAP* 1209 (2012), p. 016. arXiv: 1207.6654 [astro-ph.CO].

[88] J. Chluba. "Green's function of the cosmological thermalization problem." *Mon. Not. Roy. Astron. Soc.* 434 (2013), p. 352. arXiv: 1304.6120 [astro-ph.CO].

[89] J. Chluba. "Refined approximations for the distortion visibility function and μ-type spectral distortions." *Mon. Not. Roy. Astron. Soc.* 440.3 (2014), pp. 2544–2563. arXiv: 1312.6030 [astro-ph.CO].

[90] W. Hu and J. Silk. "Thermalization and spectral distortions of the cosmic background radiation." *Phys. Rev.* D48 (1993), pp. 485–502.

[91] J. Chluba. "Which spectral distortions does ΛCDM actually predict?" *Mon. Not. Roy. Astron. Soc.* 460.1 (2016), pp. 227–239. arXiv: 1603.02496 [astro-ph.CO].

[92] U. Seljak. "A Two fluid approximation for calculating the cosmic microwave background anisotropies." *Astrophys. J.* 435 (1994), pp. L87–L90. arXiv: astro-ph/9406050 [astro-ph].

[93] E. Pajer and M. Zaldarriaga. "A hydrodynamical approach to CMB μ-distortion from primordial perturbations." *JCAP* 1302 (2013), p. 036. arXiv: 1206.4479 [astro-ph.CO].

[94] R. Arnowitt, S. Deser, and C. W. Misner. "The Dynamics of General Relativity." *Gravitation: an introduction to current research*. 1962. Chap. 7, pp. 227–265. arXiv: gr-qc/0405109v1.

[95] S. Weinberg. "Cosmological fluctuations of short wavelength." *Astrophys. J.* 581 (2002), pp. 810–816. arXiv: astro-ph/0207375 [astro-ph].

[96] S. Dodelson. *Modern Cosmology*. 2003.

[97] K. A. Malik and D. Wands. "Cosmological perturbations." *Phys. Rept.* 475 (2009), pp. 1–51. arXiv: 0809.4944v2 [astro-ph].

[98] L. Boubekeur, P. Creminelli, J. Noreña, and F. Vernizzi. "Action approach to cosmological perturbations: the 2nd order metric in matter dominance." *JCAP* 0808 (2008), p. 028. arXiv: 0806.1016 [astro-ph].

[99] D. Baumann. *The Physics of Inflation*. URL: http://www.damtp.cam.ac.uk/user/db275/TEACHING/INFLATION/Lectures.pdf.

[100] D. Baumann, A. Nicolis, L. Senatore, and M. Zaldarriaga. "Cosmological Non-Linearities as an Effective Fluid." *JCAP* 1207 (2012), p. 051. arXiv: 1004.2488 [astro-ph.CO].

[101] S. Weinberg. *Cosmology*. 2008.

[102] H. Kurki-Suonio. *Lectures on Cosmology and CMB*. URL: http://www.courses.physics.helsinki.fi/teor/cosmology/.

[103] J. Silk. "Cosmic black body radiation and galaxy formation." *Astrophys. J.* 151 (1968), pp. 459–471.

[104] P. J. E. Peebles and J. T. Yu. "Primeval adiabatic perturbation in an expanding universe." *Astrophys. J.* 162 (1970), pp. 815–836.

[105] N. Kaiser. "Small-angle anisotropy of the microwave background radiation in the adiabatic theory." *Mon. Not. Roy. Astron. Soc.* 202 (1169 1983).

[106] M. Zaldarriaga and D. D. Harari. "Analytic approach to the polarization of the cosmic microwave background in flat and open universes." *Phys. Rev.* D52 (1995), pp. 3276–3287. arXiv: astro-ph/9504085 [astro-ph].

[107] V. Mukhanov. *Physical Foundations of Cosmology*. 2005.

[108] K. S. Thorne. "Relativistic radiative transfer: moment formalisms." *Mon. Not. Roy. Astron. Soc.* 194 (439 1981).

[109] E. Di Valentino, E. Giusarma, M. Lattanzi, O. Mena, A. Melchiorri, and J. Silk. "Cosmological Axion and neutrino mass constraints from Planck 2015 temperature and polarization data." *Phys. Lett.* B752 (2016), pp. 182–185. arXiv: 1507.08665 [astro-ph.CO].

[110] E. Di Valentino, E. Giusarma, O. Mena, A. Melchiorri, and J. Silk. "Cosmological limits on neutrino unknowns versus low redshift priors." *Phys. Rev.* D93.8 (2016), p. 083527. arXiv: 1511.00975 [astro-ph.CO].

[111] M. Gerbino, K. Freese, S. Vagnozzi, M. Lattanzi, O. Mena, E. Giusarma, and S. Ho. "Impact of neutrino properties on the estimation of inflationary parameters from current and future observations." *Phys. Rev.* D95.4 (2017), p. 043512. arXiv: 1610.08830 [astro-ph.CO].

[112] M. Gerbino, M. Lattanzi, O. Mena, and K. Freese. "A novel approach to quantifying the sensitivity of current and future cosmological datasets to the neutrino mass ordering through Bayesian hierarchical modeling" (2016). arXiv: 1611.07847 [astro-ph.CO].

[113] S. Vagnozzi, E. Giusarma, O. Mena, K. Freese, M. Gerbino, S. Ho, and M. Lattanzi. "Unveiling ν secrets with cosmological data: neutrino masses and mass hierarchy" (2017). arXiv: 1701.08172 [astro-ph.CO].

[114] F. Capozzi, E. Di Valentino, E. Lisi, A. Marrone, A. Melchiorri, and A. Palazzo. "Global constraints on absolute neutrino masses and their ordering." *Phys. Rev.* D95.9 (2017), p. 096014. arXiv: 1703.04471 [hep-ph].

[115] W. Hu and M. White. "A CMB Polarization Primer." *New Astronomy* 2 (4 1997), pp. 323–344. arXiv: astro-ph/9706147v1.

[116] Y. D. Takahashi. *Cosmic Microwave Background Polarization*. URL: http://cosmology.berkeley.edu/~yuki/CMBpol/CMBpol.htm.

[117] M. Kamionkowski, A. Kosowsky, and A. Stebbins. "Statistics of Cosmic Microwave Background Polarization." *Phys. Rev.* D55, 7368 (1997). arXiv: astro-ph/9611125v1.

[118] M. Zaldarriaga and U. Seljak. "An All-Sky Analysis of Polarization in the Microwave Background." *Phys. Rev.* D55, 1830 (1997). arXiv: astro-ph/9609170v2.

[119] X. Chen, M.-x. Huang, S. Kachru, and G. Shiu. "Observational signatures and non-Gaussianities of general single field inflation." *JCAP* 0701 (2007), p. 002. arXiv: hep-th/0605045 [hep-th].

[120] N. D. Birrell and P. C. W. Davies. *Quantum Fields in Curved Space*. 2003.

[121] D. Scott and G. Smoot. "Cosmic Microwave Background Mini-Review." *Phys. Lett.* B592, 1 (2004). arXiv: astro-ph/0601307v1.

[122] J. G. Bartlett. "Cosmic Microwave Background Polarization." *J. Phys.: Conf. Ser.* 39, 1 (2006). arXiv: astro-ph/0601576v3.

[123] *Planck* collaboration. "*Planck* 2013 results. XV. CMB power spectra and likelihood." *A&A* (2013). arXiv: 1303.5075v2 [astro-ph.CO]. In press.

[124] D. H. Lyth. "What would we learn by detecting a gravitational wave signal in the cosmic microwave background anisotropy?" *Phys. Rev. Lett.* 78, 1861 (1997). arXiv: hep-ph/9606387v1.

[125] P. André et al. "PRISM (Polarized Radiation Imaging and Spectroscopy Mission): A White Paper on the Ultimate Polarimetric Spectro-Imaging of the Microwave and Far-Infrared Sky" (2013). arXiv: 1306.2259 [astro-ph.CO].

[126] P. André et al. "PRISM (Polarized Radiation Imaging and Spectroscopy Mission): An Extended White Paper." *JCAP* 1402 (2014), p. 006. arXiv: 1310.1554 [astro-ph.CO].

[127] F. R. Bouchet et al. "COrE (Cosmic Origins Explorer) A White Paper" (2011). arXiv: 1102.2181 [astro-ph.CO].

[128] T. Matsumura et al. "Mission design of LiteBIRD" (2013). [J. Low. Temp. Phys.176,733(2014)]. arXiv: 1311.2847 [astro-ph.IM].

[129] P. Creminelli, D. L. López Nacir, M. Simonović, G. Trevisan, and M. Zaldarriaga. "Detecting Primordial B-Modes after Planck." *JCAP* 1511.11 (2015), p. 031. arXiv: 1502.01983 [astro-ph.CO].

[130] G. Cabass, L. Pagano, L. Salvati, M. Gerbino, E. Giusarma, and A. Melchiorri. "Updated Constraints and Forecasts on Primordial Tensor Modes." *Phys. Rev.* D93.6 (2016), p. 063508. arXiv: 1511.05146 [astro-ph.CO].

[131] E. Dimastrogiovanni, L. M. Krauss, and J. Chluba. "Constraints on Gravitino Decay and the Scale of Inflation using CMB spectral distortions." *Phys. Rev.* D94.2 (2016), p. 023518. arXiv: 1512.09212 [hep-ph].

[132] M. Anthonisen, R. Brandenberger, A. Laguë, I. A. Morrison, and D. Xia. "Cosmic Microwave Background Spectral Distortions from Cosmic String Loops." *JCAP* 1602.02 (2016), p. 047. arXiv: 1509.07998 [astro-ph.CO].

[133] J. M. Wagstaff and R. Banerjee. "CMB spectral distortions from the decay of causally generated magnetic fields." *Phys. Rev.* D92.12 (2015), p. 123004. arXiv: 1508.01683 [astro-ph.CO].

[134] K. E. Kunze and M. Á. Vázquez-Mozo. "Constraints on hidden photons from current and future observations of CMB spectral distortions." *JCAP* 1512.12 (2015), p. 028. arXiv: 1507.02614 [astro-ph.CO].

[135] Y. Ali-Haïmoud, J. Chluba, and M. Kamionkowski. "Constraints on Dark Matter Interactions with Standard Model Particles from Cosmic Microwave Background Spectral Distortions." *Phys. Rev. Lett.* 115.7 (2015), p. 071304. arXiv: 1506.04745 [astro-ph.CO].

[136] J. B. Dent, D. A. Easson, and H. Tashiro. "Cosmological constraints from CMB distortion." *Phys. Rev.* D86 (2012), p. 023514. arXiv: 1202.6066 [astro-ph.CO].

[137] J. Chluba, A. L. Erickcek, and I. Ben-Dayan. "Probing the inflaton: Small-scale power spectrum constraints from measurements of the CMB energy spectrum." *Astrophys. J.* 758 (2012), p. 76. arXiv: 1203.2681 [astro-ph.CO].

[138] R. Khatri and R. A. Sunyaev. "Forecasts for CMB μ- and i-type spectral distortion constraints on the primordial power spectrum on scales $8\,\mathrm{Mpc}^{-1} \lesssim k \lesssim 10^4\,\mathrm{Mpc}^{-1}$ with the future Pixie-like experiments." *JCAP* 1306 (2013), p. 026. arXiv: 1303.7212 [astro-ph.CO].

[139] S. Clesse, B. Garbrecht, and Y. Zhu. "Testing Inflation and Curvaton Scenarios with CMB Distortions." *JCAP* 1410.10 (2014), p. 046. arXiv: 1402.2257 [astro-ph.CO].

[140] K. Enqvist, T. Sekiguchi, and T. Takahashi. "Mixed Inflaton and Spectator Field Models: CMB constraints and μ distortion." *JCAP* 1604.04 (2016), p. 057. arXiv: 1511.09304 [astro-ph.CO].

[141] D. Roest. "Universality classes of inflation." *JCAP* 1401 (2014), p. 007. arXiv: 1309.1285 [hep-th].

[142] J. Garcia-Bellido and D. Roest. "Large-N running of the spectral index of inflation." *Phys. Rev.* D89.10 (2014), p. 103527. arXiv: 1402.2059 [astro-ph.CO].

[143] R. Gobbetti, E. Pajer, and D. Roest. "On the Three Primordial Numbers." *JCAP* 1509.09 (2015), p. 058. arXiv: 1505.00968 [astro-ph.CO].

[144] S. Galli, K. Benabed, F. Bouchet, J.-F. Cardoso, F. Elsner, E. Hivon, A. Mangilli, S. Prunet, and B. Wandelt. "CMB Polarization can constrain cosmology better than CMB temperature." *Phys. Rev.* D90.6 (2014), p. 063504. arXiv: 1403.5271 [astro-ph.CO].

[145] W. L. K. Wu, J. Errard, C. Dvorkin, C. L. Kuo, A. T. Lee, P. McDonald, A. Slosar, and O. Zahn. "A Guide to Designing Future Ground-based Cosmic Microwave Background Experiments." *Astrophys. J.* 788 (2014), p. 138. arXiv: 1402.4108 [astro-ph.CO].

[146] O. Doré et al. "Cosmology with the SPHEREX All-Sky Spectral Survey" (2014). arXiv: 1412.4872 [astro-ph.CO].

[147] J. Errard, S. M. Feeney, H. V. Peiris, and A. H. Jaffe. "Robust forecasts on fundamental physics from the foreground-obscured, gravitationally-lensed CMB polarization." *JCAP* 1603 (2016), p. 052. arXiv: 1509.06770 [astro-ph.CO].

[148] N. Arkani-Hamed, H.-C. Cheng, P. Creminelli, and L. Randall. "Extra natural inflation." *Phys. Rev. Lett.* 90 (2003), p. 221302. arXiv: hep-th/0301218 [hep-th].

[149] B. Feng, M.-z. Li, R.-J. Zhang, and X.-m. Zhang. "An inflation model with large variations in spectral index." *Phys. Rev.* D68 (2003), p. 103511. arXiv: astro-ph/0302479 [astro-ph].

[150] T. Kobayashi and F. Takahashi. "Running Spectral Index from Inflation with Modulations." *JCAP* 1101 (2011), p. 026. arXiv: 1011.3988 [astro-ph.CO].

[151] R. K. Jain, M. Sandora, and M. S. Sloth. "Radiative Corrections from Heavy Fast-Roll Fields during Inflation." *JCAP* 1506 (2015), p. 016. arXiv: 1501.06919 [hep-th].

[152] S. Parameswaran, G. Tasinato, and I. Zavala. "Subleading Effects and the Field Range in Axion Inflation." *JCAP* 1604.04 (2016), p. 008. arXiv: 1602.02812 [astro-ph.CO].

[153] J. Chluba. "Distinguishing different scenarios of early energy release with spectral distortions of the cosmic microwave background." *Mon. Not. Roy. Astron. Soc.* 436 (2013), pp. 2232–2243. arXiv: 1304.6121 [astro-ph.CO].

[154] J. C. Hill and E. Pajer. "Cosmology from the thermal Sunyaev-Zeldovich power spectrum: Primordial non-Gaussianity and massive neutrinos." *Phys. Rev.* D88.6 (2013), p. 063526. arXiv: 1303.4726 [astro-ph.CO].

[155] J. C. Hill, N. Battaglia, J. Chluba, S. Ferraro, E. Schaan, and D. N. Spergel. "Taking the Universe's Temperature with Spectral Distortions of the Cosmic Microwave Background." *Phys. Rev. Lett.* 115.26 (2015), p. 261301. arXiv: 1507.01583 [astro-ph.CO].

[156] J. C. Hill. "The Sunyaev-Zeldovich Effect and Large-Scale Structure." 2015. arXiv: 1510.06237 [astro-ph.CO].

[157] J. Chluba and D. Jeong. "Teasing bits of information out of the CMB energy spectrum." *Mon. Not. Roy. Astron. Soc.* 438.3 (2014), pp. 2065–2082. arXiv: 1306.5751 [astro-ph.CO].

[158] K. Basu, C. Hernandez-Monteagudo, and R. Sunyaev. "CMB observations and the production of chemical elements at the end of the dark ages." *Astron. Astrophys.* 416 (2004), pp. 447–466. arXiv: astro-ph/0311620 [astro-ph].

[159] G. De Zotti, M. Negrello, G. Castex, A. Lapi, and M. Bonato. "Another look at distortions of the Cosmic Microwave Background spectrum." *JCAP* 1603.03 (2016), p. 047. arXiv: 1512.04816 [astro-ph.CO].

[160] P. J. E. Peebles. "Recombination of the Primeval Plasma." *Astrophys. J.* 153 (1968), p. 1.

[161] Ya. B. Zeldovich, V. G. Kurt, and R. A. Sunyaev. "Recombination of hydrogen in the hot model of the universe." *Sov. Phys. JETP* 28 (1969). [Zh. Eksp. Teor. Fiz.55,278(1968)], p. 146.

[162] V. K. Dubrovich. *Sov. Astron. Lett.* 1 (196 1975).

[163] J. Chluba and R. A. Sunyaev. "Induced two-photon decay of the 2s level and the rate of cosmological hydrogen recombination." *Astron. Astrophys.* 446 (2006), pp. 39–42. arXiv: astro-ph/0508144 [astro-ph].

[164] J. A. Rubino-Martin, J. Chluba, and R. A. Sunyaev. "Lines in the Cosmic Microwave Background Spectrum from the Epoch of Cosmological Hydrogen Recombination." *Mon. Not. Roy. Astron. Soc.* 371 (2006), pp. 1939–1952. arXiv: astro-ph/0607373 [astro-ph].

[165] J. Chluba, J. A. Rubino-Martin, and R. A. Sunyaev. "Cosmological hydrogen recombination: Populations of the high level sub-states." *Mon. Not. Roy. Astron. Soc.* 374 (2007), pp. 1310–1320. arXiv: astro-ph/0608242 [astro-ph].

[166] R. Khatri, R. A. Sunyaev, and J. Chluba. "Mixing of blackbodies: entropy production and dissipation of sound waves in the early Universe." *Astron. Astrophys.* 543 (2012), A136. arXiv: 1205.2871 [astro-ph.CO].

[167] N. Aghanim et al. "Planck 2015 results. XI. CMB power spectra, likelihoods, and robustness of parameters." *Astron. Astrophys.* 594 (2016), A11. arXiv: 1507.02704 [astro-ph.CO].

[168] A. Lewis and S. Bridle. "Cosmological parameters from CMB and other data: A Monte Carlo approach." *Phys. Rev.* D66 (2002), p. 103511. arXiv: astro-ph/0205436 [astro-ph].

[169] A. Lewis. "Efficient sampling of fast and slow cosmological parameters." *Phys. Rev.* D87.10 (2013), p. 103529. arXiv: 1304.4473 [astro-ph.CO].

[170] M. Cortes, A. R. Liddle, and P. Mukherjee. "On what scale should inflationary observables be constrained?" *Phys. Rev.* D75 (2007), p. 083520. arXiv: astro-ph/0702170 [astro-ph].

[171] A. A. Starobinsky. "A New Type of Isotropic Cosmological Models Without Singularity." *Phys. Lett.* 91B (1980), pp. 99–102.

[172] E. Calabrese, A. Slosar, A. Melchiorri, G. F. Smoot, and O. Zahn. "Cosmic Microwave Weak lensing data as a test for the dark universe." *Phys. Rev.* D77 (2008), p. 123531. arXiv: 0803.2309 [astro-ph].

[173] E. Di Valentino, A. Melchiorri, and J. Silk. "Cosmological hints of modified gravity?" *Phys. Rev.* D93.2 (2016), p. 023513. arXiv: 1509.07501 [astro-ph.CO].

[174] Z. Huang. "Observational effects of a running Planck mass." *Phys. Rev.* D93.4 (2016), p. 043538. arXiv: 1511.02808 [astro-ph.CO].

[175] M. Gerbino, E. Di Valentino, and N. Said. "Neutrino Anisotropies after Planck." *Phys. Rev.* D88.6 (2013), p. 063538. arXiv: 1304.7400 [astro-ph.CO].

[176] J. B. Muñoz, D. Grin, L. Dai, M. Kamionkowski, and E. D. Kovetz. "Search for Compensated Isocurvature Perturbations with Planck Power Spectra." *Phys. Rev.* D93.4 (2016), p. 043008. arXiv: 1511.04441 [astro-ph.CO].

[177] F. Couchot, S. Henrot-Versillé, O. Perdereau, S. Plaszczynski, B. Rouillé d'Orfeuil, M. Spinelli, and M. Tristram. "Relieving tensions related to the lensing of the cosmic microwave background temperature power spectra." *Astron. Astrophys.* 597 (2017), A126. arXiv: 1510.07600 [astro-ph.CO].

[178] G. E. Addison, Y. Huang, D. J. Watts, C. L. Bennett, M. Halpern, G. Hinshaw, and J. L. Weiland. "Quantifying discordance in the 2015 Planck CMB spectrum." *Astrophys. J.* 818.2 (2016), p. 132. arXiv: 1511.00055 [astro-ph.CO].

[179] M. Escudero, H. Ramírez, L. Boubekeur, E. Giusarma, and O. Mena. "The present and future of the most favoured inflationary models after Planck 2015." *JCAP* 1602.02 (2016), p. 020. arXiv: 1509.05419 [astro-ph.CO].

[180] P. A. R. Ade et al. "Planck 2015 results. XV. Gravitational lensing." *Astron. Astrophys.* 594 (2016), A15. arXiv: 1502.01591 [astro-ph.CO].

[181] C. Heymans et al. "CFHTLenS: The Canada-France-Hawaii Telescope Lensing Survey." *Mon. Not. Roy. Astron. Soc.* 427 (2012), p. 146. arXiv: 1210.0032 [astro-ph.CO].

[182] T. Erben et al. "CFHTLenS: The Canada-France-Hawaii Telescope Lensing Survey - Imaging Data and Catalogue Products." *Mon. Not. Roy. Astron. Soc.* 433 (2013), p. 2545. arXiv: 1210.8156 [astro-ph.CO].

[183] T. D. Kitching et al. "3D Cosmic Shear: Cosmology from CFHTLenS." *Mon. Not. Roy. Astron. Soc.* 442.2 (2014), pp. 1326–1349. arXiv: 1401.6842 [astro-ph.CO].

[184] F. Beutler, C. Blake, M. Colless, D. H. Jones, L. Staveley-Smith, L. Campbell, Q. Parker, W. Saunders, and F. Watson. "The 6dF Galaxy Survey: Baryon Acoustic Oscillations and the Local Hubble Constant." *Mon. Not. Roy. Astron. Soc.* 416 (2011), pp. 3017–3032. arXiv: 1106.3366 [astro-ph.CO].

[185] A. J. Ross, L. Samushia, C. Howlett, W. J. Percival, A. Burden, and M. Manera. "The clustering of the SDSS DR7 main Galaxy sample – I. A 4 per cent distance measure at $z = 0.15$." *Mon. Not. Roy. Astron. Soc.* 449.1 (2015), pp. 835–847. arXiv: 1409.3242 [astro-ph.CO].

[186] L. Anderson et al. "The clustering of galaxies in the SDSS-III Baryon Oscillation Spectroscopic Survey: baryon acoustic oscillations in the Data Releases 10 and 11 Galaxy samples." *Mon. Not. Roy. Astron. Soc.* 441.1 (2014), pp. 24–62. arXiv: 1312.4877 [astro-ph.CO].

[187] M. Gerbino, M. Lattanzi, and A. Melchiorri. "ν generation: Present and future constraints on neutrino masses from global analysis of cosmology and laboratory experiments." *Phys. Rev.* D93.3 (2016), p. 033001. arXiv: 1507.08614 [hep-ph].

[188] C. Destri, H. J. de Vega, and N. G. Sanchez. "The CMB Quadrupole depression produced by early fast-roll inflation: MCMC analysis of WMAP and SDSS data." *Phys. Rev.* D78 (2008), p. 023013. arXiv: 0804.2387 [astro-ph].

[189] M. Zaldarriaga, L. Hui, and M. Tegmark. "Constraints from the Lyman alpha forest power spectrum." *Astrophys. J.* 557 (2001), pp. 519–526. arXiv: astro-ph/0011559 [astro-ph].

[190] P. Adshead, R. Easther, J. Pritchard, and A. Loeb. "Inflation and the Scale Dependent Spectral Index: Prospects and Strategies." *JCAP* 021 (Feb. 2011). arXiv: 1007.3748v3 [astro-ph].

[191] N. Palanque-Delabrouille et al. "Neutrino masses and cosmology with Lyman-alpha forest power spectrum." *JCAP* 1511.11 (2015), p. 011. arXiv: 1506.05976 [astro-ph.CO].

[192] N. Palanque-Delabrouille et al. "The one-dimensional Ly-alpha forest power spectrum from BOSS." *Astron. Astrophys.* 559 (2013), A85. arXiv: 1306.5896 [astro-ph.CO].

[193] C. Armendariz-Picon, T. Damour, and V. F. Mukhanov. "k - inflation." *Phys. Lett.* B458 (1999), pp. 209–218. arXiv: hep-th/9904075 [hep-th].

[194] D. Wands. "Multiple field inflation." *Lect. Notes Phys.* 738 (2008), pp. 275–304. arXiv: astro-ph/0702187 [ASTRO-PH].

[195] P. A. R. Ade et al. "Planck 2015 results. XVII. Constraints on primordial non-Gaussianity." *Astron. Astrophys.* 594 (2016), A17. arXiv: 1502.01592 [astro-ph.CO].

[196] P. Creminelli, G. D'Amico, M. Musso, and J. Noreña. "The (not so) squeezed limit of the primordial 3-point function." *JCAP* 1111 (2011), p. 038. arXiv: 1106.1462 [astro-ph.CO].

[197] C. Wagner, F. Schmidt, C.-T. Chiang, and E. Komatsu. "The angle-averaged squeezed limit of nonlinear matter N-point functions." *JCAP* 1508.08 (2015), p. 042. arXiv: 1503.03487 [astro-ph.CO].

[198] T. Falk, R. Rangarajan, and M. Srednicki. "Dependence of density perturbations on the coupling constant in a simple model of inflation." *Phys. Rev.* D46 (1992), pp. 4232–4234. arXiv: astro-ph/9208002 [astro-ph].

[199] C. Burrage, R. H. Ribeiro, and D. Seery. "Large slow-roll corrections to the bispectrum of noncanonical inflation." *JCAP* 1107 (2011), p. 032. arXiv: 1103.4126 [astro-ph.CO].

[200] L. Dai, E. Pajer, and F. Schmidt. "Conformal Fermi Coordinates." *JCAP* 1511.11 (2015), p. 043. arXiv: 1502.02011 [gr-qc].

[201] L. Dai, E. Pajer, and F. Schmidt. "On Separate Universes." *JCAP* 1510.10 (2015), p. 059. arXiv: 1504.00351 [astro-ph.CO].

[202] R. de Putter, O. Doré, and D. Green. "Is There Scale-Dependent Bias in Single-Field Inflation?" *JCAP* 1510.10 (2015), p. 024. arXiv: 1504.05935 [astro-ph.CO].

[203] P. Creminelli and M. Zaldarriaga. "CMB 3-point functions generated by non-linearities at recombination." *Phys. Rev.* D70 (2004), p. 083532. arXiv: astro-ph/0405428 [astro-ph].

[204] P. Creminelli, C. Pitrou, and F. Vernizzi. "The CMB bispectrum in the squeezed limit." *JCAP* 1111 (2011), p. 025. arXiv: 1109.1822 [astro-ph.CO].

[205] M. Alvarez et al. "Testing Inflation with Large Scale Structure: Connecting Hopes with Reality" (2014). arXiv: 1412.4671 [astro-ph.CO].

[206] L. Senatore and M. Zaldarriaga. "A Note on the Consistency Condition of Primordial Fluctuations." *JCAP* 1208 (2012), p. 001. arXiv: 1203.6884 [astro-ph.CO].

[207] T. Baldauf, U. Seljak, L. Senatore, and M. Zaldarriaga. "Galaxy Bias and non-Linear Structure Formation in General Relativity." *JCAP* 1110 (2011), p. 031. arXiv: 1106.5507 [astro-ph.CO].

[208] P. Creminelli, A. Perko, L. Senatore, M. Simonović, and G. Trevisan. "The Physical Squeezed Limit: Consistency Relations at Order q^2." *JCAP* 1311 (2013), p. 015. arXiv: 1307.0503 [astro-ph.CO].

[209] F. K. Manasse and C. W. Misner. "Fermi Normal Coordinates and Some Basic Concepts in Differential Geometry." *J. Math. Phys.* 4 (1963), pp. 735–745.

[210] P. Creminelli, J. Noreña, and M. Simonović. "Conformal consistency relations for single-field inflation." *JCAP* 1207 (2012), p. 052. arXiv: 1203.4595 [hep-th].

[211] L. Senatore and M. Zaldarriaga. "The constancy of ζ in single-clock Inflation at all loops." *JHEP* 09 (2013), p. 148. arXiv: 1210.6048 [hep-th].

[212] G. I. Rigopoulos and E. P. S. Shellard. "The separate universe approach and the evolution of nonlinear superhorizon cosmological perturbations." *Phys. Rev.* D68 (2003), p. 123518. arXiv: astro-ph/0306620 [astro-ph].

[213] D. H. Lyth, K. A. Malik, and M. Sasaki. "A General proof of the conservation of the curvature perturbation." *JCAP* 0505 (2005), p. 004. arXiv: astro-ph/0411220 [astro-ph].

[214] S. Weinberg. "Non-Gaussian Correlations Outside the Horizon." *Phys. Rev.* D78 (2008), p. 123521. arXiv: 0808.2909 [hep-th].

[215] S. Weinberg. "Non-Gaussian Correlations Outside the Horizon II: The General Case." *Phys. Rev.* D79 (2009), p. 043504. arXiv: 0810.2831 [hep-ph].

[216] V. Assassi, D. Baumann, and D. Green. "Symmetries and Loops in Inflation." *JHEP* 02 (2013), p. 151. arXiv: 1210.7792 [hep-th].

[217] M. Dias, J. Elliston, J. Frazer, D. Mulryne, and D. Seery. "The curvature perturbation at second order." *JCAP* 1502.02 (2015), p. 040. arXiv: 1410.3491 [gr-qc].

[218] K. Hinterbichler, L. Hui, and J. Khoury. "An Infinite Set of Ward Identities for Adiabatic Modes in Cosmology." *JCAP* 1401 (2014), p. 039. arXiv: 1304.5527 [hep-th].

[219] C. Cheung, A. L. Fitzpatrick, J. Kaplan, and L. Senatore. "On the consistency relation of the 3-point function in single field inflation." *JCAP* 0802 (2008), p. 021. arXiv: 0709.0295 [hep-th].

[220] D. Seery and J. E. Lidsey. "Primordial non-Gaussianities in single field inflation." *JCAP* 0506 (2005), p. 003. arXiv: astro-ph/0503692 [astro-ph].

[221] V. Desjacques, D. Jeong, and F. Schmidt. "Large-Scale Galaxy Bias" (2016). arXiv: 1611.09787 [astro-ph.CO].

[222] M. Bruni, J. C. Hidalgo, N. Meures, and D. Wands. "Non-Gaussian Initial Conditions in ΛCDM: Newtonian, Relativistic, and Primordial Contributions." *Astrophys. J.* 785 (2014), p. 2. arXiv: 1307.1478 [astro-ph.CO].

[223] M. Bruni, J. C. Hidalgo, and D. Wands. "Einstein's signature in cosmological large-scale structure." *Astrophys. J.* 794.1 (2014), p. L11. arXiv: 1405.7006 [astro-ph.CO].

[224] D. Bertacca, N. Bartolo, M. Bruni, K. Koyama, R. Maartens, S. Matarrese, M. Sasaki, and D. Wands. "Galaxy bias and gauges at second order in General Relativity." *Class. Quant. Grav.* 32.17 (2015), p. 175019. arXiv: 1501.03163 [astro-ph.CO].

[225] N. Bartolo, D. Bertacca, M. Bruni, K. Koyama, R. Maartens, S. Matarrese, M. Sasaki, L. Verde, and D. Wands. "A relativistic signature in large-scale structure." *Phys. Dark Univ.* 13 (2016), pp. 30–34. arXiv: 1506.00915 [astro-ph.CO].

[226] C. Wagner, F. Schmidt, C.-T. Chiang, and E. Komatsu. "Separate Universe Simulations." *Mon. Not. Roy. Astron. Soc.* 448.1 (2015), pp. L11–L15. arXiv: 1409.6294 [astro-ph.CO].

[227] F. Schmidt and D. Jeong. "Cosmic Rulers." *Phys. Rev.* D86 (2012), p. 083527. arXiv: 1204.3625 [astro-ph.CO].

[228] D. Jeong and F. Schmidt. "Cosmic Clocks." *Phys. Rev.* D89.4 (2014), p. 043519. arXiv: 1305.1299 [astro-ph.CO].

[229] D. Jeong and F. Schmidt. "Large-Scale Structure Observables in General Relativity." *Class. Quant. Grav.* 32.4 (2015), p. 044001. arXiv: 1407.7979 [astro-ph.CO].

[230] D. Bertacca, R. Maartens, and C. Clarkson. "Observed galaxy number counts on the lightcone up to second order: II. Derivation." *JCAP* 1411.11 (2014), p. 013. arXiv: 1406.0319 [astro-ph.CO].

[231] A. Kehagias, A. M. Dizgah, J. Noreña, H. Perrier, and A. Riotto. "A Consistency Relation for the Observed Galaxy Bispectrum and the Local non-Gaussianity from Relativistic Corrections." *JCAP* 1508.08 (2015), p. 018. arXiv: 1503.04467 [astro-ph.CO].

[232] E. Di Dio, H. Perrier, R. Durrer, G. Marozzi, A. M. Dizgah, J. Noreña, and A. Riotto. "Non-Gaussianities due to Relativistic Corrections to the Observed Galaxy Bispectrum." *JCAP* 1703.03 (2017), p. 006. arXiv: 1611.03720 [astro-ph.CO].

[233] L. Boubekeur, P. Creminelli, G. D'Amico, J. Noreña, and F. Vernizzi. "Sachs-Wolfe at second order: the CMB bispectrum on large angular scales." *JCAP* 0908 (2009), p. 029. arXiv: 0906.0980 [astro-ph.CO].

[234] N. Bartolo, S. Matarrese, and A. Riotto. "Non-Gaussianity in the Cosmic Microwave Background Anisotropies at Recombination in the Squeezed limit." *JCAP* 1202 (2012), p. 017. arXiv: 1109.2043 [astro-ph.CO].

[235] A. Lewis. "The full squeezed CMB bispectrum from inflation." *JCAP* 1206 (2012), p. 023. arXiv: 1204.5018 [astro-ph.CO].

[236] X.-L. Chen and M. Kamionkowski. "Particle decays during the cosmic dark ages." *Phys. Rev.* D70 (2004), p. 043502. arXiv: astro-ph/0310473 [astro-ph].

[237] N. Padmanabhan and D. P. Finkbeiner. "Detecting dark matter annihilation with CMB polarization: Signatures and experimental prospects." *Phys. Rev.* D72 (2005), p. 023508. arXiv: astro-ph/0503486 [astro-ph].

[238] S. Galli, F. Iocco, G. Bertone, and A. Melchiorri. "CMB constraints on Dark Matter models with large annihilation cross-section." *Phys. Rev.* D80 (2009), p. 023505. arXiv: 0905.0003 [astro-ph.CO].

[239] S. Galli, F. Iocco, G. Bertone, and A. Melchiorri. "Updated CMB constraints on Dark Matter annihilation cross-sections." *Phys. Rev.* D84 (2011), p. 027302. arXiv: 1106.1528 [astro-ph.CO].

[240] R. Diamanti, L. Lopez-Honorez, O. Mena, S. Palomares-Ruiz, and A. C. Vincent. "Constraining Dark Matter Late-Time Energy Injection: Decays and P-Wave Annihilations." *JCAP* 1402 (2014), p. 017. arXiv: 1308.2578 [astro-ph.CO].

[241] T. Baldauf, M. Mirbabayi, M. Simonović, and M. Zaldarriaga. "Large-scale structure constraints with controlled theoretical uncertainties" (2016). arXiv: 1602.00674 [astro-ph.CO].

[242] X. Chen and Y. Wang. "Quasi-Single Field Inflation and Non-Gaussianities." *JCAP* 1004 (2010), p. 027. arXiv: 0911.3380 [hep-th].

[243] N. Bartolo, S. Matarrese, and A. Riotto. "CMB Anisotropies at Second-Order. 2. Analytical Approach." *JCAP* 0701 (2007), p. 019. arXiv: astro-ph/0610110 [astro-ph].

[244] N. Bartolo and A. Riotto. "On the non-Gaussianity from Recombination." *JCAP* 0903 (2009), p. 017. arXiv: 0811.4584 [astro-ph].

[245] T. Baldauf, U. Seljak, L. Senatore, and M. Zaldarriaga. "Linear response to long wavelength fluctuations using curvature simulations." *JCAP* 1609.09 (2016), p. 007. arXiv: 1511.01465 [astro-ph.CO].

[246] L. Perotto, J. Lesgourgues, S. Hannestad, H. Tu, and Y. Y. Y. Wong. "Probing cosmological parameters with the CMB: Forecasts from full Monte Carlo simulations." *JCAP* 0610 (2006), p. 013. arXiv: astro-ph/0606227 [astro-ph].

[247] J. R. Bond, A. H. Jaffe, and L. E. Knox. "Radical compression of cosmic microwave background data." *Astrophys. J.* 533 (2000), p. 19. arXiv: astro-ph/9808264 [astro-ph].

[248] J. R. Bond, G. Efstathiou, and M. Tegmark. "Forecasting cosmic parameter errors from microwave background anisotropy experiments." *Mon. Not. Roy. Astron. Soc.* 291 (1997), pp. L33–L41. arXiv: astro-ph/9702100 [astro-ph].

[249] G. Efstathiou and J. R. Bond. "Cosmic confusion: Degeneracies among cosmological parameters derived from measurements of microwave background anisotropies." *Mon. Not. Roy. Astron. Soc.* 304 (1999), pp. 75–97. arXiv: astro-ph/9807103 [astro-ph].

[250] L. Verde, H. Peiris, and R. Jimenez. "Optimizing CMB polarization experiments to constrain inflationary physics." *JCAP* 0601 (2006), p. 019. arXiv: astro-ph/0506036 [astro-ph].

[251] M. P. Hobson, A. W. Jones, A. N. Lasenby, and F. R. Bouchet. "Foreground separation methods for satellite observations of the cosmic microwave background." *Mon. Not. Roy. Astron. Soc.* 300 (1998), p. 1. arXiv: astro-ph/9806387 [astro-ph].

[252] C. Baccigalupi, F. Perrotta, G. De Zotti, G. F. Smoot, C. Burigana, D. Maino, L. Bedini, and E. Salerno. "Extracting cosmic microwave background polarisation from satellite astrophysical maps." *Mon. Not. Roy. Astron. Soc.* 354 (2004), pp. 55–70. arXiv: astro-ph/0209591 [astro-ph].

[253] B. D. Wandelt, E. Hivon, and K. M. Gorski. "The pseudo-C_ℓ method: cosmic microwave background anisotropy power spectrum statistics for high precision cosmology." *Phys. Rev.* D64 (2001), p. 083003. arXiv: astro-ph/0008111 [astro-ph].

[254] A. Albrecht et al. "Findings of the Joint Dark Energy Mission Figure of Merit Science Working Group" (2009). arXiv: 0901.0721 [astro-ph.IM].

[255] J. S. Schwinger. "Brownian motion of a quantum oscillator." *J. Math. Phys.* 2 (1961), pp. 407–432.

[256] R. D. Jordan. "Effective Field Equations for Expectation Values." *Phys. Rev.* D33 (1986), pp. 444–454.

[257] E. Calzetta and B. L. Hu. "Closed Time Path Functional Formalism in Curved Space-Time: Application to Cosmological Back Reaction Problems." *Phys. Rev.* D35 (1987), p. 495.

[258] S. Weinberg. "Quantum contributions to cosmological correlations." *Phys. Rev.* D72 (2005), p. 043514. arXiv: hep-th/0506236 [hep-th].

[259] E. A. Lim. "Primordial non-Gaussianities." *Cambridge DAMTP Advanced Cosmology Lectures, 2012*. 2012.

COLOPHON

This document was typeset using the typographical look-and-feel `classicthesis` developed by André Miede. `classicthesis` is available for both LaTeX and LyX at:

`http://code.google.com/p/classicthesis/`

Figures 3.1, 3.4, 3.5, 5.1, 5.2, 5.3, 5.4, 5.5, 5.6, 5.7, 6.7, 7.1, 7.2, 8.1 and D.1 were obtained with the computational software *Mathematica* (version 10.2.0). *Mathematica* is available at:

`http://www.wolfram.com/mathematica/`

Final Version as of October 31, 2017 (`classicthesis` version 4.1).

DECLARATION

I declare that this thesis is my own work, which I have completed under the guidance of my supervisor and my co-supervisor. I also declare that I have cited and/or acknowledged all the results coming from published and unpublished work of other people.

Rome, October 31, 2017

Giovanni Cabass

DICHIARAZIONE

Dichiaro di essere l'autore di questa tesi, nella stesura della quale sono stato assistito dai miei relatore e correlatore. Dichiaro inoltre che sono stato attento a citare e/o riconoscere i risultati provenienti dal lavoro (pubblicato e non pubblicato) di altre persone.

Rome, 31 Ottobre 2017

Giovanni Cabass